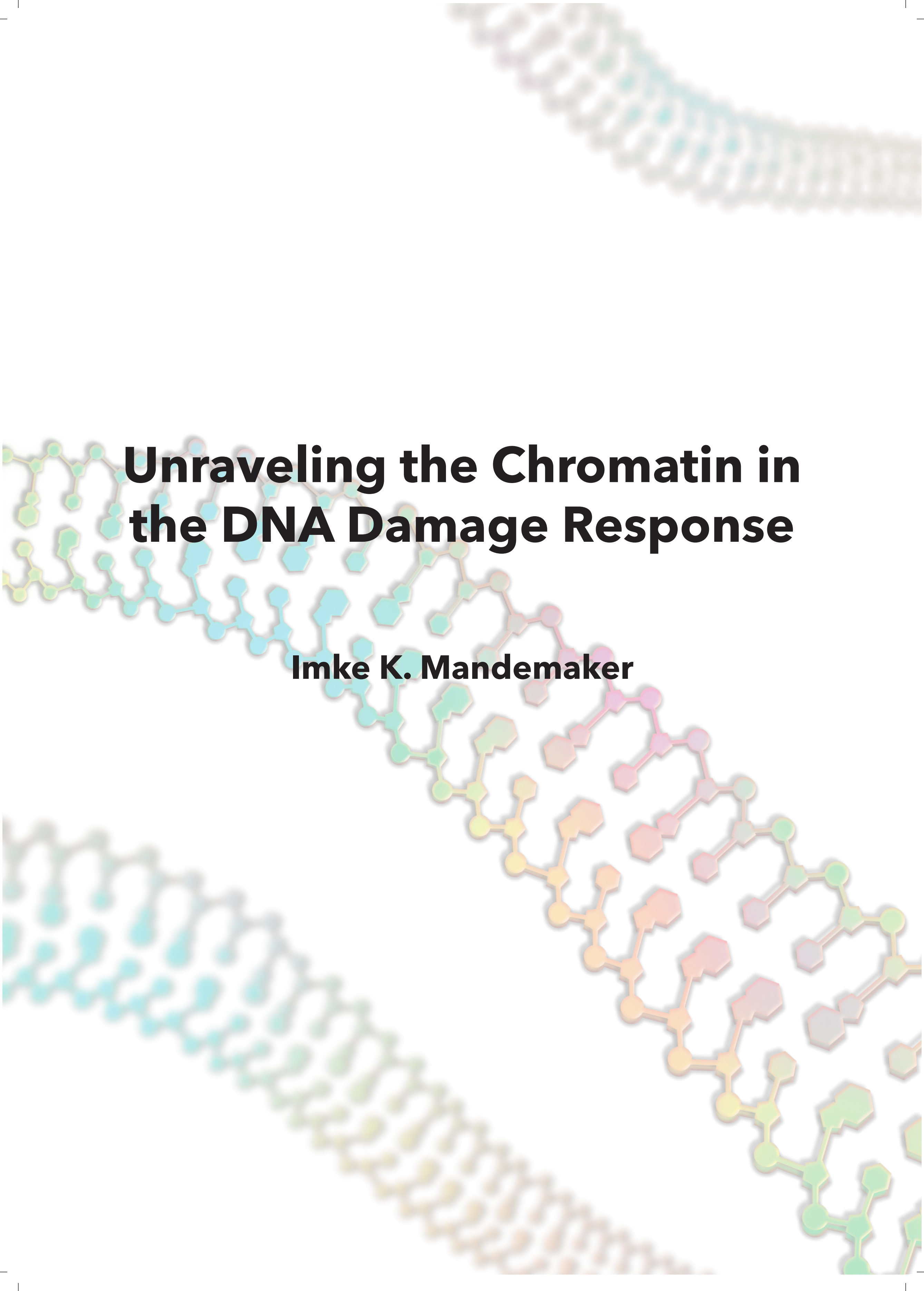

Unraveling the Chromatin in the DNA Damage Response

Imke K. Mandemaker

Colofon

ISBN: 978-94-6295-807-4

Cover design: SVDH Media
Printed by: ProefschriftMaken || www.proefschriftmaken.nl

The studies presented in this thesis were mainly performed at the department of Molecular Genetics of the Erasmus MC, Rotterdam, The Netherlands.

Copyright © Imke K. Mandemaker, 2017, Utrecht, The Netherlands

All right reserved. No part of this thesis may be reporduced, stored in a retrieval system, or transmitted in any form or by any means, without permission of the author or, when appropiate, of the publisher holding the copyrights of the published articles.

Unraveling the Chromatin in the DNA Damage Response

Ontwarren van het chromatine in de DNA schade response

Proefschrift

ter verkrijging van de graad van doctor aan de
Erasmus Universiteit Rotterdam
op gezag van de
rector magnificus

Prof.dr. H.A.P. Pols

en volgens besluit van het College voor Promoties.
De openbare verdediging zal plaatsvinden op

Woensdag 24 Januari 2018 om 15.30 uur

door

Imke Karlijn Mandemaker
geboren te Schijndel

Erasmus University Rotterdam

Promotiecommissie:

Promotor: Prof.Dr. W. Vermeulen
Overige leden: Prof.Dr. C.L. Wyman
Dr. P.J. Verschure
Dr. R.A. Poot
Copromotor: Dr. J.A. Marteijn

Table of contents

	Scope of this thesis	6
Chapter 1	Introduction	9
Chapter 2	Trichothiodystrophy causative TFIIEβ mutation affects transcription in highly differentiated tissue	19
Chapter 3	Chromatin remodeling in response to DNA damage	47
Chapter 4	Enhanced histone H1 chromatin retention after SET depletion causes DNA damage resistance	67
Chapter 5	DNA damage-induced histone H1 ubiquitylation is mediated by HUWE1 and stimulates the RNF8-RNF168 pathway	93
Chapter 6	DNA damage-induced replication stress results in PA200-proteasome mediated degradation of acetylated histones	119
Chapter 7	Discussion	151
Appendix	Summary Samenvatting Curriculum Vitae Publications PhD portfolio Acknowledgements/Dankwoord	161

SCOPE OF THIS THESIS

DNA is constantly damaged by various genotoxic agents from both external and internal sources and this has severe adverse effects on key cellular processes as transcription and replication, thereby negatively influencing cell viability. To maintain genome integrity, these harmful effects are counteracted by the DNA damage response (DDR), a complex network consisting of several signaling pathways and DNA repair mechanisms. In **Chapter 1**, we summarize how different DNA repair pathways function. We especially focus on nucleotide excision repair (NER). This DNA repair pathway is responsible for the removal of bulky helix-distorting lesions for example caused by UV-light. The biological relevance of NER is discussed with the description of several rare recessive NER-deficient disorders.

One of these disorders, Trichothiodystrophy (TTD), is characterized by brittle hair with low sulfur content, ichthyosis, developmental problems, microcephaly and impaired intelligence. About half of the TTD patients are sensitive to UV light, mostly due to mutations in TFIIH, a factor involved in both NER and transcription regulation. As mutations in TFIIH can lead to defects in both of these processes, it is difficult to distinguish if specific clinical symptoms arise from defects in either NER or transcription. To dissect the molecular mechanism underlying TTD symptoms, we performed whole genome sequencing on material from non-photosensitive TTD patients and found a mutation in the beta-subunit of general transcription factor E (TFIIEβ) in **Chapter 2**. The data presented in this chapter further suggest that TTD-specific clinical features arise from subtle transcription defects.

All DNA-transacting processes, like transcription, DNA repair and replication, take place in the context of chromatin. The chromatin structure, consisting of DNA wrapped around histone proteins, can be modified by ATP-dependent chromatin remodelers, histone chaperones and post translational modifications (PTMs). In **Chapter 3** an overview is presented of our current insights into the interplay between chromatin and the DDR. We focus on an example of how a methyl transferase and two histone chaperones stimulate the recovery of RNA synthesis in response to UV irradiation.

Thus far most research on the interplay of chromatin with DNA repair is focused on core histones and the role of linker histone H1 has remained largely unclear. Therefore we set out to study the function of histone H1 in the DDR. In **Chapter 4** we investigated the role of histone H1 chaperone SET and, interestingly, found that down regulation of SET results in increased resistance to a wide spectrum of structurally different DNA lesions that are repaired by different repair pathways. We show that co-depletion of histone H1 re-sensitizes SET-depleted cells to damage and that SET and tumor suppressor protein p53 act in the same pathway. Overall our results suggest that this decreased sensitivity in SET-depleted cells is the result of enhanced levels of chromatin bound histone H1, leading to reduced apoptosis in response to DNA damage.

In **Chapter 5** we observed, using a combination of SILAC based proteomics and an immuno-affinity procedure to specifically isolate ubiquitylated peptides, that histone H1 is a major target for ubiquitylation following UV exposure. We show that the E3 ligase HUWE1 is mediating this UV-induced H1 ubiquitylation and that this process is involved in the RNF8-RNF168-mediated DNA damage signaling pathway.

To test if, in addition to UV-induced changes in the ubiquitylation status of histones, also other UV-induced histone modifications could be observed, we performed additional quantitative mass spectrometry experiments. In **Chapter 6** we focused on changes in histone acetylation and isolated peptides with acetylated-lysines from a histone enriched fraction. Surprisingly, we found a histone-wide decrease in acetylation levels caused by UV-induced replication stress. Our results suggest that acetylated histones are specifically degraded by the PA200 proteasome complex.

In **Chapter 7**, the experimental data described in this thesis on the various roles of chromatin remodeling in response to DNA damage are being evaluated and discussed. We highlight the role of histone H1 in the DDR as our data shows that H1 is an important player by acting both in DNA damage signaling and transcription.

1

INTRODUCTION

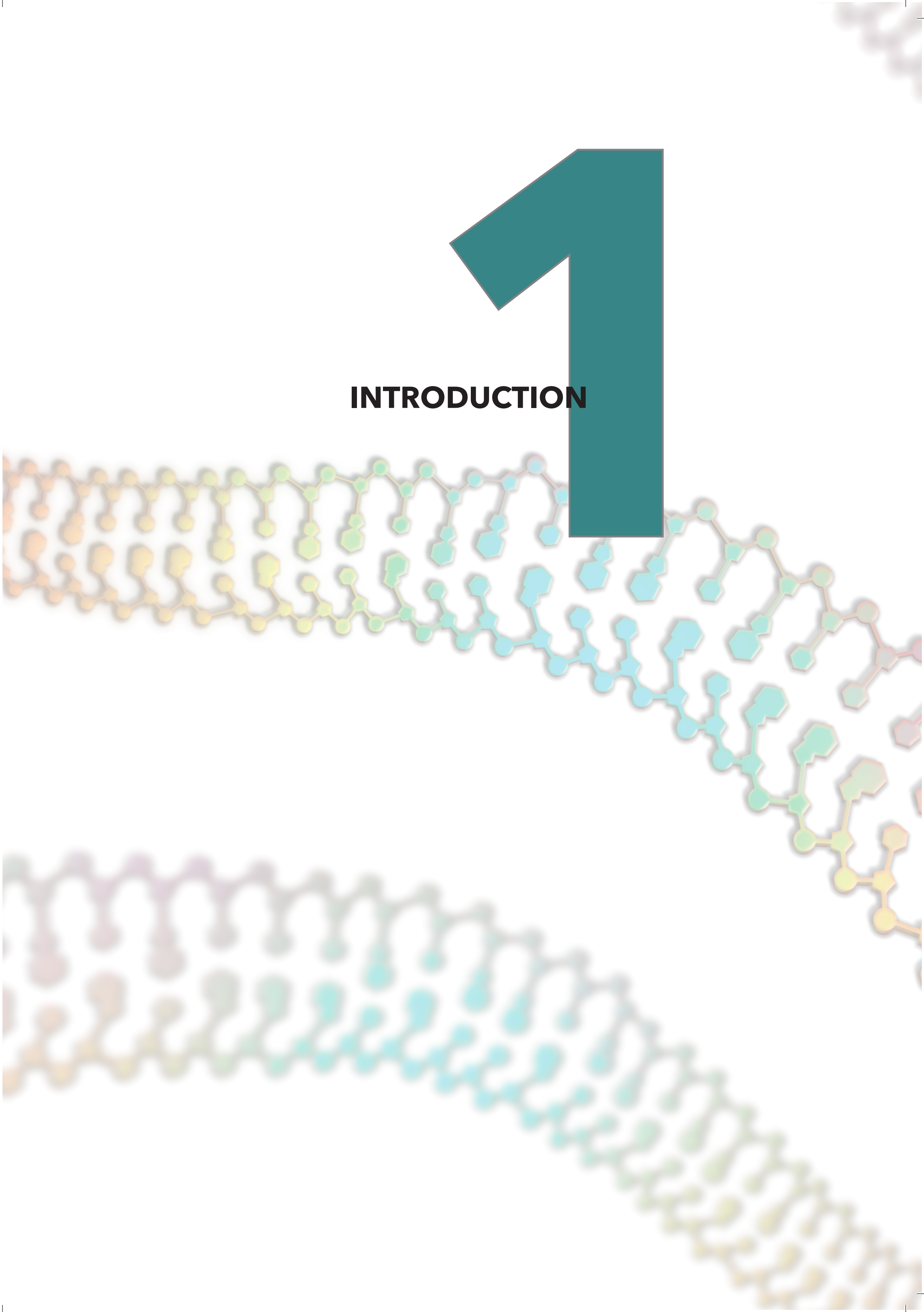

DNA DAMAGE

DNA contains all genetic information necessary for proper cellular functioning and, in contrast to RNA and proteins that have a constant turnover, it is the only biomolecule that is never completely renewed during the lifespan of a cell. Therefore, it is important that this genetic code is preserved as it is transmitted to next generations and encodes for RNA molecules. However, cells are constantly challenged by different endogenous and exogenous genotoxic agents, which can cause a wide variety of DNA lesions, threatening the integrity of the DNA thereby affecting DNA related processes, including replication of the DNA during cell division and transcription in which the DNA is copied to RNA. Damages can for instance be caused by endogenously produced reactive oxygen species (ROS) during normal cellular metabolism, which can result in base oxidations. Examples of exogenous sources of DNA damage are ionizing radiation, ultraviolet (UV) light and chemotherapeutic drugs. Different types of DNA damaging agents will induce different subsets of DNA lesions subsequently resulting in different cellular outcomes (Figure 1). Some lesions, like oxidative or UV-induced DNA damage, can be bypassed during replication leading to mutagenesis and genome instability, and as a result can lead to cancer, whereas double strand breaks (DSBs) or DNA interstrand crosslinks block the replication machinery and prevent proper chromosome segregation leading to cell death or senescence [1]. DNA damage does not only interfere with replication but can also affect transcription. For example, helix-distorting lesions, like cyclobutane pyrimidine dimers (CPDs) or 6-4 photoproducts (6-4PPs) caused by UV-light, stall elongating RNA polymerases. When the essential process of transcription is persistently blocked, this will result in severely cellular dysfunction that may finally result in apoptosis [2, 3].

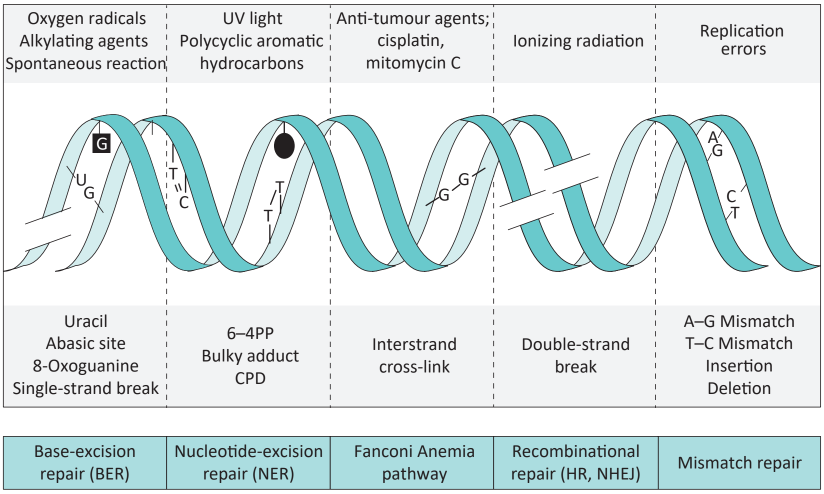
Oxygen radicals
Alkylating agents
Spontaneous reaction
UV light
Polycyclic aromatic hydrocarbons
Anti-tumour agents; cisplatin, mitomycin C
Ionizing radiation
Replication errors
G
U
G
T
C
T
T
G
G
A
G
C
T
Uracil
Abasic site
8-Oxoguanine
Single-strand break
6–4PP
Bulky adduct
CPD
Interstrand cross-link
Double-strand break
A–G Mismatch
T–C Mismatch
Insertion
Deletion
Base-excision repair (BER)
Nucleotide-excision repair (NER)
Fanconi Anemia pathway
Recombinational repair (HR, NHEJ)
Mismatch repair

Figure 1: Different types of DNA damage and DNA repair mechanisms.
Various exogenous and endogenous damaging agents constantly threaten the integrity of the DNA (top). These agents all create specific types of DNA lesions (middle) which can lead to mutagenesis, senescence or apoptosis. Luckily these damages can be recognized and repaired by dedicated DNA repair mechanisms (bottom), each responsible for a different subset of lesions. Figure adapted from Hoeijmakers [34].

DNA REPAIR

To protect the integrity of the DNA, cells have evolved a network of pathways called the DNA damage response (DDR) [4, 5]. The DDR includes signaling cascades to for example stall cell cycle progression and induce apoptosis and repair pathways that remove the DNA lesions. There are multiple DNA repair mechanisms, some specific for certain cell cycle phases or genomic locations, but each dedicated in the recognition and removal of a specific subset of lesions.

Homologous recombination (HR) and non-homologous end joining (NHEJ)

Double strand breaks are repaired by two distinct pathways, namely HR and NHEJ [6]. HR is active during the S and G2 phase of the cell cycle as it makes use of the intact sister chromatid to repair the break in an error free manner [7]. The two DNA ends are trimmed to create 3’ overhangs that can invade the homologous sister chromatid, thereby properly aligning the two DNA ends. This chromatid is used as a template to synthesize any missing DNA after which the resulting joint DNA structure, called Holliday junction, is resolved by specific endonucleases. To finalize repair the nicks are ligated back together. Compared to HR, NHEJ is a more error prone mechanism that can occur throughout all phases of the cell cycle [8]. During NHEJ the ends of the two strands are processed and then simply ligated back together, which may result in the removal or addition of several nucleotides.

Interstrand crosslink repair (ICLR)

Some chemicals, like cisplatin, can induce a covalent bond between the two strands of the DNA helix thereby blocking replication and transcription [9]. These interstrand crosslinks are highly toxic and removal of these lesions is exceptionally challenging as it requires repair on both DNA strands. The exact mechanism of ICLR is not yet fully understood, however it seems that the activities of multiple repair pathways are involved. During S-phase the Fanconi anemia (FA) pathway is involved in the recognition of replication forks that are stalled at ICLs. To date 19 proteins have been identified to play a role in the FA pathway and all together these proteins orchestrate the dual incision on either side of one of the crosslinked nucleotides thereby unhooking the lesion [9]. The repair reaction is finalized by the activities of other DNA damage repair pathways like HR [10], translesion synthesis (TLS) [11] or nucleotide excision repair (NER) [12].

Mismatch repair (MMR)

Although the DNA replication machinery is highly accurate, sometimes mistakes, like insertions, deletions and mismatches, are made [13]. MMR detects these wrongly incorporated nucleotides and specifically excises part of the newly synthesized strand containing the mismatch. To complete repair, new DNA is synthesized using the original DNA as template and a ligase seals the nick [14].

Base excision repair (BER)

Damaged nucleotides that are oxidized, deaminated or alkylated can be repaired by BER. Different types of non-helix distorting damaged bases are recognized by a set of lesion-specific DNA glycosylases that excises the damaged base from the sugar-phosphate backbone resulting in an apurinic or apyrimidinic (AP) site. This AP site is excised by an AP-endonuclease resulting in a single strand break (SSB). The nucleotide gap is repaired by DNA polymerase β or δ and the nick is subsequently sealed by a DNA ligase [15].

Nucleotide excision repair (NER)

NER removes a wide variety of different types of lesions, like cyclo-pyrimidine dimers (CPDs) and 6-4 photoproducts (64PPs) caused by UV-light, bulky adducts and intrastrand crosslinks. The reason that NER is capable to repair so many structurally different lesions is that it does not recognize a specific lesion type directly, but the resulting distortion of the DNA helix. NER consist of two distinct damage recognition sub-pathways, global genome NER (GG-NER) and transcription coupled NER (TC-NER), that detect lesions depending on their genomic context [16].

Global genome NER (GG-NER) detects helix distortions in the entire genome through the cooperative function of two protein complexes. The XPC complex, consisting of XPC, Rad23 and CETN2, constantly probes the DNA for helix distorting lesions. XPC binds with high affinity on the opposite strand of a helix destabilizing lesion. The UV-DDB protein complex is essential to detect and repair CPDs, as this type of UV-induced lesions hardly distorts the DNA helix and is therefore not recognized directly by XPC [17]. The UV-DDB complex consists of DDB1 and DDB2 and upon binding to the lesion, it flips out the damaged nucleotides, thereby kinking the DNA and facilitating the binding of XPC [18].

TC-NER specifically repairs damage in the transcribed strand of active genes as it is initiated by the stalling of RNA polymerase II (RNAPII) on lesions. During transcription elongation, RNAPII transiently interacts with TC-NER proteins and upon transcription block this interaction is enhanced to induce repair [19, 20]. The binding of UVSSA, CSA and CSB to the lesion leads to the recruitment of other downstream NER factors. To enable efficient repair also HMGN1, XAB2, TFIIS and p300 are recruited, likely to remodel the stalled transcription complex to generate access for repair proteins to bind to the lesion [21].

After damage recognition, the NER reaction proceeds into the helix unwinding and lesion verification step which is the same for both GG-NER and TC-NER (figure 2). The first protein complex that is recruited to the lesion after damage recognition is TFIIH, a general transcription initiation factor, which is involved in the opening of the transcription bubble. This complex contains two DNA helicase subunits, XPB and XPD, which are necessary to locally unwind the DNA around the lesion and confirm the presence of a NER lesion [22-24]. Next XPA is recruited to the damaged strand and the undamaged strand is coated by the single stranded DNA binding heterotrimeric RPA complex [25]. Together these proteins are involved in verification of the lesion which is an essential step necessary for the NER reaction to proceed further. After lesion verification the endonuclease XPF/ERCC1 cleaves the damaged DNA strand at the 5’ site of the lesion followed by a 3’ incision by XPG [26]. The 25-30 nucleotide long piece of DNA containing the damaged nucleotides is released from the DNA helix and the single stranded DNA gap is filled by the concerted action of PCNA, RFC and the DNA polymerases δ, ε or κ [27]. In the final step of NER, the DNA nicks are sealed by DNA ligase I or III thereby completing the repair [28].

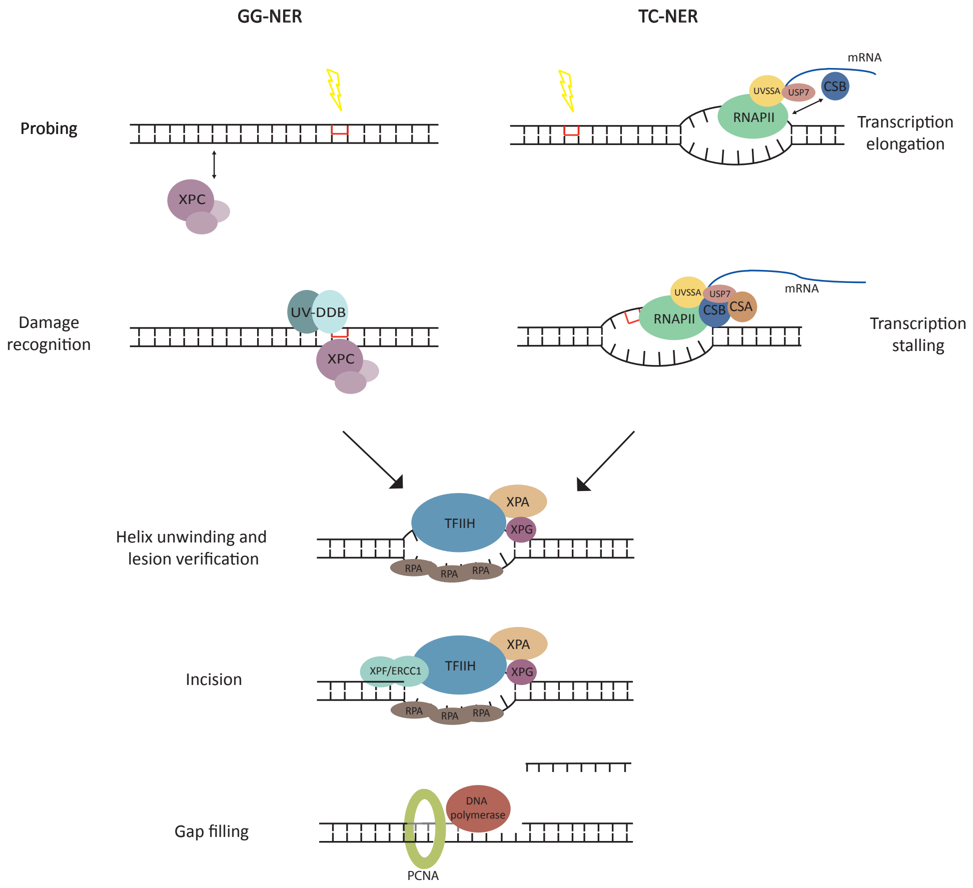
GG-NER
TC-NER
mRNA
UVSSA
USP7
CSB
RNAPII
Probing
Transcription elongation
XPC
UV-DDB
XPC
Damage recognition
UVSSA
USP7
CSB
CSA
mRNA
RNAPII
Transcription stalling
XPA
TFIIH
XPG
Helix unwinding and lesion verification
RPA
RPA
RPA
XPA
XPF/ERCC1
TFIIH
XPG
Incision
RPA
RPA
RPA
DNA polymerase
Gap filling
PCNA

Figure 2: Schematic representation of the nucleotide excision repair pathway. NER consist of two damage detection sub-pathways, transcription coupled NER (TC-NER) and global genome NER (GG-NER). GG-NER is initiated by the DDB complex together with the XPC complex that constantly probes the DNA for helix destabilizing lesions. In TC-NER the pathway is initiated by the recognition of lesion stalled RNAPII that results in stable binding of CSA, CSB and UVSSA to RNAPII. After damage recognition the DNA helix is unwound by TFIIH and together with RPA and XPA the lesion is verified. Subsequently, the endonucleases ERCC1/XPF and XPG are recruited that excise the damaged DNA. DNA polymerases fill the resulting single stranded gap and the nick is sealed by DNA ligase to finalize the repair.

The biological importance of NER is demonstrated by the severe clinical consequences associated with several rare recessive NER-deficient disorders. Xeroderma Pigmentosum (XP) is caused by mutations in the XP genes, mainly functioning in GG-NER. This syndrome is characterized by extreme UV-sensitivity and a 10,000 fold higher risk of skin cancer in patients younger than 20 years. Patients also display a scaly skin and UV-induced pigmentation abnormalities [29]. TC-NER deficiency can result in the Cockayne Syndrome (CS) or the UV-sensitive syndrome (UVSS), however these syndromes display strikingly different phenotypes. CS is characterized by growth failure, impaired neurological development, premature aging and photosensitivity. CS patients on average have a lifespan of just 12-13 years. Interestingly, in contrast to XP there is no association with an increased risk for cancer [30]. UVSS patients have much milder features compared to CS patients and usually only display cutaneous phenotypes including UV sensitivity [31].

Trichothiodystrophy (TTD) is a disorder which is linked to mutations in XPB, XPD, TTDA and TTDN1. TTD patients are usually diagnosed because of their brittle hair with low sulfur content, but they often also display ichthyosis, microcephaly, developmental problems and impaired intelligence. About half of the TTD patients also show UV-sensitivity, which is linked to mutations in XPB, XPD or TTDA. Although mutations in XPB and XPD have been identified in XP patients as well, TTD patients do not display the increased risk in skin cancer. Thus far it is not fully understood how defects in the same NER pathway, can lead to such very clinically distinct phenotypes [32]. Some of the TTD features are suggested to be attributed to a defect in transcription. It has been shown that causative TFIIH mutations result in destabilization and lower steady state levels of the TFIIH complex [32, 33]. This low level of TFIIH might not be sufficient for the transcriptional demands of tissue-specific proteins in highly differentiated cells, leading to the specific clinical features of TTD patients. However an additional NER defect cannot be excluded, as persistent lesions can also interfere with transcription. The non-photosensitive TTD patients show uncompromised NER activity and in some of these patients mutations in TTDN1 have been found. However, in many cases the causative gene has not been identified, making it difficult to dissect the exact underlying mechanism explaining the TTD phenotype.

REFERENCES

1. Vermeij, W.P., J.H. Hoeijmakers, and J. Pothof, Aging: not all DNA damage is equal. Curr Opin Genet Dev, 2014. 26: p. 124-30.
2. Derheimer, F.A., et al., RPA and ATR link transcriptional stress to p53. Proc Natl Acad Sci U S A, 2007. 104(31): p. 12778-83.
3. Conforti, G., et al., Proneness to UV-induced apoptosis in human fibroblasts defective in transcription coupled repair is associated with the lack of Mdm2 transactivation. Oncogene, 2000. 19(22): p. 2714-20.
4. Giglia-Mari, G., A. Zotter, and W. Vermeulen, DNA damage response. Cold Spring Harb Perspect Biol, 2011. 3(1): p. a000745.
5. Jackson, S.P. and J. Bartek, The DNA-damage response in human biology and disease. Nature, 2009. 461(7267): p. 1071-8.
6. van Gent, D.C., J.H. Hoeijmakers, and R. Kanaar, Chromosomal stability and the DNA double-stranded break connection. Nat Rev Genet, 2001. 2(3): p. 196-206.
7. Li, X. and W.D. Heyer, Homologous recombination in DNA repair and DNA damage tolerance. Cell Res, 2008. 18(1): p. 99-113.
8. Lieber, M.R., The mechanism of double-strand DNA break repair by the nonhomologous DNA end-joining pathway. Annu Rev Biochem, 2010. 79: p. 181-211.
9. Lopez-Martinez, D., C.C. Liang, and M.A. Cohn, Cellular response to DNA interstrand crosslinks: the Fanconi anemia pathway. Cell Mol Life Sci, 2016. 73(16): p. 3097-114.
10. Long, D.T., et al., Mechanism of RAD51-dependent DNA interstrand cross-link repair. Science, 2011. 333(6038): p. 84-7.
11. Budzowska, M., et al., Regulation of the Rev1-pol zeta complex during bypass of a DNA interstrand cross-link. EMBO J, 2015. 34(14): p. 1971-85.
12. Mouw, K.W. and A.D. D'Andrea, Crosstalk between the nucleotide excision repair and Fanconi anemia/BRCA pathways. DNA Repair (Amst), 2014. 19: p. 130-4.
13. Ganai, R.A. and E. Johansson, DNA Replication-A Matter of Fidelity. Mol Cell, 2016. 62(5): p. 745-55.
14. Jiricny, J., Postreplicative mismatch repair. Cold Spring Harb Perspect Biol, 2013. 5(4): p. a012633.
15. Hegde, M.L., T.K. Hazra, and S. Mitra, Early steps in the DNA base excision/single-strand interruption repair pathway in mammalian cells. Cell Res, 2008. 18(1): p. 27-47.
16. Marteijn, J.A., et al., Understanding nucleotide excision repair and its roles in cancer and ageing. Nat Rev Mol Cell Biol, 2014. 15(7): p. 465-81.
17. Wakasugi, M., et al., DDB accumulates at DNA damage sites immediately after UV irradiation and directly stimulates nucleotide excision repair. J Biol Chem, 2002. 277(3): p. 1637-40.
18. Sugasawa, K., Molecular mechanisms of DNA damage recognition for mammalian nucleotide excision repair. DNA Repair (Amst), 2016. 44: p. 110-7.
19. Schwertman, P., et al., UV-sensitive syndrome protein UVSSA recruits USP7 to regulate transcription-coupled repair. Nat Genet, 2012. 44(5): p. 598-602.
20. van den Boom, V., et al., DNA damage stabilizes interaction of CSB with the transcription elongation machinery. Journal of Cell Biology, 2004. 166(1): p. 27-36.
21. Vermeulen, W. and M. Fousteri, Mammalian Transcription-Coupled Excision Repair. Cold Spring Harbor Perspectives in Biology, 2013. 5(8).

22. Li, C.L., et al., Tripartite DNA Lesion Recognition and Verification by XPC, TFIIH, and XPA in Nucleotide Excision Repair. Mol Cell, 2015. 59(6): p. 1025-34.
23. Oksenych, V. and F. Coin, The long unwinding road: XPB and XPD helicases in damaged DNA opening. Cell Cycle, 2010. 9(1): p. 90-6.
24. Marteijn, J.A., J.H. Hoeijmakers, and W. Vermeulen, Check, Check...Triple Check: Multi-Step DNA Lesion Identification by Nucleotide Excision Repair. Mol Cell, 2015. 59(6): p. 885-6.
25. Sugitani, N., et al., XPA: A key scaffold for human nucleotide excision repair. DNA Repair (Amst), 2016. 44: p. 123-35.
26. Fagbemi, A.F., B. Orelli, and O.D. Scharer, Regulation of endonuclease activity in human nucleotide excision repair. DNA Repair (Amst), 2011. 10(7): p. 722-9.
27. Ogi, T., et al., Three DNA polymerases, recruited by different mechanisms, carry out NER repair synthesis in human cells. Mol Cell, 2010. 37(5): p. 714-27.
28. Moser, J., et al., Sealing of chromosomal DNA nicks during nucleotide excision repair requires XRCC1 and DNA ligase III alpha in a cell-cycle-specific manner. Mol Cell, 2007. 27(2): p. 311-23.
29. DiGiovanna, J.J. and K.H. Kraemer, Shining a light on xeroderma pigmentosum. J Invest Dermatol, 2012. 132(3 Pt 2): p. 785-96.
30. Karikkineth, A.C., et al., Cockayne syndrome: Clinical features, model systems and pathways. Ageing Res Rev, 2016.
31. Spivak, G., UV-sensitive syndrome. Mutat Res, 2005. 577(1-2): p. 162-9.
32. Stefanini, M., et al., Trichothiodystrophy: from basic mechanisms to clinical implications. DNA Repair (Amst), 2010. 9(1): p. 2-10.
33. Vermeulen, W., et al., Sublimiting concentration of TFIIH transcription/ DNA repair factor causes TTD-A trichothiodystrophy disorder. Nat Genet, 2000. 26(3): p. 307-13.
34. Hoeijmakers, J.H., Genome maintenance mechanisms for preventing cancer. Nature, 2001. 411(6835): p. 366-74.

2

TRICHOTHIODYSTROPHY CAUSATIVE TFIIEβ MUTATION AFFECTS TRANSCRIPTION IN HIGHLY DIFFERENTIATED TISSUE

Arjan F. Theil[1], Imke K. Mandemaker[1,†], Emile van den Akker[2,†], Sigrid M.A. Swagemakers[3], Anja Raams[1], Tatjana Wüst[2], Jurgen A. Marteijn[1], Jacques C. Giltay[4], Max M. Colombijn[5], Ute Moog[6], Urania Kotzaeridou[7], Mehrnaz Ghazvini[8], Marieke von Lindern[2], Jan H.J. Hoeijmakers[1], Nicolaas G.J. Jaspers[1], Peter J. van der Spek[3] and Wim Vermeulen[1]

[1]Department of Molecular Genetics, Cancer Genomics Netherlands, Erasmus MC, Rotterdam, The Netherlands; [2]Sanquin Research, Department of Hematopoiesis/Landsteiner Laboratory, Academic Medical Centre, University of Amsterdam, Amsterdam, The Netherlands; [3]Department of Bioinformatics, Erasmus MC Rotterdam, The Netherlands; [4]Department of Genetics, University Medical Center Utrecht, Utrecht, The Netherlands; [5]Rivas Zorggroep; location Beatrixziekenhuis, Gorinchem, The Netherlands; [6]Institute of Human Genetics, Heidelberg University, Heidelberg, Germany; [7]University Children's Hospital Heidelberg, Heidelberg, Germany; [8]Department of Developmental Biology, iPS core facility, Erasmus MC, Rotterdam, The Netherlands. [†] These authors have contributed equally.

Published in Human Molecular Genetics 2017

ABSTRACT

The rare recessive developmental disorder Trichothiodystrophy (TTD) is characterized by brittle hair and nails. Patients also present a variable set of poorly explained additional clinical features, including ichthyosis, impaired intelligence, developmental delay and anemia. About half of TTD patients are photosensitive due to inherited defects in the DNA repair and transcription factor II H (TFIIH). The pathophysiological contributions of unrepaired DNA lesions and impaired transcription have not been dissected yet. Here, we functionally characterize the consequence of a homozygous missense mutation in the general transcription factor II E, subunit 2 (GTF2E2/TFIIEβ) of two unrelated non-photosensitive TTD (NPS-TTD) families. We demonstrate that mutant TFIIEβ strongly reduces the total amount of the entire TFIIE complex, with a remarkable temperature-sensitive transcription defect, which strikingly correlates with the phenotypic aggravation of key clinical symptoms after episodes of high fever. We performed induced pluripotent stem (iPS) cell reprogramming of patient fibroblasts followed by in vitro erythroid differentiation to translate the intriguing molecular defect to phenotypic expression in relevant tissue, to disclose the molecular basis for some specific TTD features. We observed a clear hematopoietic defect during late-stage differentiation associated with hemoglobin subunit imbalance. These new findings of a DNA repair-independent transcription defect and tissue-specific malfunctioning provide novel mechanistic insight into the etiology of TTD.

INTRODUCTION

Trichothiodystrophy (TTD) is a rare recessive disorder, characterized by brittle hair and nails, due to a low content of sulfur-rich proteins in keratinocytes. Patients present a variable combination of additional symptoms including, ichthyosis, impaired intelligence, decreased fertility, microcephaly, developmental delay, anemia and progeroid features (1). Approximately, 50% of the TTD patients are sun(photo)-sensitive, caused by mutations in the xeroderma pigmentosum group B (XPB/ERCC3), group D (XPD/ERCC2) or trichothiodystrophy group A (TTDA/GTF2H5) genes (2,3), each encoding for subunits of the transcription factor IIH (TFIIH) (4). In addition to an essential role of TFIIH in transcription initiation, this complex is also pivotal for nucleotide excision repair (NER). These mutations impair NER, which is the only DNA repair system in mammals capable of removing sun-induced DNA damage and thus easily explain photo-sensitivity. The additional features are thought to be derived by subtle defects in the transcription function of TFIIH.

We previously proposed that reduced stability of mutant TFIIH in TTD patients may cause some of the TTD-specific clinical features, which are mainly apparent in terminally differentiated tissues (3). Within late-stage differentiated cells, the majority of genes become transcriptionally silenced, including genes encoding for basal transcription factors such as TFIIH. The amount of proteins encoded by transcriptionally "switched off" genes in these cells thus depends on the stability of their residual mRNAs and proteins produced at prior stages. We have shown that TTD-causing mutations in TFIIH genes affect the stability of the entire complex and that the steady-state level of each subunit becomes strongly reduced (2,5,6). In cultured fibroblast, this reduced amount appeared sufficient to provide normal transcription levels. However, at the final stages of cellular differentiation when de novo synthesis is switched off, the reduced TFIIH stability in TTD cells may result in too low amounts of TFIIH to support sufficient transcription of tissue-specific proteins. The observed reduced transcription of the SPRR2 gene in terminally differentiated keratinocytes from a TTD-mimicking mouse-model (7) supported this hypothesis. SPRR2 is a sulfur-rich matrix protein, only expressed at very late stages of differentiation, which crosslinks keratin filaments to provide mechanical strength to skin and hair cells. In terminally differentiated red blood cells, TTD-specific TFIIH mutations may cause imbalanced globin mRNA expression, explaining the relatively frequent anemic features of TTD (1,8). It is however not excluded that unrepaired (endogenously produced) DNA lesions in transcription units, as a consequence of the DNA repair defect associated with mutated TFIIH, may also contribute to reduced transcription in late-stage differentiated cells. Indeed, endogenous metabolic stress and environmental cues do generate a variety of DNA lesions, which may play a role in the pathogenesis of accelerating aging (9) and other degenerative diseases (10,11).

We hypothesize that a large of part of the clinical features associated with repair-proficient non-photosensitive TTD (NPS-TTD) are based on gene expression defects (12). In only a minority of NPS-TTD patients causative mutations were found in genes encoding for the M-phase-specific PLK1 interacting protein (MPLKIP/TTDN1) (13) or the β subunit of the transcription factor IIE (GTF2E2/TFIIEβ) (14) and in an isolated case in the RNF113A gene (15). Nevertheless, thus far no obvious experimental evidence for transcription malfunctioning in NPS-TTD patient cells has been provided. Here, we present the genetic and functional analysis of NPS-TTD cases with homozygous GTF2E2 mutations. We showed that fibroblasts derived from these patients exhibit a clear transcription defect, however only when cultured at elevated temperatures. We used induced pluripotent stem cell (iPS) reprogramming of patient fibroblasts followed by in vitro erythroid differentiation to show hemoglobin protein imbalance in late-stage differentiated erythroid cells, in line with patients' anemic features.

RESULTS

Genetic analysis of non-photosensitive TTD patients

Recently, two unrelated NPS-TTD patients were identified with different mutations in the gene encoding for the beta subunit of transcription initiation factor II E (TFIIEβ/GF2E2) (14), suggesting impaired transcription in these patients. To provide functional evidence for affected transcription in NPS-TTD, we first performed genetic analyses among a selected group of NPS-TTD patients to identify possible other mutations in transcription factors.

Patient TTD218UT is of Moroccan origin and was born to consanguineous parents. She was referred to the clinical geneticist at 1.5 years of age with brittle hair (low cysteine content and tiger-tail banding pattern), ichthyosis, microcephaly (−2.5 SD), psychomotor retardation, short stature (−2.5 SD) and microcytic anemia. She showed recurrent aggravation of hair-loss by tufted breakage at the scalp boundary immediately following episodes of infection-induced fever. Also upon long-term exposure to the heat of the sun, she appears to have increased hair-loss. At the age of 8 years, she shows no signs of progressive deterioration. She has a happy and friendly personality with an IQ of 54 (at 7 years of age). She has a limited physical endurance. Laboratory investigation revealed microcytic hypochromic anemia (Hb 6.5) without sequence anomalies nor deletions or duplications of the genes encoding for the alpha or beta globin chains (not shown). We performed whole genome sequencing on patient's DNA, using the sequencing-by-ligation method from Complete Genomics (16,17). Surprisingly, we identified a homozygous variant in the GTF2E2/TFIIEβ gene, creating a missense mutation (c.C559T [p.Asp187Tyr]). This mutation is identical to one of the mutations in GTF2E2/TFIIEβ previously described by Kuschal et al. (14). Its homozygous presence was confirmed by Sanger sequencing of cDNA generated from patient's cells and found to co-segregate with the phenotype within the family (Fig. 1A and B).

Additional Sanger sequencing of the TFIIE subunits among another group of selected NPS-TTD patients revealed the identification of the same homozygous mutation (c.G559T in GTF2E2/TFIIEβ) in two sibs, TTD241HE and TTD275HE. These patients are born to consanguineous parents of Moroccan origin, which are both heterozygous for this mutation (Fig. 1C) and are not related to patient TTD218UT. Patient TTD241HE was diagnosed at 18 months of age with brittle hair (tiger-tail banding pattern), dysmorphic features, developmental delay, moderate intellectual disability, microcephaly, difficulty swallowing and failure to thrive, cheerful character, mild Ichthyosis, growth retardation (length −4.7 SD, weight −2.6 SD), occipitofrontal circumference (OFC) (−3.1 SD), hypertonia, microcytic hypochromic anemia

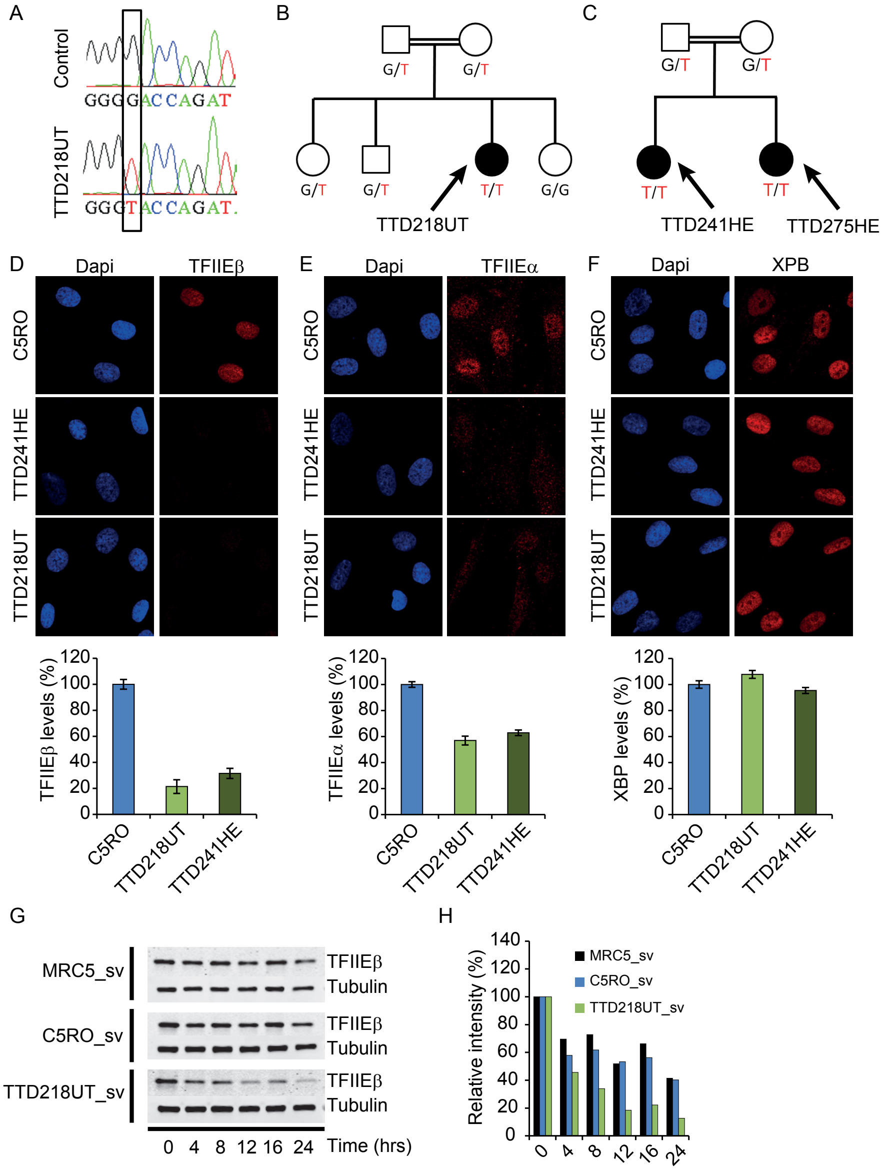

Figure 1. TFIIE protein levels and stability is reduced in TFIIEβ-mutated TTD cells. A) Sanger sequencing profiles of TFIIEβ cDNA. TTD218UT shows homozygosity for the c.G559T missense mutation. (B,C) TFIIEβ mutations segregating in the patients' families. (D–F) Immuno-fluorescence analysis of TTD218UT and TTD251HE fibroblasts compared with wild-type control (C5RO) cells, stained for (D) TFIIEβ, (E) TFIIEα or (F) XPB (TFIIH) and DNA was stained with DAPI (blue). Quantification of the mean intensities (n = 50 nuclei), expressed as percentage of the mean intensity in normal cells, is shown beneath the representative images. Error bars indicate SEM. (G) Immuno-blot analysis to determine protein stability of TFIIEβ after cycloheximide (100 μM) treatment (for indicated times in hours) of Sv40-immoratlized patient cells (TTD218UT_sv) compared with two wild-type controls (MRC5_sv, C5RO-sv). (H) Quantification of TFIIEβ band intensities normalized to tubulin were expressed as percentages of t=0 values.

and recurrent infections. At 6 years of age, she still showed spasticity, ataxia and mild cognitive retardation without significant speech, but no signs of progressive deterioration. She has one affected younger sib (TTD275HE), also diagnosed with brittle hair, dysmorphic features, mild developmental delay, microcephaly, mild difficulty swallowing, no failure to thrive, cheerful character, mild ichthyosis, additional left thumb, no recurrent infections and growth retardation were noticed.

Functional analysis of DNA repair capacity

We consider this TFIIEβ mutation as likely causative for some of the NPS-TTD patients, in line with our hypothesis that one of the prime causes for this form of TTD is based on subtle transcriptional defects. Since TFIIE is closely associated with TFIIH's transcription function (18,19), it is not excluded that mutant TFIIE may influence TFIIH's repair function. To that aim, we thoroughly examined the cellular NER capacity in fibroblasts of patient TTD218UT and TTD241HE. Patients' fibroblast were not hypersensitive to UV-light and exhibited proficient unscheduled DNA repair synthesis (UDS) and recovery of RNA synthesis after UV irradiation (RRS), indicating that both global-genome and transcription-coupled NER are not affected (Supplementary Material, Figs S1 and S2).

TFIIE protein levels and stability

The general transcription factor TFIIE consists of two subunits; GTF2E1/TFIIEα and GTF2E2/TFIIEβ (20–22) and is a crucial component of the transcription preinitiation complex required for transcription initiation and promoter opening by facilitating loading and stable binding of TFIIH (18,23,24). Since TTD-causing mutations in TFIIH destabilize the entire complex (25) and because this frail TFIIH was suggested to cause TTD-specific transcription features (3), we wondered whether also this TFIIEβ mutation affects TFIIE stability. Immuno-fluorescence analysis showed that the steady-state levels of TFIIEβ and TFIIEα were strongly reduced to approximately 20 and 60%, respectively, of TFIIE levels in wild-type cells assayed in parallel. Whereas the levels of TFIIH (assessed with anti-XPB antibody) appeared unaffected, as expected (Fig. 1D–F, Supplementary Material, Fig. S3A–C).

Immuno-blot analysis of cell-free extracts confirmed the low steady-state levels of both TFIIE subunits (Supplementary Material, Fig. S3D–E). Since quantitative RT-PCR showed that the mRNA levels of both TFIIE subunits were unaffected (data not shown), it is likely that the reduced TFIIE levels are derived from protein instability. Western blot analysis on protein extracts isolated from cells incubated for different times in the presence of the translation inhibitor cycloheximide showed a strongly reduced stability of mutated TFIIEß, as compared with wild-type TFIIEß (Fig. 1G and H). The levels of both subunits can be fully restored by reintroducing wild-type TFIIEβ cDNA in the patient cells (Supplementary Material, Fig. S4). Together, these data show that the single amino-acid substitution p.Asp187Tyr in the beta subunit of TFIIE causes instability of the entire complex.

Transcription levels

It is to be expected that with such a severe reduction of the cellular content of TFIIE, the overall transcription would be impaired. Moreover, previous studies (26) have shown that amino acid substitutions p.Ile171Ser and p.Ile189Ser, both in close

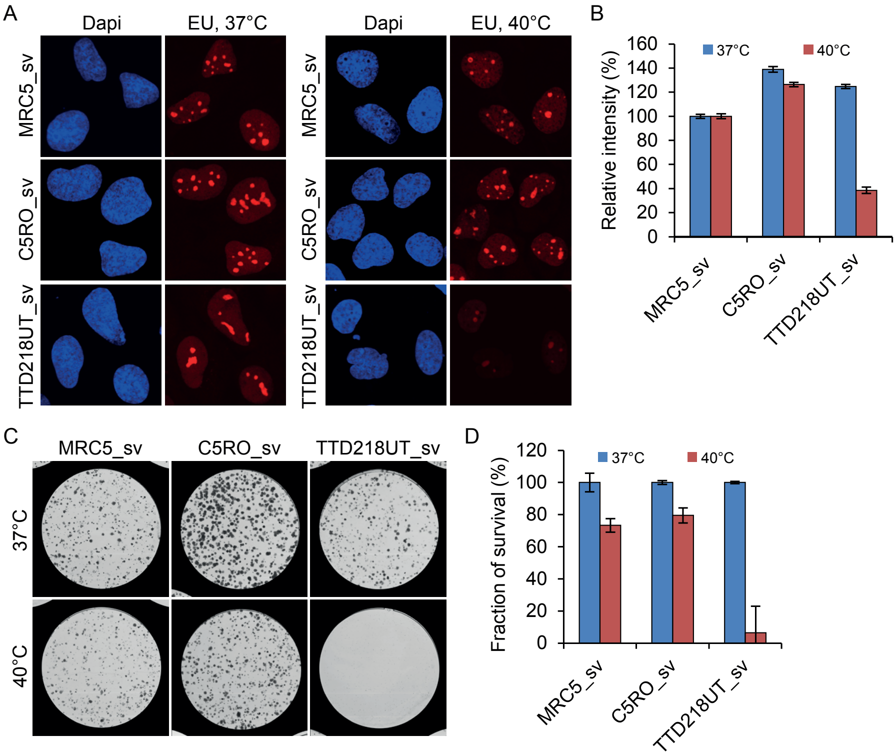

Figure 2. Transcription and cell survival is reduced at 40°C in TFIIEβ-mutated TTD cells. (A) Transcription levels after incubation for 72 h at 37 °C or 40 °C, measured by pulse-labeling with ethynyl-uridine (EU) and subsequent fluorescent staining of incorporated EU, of Sv40-immortalized patient cells (TTD218UT_sv), compared with wild-type controls (MRC5_sv, C5RO-sv). DNA was stained with DAPI (blue). (B) Quantification of the mean intensities (n = 50), expressed as percentages of intensity in MRC5_sv. Error bars indicate SEM. (C,D) Coomassie staining and quantification of colonies (D) of TTD218UT_sv, MRC5_sv and C5RO-sv cells formed after 12 days culturing at 37 °C (blue bars) or 40 °C (red bars) (n = 2).

proximity of patient's TFIIEβ mutation (c.G559T [p.Asp187Tyr]), affect XPB helicase activity and severely reduce transcriptional capacity in cell-free in vitro assays. Surprisingly however, basal transcription levels, assayed by ethynyl uridine (EU) pulse labeling, were not affected in patient cells under standard culture conditions (Fig. 2A and B, Supplementary Material, Fig. S5A and B). Despite the strong reduction in steady-state levels of TFIIE, the remaining amount is apparently sufficient to support normal levels of transcription. Therefore, we searched for experimental conditions in which TFIIE levels may become limiting to transcription. We became aware that upon recurrent infections patient TTD218UT experiences reversible fever-dependent worsening of her brittle hair phenotype, most likely due to a further decrease or inactivation of the already low amounts of mutant TFIIE. Recurrent infections have also been reported for patient TTD241HE, however, fever-dependent worsening of any clinical feature could not be confirmed. Previously, we have found that a specific TTD-causative mutation in XPD (c.C2050T [p.Arg658Cys]) causes thermo-lability of the entire TFIIH complex, which was also accompanied by fever-dependent worsening of the TTD-specific hair phenotype in these patients (6). Incubation of cells derived from these XPD-TTD patients at elevated temperature showed a strong temperature-dependent reduction of transcription and severely reduced viability of the cells. Upon culturing of TFIIEβ-mutated TTD218UT and TTD241HE cells for 3 days at 40 °C, we observed a strikingly reduced transcription as compared with normal cells exposed to the same temperature (Fig. 2A and B, Supplementary Material, Fig. S5A and B).

To determine the effect of prolonged exposure to elevated temperatures, we performed a colony survival assay on patient-derived cells that were incubated for 12 days at 40 °C. This extended culturing at higher temperature induced a dramatic reduction in colony-forming ability of the TTD218UT cells compared with control cells (Fig. 2C and D). The chronic exposure to higher temperatures likely depletes TFIIE levels to such an extent that they become too low to allow sufficient transcription to support cellular survival.

Erythroid differentiation of human iPS cells

Proliferating cultured fibroblasts are likely not representative to mimic the in vivo conditions that determine the TTD-specific symptoms, particularly since these are mainly apparent in terminally differentiated tissues, such as hair-follicles (brittle hair), epidermal keratinocytes (ichthyosis), neurons (impaired neurologic functions) and erythrocytes (anemia). Patients harboring a TFIIEβ mutation present microcytic anemia [this study and (14)], characterized by a reduced mean cell volume (MCV), which might be the consequence of reduced iron binding or a defect in late-stage erythroid differentiation driven by transcriptional problems.

To recapitulate the TTD-phenotype in this patient, induced pluripotent stem (iPS) cells may offer a powerful platform to investigate genotype–phenotype relationship in relevant tissue. To this aim, we established an iPS clone reprogrammed from TTD218UT primary fibroblasts, and two control iPS cell lines obtained from healthy individuals, one reprogrammed from primary fibroblasts and one reprogrammed from a blood sample. Isolated iPS clones were selected on the basis of normal karyotypes, and thoroughly screened for expression of pluripotency markers (e.g. OCT4, Nanog) and absence of expression of differentiation markers (e.g. GFAP, AFP) (27), all of which were normal (data not shown). To investigate whether the TFIIEβ mutation could account for hematological malfunctions, we used a two-phased liquid culture system, including an expansion and a differentiation phase (28). Wild type and patient iPS cells were similar in their ability to differentiate into a homogenous population of CD71+/CD235+ erythroblasts (Supplementary Material, Fig. S7). Also, the cumulative and relative number of erythroid cells generated during the expansion phase, prior to erythroid differentiation, did not differ (data not shown), suggesting that proliferation is not affected. Comparing erythroblast differentiation at 37 °C and a fever-mimicking temperature of 39 °C indicated that differentiation to CD71+/CD235+ erythroblasts was still similar among all iPS-derived erythroblasts (Supplementary Material, Fig. S7). However, the cell size and number of multinuclear erythroblasts were increased in terminally differentiated TTD-erythroblasts, which were even more affected at 39 °C (Fig. 3A–C, Supplementary Material, Fig. S6). Flow cytometric analysis revealed an increase of cells with high forward and/or side

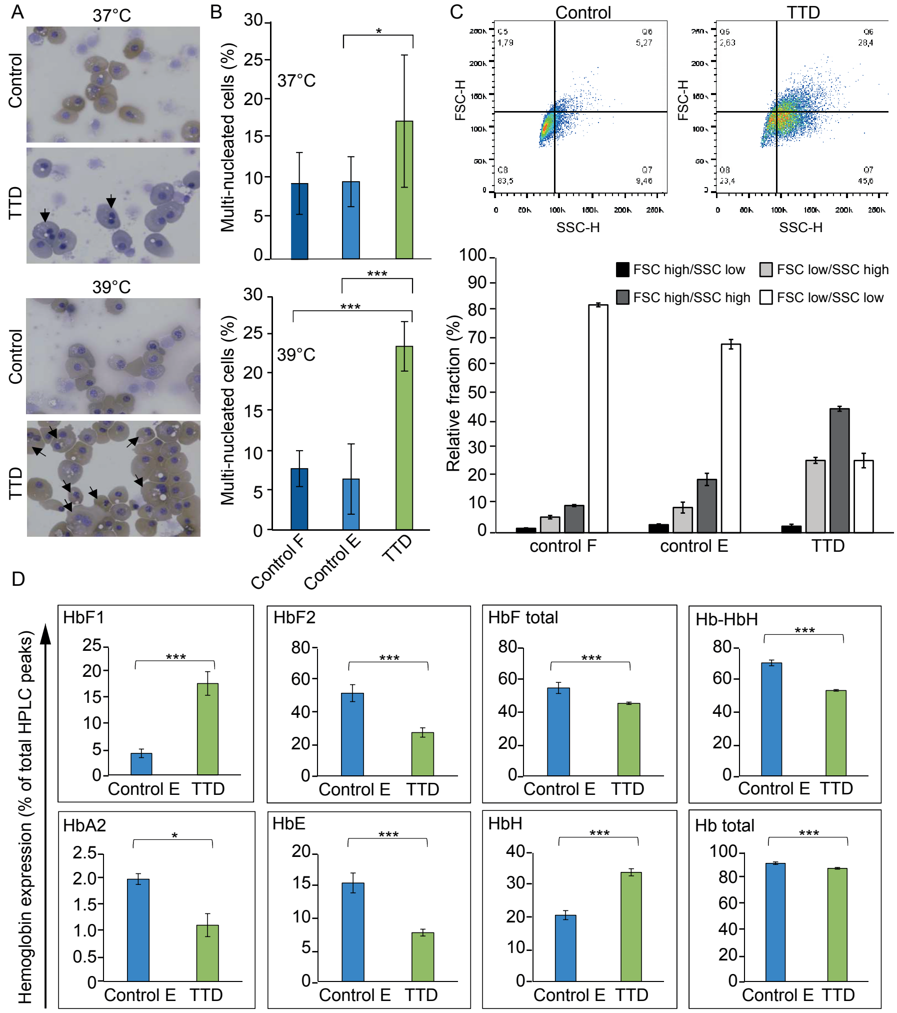

Figure 3. Affected Hematopoiesis in iPS-derived erythroid cells of TTD patients. In vitro erythroblast differentiation performed on iPS cells derived from TTD218UT (TTD) fibroblasts, control fibroblasts (control F) and peripheral blood mononuclear cell derived erythroblasts (control E).(A) Cytospins and Giemsa-Grünwald staining of in vitro differentiated erythroblasts. Arrows indicate multinucleated cells. (B) Quantification of multinucleated cells, expressed as a percentage of total cells [>500 cells, counted by two independent researchers (N = 2)]. (C) Dot plots of flow-cytometric analysis of differentiated erythroid control and TTD cells. Lower bar graph depicts the quantification of the gated dot-plots [Q8=FSC^{low}/SSC^{low} (normal size and intracellular structures); Q5=FSC^{high}/SSC^{low} (bigger cells); Q6=FSC^{high}/SSC^{high} (bigger cells, more intracellular structures); Q7=FSC^{low}/SSC^{high} (normal size, more intracellular structure); N = 5 for each. Error bars represent standard deviation] (D) HPLC analysis of different hemoglobin variants. Bar graphs depict the percentage of hemoglobin variants: “HbF total” = sum of HbF1 and HbF2, Hb-HbH = sum of all non-aberrant hemoglobin variants, HbA2, HbE, HbH represent the peaks identified as HbH, probably representing HbBarts (beta tetramers or gamma tetramers respectively) and “Hb Total” = sum of all the peaks. Experiments represent an N = 3 for TTD and N = 6 for control iPS-derived erythroid cells. Error bars represent standard deviation and student t-test was performed to calculate significance, * <0.05 and ***< 0.01.

scatter of TTD-derived erythroid cells at 37 °C compared with control cells (Fig. 3C), suggesting defective cytokinesis and cell size control, two important aspects heavily controlled during erythropoiesis (29). Several TTD patients have microcytic hypochromic anemia, which may suggest a disturbed hemoglobin synthesis. Hemoglobin consists of two subunits from the alpha locus and two subunits from the beta locus. The beta locus produces β and δ subunits for adult HbA and HbA2, respectively, γ1 and γ2 for fetal HbF1 and HbF2, and ε for embryonal HbE. Subunit imbalance can present as microcytic hypochromic anemias and thalassemia-like phenotypes (30), as observed among TTD patients without additional mutations in globin subunits (8). Hemoglobins cannot be compared between adult erythrocytes and iPS-derived mature erythroblasts because iPS-derived cells execute an embryonic/fetal program. However iPS-derived cells can be compared among each other. HPLC analysis (31) of iPS-derived erythroid cells showed reduced levels of HbF, HbA2 and HbE in TTD cells, with increased hemoglobin H (HbH/barts; tetramers of beta locus globins only) (Fig. 3D, Supplementary Material, Fig. S8). This may indicate an underproduction of alpha globin chains in TTD cells causing increased tetramerization of γ globin or β globin chains and reduced HbF, HbA2 and HbE. Control cells primarily express HBF2, and low levels of HBF1, contrary to TTD cells that express significantly higher levels of HBF1 with a concomitant reduction of HBF2. These results suggest a disturbed hemoglobin regulation during erythropoiesis in TTD iPS-derived erythroid cells. Reduced stability and functionality of TFIIE in TTD may lead to reduced expression of specific high abundant mRNAs e.g. the globin genes during erythroid differentiation. We suggest that in TTD patient-derived iPS cells the beta locus generates several subtypes of globin polypeptides, which cannot be matched by the reduced expression of the α-chain from the alpha locus, resulting in HbH formation, anemia and microcytic hypochromic erythrocytes.

DISCUSSION

We have identified a homozygous missense mutation (c.G559T [p.Asp187Tyr]) in the beta subunit of TFIIE (GTF2E2/TFIIEβ) (Fig. 1A–C) in two non-related families of Moroccan origin with non-photosensitive TTD (NPS-TTD). This same mutation was earlier identified as causative for NPS-TTD in another non-related Moroccan NPS-TTD patient (14). In addition, in the same study by Kuschal et al. another homozygous missense mutation in TFIIEβ (c.448 G > C [p.Ala150Pro]) was identified in one NPS-TTD patient from Asian origin. Together, these TFIIEβ mutations in four non-related families firmly establish a causative genetic relationship between mutated TFIIEβ and NPS-TTD.

We further noticed that this mutation in TFIIEβ [c.G559T (p.Asp178Tyr)] causes a severe reduction in the cellular amount of this protein (Fig. 1D). Strikingly, also the alpha subunit of TFIIE (TFIIEα) appeared significantly reduced by the mutation in the beta subunit (Fig. 1E), eventually leading to a strong reduction of the entire two-subunit TFIIE complex in cultured cells of these patients. Since this amino acid substitution is in close proximity of the predicted interaction-site of TFIIEβ with the winged-helix domain of TFIIEα (32), it is anticipated to compromise complex formation, which may explain the observed fragility of the entire complex. In addition, it is likely that a mutation causing instability of one subunit renders the entire complex unstable, as previously found for other protein complexes, including TTD-causing mutations of TFIIH (5,25).

Strikingly, however, this decline in the amount of an essential transcription initiation factor did not result in a measurable effect on the overall transcription when cells were grown under standard optimal culturing conditions (Fig. 2A). Only under specific conditions, i.e. incubation at elevated temperatures (Fig. 2B) or terminal differentiation (Fig. 3), we were able to observe phenotypic consequences of this hypomorphic GTF2E2/TIIEβ allele. This fever-dependent worsening of clinical symptoms is apparently not solely dependent on the pathogenic mutation, since this peculiar phenotype was not clinically confirmed in patients TTD241HE and TTD275HE. This apparent discrepancy could be explained by an incomplete or reduced penetrance of the disease-causing allele. Also, the patient's body temperature might not always reach the critical height and duration to observe worsening of TTD-specific features, which is off course much better controlled within a cellular in vitro assay. We previously reported on a similar thermo-sensitive TTD-causing mutation in the XPD subunit of TFIIH (6) that is also associated with fever-dependent aggravation of TTD-specific features. Hyperthermia generally causes partial denaturation of cellular proteins and may affect protein complex formation. We thus envisage that fever-driven hyperthermia will further reduce the already compromised, mutation-derived, protein stability of TFIIE complexes in TTD patient cells. The number of available TFIIE complexes will thus decline to such an extent that eventually transcription will be affected. The consistent presence of presumably hypomorphic variants in these TTD patients is expected, since general transcription factors, such as TFIIE, are highly conserved and essential proteins in mammals, so fully inactivating mutations (nonsense, frame-shift) are likely not tolerated. Similarly, all reported cases with TFIIH mutations, including the TTD-causative ones, carry at least one hypomorphic allele (33). This is in line with previous reports that complete ablation of the TFIIH subunits XPB and XPD in mice (Xpb−/− or Xpd−/−) resulted in very early embryonic lethality already at the two cell stage (34,35).

Until recently, it appeared rather difficult to extrapolate TTD-causing mutations to disease-specific phenotypic expression through available cellular and biochemical assays. However, with the here applied iPS reprogramming of patient-derived fibroblasts to stem cell-like cells and the subsequent in vitro differentiation into erythroid progenitors we were now able to show such a correlation. The observed disturbance of the delicate balance of hemoglobin-forming polypeptide production in late-stage erythroid progenitors underscores our hypothesis that at least part of the TTD-specific features are a consequence of affected transcription. It is further important to note that transcriptional defects associated with TTD mutations are mainly instigated by a stability problem of either TFIIE (this paper) or TFIIH (5,25), rather than a direct failure in transcription initiation. Hence, we speculate that fragility-causing mutations in other basal factors required for gene-expression, i.e. transcription-maturation, splicing [shown recently for mutations within RNF113A (36)] or even protein translation may result in TTD-like diseases. It is thus important to further investigate possible gene-expression functions of other identified genes (e.g. MPLKIP/TTDN1) and not-yet-identified NPS-TTD causing genes.

MATERIALS AND METHODS

Massive parallel sequencing

Massive parallel sequencing (software version 2.5.0.37) was done as described previously (16). Briefly, the human genome sequencing procedures include DNA library construction, DNA Nano-Ball (DNB) generation, DNB array self-assembling, cPAL-based sequencing and imaging. Image data analyses including base calling, DNB mapping, and sequence assembly. Reads were mapped to the National Center for Biotechnology Information (NCBI) reference genome, build 37. Variants were annotated using NCBI build 37 and dbSNP build 137. Data were provided as lists of sequence variants (SNPs and short indels) relative to the reference genome. Analysis of the massive parallel sequencing data was performed using Complete Genomics analysis tools (cga tools version 1.8.0 build 1; http://www.completegenomics.com/sequence-data/cgatools/) and TIBCO/Spotfire version 7.0.1 (http://spotfire.tibco.com/).

Ethics statement

Prior to our experimental onset, we obtained written informed consent from the patient's family and all clinical investigations have been conducted according to the Declaration of Helsinki, developed by The World Medical Association (WMA).

Cell culture

Primary fibroblasts: TTD218UT (TTD), TTD241HE (TTD), C4RO (wild-type) and C5RO (wild-type), were cultured in Ham's F10 medium (BE02-014F, Lonza) supplemented with 10% fetal bovine serum (S1810, Biowest) and 1% penicillin-streptomycin (P0781, Sigma-Aldrich) at 37 °C, 20% O_2 and 5% CO_2.

SV40-immortalized human fibroblasts: TTD218UT-sv (TTD), TTD218UT-sv stably expressing TFIIEβWT-GFP, MRC5_sv (wild-type) and C5RO_sv (wild-type), were cultured in a 1: 1 mixture of DMEM (BE12-604F/U1) and Ham's F10 medium (BE02-014F, Lonza) supplemented with 10% fetal bovine serum (S1810, Biowest) and 1% penicillin-streptomycin (P0781, Sigma-Aldrich) at 37 °C, 20% O_2 and 5% CO_2.

Human iPS cells: were cultured feeder free in E8 medium (Thermo Fisher Scientific), on matrigel (BD-biosciences)-coated plates. Medium was changed every other day and cells were passaged every 4–5 days, using ReLeSR (Stem cell technologies) as described by manufacturers with a split-ratio of 1: 20. iPS were differentiated as whole colonies derived from single cells (28). In short, iPS were made into single cells using TrypLselect (Lifetech) and 100–150 cells were plated onto 6 cm dishes. Colonies were allowed to expand to 400 μm size upon which media was changed to differentiation media containing 20 ng/ml BMP4, 40 ng/ml VEGF and 50 ng/ml bFGF in Stemline II (sigma-aldrich), media was refreshed after 3 days. At day 6, this medium was replaced by serum- free humanized IMDM-based medium (Cellquin) (37) supplemented with 1 μg/ml interleukin 3, 10 μg/ml interleukin 6, 100 ng/ml SCF, 25 ng/ml Nplate (TPO agonist), 40 ng/ml VEGF, 20 ng/ml BMP4 and 1 U/ml Erythropoietin. Cells were refreshed every 2 days and erythroid progenitors harvested between day 9 and 15 were cultured as described before in (28).

Antibodies

Primary antibodies used: α-TFIIEβ (ab187143; Abcam), α-TFIIEα (H00002960-B01, Abnova), α-TFIIEα (#1G6; gift from J.M. Egly), α-XPB (sc-293, Santa Cruz Biotechnology), α-GFP (ab290, Abcam) and α-Tubulin (T5168, Sigma-Aldrich).

Secondary antibodies used: CF770 anti-rabbit (SAB4600215, Sigma-Aldrich), CF680 anti-mouse (SAB4600199, Sigma-Aldrich), IRDye 800CW Donkey anti-mouse (926-32212, LI-COR), Alexa Fluor 555 goat anti-mouse (A21424, Invitrogen), Alexa Fluor 555 goat anti-rabbit (A21429, Invitrogen) and Alexa Fluor 488 goat anti-rabbit (A11034, Invitrogen), α-CD71 (Miltenyi Biotech), α-CD235 (BD Biosciences).

Western blot analysis

Whole cell extracts were prepared by direct lysis of isolated cell pellets in SDS–PAGE protein sample buffer reagent, separated on 8% SDS-PAGE gel, blotted onto Immobilon-FL membrane (IPFL00010, Merck Millipore Ltd.), stained with specific primary and secondary antibodies and analyzed using an Odyssey imager (LI-COR).

Protein stability

Cells were plated on 6 cm dishes and incubated overnight under normal culture conditions. Cells were treated with 100 μM Cycloheximide (CHX) and harvested at different time-points (0, 4, 8, 12, 16 and 24 h) after treatment. Whole-cell extracts were obtained by direct lysis in sample buffer. The signal intensities were measured and normalized to Tubulin. Signal intensities were plotted as the percentage of TFIIEβ levels after CHX treatment compared with the signal intensities of the non-treated samples (set at 100%).

Colony-forming ability/survival

Cells were plated on 10 cm dishes (1500 cells/dish, 40 °C survival), in triplicate. After 24 h, cells were continuously incubated at 37 °C or 40 °C for approximately 2 weeks. Colonies were fixed and stained with 0.1% Brilliant Blue R (Sigma) and counted (Gelcount, Oxford Optronix Ltd.). The survival was plotted as the percentage of colonies obtained after treatment compared with the mean number of colonies from the mock-treated cells (set at 100%).

Transcription capacity measured by EU incorporation

Cells were grown onto 24 mm cover slip and cultured for 1 day prior to the experiments. The cells were washed once with PBS and incubated for 2 h in culture medium containing 100 μM 5-ethynyl-uridine (EU). After EU incorporation, cells were fixed in 4% formaldehyde/PBS, washed twice with 3% BSA/PBS, permeabilized for 20 min in 0.5% Triton/PBS and washed once with PBS. Cells were incubated for 30 min with fluorescent dye coupling buffer containing 10 mM CuSO4 and Alexa Fluor 594 azide (Click-iT, Thermo Fisher Scientific). After washing with PBS, cells were mounted in vectashield, containing 1.5 μg/ml DAPI. The mean fluorescence is determined with a confocal microscope (Zeiss LSM 700) from at least 50 cells. Images were processed using ImageJ and the average fluorescence intensity in the nucleus of MRC5_sv wild-type cells was set at 100%.

Immuno fluorescence

Cells were grown on glass cover slips (24 mm) for 1 day prior to the experiments and washed with PBS, fixed with 2% paraformaldehyde for 15 min, washed with PBS, washed 2 times 10 min with 0.1% Triton X-100/PBS and incubated for 15 min with PBS+ (PBS containing 0.15% glycine and 1% BSA). Cells were incubated overnight at 4 °C with primary antibodies in a moist chamber. The next day, cover slips were washed 2 times 10 min with PBS/Triton X-100 and washed once with PBS+. Cells were incubated for 1 h with secondary antibodies at room temperature in moist chamber and again washed three times in PBS/Triton X-100. Samples were embedded in Vectashield mounting medium (Vector Laboratories, containing 1.5 µg/ml DAPI). The mean fluorescence is determined with a confocal microscope (Zeiss LSM 700) from at least 50 cells. Images were processed using ImageJ.

Generation of human iPS cells

Primary fibroblasts from patient TTD218UT and control fibroblasts were reprogrammed through lentiviral transduction of human genes OCT4, SOX2, c-MYC and KLF4, using engineered color-coded lentiviral vectors (27).

Flow cytometry

Cells were washed once in PBS, resuspended in PBS with 0.5% BSA and stained with appropriate antibodies for 1 h as indicated in the figure legends. Cells were washed in PBS and flow cytometry experiments were performed with BD FACS CantoII or BD LSRII + HTS (BD Bioscsiences, Franklin Lakes, NJ). The data were analyzed with FACSDiva Software (BD Biosciences, Franklin Lakes, NJ) and FlowJo Software (Tree Star, Ashland, OR).

Cytospin preparation

Cells (5×10^5) were cytospun onto glass slides, fixed in methanol, and stained with benzidine to visualize haemoglobin and DIFCO B/C. Images were taken with a Zeiss Axioscope A1 macroscope (50x lens) and processed using Adobe Photoshop 9.0 (Adobe Systems Inc.; CA, USA).

HPLC to detect hemoglobin variants

Separation of the various Hb fractions was performed by high-performance cation-exchange liquid chromatography (CE-HPLC) on Waters Alliance 2690 equipment (Waters, Milford, MA, USA) according to (31). In short, the protocol consisted of a 30-min elution over a combined 20–200 mM NaCl and pH 7.0–6.6 gradient in 20 mM BisTris/HCl, 2 mM KCN. The column, a PolyCAT A 100/4.6-mm, 3 µm, 1500 Å column, was purchased from PolyLC (Columbia, MD, USA).

ACKNOWLEDGEMENTS

We thank the Optical Imaging Centre (OIC) of the Erasmus MC for microscopy support. Funding was provided by Dutch Science Organization (NWO), ALW division (grant numbers 864.13.004 and 854.11.002), ZonMW division (grant number

912.12.132) and by the European Research Council (ERC; grant numbers 233424 and 340988). Funding to pay the Open Access publication charges for this article was provided by the European Research Council, grant ERC-ID 340988.

SUPPLEMENTAL METHODS AND FIGURES

[methyl-3H]-thymidine survival

Fibroblasts were plated in 6-well culture dishes (7500 cells per well) in quadruplicate (0 J/m^2) or triplicate (others) in 3 ml medium. Two day after seeding, cells were washed with PBS and UV irradiated (0-8 J/m^2; 254 nm Philips TUV lamp). Five days after irradiation cells were pulse-labeled with [methyl-3H]-thymidine (40-60 Ci/mmol; 5 µCi/ml; Amersham Biosciences), chased for 30 minutes in unlabeled medium, washed with PBS, lyzed in 0.25 M NaOH and harvested. Cell lysates were transferred into scintillation flasks and supplemented with 7.5 ml Hionic Fluor scintillation fluid (Packard). Each sample was counted in the scintillation counter for 10 minutes and results were expressed as the percentage of counts obtained from the non-treated dishes (set as 100%).

Unscheduled DNA synthesis (UDS) assay

For UDS 1 x 105 cells were seeded onto 24 mm cover slips and UV irradiated with 16 J/m^2 after 1 day. The cells were washed once with PBS and incubated for 3 hours in culture medium containing 10 µM 5-ethynyl-2'-deoxyuridine (EdU; Thermo Fisher Scientific). After EdU incorporation, cells were fixed in 4% formaldehyde/PBS, washed twice with 3% BSA/PBS, permeabilized for 20 minutes in 0.5% Triton/PBS and washed once with PBS. Cells were incubated for 30 minutes with fluorescent dye coupling buffer containing 10 mM $CuSO_4$ and Alexa Fluor 594 azide (Click-iT, Thermo Fisher Scientific). After washing with PBS, cells were mounted in vectashield, containing 1.5 µg/ml DAPI. UDS levels were expressed as a percentage of the average fluorescence intensity in the nucleus of wild-type cells, which was set at 100%. The mean fluorescence is determined with a confocal microscope (Zeiss LSM 700) from at least 50 cells. Images were processed using ImageJ.

Recovery of RNA synthesis (RRS) assay

For RRS 1 x 105 cells were seeded onto 24 mm cover slips and UV irradiated with 8 J/m^2 after 1 day. The cells were washed once with PBS and incubated for 2 h in culture medium containing 100 µM 5-ethynyl-uridine (EU) at different time-points after UV (2 hours or 24 hours). After EU incorporation, cells were fixed in 4% formaldehyde/PBS, washed twice with 3% BSA/PBS, permeabilized for 20 minutes in 0.5% Triton/PBS and washed once with PBS. Cells were incubated for 30 minutes with fluorescent dye coupling buffer containing 10mM $CuSO_4$ and Alexa Fluor 594 azide (Click-iT, Thermo Fisher Scientific). After washing with PBS, cells were mounted in vectashield, containing 1.5 µg/ml DAPI. RRS levels were expressed as a percentage of the average fluorescence intensity in the nucleus of non-irradiated wild-type cells, which was set at 100%. The mean fluorescence is determined with a confocal microscope (Zeiss LSM 700) from at least 50 cells. Images were processed using ImageJ.

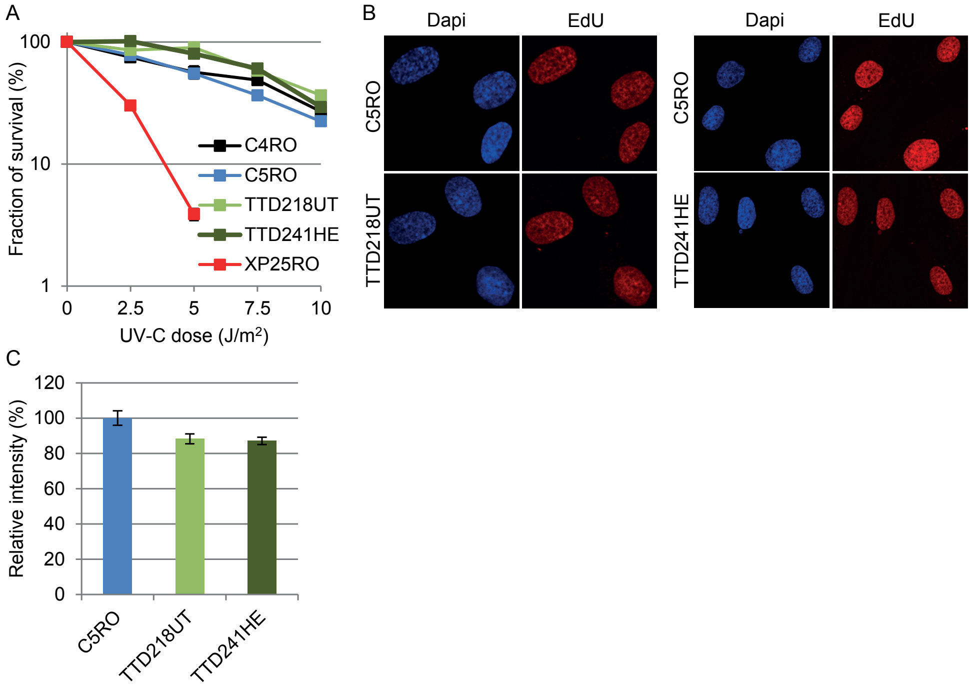

Figure S1. Characterization of DNA Repair capacity.

(A) UV-survival assay measuring UV sensitivities in triplicate culture dishes of patient fibroblasts (TTD218UT, TTD251HE), NER-defective XP-A cells (XP25RO) and NER-proficient (wild-type) controls (C4RO, C5RO). (B) Global NER activities measured as UV-induced unscheduled DNA synthesis (UDS) using EdU incorporation, visualized by fluorescence-conjugated azide (Click-iT assay). Shown are representative pictures from the UDS experiment performed on primary fibroblasts of TTD218UT (left panel) or TTD241HE (right panel) and compared to C5RO primary fibroblasts. UDS-derived fluorescence is shown in red and nuclear staining in blue (DAPI). (C) Quantification of the UDS experiments. Mean intensities of at least 50 nuclei are expressed as percentages of those in normal cells assayed in parallel. The error bars indicate SEM.

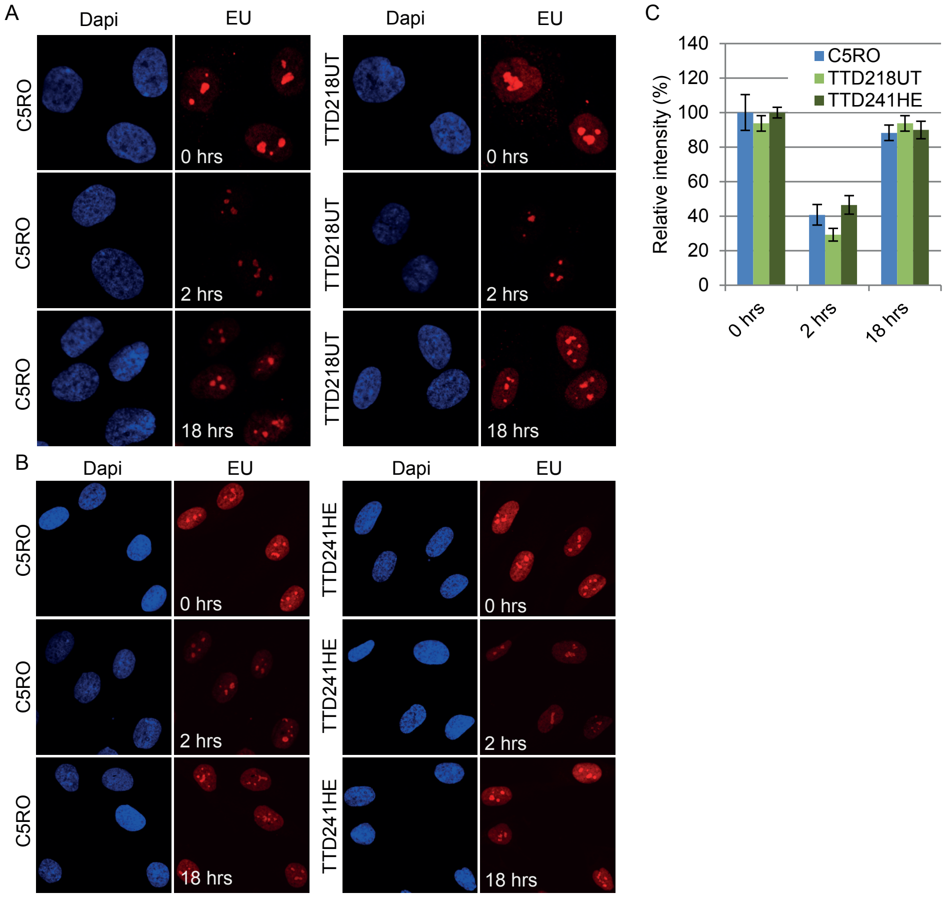
A
Dapi
EU
Dapi
EU
C5RO
TTD218UT
0 hrs
2 hrs
18 hrs
B
Dapi
EU
Dapi
EU
C5RO
TTD241HE
0 hrs
2 hrs
18 hrs
C
Relative intensity (%)
0
20
40
60
80
100
120
140
C5RO
TTD218UT
TTD241HE
0 hrs
2 hrs
18 hrs

Figure S2. Characterization of recovery of RNA Synthesis.
Transcription-coupled NER activities measured as recovery of RNA Synthesis (RRS) in UV-exposed primary fibroblasts using EU incorporation and subsequent Click-iT Assay. (A-B) Shown are representative pictures at the indicated time points (time of EU pulse-labeling after UV irradiation) from the RRS experiment performed on primary fibroblasts of TTD218UT (A) or TTD241HE (B) and compared to C5RO primary fibroblasts. RRS-derived fluorescence is shown in red and nuclear staining in blue (DAPI). (C) Quantification of the EU-incorporation (measure for RNA synthesis) at the indicated time points after UV. Mean intensities of at least 50 nuclei are expressed as percentages of those in normal cells. The error bars indicate SEM.

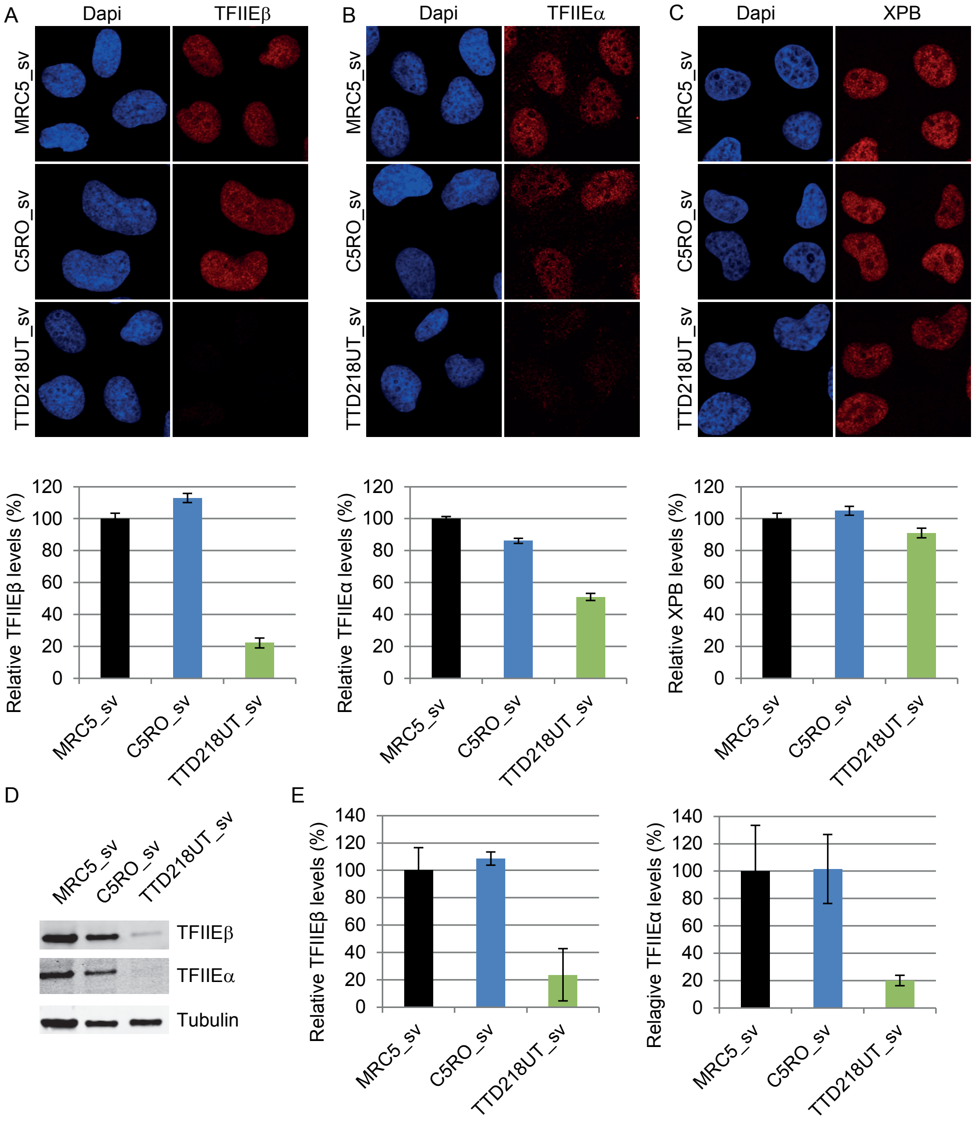

Figure S3. TFIIE protein level is reduced in TFIIEβ-mutated TTD cells.
(A-C) Immuno-fluorescence analysis of TTD218UT_sv and wild-type control (C5RO_sv and MRC5_sv) cells, stained for (A) TFIIEβ, (B) TFIIEα or (C) XPB (TFIIH) and DNA was stained with DAPI (blue). Quantification of the mean intensities (n=50 nuclei), expressed as percentage of the mean intensity in normal cells, is shown beneath the representative images. Error bars indicate SEM. (D) Immuno-blot analysis to determine TFIIE protein levels of Sv40-immoratlized patient cells (TTD218UT_sv) compared to two wild-type controls (MRC5_sv, C5RO-sv). (E) Quantification of the immune-blot. The band intensities of TFIIEβ or TFIIEα were normalized to Tubulin and expressed as percentage of control cells.

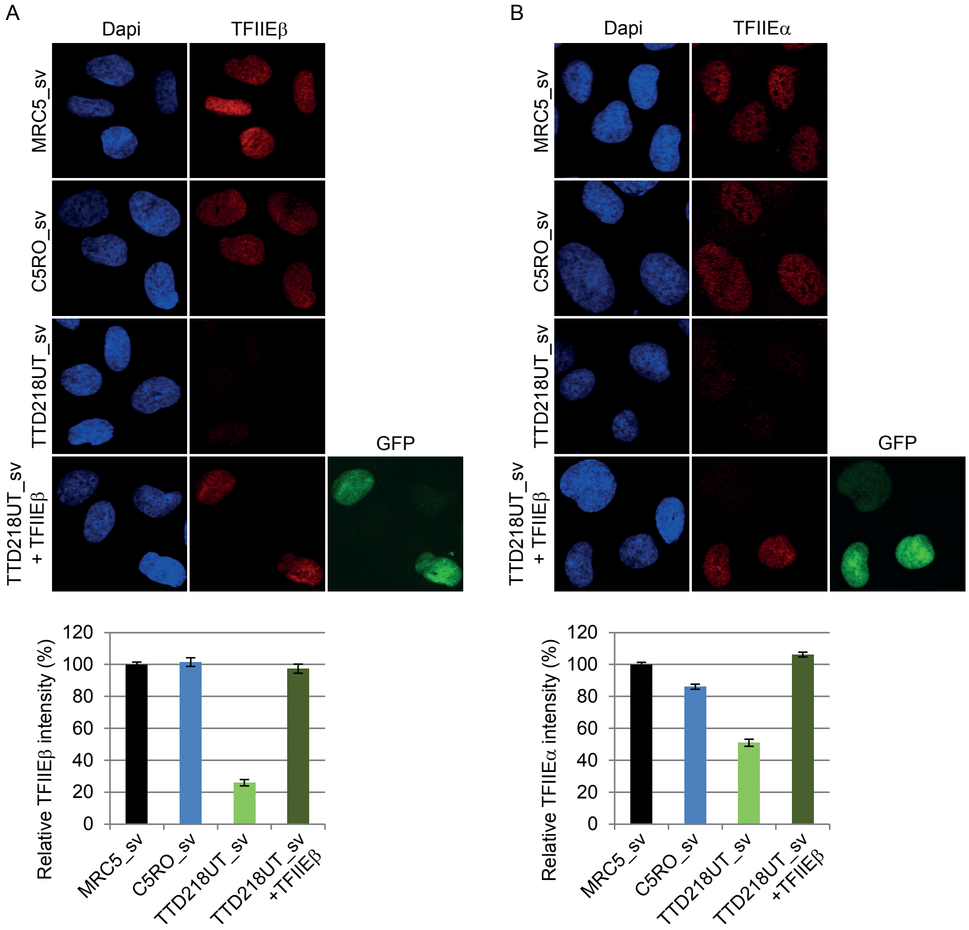
A
Dapi
TFIIEβ
GFP
MRC5_sv
C5RO_sv
TTD218UT_sv
TTD218UT_sv + TFIIEβ
Relative TFIIEβ intensity (%)
0
20
40
60
80
100
120
MRC5_sv
C5RO_sv
TTD218UT_sv
TTD218UT_sv +TFIIEβ
B
Dapi
TFIIEα
GFP
MRC5_sv
C5RO_sv
TTD218UT_sv
TTD218UT_sv + TFIIEβ
Relative TFIIEα intensity (%)
0
20
40
60
80
100
120
MRC5_sv
C5RO_sv
TTD218UT_sv
TTD218UT_sv +TFIIEβ

Figure S4. TFIIEβ complementation in TTD218UT_sv cells.
Shown are representative pictures of an immuno-fluorescence experiment performed with MRC5_sv, C5RO_sv, TTD218UT_sv and TTD218UT_sv cells complemented with TFIIEβ^{WT}-GFP. Cells were fixed and stained for (A) TFIIEβ (B) TFIIEα, and DNA was stained with DAPI. Quantification of the immuno-fluorescence experiments is shown below the images. Mean intensities of at least 50 nuclei are expressed as percentages of those in normal cells, is shown beneath the representative images. The error bars indicate SEM. TFIIEβ^{WT}-GFP expressing cells are indicated under the images marked with GFP.

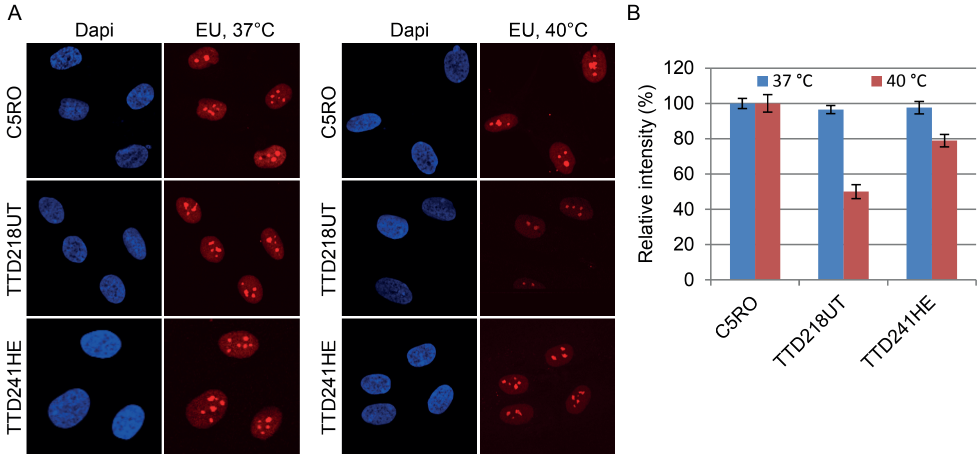
A
Dapi
EU, 37°C
Dapi
EU, 40°C
C5RO
TTD218UT
TTD241HE
C5RO
TTD218UT
TTD241HE
B
Relative intensity (%)
120
100
80
60
40
20
0
37 °C
40 °C
C5RO
TTD218UT
TTD241HE

Figure S5. Transcription levels in primary fibroblasts at 37°C and 40°C.
(A) Overall transcription in patient fibroblasts TTD218UT (middle panel) and TTD241HE (bottom panel) and wild-type control cells, C5RO (top panel). Cells were cultured for 72 hours at 37°C or 40°C (as indicated) and transcription levels were measured by incorporated ethynyl-uridine using a Click-iT assay. (B) Quantification of the transcription experiment. Mean intensities of at least 50 nuclei are expressed as percentages of those in normal cells. The error bars indicate the SEM.

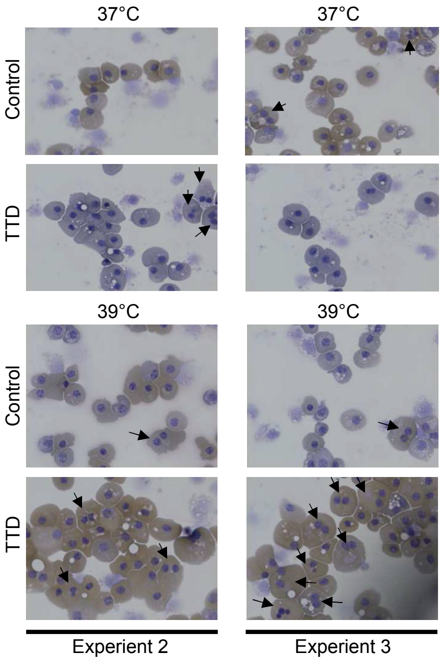
37°C
37°C
Control
TTD
39°C
39°C
Control
TTD
Experient 2
Experient 3

Figure S6. iPSC erythroid differentiation.
In vitro erythroblast differentiation as performed and shown in Figure 3A were performed in triplicate. Shown are representative pictures of the second (left panel) and third experiment (right panel) of cytospins and Giemsa-Grünwald staining. Arrows indicate multinucleated cells. Quantification of multinucleated cells are shown in Figure 3B.

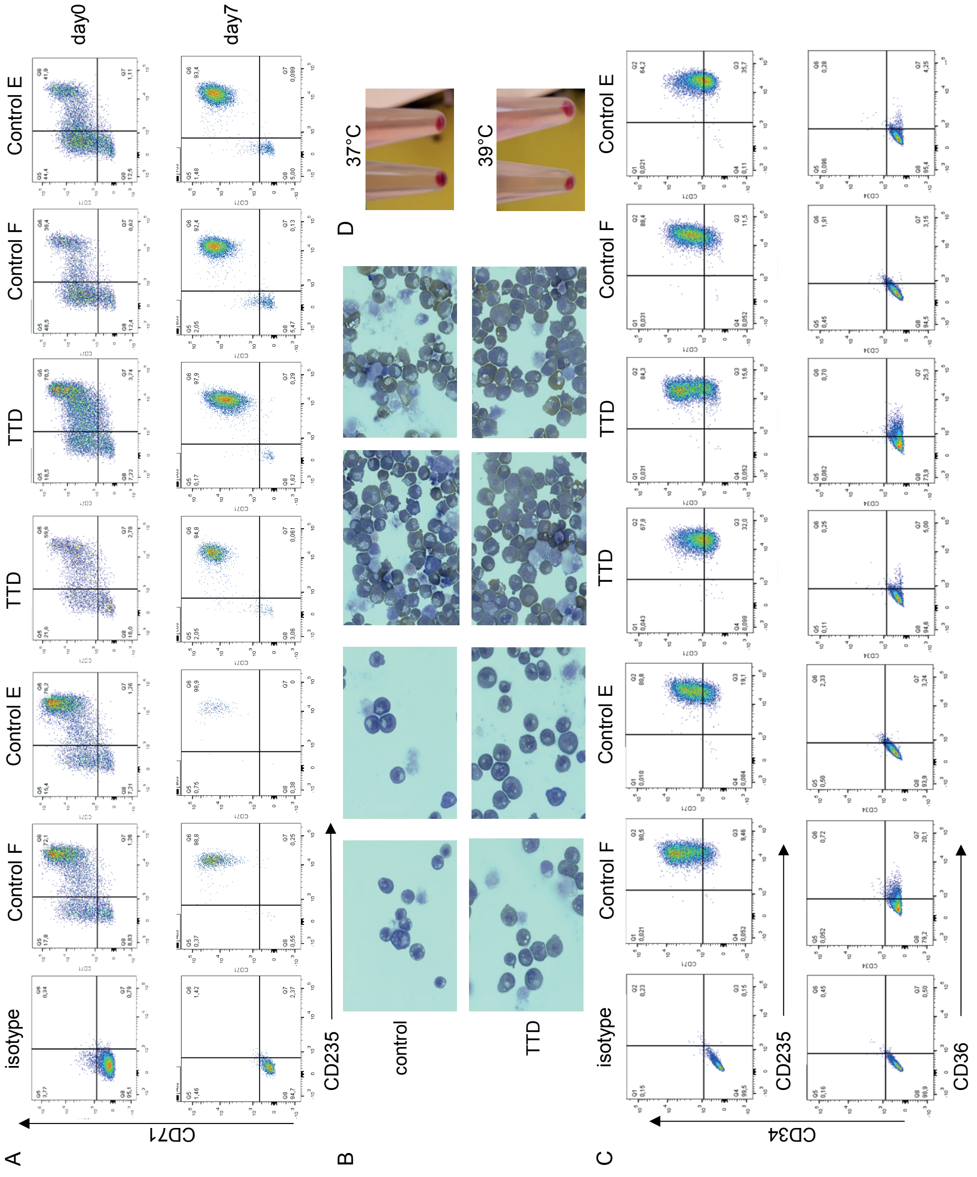

Figure S7. iPSC erythroid specification and differentiation.
iPS cells, derived from TTD218UT (TTD) fibroblasts, control fibroblasts (control F) and peripheral blood mononuclear cell (control E) were differentiated to erythroblasts, which were further expanded and subsequently differentiated to poly/orthochromatic normoblasts as indicated in material and methods. (A) Cells were harvested as suspension cells from the iPSC colony differentiation after 12 days. Panels represent flow cytometry dot plots from 2 independent experiments depicting CD71 versus CD235 (or GPA) to assess the purity, production and differentiation status of erythroid cells as described before (1) at the day of harvest (day 0, upper panels) and after 7 days (lower panels) of erythroblast expansion on Epo, SCF and Dex using a culture system as described before (2). CD71+CD235+ cells are defined as erythroid cells. Note

that at the day of harvest (day 0) erythroid cells are identified but purity is still low. However, after 7 days of expansion the cells are primarily CD71+/CD235+ erythroblasts (>93%) and contaminating non-erythroid cells are limited. (B) Cytospins of the 7 days expanded cultures in A were stained with Giemsa/Max Grunwald and benzidine (haemoglobin stains brown). A low seeding cytospin and high seeding cytospins are depicted for control (upper panels) and TTD (lower panels), which look similar in all aspects. Note the absence of the multinucleated and cell size phenotype in the TTD sample as observed later in poly/orthochromatic cells during terminal differentiation (see main text). (C) Expanded erythroblasts of A and B were terminally differentiated for 3 days as indicated in material and methods at 37°C and 39°C as depicted. Erythroblast differentiation is accompanied with decreased expression of CD71 but maintained expression of CD235 and absence of CD34 and CD36. Flow cytometry dot plots depict CD71/CD235 in upper panels and CD34/CD36 in the lower panels. Please note the decreased expression of CD71 compared to figure A, indicating differentiation which is similar between control and TTD (patient). CD34 and CD36 are absent at this stage (lower panels) and no differences were observed between control and TTD samples. (D) Erythroid cells after 3 days of differentiation were pelleted and photographed to show hemoglobinization, which was comparable between control and TTD at both 37°C and 39°C. These data indicate that erythroid specification of iPSC lines is not blocked and that differentiation of erythroblasts can progress normally as defined by marker expression.

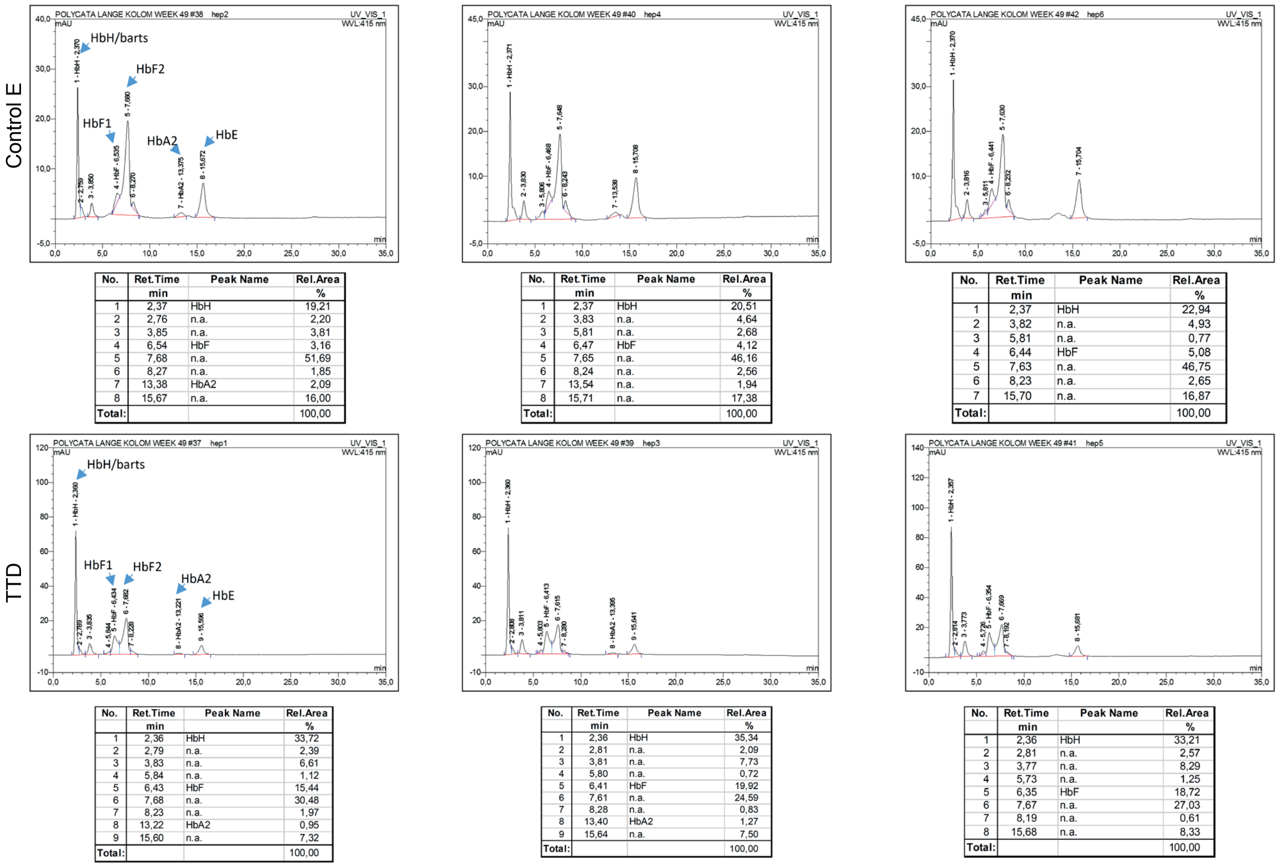

No.	Ret.Time min	Peak Name	Rel.Area %
1	2,37	HbH	19,21
2	2,76	n.a.	2,20
3	3,85	n.a.	3,81
4	6,54	HbF	3,16
5	7,68	n.a.	51,69
6	8,27	n.a.	1,85
7	13,38	HbA2	2,09
8	15,67	n.a.	16,00
Total:			100,00

No.	Ret.Time min	Peak Name	Rel.Area %
1	2,37	HbH	20,51
2	3,83	n.a.	4,64
3	5,81	n.a.	2,68
4	6,47	HbF	4,12
5	7,65	n.a.	46,16
6	8,24	n.a.	2,56
7	13,54	n.a.	1,94
8	15,71	n.a.	17,38
Total:			100,00

No.	Ret.Time min	Peak Name	Rel.Area %
1	2,37	HbH	22,94
2	3,82	n.a.	4,93
3	5,81	n.a.	0,77
4	6,44	HbF	5,08
5	7,63	n.a.	46,75
6	8,23	n.a.	2,65
7	15,70	n.a.	16,87
Total:			100,00

No.	Ret.Time min	Peak Name	Rel.Area %
1	2,36	HbH	33,72
2	2,79	n.a.	2,39
3	3,83	n.a.	6,61
4	5,84	n.a.	1,12
5	6,43	HbF	15,44
6	7,68	n.a.	30,48
7	8,23	n.a.	1,97
8	13,22	HbA2	0,95
9	15,60	n.a.	7,32
Total:			100,00

No.	Ret.Time min	Peak Name	Rel.Area %
1	2,36	HbH	35,34
2	2,81	n.a.	2,09
3	3,81	n.a.	7,73
4	5,80	n.a.	0,72
5	6,41	HbF	19,92
6	7,61	n.a.	24,59
7	8,28	n.a.	0,83
8	13,40	HbA2	1,27
9	15,64	n.a.	7,50
Total:			100,00

No.	Ret.Time min	Peak Name	Rel.Area %
1	2,36	HbH	33,21
2	2,81	n.a.	2,57
3	3,77	n.a.	8,29
4	5,73	n.a.	1,25
5	6,35	HbF	18,72
6	7,67	n.a.	27,03
7	8,19	n.a.	0,61
8	15,68	n.a.	8,33
Total:			100,00

Figure S8

Figure S8. Hemoglobinization in erythroid cells.
HPLC graphs and corresponding hemoglobin peak calling were obtained as indicated in material and methods. The called peaks depicted as bar graphs shown in the main Figure (Figure 3D) as percentages of hemoglobin variants, are indicated in the HPLC.

REFERENCES

1 Faghri, S., Tamura, D., Kraemer, K.H. and Digiovanna, J.J. (2008) Trichothiodystrophy: a systematic review of 112 published cases characterises a wide spectrum of clinical manifestations. J. Med. Genet., 45, 609-621.

2 Stefanini, M., Botta, E., Lanzafame, M. and Orioli, D. (2010) Trichothiodystrophy: from basic mechanisms to clinical implications. DNA Repair (Amst), 9, 2-10.

3 Theil, A.F., Hoeijmakers, J.H. and Vermeulen, W. (2014) TTDA: big impact of a small protein. Exp. Cell Res., 329, 61-68.

4 Compe, E. and Egly, J.M. (2012) TFIIH: when transcription met DNA repair. Nat Rev Mol. Cell Biol., 13, 343-354.

5 Vermeulen, W., Bergmann, E., Auriol, J., Rademakers, S., Frit, P., Appeldoorn, E., Hoeijmakers, J.H. and Egly, J.M. (2000) Sublimiting concentration of TFIIH transcription/DNA repair factor causes TTD-A trichothiodystrophy disorder. Nat. Genet., 26, 307-313.

6 Vermeulen, W., Rademakers, S., Jaspers, N.G., Appeldoorn, E., Raams, A., Klein, B., Kleijer, W.J., Hansen, L.K. and Hoeijmakers, J.H. (2001) A temperature-sensitive disorder in basal transcription and DNA repair in humans. Nat. Genet., 27, 299-303.

7 de Boer, J., de Wit, J., van Steeg, H., Berg, R.J., Morreau, H., Visser, P., Lehmann, A.R., Duran, M., Hoeijmakers, J.H. and Weeda, G. (1998) A mouse model for the basal transcription/DNA repair syndrome trichothiodystrophy. Mol. Cell, 1, 981-990.

8 Viprakasit, V., Gibbons, R.J., Broughton, B.C., Tolmie, J.L., Brown, D., Lunt, P., Winter, R.M., Marinoni, S., Stefanini, M., Brueton, L. et al. (2001) Mutations in the general transcription factor TFIIH result in beta-thalassaemia in individuals with trichothiodystrophy. Hum. Mol. Genet., 10, 2797-2802.

9 Vermeij, W.P., Hoeijmakers, J.H. and Pothof, J. (2016) Genome Integrity in Aging: Human Syndromes, Mouse Models, and Therapeutic Options. Annu. Rev. Pharmacol. Toxicol., 56, 427-445.

10 Hasty, P., Campisi, J., Hoeijmakers, J., van Steeg, H. and Vijg, J. (2003) Aging and genome maintenance: lessons from the mouse? Science, 299, 1355-1359.

11 Cooke, M.S., Evans, M.D., Dizdaroglu, M. and Lunec, J. (2003) Oxidative DNA damage: mechanisms, mutation, and disease. FASEB J, 17, 1195-1214.

12 Vermeulen W., van Vuuren A.J., Chipoulet M., Schaeffer L., Appeldoorn E., Weeda G., Jaspers N.G., Priestley A., Arlett C.F., Lehmann A.R. et al. (1994) Three unusual repair deficiencies associated with transcription factor BTF2(TFIIH): evidence for the existence of a transcription syndrome. Cold Spring Harb. Symp. Quant. Biol., 59, 317–329.

13 Heller, E.R., Khan, S.G., Kuschal, C., Tamura, D., DiGiovanna, J.J. and Kraemer, K.H. (2015) Mutations in the TTDN1 gene are associated with a distinct trichothiodystrophy phenotype. J. Invest. Dermatol., 135, 734-741.

14 Kuschal, C., Botta, E., Orioli, D., Digiovanna, J.J., Seneca, S., Keymolen, K., Tamura, D., Heller, E., Khan, S.G., Caligiuri, G. et al. (2016) GTF2E2 Mutations Destabilize the General Transcription Factor Complex TFIIE in Individuals with DNA Repair-Proficient Trichothiodystrophy. Am. J. Hum. Genet., 98, 627-642.

15 Corbett, M.A., Dudding-Byth, T., Crock, P.A., Botta, E., Christie, L.M., Nardo, T., Caligiuri, G., Hobson, L., Boyle, J., Mansour, A. et al. (2015) A novel X-linked trichothiodystrophy associated with a nonsense mutation in RNF113A. J. Med.

Genet., 52, 269-274.

16 Drmanac, R., Sparks, A.B., Callow, M.J., Halpern, A.L., Burns, N.L., Kermani, B.G., Carnevali, P., Nazarenko, I., Nilsen, G.B., Yeung, G. et al. (2010) Human genome sequencing using unchained base reads on self-assembling DNA nanoarrays. Science, 327, 78-81.

17 Swagemakers, S.M., Jaspers, N.G., Raams, A., Heijsman, D., Vermeulen, W., Troelstra, C., Kremer, A., Lincoln, S.E., Tearle, R., Hoeijmakers, J.H. et al. (2014) Pollitt syndrome patients carry mutation in TTDN1. Meta Gene, 2, 616-618.

18 Sainsbury, S., Bernecky, C. and Cramer, P. (2015) Structural basis of transcription initiation by RNA polymerase II. Nat. Rev. Mol. Cell Biol., 16, 129-143.

19 Nogales, E., Louder, R.K. and He, Y. (2017) Structural Insights into the Eukaryotic Transcription Initiation Machinery. Annu. Rev. Biophys., 46, 59-83.

20 Itoh, Y., Unzai, S., Sato, M., Nagadoi, A., Okuda, M., Nishimura, Y. and Akashi, S. (2005) Investigation of molecular size of transcription factor TFIIE in solution. Proteins, 61, 633-641.

21 Hayashi, K., Watanabe, T., Tanaka, A., Furumoto, T., Sato-Tsuchiya, C., Kimura, M., Yokoi, M., Ishihama, A., Hanaoka, F. and Ohkuma, Y. (2005) Studies of Schizosaccharomyces pombe TFIIE indicate conformational and functional changes in RNA polymerase II at transcription initiation. Genes Cells, 10, 207-224.

22 Jawhari, A., Uhring, M., De Carlo, S., Crucifix, C., Tocchini-Valentini, G., Moras, D., Schultz, P. and Poterszman, A. (2006) Structure and oligomeric state of human transcription factor TFIIE. EMBO Rep., 7, 500-505.

23 Chen, H.T., Warfield, L. and Hahn, S. (2007) The positions of TFIIF and TFIIE in the RNA polymerase II transcription preinitiation complex. Nat. Struct. Mol. Biol., 14, 696-703.

24 Grunberg, S., Warfield, L. and Hahn, S. (2012) Architecture of the RNA polymerase II preinitiation complex and mechanism of ATP-dependent promoter opening. Nat. Struct. Mol. Biol., 19, 788-796.

25 Botta E., Nardo T., Lehmann A.R., Egly J.M., Pedrini A.M., Stefanini M. (2002) Reduced level of the repair/transcription factor TFIIH in trichothiodystrophy. Hum. Mol. Genet., 11, 2919–2928.

26 Lin, Y.C. and Gralla, J.D. (2005) Stimulation of the XPB ATP-dependent helicase by the beta subunit of TFIIE. Nucleic Acids Res, 33, 3072-3081.

27 Warlich, E., Kuehle, J., Cantz, T., Brugman, M.H., Maetzig, T., Galla, M., Filipczyk, A.A., Halle, S., Klump, H., Scholer, H.R. et al. (2011) Lentiviral vector design and imaging approaches to visualize the early stages of cellular reprogramming. Mol. Ther., 19, 782-789.

28 van den Akker, E., Satchwell, T.J., Pellegrin, S., Daniels, G. and Toye, A.M. (2010) The majority of the in vitro erythroid expansion potential resides in CD34(-) cells, outweighing the contribution of CD34(+) cells and significantly increasing the erythroblast yield from peripheral blood samples. Haematologica, 95, 1594-1598.

29 Dolznig, H., Bartunek, P., Nasmyth, K., Mullner, E.W. and Beug, H. (1995) Terminal differentiation of normal chicken erythroid progenitors: shortening of G1 correlates with loss of D-cyclin/cdk4 expression and altered cell size control. Cell Growth Differ., 6, 1341-1352.

30 Cao, A. and Galanello, R. (2010) Beta-thalassemia. Genet Med, 12, 61-76.

31 van Zwieten, R., Veldthuis, M., Delzenne, B., Berghuis, J., Groen, J., Ait Ichou,

F., Clifford, E., Harteveld, C.L. and Stroobants, A.K. (2014) Hemoglobin analyses in the Netherlands reveal more than 80 different variants including six novel ones. Hemoglobin, 38, 1-7.

32 Miwa, K., Kojima, R., Obita, T., Ohkuma, Y., Tamura, Y. and Mizuguchi, M. (2016) Crystal Structure of Human General Transcription Factor TFIIE at Atomic Resolution. J. Mol. Biol., 428, 4258-4266.

33 Hashimoto S., Egly J.M. (2009) Trichothiodystrophy view from the molecular basis of DNA repair/ transcription factor TFIIH. Hum. Mol. Genet., 18, R224–R230.

34 de Boer J., Donker I., de Wit J., Hoeijmakers J.H., Weeda G. (1998) Disruption of the mouse xeroderma pigmentosum group D DNA repair/ basal transcription gene results in preimplantation lethality. Cancer Res., 58, 89–94.

35 Andressoo J.O., Weeda G., de Wit J., Mitchell J.R., Beems R.B., van Steeg H., van der Horst G.T., Hoeijmakers J.H. (2009) An Xpb mouse model for combined xeroderma pigmentosum and cockayne syndrome reveals progeroid features upon further attenuation of DNA repair. Mol. Cell Biol., 29, 1276–1290.

36 Wu N.Y., Chung C.S., Cheng S.C. (2017) Role of Cwc24 in the First Catalytic Step of Splicing and Fidelity of 5' Splice Site Selection. Mol. Cell Biol., 37

37 Migliaccio G., Sanchez M., Masiello F., Tirelli V., Varricchio L., Whitsett C., Migliaccio A.R. (2010) Humanized culture medium for clinical expansion of human erythroblasts. Cell Transplant, 19, 453–469.

3

CHROMATIN REMODELING IN RESPONSE TO DNA DAMAGE

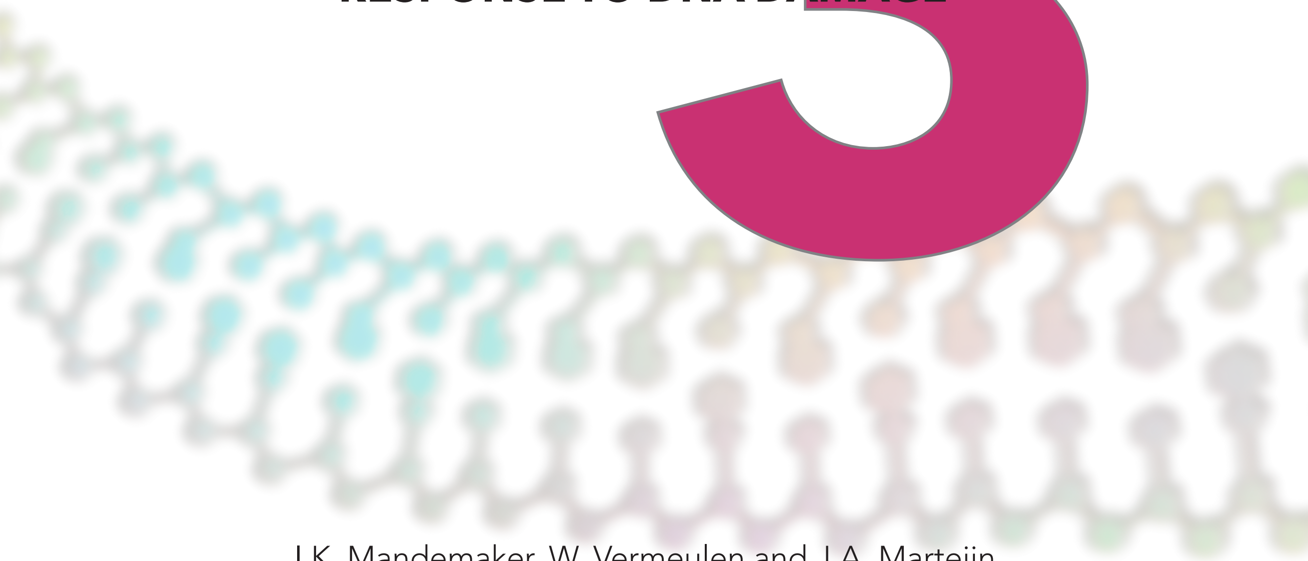

I.K. Mandemaker, W. Vermeulen and J.A. Marteijn

Department of Molecular Genetics, Erasmus Medical Centre, 3015 GE
Rotterdam, The Netherlands

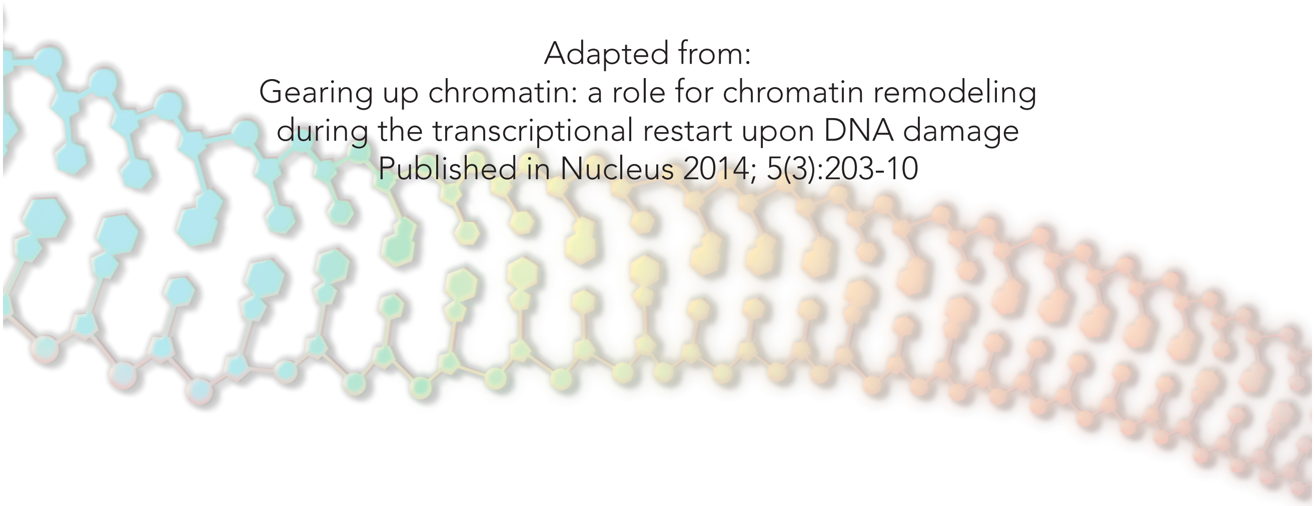

Adapted from:
Gearing up chromatin: a role for chromatin remodeling
during the transcriptional restart upon DNA damage
Published in Nucleus 2014; 5(3):203-10

ABSTRACT

The macromolecular complex of DNA wrapped around histone octamers is called chromatin. Chromatin packages the DNA into a highly condensed structure and affects all DNA transacting processes, like transcription, replication and repair. The access-repair-restore model describes the importance of chromatin remodeling during the DNA damage response, for example, to allow DNA repair proteins to access damaged DNA and to activate DNA damage signaling. The concept of this model is nicely exemplified during the last crucial step of the transcription coupled nucleotide excision repair (TC-NER), the transcription restart. During transcription, RNA polymerase may encounter DNA lesions, which causes stalling of transcription. To overcome the RNA polymerase blocking lesions, the transcribed strand is repaired by a dedicated repair mechanism, called TC-NER. After repair is completed, it is essential that transcription restarts. So far the regulation and exact molecular mechanism of this transcriptional restart upon genotoxic damage has remained elusive. Recently, three different chromatin modifying factors, HIRA, FACT and Dot1L, were identified to stimulate transcription restart after DNA damage. These factors either incorporate new histones or establish specific chromatin marks which will gear up the chromatin to subsequently promote transcription recovery. This adds a new layer to the current model of chromatin remodeling necessary for repair and indicates that this specific form of transcription, i.e. the transcriptional restart upon DNA damage, needs specific chromatin remodeling events.

CHROMATIN STRUCTURE AND REMODELING

Just like other DNA transacting processes, the DNA damage response (DDR), including the different DNA repair pathways, is highly influenced and regulated by chromatin. This macromolecular complex, consisting of DNA and proteins and functioning in organizing the DNA, can be a barrier for proteins to access the DNA. Although the main molecular mechanisms of DNA repair pathways are quite well understood, their interplay with the chromatin remains largely elusive. Chromatin is often considered as a barrier for repair proteins to access the DNA and more evidence is arising that chromatin remodelers and histone modifying enzymes are active players in the DDR [1]. Two specific chromatin states have been distinguished based on the density of the structure; heterochromatin and euchromatin. Heterochromatin is a highly compact structure which consists mainly of transcriptionally silenced genes and repetitive sequences like telomeres. The compact structure makes it less accessible for proteins thereby silencing transcription and inhibiting DNA repair. Euchromatin is a more open and accessible structure than heterochromatin and enriched with actively transcribed genes. These two chromatin states are not rigid and the chromatin can be restructured to the other state.

The main repeating building blocks of chromatin are nucleosomes, consisting of about 147 base pairs DNA wrapped around 8 core histone proteins. The histone core is made up of a H3/H4 heterotetramer flanked by two H2A/H2B dimers [2]. Nucleosomes are connected together with on average 20-80 nucleotides of linker DNA. This linker DNA can be bound by histone H1 at the entry and exit point from the nucleosome. Histone H1 also interacts with the nucleosome and keeps the DNA wrapped around the histone core in place, thereby stabilizing and compacting the nucleosome structure [3]. Histone H1 is one of the most important proteins that defines the higher order structure of the chromatin, however the exact function of histone H1 is not fully understood yet. For instance, it has been shown that histone H1 can be both a positive and a negative regulator of transcription [3].

There are many histone variants, differing from each other from a few amino acids up to the addition of large domains.. These variants regularly are differentially expressed in distinct cell types, during specific phases of the cell cycle or are incorporated into particular chromatin locations. The variants can differ in binding strength, structure and the recruitment of interactors thereby presenting different functions in the regulation of, for example, the cell cycle, transcription and DNA repair [4]. One such variant is the ubiquitously expressed histone H2A variant H2AX, which has an additional C-terminal domain containing a specific phosphorylation site that plays an important role in the DDR [5].

The structure of the chromatin can be altered by three different groups of proteins; ATP-dependent chromatin remodelers, histone modifying enzymes and histone chaperones. There are 4 different families of chromatin remodeling complexes: ISWI, SWI/SNF, INO80 and CHD, which use the energy of ATP to catalyze the disruption of the interaction between histones and the DNA. ATP-dependent chromatin remodelers can evict histones or even entire nucleosomes from the chromatin or slide nucleosomes along the DNA, changing the accessibility of the DNA (Figure 1). Chromatin remodelers have been shown to be involved in both transcription repression and activation, cell cycle regulation and DNA repair [6]. Histone modifying enzymes alter the chromatin structure by the covalent attachment of chemical groups or small proteins on specific amino acids of histones. The different post-translational modifications (PTMs) identified on histones include acetylation, phosphorylation, ubiquitylation, sumoylation, methylation and poly-ADP-ribosylation. Histones can be heavily modified by PTMs in response to cellular and environmental cues, especially on the C-terminal and N-terminal tails that protrude from the nucleosomes. These PTMs can affect the net charge, binding affinity or stability of histones. For instance, modification by acetylation neutralizes the positive charge of the lysine it is attached to, thereby decreasing the binding affinity between the histone and the DNA. Histone modifications can also function as a binding platform for proteins that specifically recognize the modified form and thereby bind to the chromatin [7]. The third group of chromatin rearranging proteins is the histone chaperones. Histone chaperones facilitate the assembly and disassembly of nucleosomes and have in general either preferential binding for histones H2A-H2B or for histones H3-H4. Histone chaperones function in three different ways. First, they can directly deposit histones onto the DNA for nucleosome assembly. Second, chaperones can facilitate the shuttling of newly synthesized histones from the cytoplasm into the nucleus. And third, histone chaperones can bind histones and keep them as a soluble pool ready to use during stress conditions [8]. Together these chromatin remodeling proteins ensure that the chromatin is a compact, yet very dynamic structure that can be adapted from a dense structure to protect the DNA from the binding of unwanted proteins to a more open conformation that allows DNA transacting processes to take place.

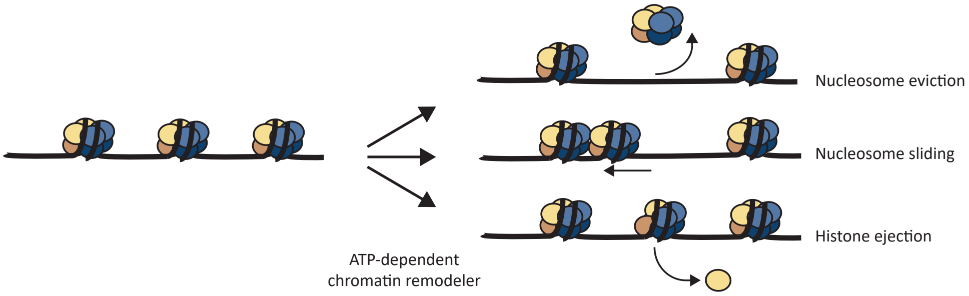

Figure 1. Mechanisms of ATP-dependent chromatin remodelers.
ATP-dependent chromatin remodelers use the energy from ATP hydrolysis to alter the chromatin structure by facilitating the eviction of complete nucleosomes (top), the sliding of nucleosomes along the DNA (middle) or the ejection of histones (bottom).

CHROMATIN REMODELING DURING THE DNA DAMAGE RESPONSE

DNA damage occurs throughout the DNA, also in highly condensed chromatin regions like heterochromatin. The postulated 'access-repair-restore' model proposes that the chromatin organization presents a barrier for repair proteins and that chromatin needs to be reorganized to provide a more open conformation to allow access for repair proteins to bind the lesions. Following repair, the chromatin needs to be restored to pre-damaged conditions to preserve epigenetic information [9]. However, over the years it became clear that chromatin is not only a barrier for repair but also an optimal platform for the regulation of repair and initiation of damage signaling events [10] (Figure 2). Although this model holds for many types of DNA damage, below we will only focus on chromatin remodeling in response to UV irradiation.

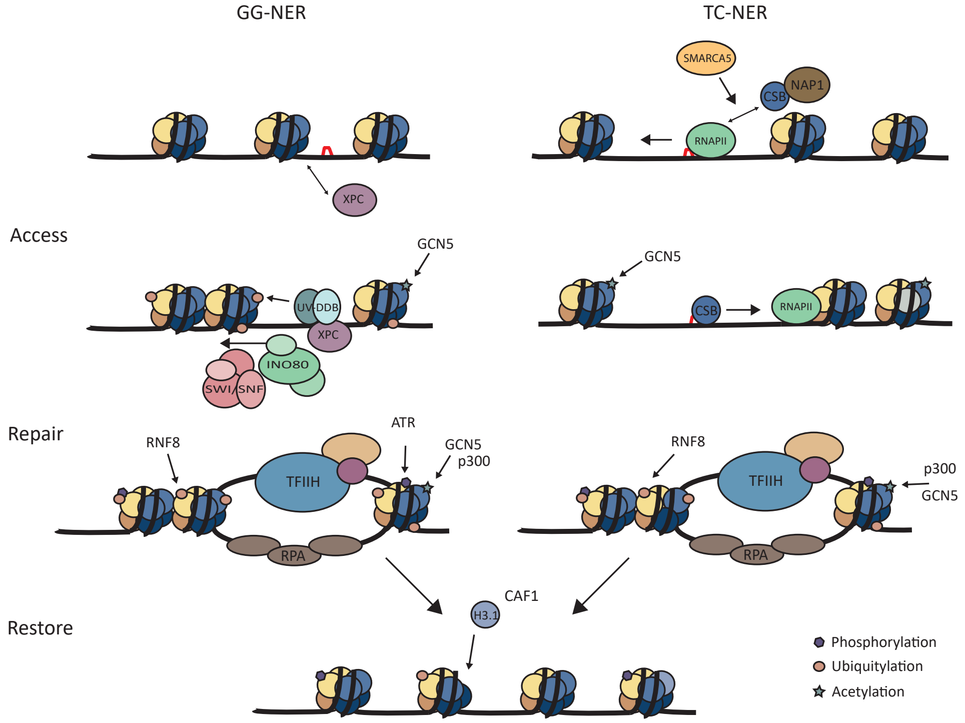
GG-NER
TC-NER
SMARCA5
NAP1
CSB
RNAPII
XPC
Access
GCN5
GCN5
UV-DDB
XPC
CSB
RNAPII
INO80
SWI/SNF
Repair
RNF8
ATR
GCN5
p300
TFIIH
RPA
RNF8
TFIIH
p300
GCN5
RPA
CAF1
H3.1
Restore
Phosphorylation
Ubiquitylation
Acetylation

Figure 2. Chromatin remodeling in the UV-DDR.
Schematic representation of chromatin remodeling after UV-induced DNA damage. The concerted action of ATP-dependent chromatin remodelers, histone modifying enzymes and histone chaperones opens up the chromatin structure to allow repair proteins to bind the lesion. Histones are ubiquitylated by the UV-DDB complex as well as the E3 ligase RNF8 and histone acetyltransferase GCN5 is recruited to the lesions where it acetylates histone H3K9/K14 resulting in more accessible nucleosomes thereby promoting the recruitment of NER proteins and repair. Histone acetyltransferase p300 interacts with PCNA and the newly synthesized DNA and is suggested to be involved in chromatin relaxation, although its exact function remains unclear. Also DNA damage signaling is induced by phosphorylation of histone H2AX by ATR.

Almost 40 years ago it was already shown that indeed chromatin has a more open structure after DNA damage. Regions undergoing repair are more sensitive to micrococcal nuclease digestion than other regions, indicating that DNA is more accessible during repair [11]. This process might be facilitated by several ATP-dependent chromatin remodelers. For example, chromatin remodelers from the SWI/SNF and INO80 family have been linked to GG-NER and are shown to stimulate repair and to be required for optimal UV survival [12]. Even though transcription requires a more open chromatin structure, chromatin remodeling also plays an important role during TC-NER, just like in GG-NER. Several chromatin modulating activities have been found to facilitate TC-NER, including the p300 histone acetyltransferase (HAT), the chaperone NAP1 and the, for TC-NER crucial, SNF2/ SWI2 ATPase CSB [13-17]. The TC-NER factor CSB itself contains a SWI2/SNF2 ATPase domain and has in vitro chromatin remodeling activity. The chromatin is not only restructured by ATP-dependent chromatin remodelers after UV-induced damage, as it has also been shown that several histone chaperones affect the repair process. For example the chromatin remodeling function of CSB is stimulated by the histone chaperone NAP1 [15-17]. Moreover, the recruitment of CSB to sites of UV damage is regulated by het ISWI ATPase subunit SMARCA5, which is essential for UV survival [18].

In addition, several histone modifications have been described to be involved at different stages of the DDR induced by UV irradiation (UV-DDR). One of the most characterized DNA damaged induced histone modification is the phosphorylation of histone H2AX at serine 139 (yH2AX), which is induced after DSBs, UV damage and replication stress [19-21]. This modification of H2AX stimulates repair of DSBs and initiates a signaling cascade that activates DNA damage checkpoints [22]. After UV irradiation in non-cycling cells the phosphorylation of H2AX is dependent on GG-NER and also on protein kinase ATR, which is most likely activated by the binding of ATRIP and TOPBP1 to RPA coated single stranded DNA generated during the NER reaction [19, 23-25]. The induction of yH2AX results in the recruitment of MDC1 to the damage which in turn leads to the recruitment of the E3 ubiquitin ligase RNF8 [24]. RNF8 is implicated in the DDR after UV-irradiation, replication stress and DSBs [24, 26, 27]. Together with the E2-enzyme UBC13, RNF8 poly-ubiquitylates histone H1 upon DSBs. This results in recruitment of the E3-ligase RNF168 which interacts via its UDM1 domain with the K63-linked poly-ubiquitylated histone H1. Subsequently, RNF168 ubiquitylates histone H2A on lysine 13-15, stimulating recruitment of downstream factors, including 53BP1 and BRCA1 [26, 28]. It is likely that this pathway is also activated during the UV-DDR as RNF8-dependent histone H2A ubiquitylation is also observed after UV-irradiation [24]. Besides stimulating recruitment of DDR factors, histone ubiquitylation also leads to a more accessible chromatin structure. For instance, UV-induced ubiquitylation of the core histones H2A, H3 and H4 by the E3 ligase complex containing DDB1, DDB2, Cul4 and RBX1 (CRL4DDB2) destabilizes nucleosomes [29-31]. In contrast, in yeast also deubiquitylation of histones is shown to stimulate DNA repair, as Ubp8 and Ubp10-dependent histone H2B deubiquitylation in response to RNAPII stalling at UV-induced lesions is necessary for efficient repair of lesions [32]. Besides phosphorylation and ubiquitylation, also histone acetylation plays a key role in chromatin remodeling after UV irradiation. The histone acetyl transferases (HATs) GCN5 and p300 are described to function in the UV-DDR. GCN5 was shown to stimulate NER at the MFA2 locus in yeast by acetylating histone H3 thereby making the DNA more accessible [33]. Also, in human cells GCN5 acetylates histone H3 at sites of UV damage. Depletion of this HAT results in impaired recruitment of NER factors leading to inefficient repair [34]. Like GCN5, the HAT p300 is also recruited to UV lesions where it is hypothesized to be involved in global chromatin relaxation after UV irradiation in a p53 dependent manner [35].

Modifying and restructuring of the chromatin plays an important role in DNA repair and signaling. However, the restore step of the access-repair-restore model [9] seems to entail more than only the removal of DNA damage signaling markers and the maintenance of epigenetic information. Recently, an important novel layer is added to the model in which chromatin remodeling is also involved in the stimulation the final step of TC-NER, the transcription restart [36]. Below we discuss in more detail how two histone chaperones and a methyl transferase function in the remodeling of chromatin to promote the recovery of transcription levels in response to UV.

REPAIR OF TRANSCRIPTION BLOCKING LESIONS

Gene transcription is an essential process for proper cellular function. However, translocating RNA polymerases may encounter lesions in the DNA template that impede the transcription machinery and cause slowing down or even stalling of these polymerases, thereby depriving cells from essential RNA molecules or triggering a signaling response leading to apoptosis [37]. In some cases RNA Polymerase II (RNAPII) might bypass lesions, an activity most likely depending on two flexible regions of the Rpb1 subunit of RNAPII [38]. However, this translesion synthesis might result in aberrant transcripts [39]. Therefore, more preferably, these RNA polymerase blocking DNA lesions are repaired in order to restore transcription and thereby proper cellular functioning [40]. An example of transcription blocking lesions are cyclobutane-pyrimidine dimers (CPD) and 6-4 pyrimindinepyrimidone photo products (64PP), which are the most abundant occurring DNA lesions upon UV irradiation. Transcription coupled nucleotide excision repair (TC-NER) is a dedicated branch of the nucleotide excision repair (NER) pathway, which removes transcription-blocking lesions specifically from transcribed strands [14]. RNAPII constantly interacts with TC-NER proteins, so that upon stalling the lesions can rapidly be recognized and repaired. For example, CSB transiently interacts with RNAPII. Upon lesion stalling of RNAPII, CSB gets more tightly associated [41], resulting in recruitment of CSA to the damage [13]. Recently, also two other crucial TC-NER factors, UVSSA and USP7, were shown to interact with RNAPII in unperturbed conditions [42]. Together these proteins are involved in the damage recognition step and play a crucial role in the formation and function of the complete TC-NER complex (Figure 3, left side). Lesions located throughout the genome are targeted by the global genome repair (GG-NER) pathway. GG-NER is initiated by the concerted action of the XPC and DDB2 DNA damage sensing protein complexes. TC-NER and GG-NER only differ in the DNA damage recognition after which TFIIH is recruited, which partially unwinds the damaged DNA and plays an important role, together with XPA and RPA, in the damage verification. Next the endonucleases XPF/ERCC1 and XPG incise the damaged DNA strand and remove about 30 nucleotides. DNA polymerases synthesize new DNA over the single-stranded gap followed by the sealing of the nick by DNA ligases I or III to complete the NER reaction [43]. Importantly, in the specific case of TC-NER, an essential step for proper cellular functioning, is that transcription needs to resume after repair is completed [14, 40]. This recovery of RNA synthesis (RRS) can be measured by pulse chase labeling with uridine analogs and is commonly used to determine TC-NER efficiency [44]. The biological relevance of a failure to restart transcription upon DNA damage, due to an impaired TC-NER, is illustrated by patients with inborn TC-NER defects. Inactivating mutations in UVSSA result for example in the UV sensitive syndrome characterized by a hypersensitivity to UV-irradiation. While patients with nonfunctional CSA or CSB exhibit additional severe clinical features such as growth and development failure and premature segmental aging [40, 45].

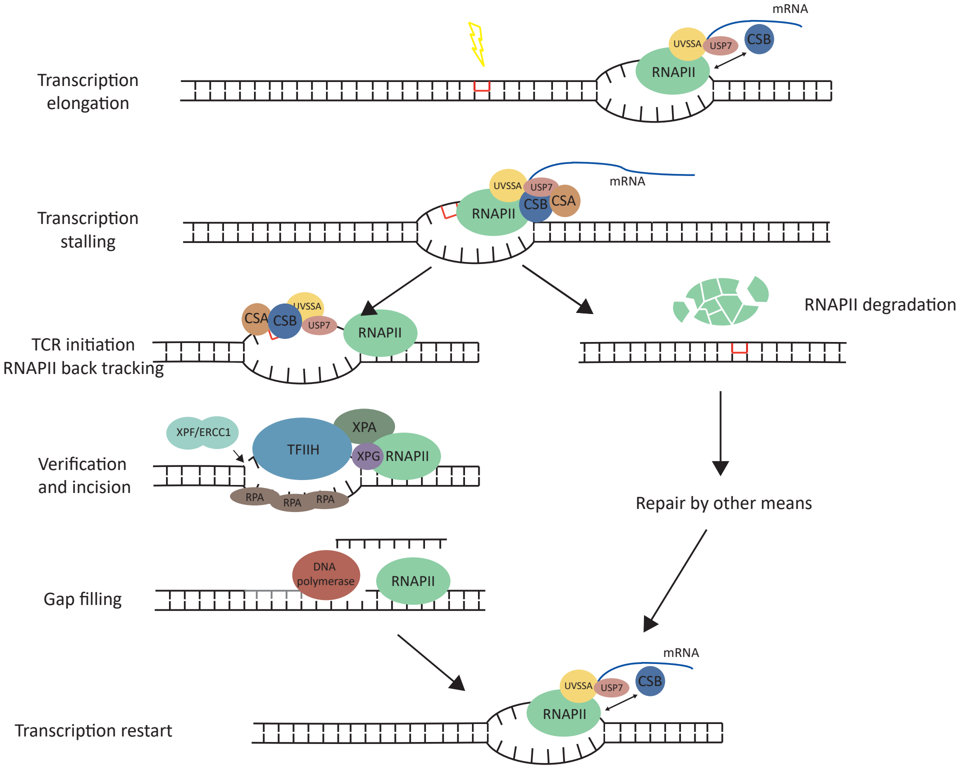
mRNA
UVSSA
USP7
CSB
RNAPII
Transcription elongation
UVSSA
USP7
mRNA
RNAPII
CSB
CSA
Transcription stalling
CSA
UVSSA
CSB
USP7
RNAPII
RNAPII degradation
TCR initiation
RNAPII back tracking
XPF/ERCC1
XPA
TFIIH
XPG
RNAPII
Verification and incision
RPA
RPA
RPA
Repair by other means
DNA polymerase
RNAPII
Gap filling
mRNA
UVSSA
USP7
CSB
RNAPII
Transcription restart

Figure 3. Model of mammalian transcription coupled repair.
During transcription UVSSA, USP7 and CSB transiently interacts with RNAPII. When the polymerase encounters a lesion in the DNA, the stalled complex will block access of the repair proteins to the lesion. Therefore, RNAPII has to be either moved back along the DNA to enable TC-NER initiation by CSB, UVSSA, USP7 and CSA (left side) or degraded to allow repair by other repair mechanisms (right side). In TC-NER, the DNA is unwound by TFIIH which together with XPA is responsible for the damage verification. The endonucleases XPF/ERCC1 and XPG are positioned by RPA and cleave the damaged DNA strand and remove about 30 bases around the damage. DNA polymerases fill the single-stranded gap followed by ligation of the nick by DNA ligases I or III to complete the NER reaction. Upon damage removal the transcription need to restart for proper cellular functioning.

Importantly, when RNAPII is stalled at a lesion the damaged bases are enclosed in the active polymerase complex, thereby shielding the damage from repair factors [46]. Therefore, to make the lesion accessible for repair, the stalled RNAPII has to be removed or backtracked. Currently, there are two not mutually exclusive models, describing the displacement of the polymerase from the DNA lesion. RNAPII might reverse translocate along the DNA resulting in the initiation of TC-NER [40, 47, 48] (Figure 3, left side). If the RNAPII blocking lesion cannot be resolved efficiently by the above process, the stalled RNAPII may be ubiquitylated resulting in the dissociation and subsequent degradation of the large subunit of the RNA polymerase complex, RPB1, [49], thereby making the lesion accessible for other repair systems (Figure 3, right side).

TRANSCRIPTION RESTART AFTER UV DAMAGE REQUIRES CHROMATIN REMODELING

After completion of DNA repair in the transcribed strand of an expressed gene, the transcription machinery needs to be restarted in order to restore normal expression levels of the affected gene. Whether specific proteins, besides the essential repair proteins, are involved in the transcriptional restart after repair has so far remained elusive. Specific histone variants and histone PTMs play an important role in gene expression regulation and therefore it is expected that chromatin organization is also important for RRS. Recently three different papers identified chromatin modulating factors implicated in the transcription restart after DNA repair [50-52]. Together these papers show that repair of the transcribed strand alone is not sufficient for the cell to restore expression levels of the affected genes, but that specific chromatin modifications and remodeling events are crucial as well.

Two of these papers [50, 51] identified the involvement of key histone chaperones during the TC-NER reaction directly resulting in nucleosome remodeling. Previously it was shown that the histone chaperone “Histone regulator A” (HIRA) is involved in chromatin remodeling in the response to double strand breaks (DSBs) and is also recruited to UV-A-induced lesions [53]. The HIRA chaperone deposits the histone variant H3.3 in transcriptionally active chromatin [54]. Knockdown of HIRA does not affect recruitment of NER factors nor the repair synthesis, indicating that HIRA is not involved in GG-NER [50]. However, downregulation of HIRA resulted in an impaired RRS after UVC damage to an extent comparable to TC-NER-deficient cells, implying an important role in transcription recovery [50]. The HIRA function at transcription blocking DNA lesions was elegantly shown using SNAP-tagged histones, enabling to specifically identify novel incorporated H3.3 at the damaged site [50]. As H3.3 is normally present in transcriptional active chromatin and carries specific modifications, that either promote transcription or exclude transcription inhibiting factors from the chromatin [55], it is very likely that H3.3 incorporation at sites of UV damage plays an essential role during transcription recovery upon DNA damage.

In addition it was shown that the histone chaperone FACT (Facilitating Chromatin Transcription) is also involved in transcription recovery upon UV damage. FACT is a heterodimer, consisting of the SPT16 and SSRP1 subunits and is a known H2A/H2B chaperone [56]. FACT was already known to function in the UV damage response where it acts in p53 signaling together with casein kinase 2 [57]. Both subunits of FACT are recruited to the site of local UV damage, however, only SPT16 depletion results in an impaired recovery of RNA synthesis after UV damage. These data suggest a specific role for SPT16 in the transcription recovery after UV damage, besides its other functions together with SSRP1 [51, 56]. In line with this, SPT16 downregulation results in a UV-hypersensitivity whereas knock down of SSRP1 does not affect the UV-sensitivity. The combination of fluorescence recovery after photobleaching (FRAP) and local UV damage induction uncovered a SPT16-dependent enhanced removal and incorporation of new H2A/H2B dimers at the site of local UVC damage [51]. The postulated function of the FACT-dependent H2A/H2B exchange, during normal transcription, is to enable translocation of RNAPII along the chromatin by destabilizing the nucleosomes [56]. After DNA damage the SPT16 activity might result in a prolonged plasticity of the chromatin, as shown by the increased H2A/H2B turnover at UV-damage [57]. A possible function of this SPT16-mediated chromatin plasticity is to facilitate backtracking of stalled RNAPII, a crucial step in TC-NER [40, 49, 58]. When RNAPII is not efficiently pulled back from the lesion to allow access of repair factors, the polymerase might get poly-ubiquitylated and degraded, referred to as the "last resort". Turnover of RNAPII may lead to a delay in transcription recovery after UV damage repair since new RNAPII has to be loaded onto this transcribed gene [49]. Instead of playing a role in backtracking, it is also conceivable that the SPT16-mediated H2A/H2B exchange is necessary for forward movement of the RNAPII. This can either be necessary for the restart of transcription by the stalled polymerase after the blocking lesion has been successfully repaired, or it might be involved in lesion bypass synthesis. This latter, more remote, scenario is unfavorable as it might result in aberrant transcripts [59]. Another possibility is that the chromatin remodeling stimulates the recruitment of other (unknown) factors involved in repair or specifically involved in transcription restart after UV-C damage.

Strikingly, while both histone chaperones are suggested to play an important role specifically for transcription restart after repair, both factors are recruited to sites of UV-damage with comparable accumulation kinetics as early NER-factors. This early response was further corroborated as both factors are still recruited in XPA- or XPG-deficient patient cells in which both GG-NER, and more importantly, TC-NER cannot take place [50, 51]. In line with this it was shown that repair is also not a pre-requisite for both histone H3.3 deposition or H2A/H2B exchange [50, 51]. HIRA is shown to only remain transiently enriched at DNA lesions as its recruitment decreased already 1h after damage infliction, while it takes much longer to fully restore expression levels to pre-damage levels (20-24h) [50]. However the maximum levels of H3.3 are reached after 1 hour and remain stable until transcription restarts. These results indicate that HIRA functions early during TC-NER in order to prepare the damaged chromatin for transcription recovery. In contrast to HIRA accumulation, SPT16 remains present for longer periods at sites of damage. This difference between HIRA and SPT16 colocalization with DNA lesions is in line with their chromatin remodeling functions. HIRA causes the incorporation of the histone variant H3.3, which remains stably incorporated in the chromatin, thereby most likely replacing other H3 histone variants. However UV stimulates a continuous exchange of H2A/H2B at sites of damage, which most logically needs long lasting histone chaperone activity of SPT16 and therefore explains the persistent enrichment of SPT16 at damaged sites.

The question remains how these factors are specifically recruited to sites of stalled RNAPII as the recruitment of both HIRA and SPT16 is independent of repair. The recruitment of FACT is transcription independent, indicating it is either a very early step in the NER pathway or a parallel process which happens independent of NER and transcription [51]. During transcription the recruitment of FACT is mediated by the histone methyltransferase SETD2 [60]. It is thus possible that also in the UV damage response specific histone modifications, will mediate the FACT recruitment. The HIRA recruitment was shown to depend on the ubiquitylation activity of Cul4/DDB1 [50]. However, thus far there is no indication that HIRA is ubiquitylated itself or that it can interact directly with ubiquitylated proteins. Since, HIRA is able to bind to naked DNA [61], it is possible that the DDB1-CUL4 ubiquitin ligase activity toward nucleosomes might result in the generation of nucleosome sparse DNA, making it available for HIRA binding [62].

POST TRANSLATIONAL MODIFICATIONS REGULATE TRANSCRIPTION RESTART AFTER UV DAMAGE

Besides regulating the recruitment of histone chaperone to sites of DNA damage, post translational histone modifications are well established to regulate the promoter activity. Transcription normally requires specifically marked chromatin in order to open up the chromatin and stimulate transcription initiation. These marks consist, among others, of high levels of H4K16 and H4K20 acetylation and methylation of lysine 4, 36 and 79 on histone H3, compared with heterochromatin [56, 63]. A large group of proteins is responsible for creating, maintaining or removing these modifications. For instance, the yeast lysine methyltransferase DOT1, that specifically methylates H3K79, is an important transcription regulator [64, 65].

The mammalian homolog of DOT1, DOT1 like protein (DOT1L), is part of a complex, containing several myeloid or mix-lineage leukemia fusion partners. Besides regulating H3K79 di- and tri-methylation in transcription [66], DOT1L also stimulates recruitment of 53BP1 to DSBs and has a, thus far unknown, function in the UV damage response [67, 68]. Recent findings show that knock out of DOT1L, in mouse embryonic fibroblasts, leads to increased UV sensitivity [52]. Interestingly, DOT1L depletion does not influence GG-NER nor TC-NER, but does result in a strong impairment of transcription recovery after UV damage [52]. As loss of DOT1L and the subsequent reduction of H3K79 methylation normally results in the repression of transcription, the authors tested if general chromatin relaxation could overcome the effect of DOT1L absence by using Trichostatin A. Treatment with this class I Histone deacetylase inhibitor resulted in a rescue of the DOT1L phenotype, both in transcription recovery and UV-survival, suggesting that DOT1L normally results in an open chromatin structure around the promoter of UV-repressed genes to allow transcription re-initiation [52]. These data suggest a transacting effect of DOT1L at the promoters, in contrast to HIRA and FACT which most likely act in the vicinity of the lesions. In line with this, Oksenych and colleagues show that in absence of DOT1L, the transcription initiation machinery is not assembled at promoters after UV irradiation, while in wild type cells the machinery reassembles 6-10h after irradiation [52].

Specific histone modifications, associated with either active or repressive chromatin regions were tested in the promoter region of the DFHR gene. Over time the WT cells show a gradual increase in H4 acetylation and 6h after irradiation there is a large increase in DOT1L-mediated H3K79 dimethylation in these cells [52]. However no signs of these active chromatin marks are found after irradiation of DOT1L-depleted cells [52]. In addition, the heterochromatin H3K9me2 mark is upregulated after UV in DOT1L-depleted cells in comparison to WT MEFs [52]. DOT1L-mediated H3K79 trimethylation plays a role in transcription restart after UV by creating an active open chromatin state at promoters to allow reassembly of the pre-initiation complex. Dot1L trimethylates H3K79, a lysine in the core region of the histone, which is distinctive since most modifications occur on histone tails [69]. H3K79 methylation might serve as a first landmark for chromatin remodeling, preceding the recruitment of other modifiers and histone modifications [52]. Most likely, Dot1L functions in transcription recovery by limiting the spreading of heterochromatin marks at promoters immediately after irradiation, which allows RNAPII to re-accumulate at the promoters to re-activate transcription as soon as the UV damage is repaired [52].

SPECIFIC CHROMATIN REMODELING FOR TRANSCRIPTIONAL RESTART UPON DNA DAMAGE

An interesting question remains whether most chromatin modifying enzymes are implicated or whether only specific factors have acquired or adapted a specific role in the DDR. In addition it is currently unknown whether these factors are specifically involved in transcription resumption upon transcription blocking DNA damage or are also involved in the recovery of other transcription pausing events. Methyltransferases, like DOT1L, MYST2 and G9a, are involved in facilitating an open chromatin environment and might therefore play a role in general transcription initiation. Interestingly, only the chromatin modifier DOT1L was found to be specifically required for transcription restart after UV damage, as MYST2 and G9a do not play a role during RRS [52]. The effect of DOT1L on transcription restart is specific for transcription inhibition upon genotoxic insults, since after incubation with the transcription inhibitor DRB transcription can be restarted in a DOT1L independent manner [52]. A similar, specific involvement in transcription restart upon DNA damage holds for FACT and HIRA, as experiments show that another H3.3 chaperone DAXX did not have an effect on the UV-induced H3.3 incorporation [50]. In line with this, the SPT16 subunit of the H2A/H2B chaperone FACT is essential for H2A/H2B exchange after UV, while the SPT16 binding partner SSRP1, required for the canonical FACT function or other H2A/H2B chaperones, like NAP1L1, seem not to be involved [51]. The activities HIRA, FACT and DOT1L are thought to play a role in the priming of the chromatin for proper transcription recovery. Just like the methyltransferase activity of DOT1L, most likely the incorporation of H3.3 and eviction of the nucleosomal H2A/H2B histones results in a temporarily open chromatin state. This indicates that transcription activation upon DNA damage needs extra chromatin plasticity compared to normal transcription, as for example HIRA and DOT1L are not needed for transcription restart upon DRB inhibition [50, 52]. Together these findings suggest that there is a specific form of transcription; namely the recovery of RNA synthesis upon genotoxic insults, which needs specific chromatin changes to be fully functional.

DISCUSSION

It should be noted that at this moment it cannot be excluded that HIRA and FACT chromatin remodeling activities facilitate TC-NER and therefore these proteins are crucial factors for transcription restart in an indirect manner. This might also explain their presence early in the TC-NER reaction. Crucial experiments to specifically measure TC-NER repair capacity, like for example strand specific repair assays, should point out if HIRA and FACT activity affects repair or specifically transcription recovery as was shown for DOT1L.

It is not known whether the activities of HIRA, FACT and DOT1L are always needed together to stimulate RRS, or that subsets of these chromatin remodelers are needed under specific conditions. As discussed before, lesion stalled RNAPII is either degraded or reverse translocated to allow repair and finally transcription restart. Different chromatin remodeling activities could be needed for these different events and might explain the involvement of different chromatin remodelers in the transcription restart. For example, the RNAPII backtracking followed by damage removal by TC-NER (Figure 4) could be stimulated through enhancing the chromatin plasticity by FACT, which is in line with the early FACT recruitment to the damaged site. In case of degradation of the RNAPII upon stalling at the lesion, either an already active transcription complex, that did not encounter this lesion yet will continue transcription, or a new transcription complex needs to be built up at the promoter. In this latter event DOT1L activity, which promotes re-accumulation of the transcription machinery at promoters [52], might be specifically important (Figure 4). Further studies will have to point out when exactly specific remodeling activities are needed and how the interplay between histone chaperones and modifiers is defined.

The incorporation of new histones will result in a loss of pre-damage PTMs as new histones can carry specific modifications different from the old nucleosomal histones. So, incorporation of these histones upon damage will result in a defined chromatin region with specific post translational modifications. These new modifications might either stimulate transcription restart itself or recruit other factors needed for transcription recovery. Interestingly, the recently identified UV-specific interaction partner of TFIIH, ELL is not involved in repair but knock down results in an impaired recovery of RNA synthesis [70]. FRAP data shows that, in absence of ELL, upon UV irradiation a larger immobile fraction of RNAPII was observed, suggesting that without ELL RNAPII remains stalled upon repair. ELL might be a promoting factor necessary for transcription restart itself, or may serve as a binding site for other factors that are needed to stimulate RNAPII to initiate transcription after repair is finished [70]. Recently different NER factors, including XPC and ERCC1, were suggested to be involved in transcriptional control as well. These proteins might regulate changes in the epigenetic landscape or are suggested to induce chromatin looping and CTCF recruitment to facilitate transcription initiation. Even though these effects were found to be gene and most likely cell type specific, it might be interesting to study whether this activity is involved in transcription recovery upon UV-damage [71-73].

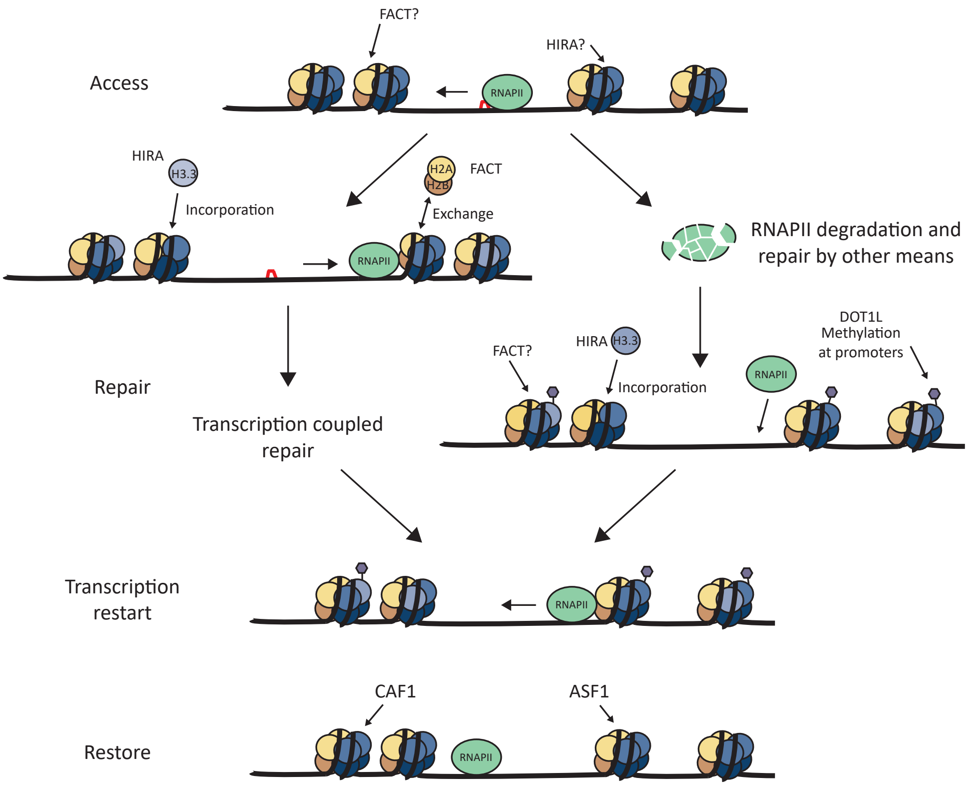
FACT?
HIRA?
Access
RNAPII
HIRA
H3.3
Incorporation
H2A
H2B
FACT
Exchange
RNAPII
RNAPII degradation and
repair by other means
DOT1L
Methylation
at promoters
FACT?
HIRA
H3.3
Incorporation
RNAPII
Repair
Transcription coupled
repair
Transcription
restart
RNAPII
CAF1
ASF1
Restore
RNAPII

Figure 4. Chromatin remodeling during the transcriptional restart upon DNA damage. This model shows an overview of chromatin remodeling necessary for transcriptional restart after UV damage. When RNAPII is stalled by a lesion, the damaged site has to be made accessible for repair. This is done by chromatin remodelers like NAP1L1, p300 and HMGN1 (not shown), which are most likely involved in the reverse translocation of RNAPII. FACT mediates H2A/H2B exchange which might give the chromatin extra plasticity needed for this backtracking. In another scenario, if RNAPII is degraded, other repair mechanisms will remove the damage and in order for transcription to restart new RNAPII has to be loaded onto the DNA. As DOT1L is a histone methyltransferase that prevents heterochromatin spreading and might therefore stimulates loading of new RNAPII after it has been degrades upon DNA damage. Both these pathways could be stimulated by the incorporation of new histone H3.3 by HIRA. DOT1L and FACT might also play a role in either of these events. This chromatin remodeling provides an specific environment stimulating the transcription restart after DNA damage. When transcription rates are recovered, the DNA can be remodeled back to its predamaged state to maintain epigenetic information by for instance CAF1 and ASF1.

These three recent studies show that in addition to the in this model suggested chromatin modifications, specific chromatin changes are needed for proper transcription restart upon UV-damage [50-52]. Histone H3.3 is normally present in actively transcribed chromatin regions and therefore incorporation of H3.3 at damaged sites by HIRA will provide a transcription stimulating environment. FACT-mediated H2A/H2B exchange will most likely give the chromatin extra plasticity needed for RNAPII movement or recruitment of other involved factors. In addition, DOT1L is preventing a heterochromatin structure that would block transcription recovery after repair. All together these factors create a specific chromatin environment of newly incorporated histones and their chromatin marks so that after the lesion is repaired, RNAPII can restart transcription to restore mRNA expression levels.

OUTLOOK

According to the access-repair-restore model, chromatin remodeling may be implicated before and after DNA repair, thereby maintaining proper cellular functioning [9]. These transcription restart-associated chromatin restructuring activities have added a novel layer to the access-repair-restore model in which the chromatin is geared up for proper transcription restart already before the actual damage is repaired. Also after repair and transcription restart have taken place, more remodeling might be needed to restore the chromatin to pre-damaged conditions thereby preserving the epigenetic information of the damage region [36, 74]. The assays used to monitor chromatin plasticity upon DNA damage, including live-cell histone exchange assays and visualization of newly incorporated histone at sites of damage, will enable us to further study the involvement of specific histone variants and the role of other histone chaperones in the response to DNA damage. Furthermore, recent advances in proteomics will enable us to uncover specific histone PTMs that are crucial to overcome the detrimental consequences UV-induced DNA lesions. Altogether this will further fuel in-depth research to detect roles of the changes in the chromatin landscape upon genotoxic events.

REFERENCES

1. Groth, A., et al., Chromatin challenges during DNA replication and repair. Cell, 2007. 128(4): p. 721-33.
2. Zhu, P. and G. Li, Structural insights of nucleosome and the 30-nm chromatin fiber. Curr Opin Struct Biol, 2016. 36: p. 106-15.
3. Hergeth, S.P. and R. Schneider, The H1 linker histones: multifunctional proteins beyond the nucleosomal core particle. EMBO Rep, 2015. 16(11): p. 1439-53.
4. Zink, L.M. and S.B. Hake, Histone variants: nuclear function and disease. Curr Opin Genet Dev, 2016. 37: p. 82-9.
5. Yuan, J., R. Adamski, and J. Chen, Focus on histone variant H2AX: to be or not to be. FEBS Lett, 2010. 584(17): p. 3717-24.
6. Clapier, C.R. and B.R. Cairns, The biology of chromatin remodeling complexes. Annu Rev Biochem, 2009. 78: p. 273-304.
7. Kouzarides, T., Chromatin modifications and their function. Cell, 2007. 128(4): p. 693-705.
8. Burgess, R.J. and Z. Zhang, Histone chaperones in nucleosome assembly and human disease. Nat Struct Mol Biol, 2013. 20(1): p. 14-22.
9. Smerdon, M.J., DNA repair and the role of chromatin structure. Curr Opin Cell Biol, 1991. 3(3): p. 422-8.
10. Polo, S.E. and G. Almouzni, Chromatin dynamics after DNA damage: The legacy of the access-repair-restore model. DNA Repair (Amst), 2015. 36: p. 114-21.
11. Smerdon, M.J., T.D. Tlsty, and M.W. Lieberman, Distribution of ultraviolet-induced DNA repair synthesis in nuclease sensitive and resistant regions of human chromatin. Biochemistry, 1978. 17(12): p. 2377-86.
12. Lans, H. and W. Vermeulen, Nucleotide Excision Repair in Caenorhabditis elegans. Mol Biol Int, 2011. 2011(542795).
13. Fousteri, M., et al., Cockayne syndrome A and B proteins differentially regulate recruitment of chromatin remodeling and repair factors to stalled RNA polymerase II in vivo. Molecular Cell, 2006. 23(4): p. 471-82.
14. Hanawalt, P.C. and G. Spivak, Transcription-coupled DNA repair: two decades of progress and surprises. Nature Reviews Molecular Cell Biology, 2008. 9(12): p. 958-970.
15. Citterio, E., et al., ATP-dependent chromatin remodeling by the Cockayne syndrome B DNA repair-transcription-coupling factor. Molecular and Cellular Biology, 2000. 20(20): p. 7643-7653.
16. Selzer, R.R., et al., Differential requirement for the ATPase domain of the Cockayne syndrome group B gene in the processing of UV-induced DNA damage and 8-oxoguanine lesions in human cells. Nucleic Acids Research, 2002. 30(3): p. 782-793.
17. Cho, I., et al., ATP-dependent chromatin remodeling by Cockayne syndrome protein B and NAP1-like histone chaperones is required for efficient transcription-coupled DNA repair. Plos Genetics, 2013. 9(4): p. e1003407.
18. Aydin, O.Z., et al., Human ISWI complexes are targeted by SMARCA5 ATPase and SLIDE domains to help resolve lesion-stalled transcription. Nucleic Acids Res, 2014. 42(13): p. 8473-85.
19. Hanasoge, S. and M. Ljungman, H2AX phosphorylation after UV irradiation is triggered by DNA repair intermediates and is mediated by the ATR kinase. Carcinogenesis, 2007. 28(11): p. 2298-304.
20. Rogakou, E.P., et al., DNA double-stranded breaks induce histone H2AX phosphorylation on serine 139. J Biol Chem, 1998. 273(10): p. 5858-68.
21. Ward, I.M. and J. Chen, Histone H2AX is phosphorylated in an ATR-dependent

manner in response to replicational stress. J Biol Chem, 2001. 276(51): p. 17759-62.
22. Bartek, J. and J. Lukas, DNA damage checkpoints: from initiation to recovery or adaptation. Curr Opin Cell Biol, 2007. 19(2): p. 238-45.
23. Nam, E.A. and D. Cortez, ATR signalling: more than meeting at the fork. Biochem J, 2011. 436(3): p. 527-36.
24. Marteijn, J.A., et al., Nucleotide excision repair-induced H2A ubiquitination is dependent on MDC1 and RNF8 and reveals a universal DNA damage response. J Cell Biol, 2009. 186(6): p. 835-47.
25. Marteijn, J.A., et al., Understanding nucleotide excision repair and its roles in cancer and ageing. Nat Rev Mol Cell Biol, 2014. 15(7): p. 465-81.
26. Thorslund, T., et al., Histone H1 couples initiation and amplification of ubiquitin signalling after DNA damage. Nature, 2015. 527(7578): p. 389-93.
27. Sy, S.M., et al., Critical roles of ring finger protein RNF8 in replication stress responses. J Biol Chem, 2011. 286(25): p. 22355-61.
28. Mattiroli, F., et al., RNF168 ubiquitinates K13-15 on H2A/H2AX to drive DNA damage signaling. Cell, 2012. 150(6): p. 1182-95.
29. Kapetanaki, M.G., et al., The DDB1-CUL4ADDB2 ubiquitin ligase is deficient in xeroderma pigmentosum group E and targets histone H2A at UV-damaged DNA sites. Proc Natl Acad Sci U S A, 2006. 103(8): p. 2588-93.
30. Lan, L., et al., Monoubiquitinated histone H2A destabilizes photolesion-containing nucleosomes with concomitant release of UV-damaged DNA-binding protein E3 ligase. J Biol Chem, 2012. 287(15): p. 12036-49.
31. Wang, H., et al., Histone H3 and H4 ubiquitylation by the CUL4-DDB-ROC1 ubiquitin ligase facilitates cellular response to DNA damage. Mol Cell, 2006. 22(3): p. 383-94.
32. Mao, P., et al., UV damage-induced RNA polymerase II stalling stimulates H2B deubiquitylation. Proc Natl Acad Sci U S A, 2014. 111(35): p. 12811-6.
33. Yu, Y., et al., UV irradiation stimulates histone acetylation and chromatin remodeling at a repressed yeast locus. Proc Natl Acad Sci U S A, 2005. 102(24): p. 8650-5.
34. Guo, R., et al., GCN5 and E2F1 stimulate nucleotide excision repair by promoting H3K9 acetylation at sites of damage. Nucleic Acids Res, 2011. 39(4): p. 1390-7.
35. Rubbi, C.P. and J. Milner, p53 is a chromatin accessibility factor for nucleotide excision repair of DNA damage. EMBO J, 2003. 22(4): p. 975-86.
36. Soria, G., S.E. Polo, and G. Almouzni, Prime, repair, restore: the active role of chromatin in the DNA damage response. Molecular Cell, 2012. 46(6): p. 722-34.
37. Ljungman, M., The transcription stress response. Cell Cycle, 2007. 6(18): p. 2252-7.
38. Walmacq, C., et al., Mechanism of Translesion Transcription by RNA Polymerase II and Its Role in Cellular Resistance to DNA Damage. Molecular Cell, 2012. 46(1): p. 18-29.
39. Marietta, C. and P.J. Brooks, Transcriptional bypass of bulky DNA lesions causes new mutant RNA transcripts in human cells. EMBO Rep, 2007. 8(4): p. 388-93.
40. Vermeulen, W. and M. Fousteri, Mammalian Transcription-Coupled Excision Repair. Cold Spring Harbor Perspectives in Biology, 2013. 5(8).
41. van den Boom, V., et al., DNA damage stabilizes interaction of CSB with the

transcription elongation machinery. Journal of Cell Biology, 2004. 166(1): p. 27-36.

42. Schwertman, P., et al., UV-sensitive syndrome protein UVSSA recruits USP7 to regulate transcription-coupled repair. Nat Genet, 2012. 44(5): p. 598-602.
43. Schärer, O.D., Nucleotide excision repair in eukaryotes. Cold Spring Harb Perspect Biol, 2013. 5(10).
44. Mayne, L.V. and A.R. Lehmann, Failure of RNA synthesis to recover after UV irradiation: an early defect in cells from individuals with Cockayne's syndrome and xeroderma pigmentosum. Cancer Res, 1982. 42(4): p. 1473-8.
45. Laugel, V., Cockayne syndrome: the expanding clinical and mutational spectrum. Mech Ageing Dev, 2013. 134(5-6): p. 161-70.
46. Tornaletti, S., D. Reines, and P.C. Hanawalt, Structural characterization of RNA polymerase II complexes arrested by a cyclobutane pyrimidine dimer in the transcribed strand of template DNA. Journal of Biological Chemistry, 1999. 274(34): p. 24124-30.
47. Saeki, H. and J.Q. Svejstrup, Stability, Flexibility, and Dynamic Interactions of Colliding RNA Polymerase II Elongation Complexes. Molecular Cell, 2009. 35(2): p. 191-205.
48. Lagerwerf, S., et al., DNA damage response and transcription. DNA Repair, 2011. 10(7): p. 743-750.
49. Wilson, M.D., M. Harreman, and J.Q. Svejstrup, Ubiquitylation and degradation of elongating RNA polymerase II: The last resort. Biochimica Et Biophysica Acta-Gene Regulatory Mechanisms, 2013. 1829(1): p. 151-157.
50. Adam, S., S.E. Polo, and G. Almouzni, Transcription Recovery after DNA Damage Requires Chromatin Priming by the H3.3 Histone Chaperone HIRA. Cell, 2013. 155(1): p. 94-106.
51. Dinant, C., et al., Enhanced chromatin dynamics by FACT promotes transcriptional restart after UV-induced DNA damage. Mol Cell, 2013. 51(4): p. 469-79.
52. Oksenych, V., et al., Histone Methyltransferase DOT1L Drives Recovery of Gene Expression after a Genotoxic Attack. Plos Genetics, 2013. 9(7).
53. Yang, X., et al., Histone acetyltransferase 1 promotes homologous recombination in DNA repair by facilitating histone turnover. Journal of Biological Chemistry, 2013. 288(25): p. 18271-82.
54. Skene, P.J. and S. Henikoff, Histone variants in pluripotency and disease. Development, 2013. 140(12): p. 2513-24.
55. Szenker, E., N. Lacoste, and G. Almouzni, A developmental requirement for HIRA-dependent H3.3 deposition revealed at gastrulation in Xenopus. Cell Rep, 2012. 1(6): p. 730-40.
56. Reinberg, D. and R.J. Sims, 3rd, de FACTo nucleosome dynamics. Journal of Biological Chemistry, 2006. 281(33): p. 23297-301.
57. Keller, D.M. and H. Lu, p53 serine 392 phosphorylation increases after UV through induction of the assembly of the CK2.hSPT16.SSRP1 complex. Journal of Biological Chemistry, 2002. 277(51): p. 50206-13.
58. Fousteri, M. and L.H. Mullenders, Transcription-coupled nucleotide excision repair in mammalian cells: molecular mechanisms and biological effects. Cell Research, 2008. 18(1): p. 73-84.
59. Saxowsky, T.T. and P.W. Doetsch, RNA polymerase encounters with DNA damage: transcription-coupled repair or transcriptional mutagenesis? Chemical Reviews, 2006. 106(2): p. 474-88.
60. Carvalho, S., et al., Histone methyltransferase SETD2 coordinates FACT recruitment with nucleosome dynamics during transcription. Nucleic

Acids Research, 2013. 41(5): p. 2881-93.

61. Ray-Gallet, D., et al., Dynamics of histone H3 deposition in vivo reveal a nucleosome gap-filling mechanism for H3.3 to maintain chromatin integrity. Molecular Cell, 2011. 44(6): p. 928-41.
62. Nouspikel, T., Multiple roles of ubiquitination in the control of nucleotide excision repair. Mech Ageing Dev, 2011. 132(8-9): p. 355-65.
63. Campos, E.I. and D. Reinberg, Histones: annotating chromatin. Annu Rev Genet, 2009. 43: p. 559-99.
64. Feng, Q., et al., Methylation of H3-lysine 79 is mediated by a new family of HMTases without a SET domain. Curr Biol, 2002. 12(12): p. 1052-8.
65. Lacoste, N., et al., Disruptor of telomeric silencing-1 is a chromatin-specific histone H3 methyltransferase. Journal of Biological Chemistry, 2002. 277(34): p. 30421-4.
66. Nguyen, A.T. and Y. Zhang, The diverse functions of Dot1 and H3K79 methylation. Genes Dev, 2011. 25(13): p. 1345-58.
67. Huyen, Y., et al., Methylated lysine 79 of histone H3 targets 53BP1 to DNA double-strand breaks. Nature, 2004. 432(7015): p. 406-11.
68. Bostelman, L.J., et al., Methylation of histone H3 lysine-79 by Dot1p plays multiple roles in the response to UV damage in Saccharomyces cerevisiae. DNA Repair (Amst), 2007. 6(3): p. 383-95.
69. Luger, K., et al., Crystal structure of the nucleosome core particle at 2.8 A resolution. Nature, 1997. 389(6648): p. 251-60.
70. Mourgues, S., et al., ELL, a novel TFIIH partner, is involved in transcription restart after DNA repair. Proc Natl Acad Sci U S A, 2013. 110(44): p. 17927-32.
71. Fong, Y.W., C. Cattoglio, and R. Tjian, The intertwined roles of transcription and repair proteins. Molecular Cell, 2013. 52(3): p. 291-302.
72. Kamileri, I., I. Karakasilioti, and G.A. Garinis, Nucleotide excision repair: new tricks with old bricks. Trends Genet, 2012. 28(11): p. 566-73.
73. Le May, N., et al., XPG and XPF endonucleases trigger chromatin looping and DNA demethylation for accurate expression of activated genes. Mol Cell, 2012. 47(4): p. 622-32.
74. Polo, S.E., D. Roche, and G. Almouzni, New histone incorporation marks sites of UV repair in human cells. Cell, 2006. 127(3): p. 481-493.

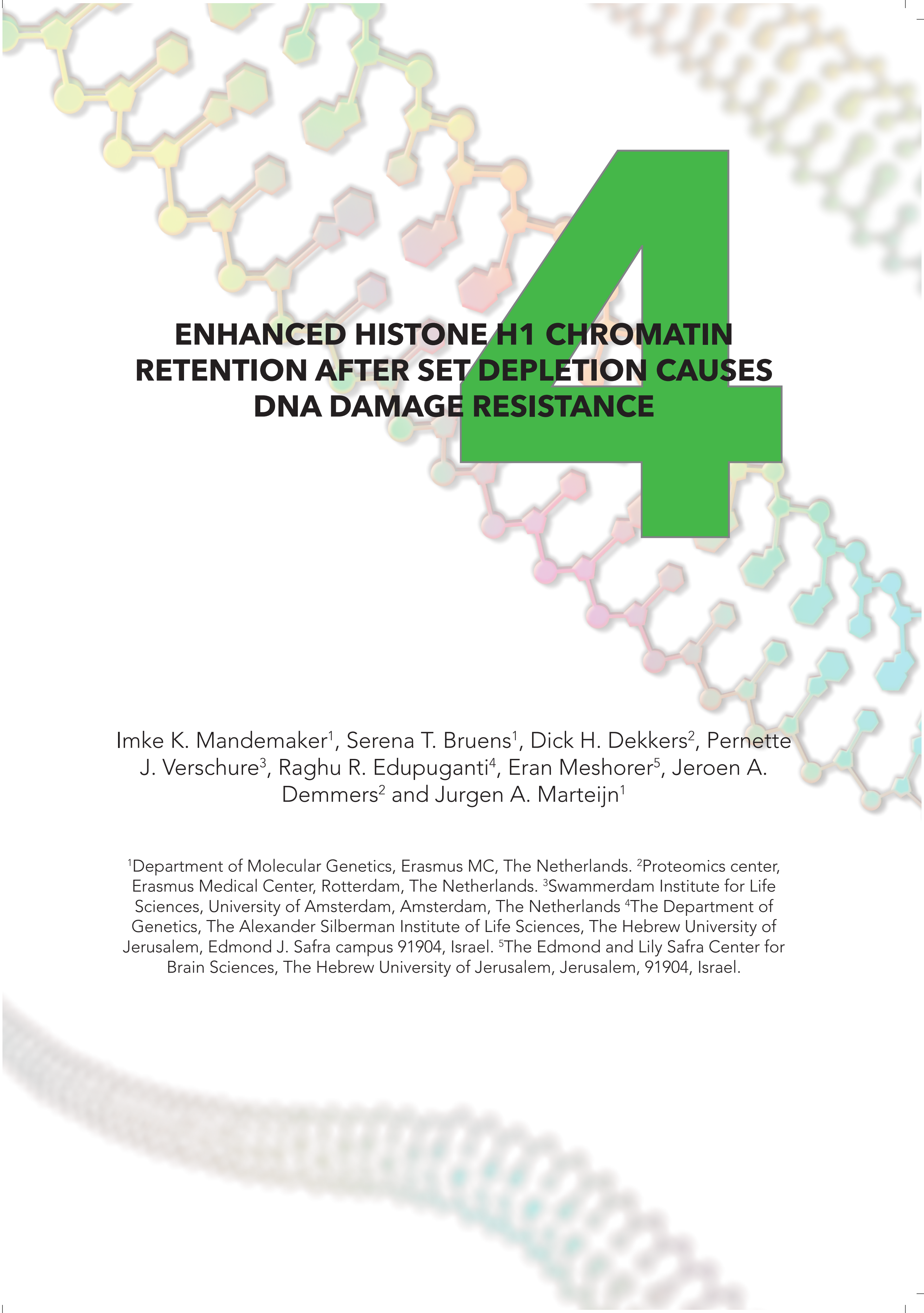

4

ENHANCED HISTONE H1 CHROMATIN RETENTION AFTER SET DEPLETION CAUSES DNA DAMAGE RESISTANCE

Imke K. Mandemaker[1], Serena T. Bruens[1], Dick H. Dekkers[2], Pernette J. Verschure[3], Raghu R. Edupuganti[4], Eran Meshorer[5], Jeroen A. Demmers[2] and Jurgen A. Marteijn[1]

[1]Department of Molecular Genetics, Erasmus MC, The Netherlands. [2]Proteomics center, Erasmus Medical Center, Rotterdam, The Netherlands. [3]Swammerdam Institute for Life Sciences, University of Amsterdam, Amsterdam, The Netherlands [4]The Department of Genetics, The Alexander Silberman Institute of Life Sciences, The Hebrew University of Jerusalem, Edmond J. Safra campus 91904, Israel. [5]The Edmond and Lily Safra Center for Brain Sciences, The Hebrew University of Jerusalem, Jerusalem, 91904, Israel.

ABSTRACT

Many chromatin remodeling and modifying proteins are involved in the DNA damage response by stimulating repair or inducing DNA damage signaling. Here we identified SET as an H1-interacting protein. Interestingly, down regulation of SET results in increased resistance to a wide variety of DNA damaging agents. We found that this increased resistance is not the result of an inhibitory effect of SET on DNA repair, but rather the consequence of a suppressed apoptotic response to DNA damage. We further provide in vivo evidence, using live cell imaging techniques, that the histone chaperone SET is responsible for the eviction of H1 from chromatin. Simultaneous knock down of H1 and SET re-sensitizes cells to DNA damage, indicating that the increased DNA damage resistance in SET-depleted cells is the result of enhanced retention of H1 on chromatin. Recently, it was shown that DNA damage-induced H1 binding at promoters suppresses the expression of p53-responsive genes. In line with this observation, we found that SET and p53 are epistatic in attenuating DNA damage-induced cell death. Our studies uncovered a new role for SET in the DNA damage response, in which its H1 chaperoning function is necessary for induction of apoptosis in response to DNA damage.

INTRODUCTION

The integrity of DNA needs to be maintained to ensure proper cellular functioning and prevent genome instability. However, DNA is constantly challenged by exogenous and endogenous DNA damaging agents that can cause a wide variety of lesions. Cells have evolved a sophisticated network of different pathways called the DNA damage response (DDR) [1] to properly respond to genomic insults. This DDR includes activation of different DNA repair mechanisms, each endowed to detect and remove specific subsets of DNA lesions [2], and a complex damage signaling network to control cell cycle progression, transcriptional reprogramming and apoptosis when the damage is beyond repair. One of the main players in the DDR is the tumor suppressor protein p53 which is involved in regulating these processes by activating specific transcriptional programs following DNA damage [3]. The DDR may act in different genomic environments or cell cycle phases, but have in common that these take place in the context of chromatin. Chromatin is generally considered to be an obstacle for repair proteins to access DNA lesions, but is also shown to serve as an important regulatory platform for many DNA damage signaling events including regulation of transcription [3-6]. In accordance with the important role of chromatin in the DDR, many proteins have been implicated in regulating chromatin changes in response to DNA damage, including ATP-dependent chromatin remodelers, histone modifying enzymes and histone chaperones [4, 6-9]. For example, the DDR-kinases ATM and ATR are involved in the phosphorylation of histone H2AX (yH2AX), which stimulates the assembly of repair complexes and is involved in the regulation of cell cycle checkpoints [10]. Deletion of the two catalytic ATPase subunits of the SWI/SNF complex, BRG1 and BRM, interferes with the induction of yH2AX and impairs repair [11]. Furthermore, histone chaperones are involved in the DDR by assembling and disassembling chromatin during the processes of repair or by replacing histones by specific histone variants. HIRA, for instance, deposits newly synthesized histone H3.3 onto the chromatin at damaged sites, thereby promoting transcriptional restart after UV irradiation [12].

Although thus far most research has focused on the remodeling, modifications and exchange of core histones and their variants, increasing evidence shows that also the linker histone H1 plays an important role in the DDR. Mouse embryonic stem cells that have 50% reduced H1 levels (TKO H1 mES cells) show enhanced phosphorylation of H2AX and Chk1 and enhanced survival after treatment with DNA damaging agents [13]. However, the exact effect of histone H1 depletion on cellular survival after DNA damage is not completely clear yet, particularly as another report found that H1-depleted cells were more sensitive to genotoxic agents [14]. Recently, a more specific role for H1 in the DDR was shown by two reports describing that H1 is an important ubiquitin substrate in the RNF8/RNF168 pathway [15][Chapter 5]. Ubiquitylation of H1 leads to the recruitment RNF168 that triggers ubiquitylation of core histones and eventually leads to the binding of downstream DDR factors such as 53BP1 and BRCA1. Together these data indicate that histone H1 is an important regulator of the DDR.

In this study we set out to further investigate the role of histone H1 in the DDR by first determining the H1 interactome. Among many other chromatin-associated factors, we identified SET as one of the H1 interacting proteins. Since SET was previously identified as a histone H1 chaperone [16], we here focused on the role of SET in DDR. SET was first identified as an inhibitor of protein phosphatase 2A (PP2A) [17] and overexpression of SET is found to be involved in the initiation of various types of cancer [18, 19]. SET has opposing functions in transcription, as it represses transcription by inhibiting the activity of CBP/p300 [20, 21], but also stimulates transcription by remodeling the chromatin [22, 23]. Here we show that down regulation of SET results in a remarkable enhanced resistance to a wide variety of genotoxic agents, without stimulating DNA repair. Live cell imaging studies showed that SET is involved in the dissociation of H1 from chromatin. This suggests that depletion of SET will result in increased H1 levels binding to the chromatin. Interestingly, knockdown of H1 reversed the increased DNA damage resistance induced by SET depletion, suggesting that this effect is directly caused by its H1 chaperone activity. Enhanced promoter binding of histone H1 has been shown to negatively influence the expression of p53-regulated genes in response to DNA damage [14]. In line with this, we observed that p53 and SET are epistatic for the increased resistance to genotoxic stress. Together our data suggests that both histone H1 and SET play an important role in the response to DNA damage.

RESULTS

SET depletion leads to DNA damage resistance

H1 deposition at the chromatin plays an important role in the DDR regulation[13, 14]. However, compared to core histones, relatively little is known about proteins that regulate histone H1 modifications and its dynamic deposition into the chromatin. To identify factors involved in H1 regulation, we performed quantitative proteomics on chromatin-bound proteins enriched for H1 by using GFP-pull downs in GFP-H1.2 expressing cells. As expected, we found core histones copurifying with GFP-H1.2, suggesting that GFP-tagged histone H1.2 is correctly incorporated into the chromatin and that the GFP-tag does not interfere with the H1-nucleosome interaction (Supplemental Table 1). In addition to many proteins known to be chromatin-bound, such as the high mobility group proteins and transcription regulators, we identified the oncoprotein SET as H1 interactor (Supplemental Table 1). We were particularly interested in SET since it was previously suggested to function as a H1 chaperone [16, 24].

To address the involvement of SET in the DNA damage response, we performed clonogenic survival experiments following UV exposure with mouse embryonic stem (ES) cells in which SET is knocked down (KD) by stable shRNA expression (Fig. 1A). Surprisingly, shSET expressing cells were less sensitive to UV irradiation than cells expressing a non-targeting control shRNA (Fig. 1B). This effect is not specific for ES cells, as increased UV-resistance was also observed in U2OS cells following siRNA-mediated SET knockdown using a pool of 4 different siRNAs against SET (siSET sp) (Fig. 1C-D). Off target effects could be excluded as a similar UV-resistance was observed with a single siRNA targeting SET (siSET a), that is not present in the siSET pool (Fig. 1C-D). To uncover the cause of SET knockdown induced resistance to DNA damage, we tested whether SET influences the cell cycle, as a reduced proliferation rate may result in less UV-induced replication stress. However, no

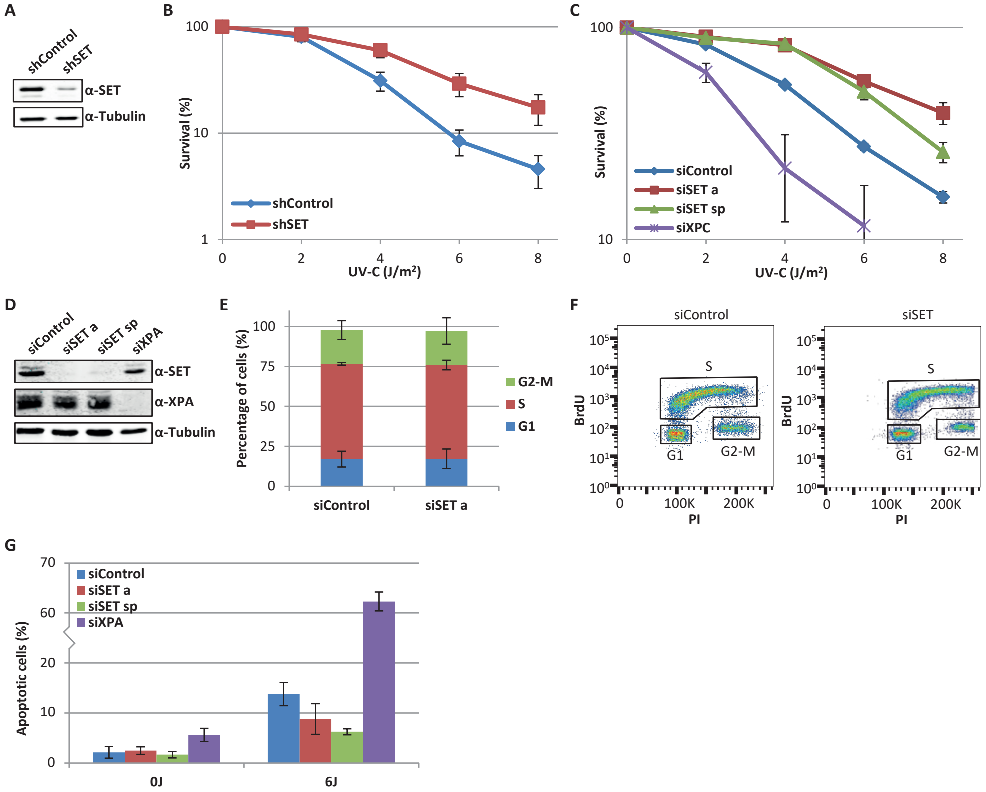

Figure 1: Depletion of SET leads to enhanced cellular survival after UV-induced DNA damage.

(A) Western blot showing the expression levels of SET in mES cells. (B-C) Clonogenic UV-survivals in (B) mES cells expressing shControl or shSET and (C) U2OS cells transfected with either siControl, siXPC, siSET or an siRNA smart pool containing 4 sequences targeting SET. The relative colony survival, normalized to 0 J/m^2, is plotted against the UV-C dose. N=3-6 individual experiments, error bars represent SEM. (D) Western blot of whole cell extracts from U2OS cells showing the knock down efficiency of the different siRNAs. Tubulin is used as a loading control. (E) Cell cycle analysis with BrdU (5 μM) incorporation and PI (2 μg/ml) staining of U2OS cell transfected with the indicated siRNAs followed by FACS analysis. N=2 individual experiments and error bars represent SEM. (F) Cell cycle analysis by incorporation of BrdU (5 μM) and PI (2 μg/ml) in mES cells expressing indicated shRNAs. (G) Quantification of percentage of apoptotic cells after UV irradiation (6 J/m^2) and addition of caspase inhibitor Q-VD-OPH (20 μM). Average ±SEM of at least 5 experiments is shown.

difference in cell cycle distribution in either SET-depleted U2OS (Fig. 1E-F) or mES cells (Supplemental fig. 1A-B) was observed, indicating that the observed higher UV-resistance in SET-depleted cells is not a consequence of changes in proliferation rate. In addition to proliferation, also the level of apoptosis is an important determinant for colony survival following DNA damage [25]. To sensitively quantify the amount of apoptotic cells we treated cells with the pan-caspase inhibitor Q-VD-OPH, which arrests the apoptotic process and resulting in the accumulation of apoptotic cells without affecting the release of cytochrome C from mitochondria (Supplemental fig. 1C). As expected an UV-induced increase in apoptotic cells was observed 32h after UV irradiation, which was further increased upon depletion of the essential NER factor XPA (Fig. 1G). SET KD resulted in fewer apoptotic cells after UV-induced DNA damage, suggesting that the increased UV-induced DNA damage resistance upon SET depletion is the result of reduced induction of apoptosis.

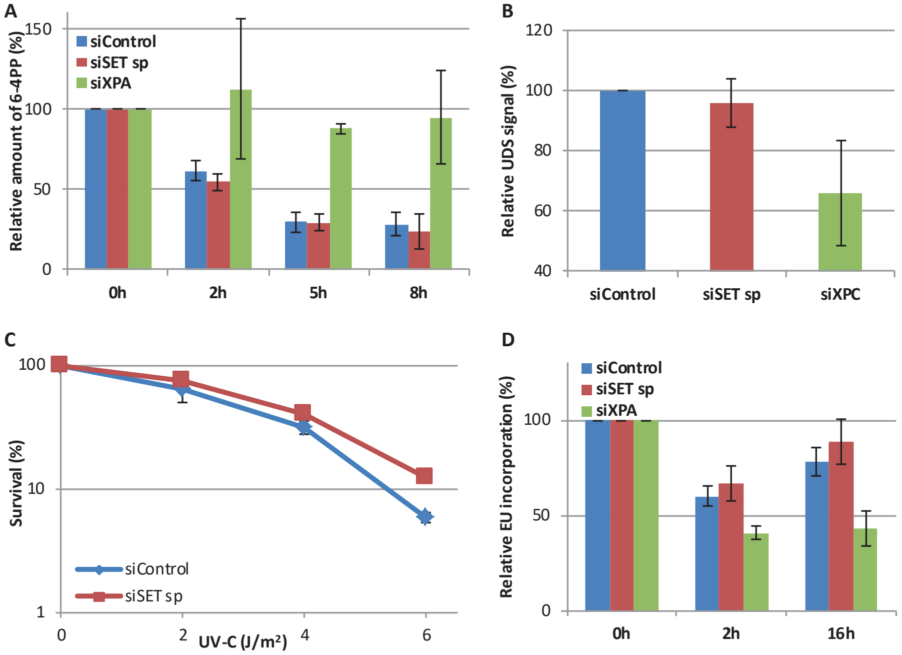

Figure 2: Depletion of SET does not affect NER efficiency.
(A) Quantification of relative amount of 6-4PP at different time points after UV irradiation (10 J/m^2). Amount of 6-4PP was quantified by immunofluorescence intensity and data was normalized to the 0 hour time point. N=3 (≥100 cells per experiment) and error bars represent SEM. (B) Unscheduled DNA synthesis measured by the incorporation of EdU (20 μM) over 3 hours in non-S-phase C5RO cells after UV irradiation (16 J/m^2). UDS levels in siControl cells were set as 100%. N=2-3 experiments, with at least 100 cells analyzed per experiment, error bars represent SEM. (C) Clonogenic UV-survival in XP4PA (XPC deficient) cells transfected with the indicated siRNAs. The relative colony survival, normalized to 0 J/m^2, is plotted against the UV-C dose. Average ±SEM of 2 independent experiments. (D) RNA synthesis determined by quantifying the amount of EU (100 μM) incorporation. Amount of EU incorporation 2 and 16 h after UV treatment is normalized to levels in undamaged cells. Mean ±SEM of 3 experiments, in which at least 75 cells were analyzed, is shown.

The increased survival in SET-depleted cells is independent of repair

To test whether SET influences DNA repair efficiency we quantified NER activity following UV-induced DNA damage using different assays. First we quantified the removal of UV-induced 6-4 photoproducts (6-4PPs) by NER. No change in the removal of UV-induced 6-4PP lesions was observed in SET KD cells compared to control cells (Fig. 2A), while a clear reduction in 6-4PP removal was observed in cells in which the crucial NER factor XPA was depleted. In line with this, no difference in unscheduled DNA synthesis (UDS) [26], a measure for the final gap-filling step of NER, was observed following SET knockdown, while depletion of XPC resulted in the expected decrease of the UDS signal (Fig. 2B). Together these data indicate that NER-mediated DNA damage removal and the subsequent gap-filling synthesis are not affected by SET depletion and suggest that SET knockdown mediated damage resistance is not caused by an increased repair activity. To further corroborate this we performed a clonogenic survival assay in cells deficient for global genome repair (GG-NER), one of the sub-pathways of NER. Although these XP-C cells are very sensitive to UV irradiation, we still observed a better survival after SET KD (Fig. 2C), indicating that the enhanced survival is not dependent on functional GG-NER and is most likely a parallel process. As the above assays mainly monitor the activity of GG-NER, we also tested whether SET influences TC-NER, the NER sub-pathway that specifically removes damages in the transcribed strand of actively expressed genes. TC-NER efficiency was assessed by the recovery of RNA synthesis (RRS) after UV-induced transcription inhibition by quantifying transcription rates using pulse labeling with the uridine analog EU [27]. Sixteen hours after UV irradiation, the RRS is clearly reduced in XPA-depleted (deficient in GG-NER and TC-NER) cells as compared to siControl transfected cells (Fig. 2D). However, RRS levels were similar in SET-depleted cells to control transfected cells (Fig. 2D), indicating that TC-NER efficiency is not affected by SET.

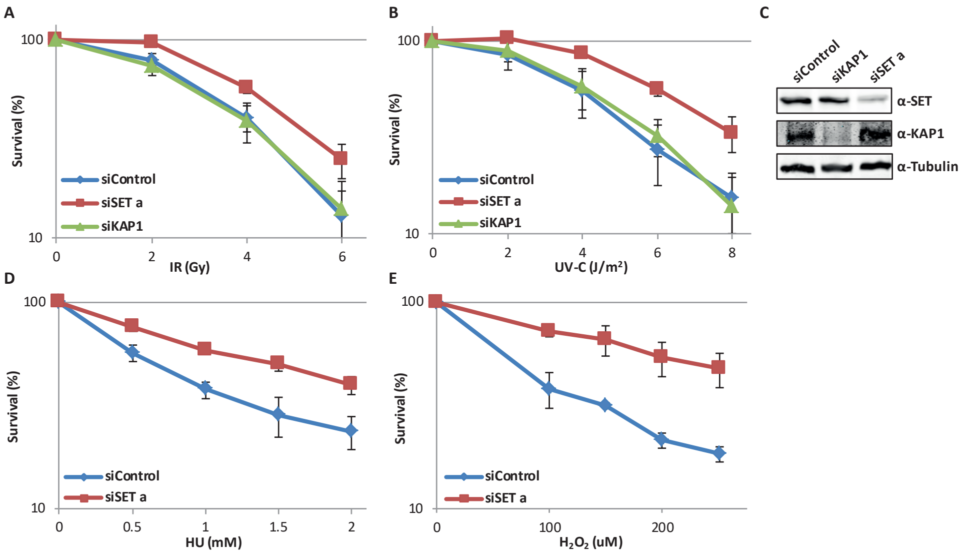

Figure 3: SET depletion leads to increased resistance to a wide variety of DNA damaging agents.
(A-B) Colony survivals of U2OS cells transfected with siControl, siSET a or siKAP1 treated with ionizing irradiation (A) or UV-C (B). Relative colony survival, normalized to untreated sample, is plotted against the dose. Average ±SEM of 3 experiments is shown. (C) Western blot of whole cell extract from U2OS cells showing KD efficiency of the used siRNA. Blots are stained with antibodies against SET, KAP1 and tubulin. (D-E) Clonogenic survival assays of U2OS cells transfected with the indicated siRNAs treated with hydroxyurea (D) or hydrogen peroxide (E). Relative colony number was normalized to non-treated conditions. Average ±SEM of 2 individual experiments.

Previously it was shown that SET also affects the cellular survival after DNA double strand break induction [28]. In line with this, we observed that SET down regulation also leads to increased resistance to ionizing radiation in both U2OS (Fig. 3A) and ES cells (Supplemental fig. 2A). In response to double strand breaks SET densifies chromatin via KAP1-dependent recruitment of HP1, leading to a shift in the balance between homologous recombination (HR) and non-homologous end joining (NHEJ) [28]. However, NHEJ and HR are not the major repair pathways involved in UV-survival and therefore it is not likely that a difference in these pathways is the reason for the UV-resistance in SET-depleted cells. In line with this, KAP1-depleted cells show a similar survival as control cells both after UV or IR treatments (Fig. 3A-C). This implies that enhanced survival in SET KD cells is not mediated by reduced KAP1-dependent chromatin compaction or by its effect on NHEJ and HR.

As SET has a role in the survival after UV and IR induced DNA damage, we tested whether SET also has also a role in the response to other types of DNA lesions. Therefore we performed clonogenic survival assays using different agents, including hydrogen peroxide, hydroxyurea, mitomycin C and Illudin S. These DNA damaging agents generate structurally very different DNA lesions and are repaired by different mechanisms: hydrogen peroxide and potassium bromate mainly induce oxidative base damage which are targeted by base excision repair; while mitomycin C creates DNA interstrand cross-links that are repaired by the Fanconi Anemia pathway. Interestingly, SET KD resulted in higher cellular resistance to all agents tested (Fig. 3 and Supplemental Fig. 2). SET knockdown also resulted in an increased survival following hydroxyurea-induced replication stress (Fig 3D). As it is highly unlikely that SET is directly involved in all these repair pathways, these data suggest that the enhanced resistance in SET-depleted cells is not the result of enhanced repair, but that SET more likely affects a cellular response that is common between different types of DNA lesions.

Altered DNA damage signaling is not the cause of the enhanced survival in SET-depleted cells

We set out to identify the responsible molecular mechanism that, in a damage-type independent manner, resulted in the increased cell survival and the reduction of damage-induced apoptosis upon SET depletion. DNA damage signaling by phosphorylation of histone H2AX (yH2AX) is a likely candidate as this common and abundant PTM plays an important role in the DDR and is induced after many different types of DNA damage [29-34]. Furthermore, previous studies have indicated that SET depletion resulted in an increased yH2AX signaling following double-strand break induction [28]. To test if SET also affects yH2AX signaling after different types of DNA damage, we studied H2AX phosphorylation following replication stress. Lac repressors (LacR) were expressed in U2OS cells that harbor an integrated array of 256 repeats of the Lac operon (LacO) (Fig. 4A). Tethering of the LacR to de LacO-locus blocks replication fork progression and thereby induces replication stress, resulting in H2AX phosphorylation [35]. Cells were transfected with the LacR vectors and 36h later the yH2AX signal was assed at the operon. We observed a more than two-fold reduction in yH2AX signal when mCherry-SET-LacR was targeted to LacO compared to the mCherry-LacR (Fig. 4B-C). This reduction in yH2AX signaling is not caused by a reduction in histone H2AX levels at the operon, as these are not affected by SET tethering (Fig. 4D). Together this indicates that SET overexpression represses yH2AX signaling.

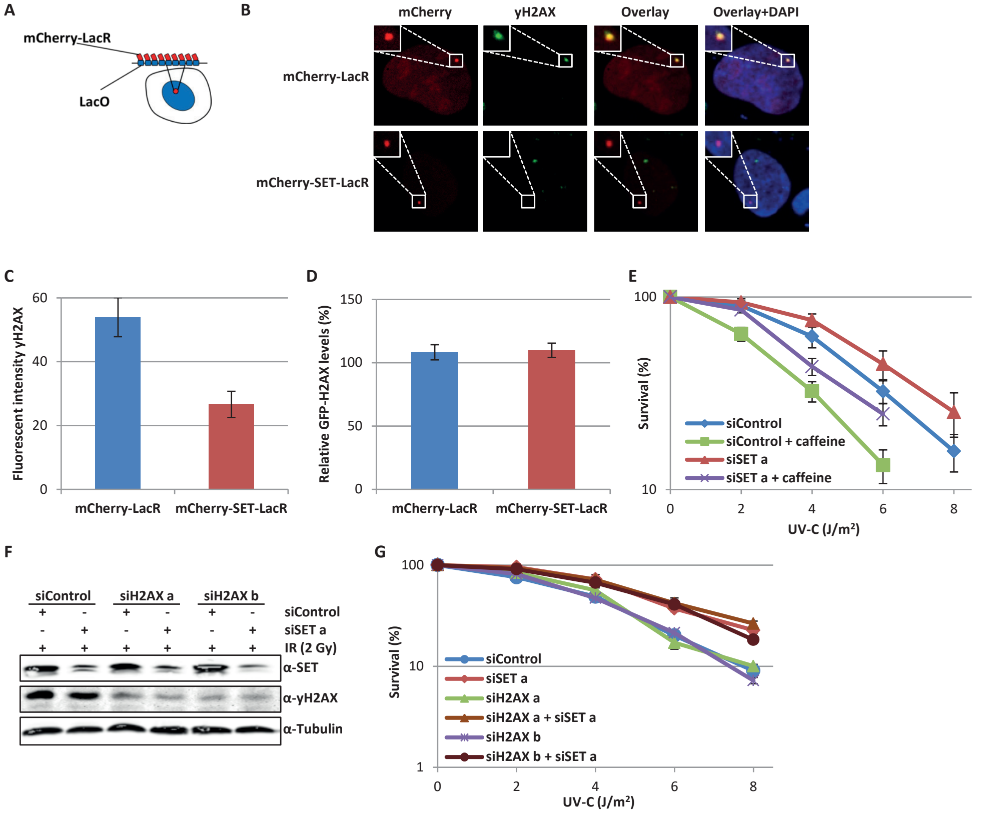

Figure 4: Altered DNA damage signaling is not the cause of the enhanced survival in SET-depleted cells.
(A) Graphical representation of U2OS LacO cells, containing 256 repeats of the Lac operon at a defined DNA locus. A Lac repressor specifically binds this operon, visualizing the locus by an fusion of the LacR with mCherry. (B) Representative immunofluorescence images of U2OS in which the indicated mCerry-LacR containing proteins are targeted to the LacO. yH2AX signal was determined by antibody staining. (C) Quantification of yH2AX signal at the lacO. Average ±SEM of 8 experiments with 25 cells analyzed per experiment. (D) Quantification of GFP-H2AX levels at the LacO of U2OS cells expressing the indicated LacR vectors. GFP-H2AX levels at the LacO are normalized to the average levels in the nucleus. Average ±SEM of at least 18 cells. (E) Colony UV-survival experiments of cells treated with caffeine. Percentage of surviving colonies, normalized to 0 J/m^2, is plotted against UV-C dose. Average of 4 experiments is shown, error bars represent SEM. (F) Representative western blot from whole cell extracts from U2OS cells transfected with the indicated siRNAs showing the protein levels of SET, yH2AX and tubulin. One hour prior to lysis, cells were irradiated with 2 Gy to induce yH2AX signaling. (G) Clonogenic UV-survival of cells transfected with siRNAs targeting histone H2AX. The relative colony survival, normalized to 0 J/m^2, is plotted against the UV-C dose. Average ±SEM of 2 independent experiments.

However, the fact that yH2AX signaling is repressed after SET overexpression does not indicate that altered yH2AX signaling is also the cause of the observed enhanced DNA damage survival in SET-depleted cells. To test this, we performed colony survival assays in which H2AX phosphorylation was suppressed by inhibition of the PI3K-like protein kinases ATR, ATM and DNA-PK, key mediators of DNA damage signaling [36, 37]. As expected, inhibition of these kinases by caffeine [38, 39] resulted in sensitization to UV [40] (Fig. 4E). Importantly, caffeine treated cells still presented an increased resistance to DNA damage upon SET depletion. Similar effects of SET depletion on cell survival were observed when ATM and DNA-PK were inhibited with specific inhibitors (Supplemental fig. 3). Importantly, also depleting histone H2AX by 2 different siRNA's, resulting in the absence of H2AX phosphorylation upon DNA damage (Fig. 4F), did not affect the SET knockdown induced UV-resistance (Fig. 4G). Together our data suggest that, although yH2AX signaling is affected by SET, it is not functionally involved in the increased resistance of SET-depleted cells to DNA damage.

The enhanced survival in SET-depleted cells is dependent on histone H1

Remodeling of the chromatin environment is important for a proper DDR [7, 41] and interestingly SET was previously implicated in nucleosome assembly and histone H1 chaperoning [16]. More specifically, in vitro data indicate that SET plays mainly a role in the eviction of H1 from the chromatin [24]. To study the function of SET in living cells, we first tested the effect of SET on H1 chromatin binding using live cell fluorescent recovery after photo bleaching (FRAP) studies on GFP-H1.2 expressing cells. In accordance with previous data [16], we observed a slower recovery of the fluorescent intensity of GFP-H1.2 upon SET knock down (KD) (Fig. 5A). The increased immobilized H1 fraction denotes a lower exchange rate of GFP-H1.2 molecules with chromatin, which can either be the result of a decreased incorporation or reduced removal of H1 molecules. In order to distinguish whether SET is mainly involved in H1 loading or unloading, we transfected mCherry-SET-LacR in LacO-array containing U2OS cells expressing GFP-H1.2, thereby inducing a local overexpression of SET (Fig. 5B). Interestingly, reduced GFP-H1.2 levels at the operon were found in cells expressing mCherry-SET-LacR, but not in cells expressing mCherry-LacR (Fig. 5C). A similar experiment with GFP-Histone H3, showed that SET tethering to the LacO has no effect on H3 levels, indicating that the histone chaperone activity of SET is specific for histone H1 (Fig. 5D). In line with previous in vitro data, these in vivo imaging experiments show that SET functions by evicting histone H1 from the chromatin (Fig. 5A-C).

This suggests that SET depletion will result in enhanced retention of histone H1 on chromatin, which might subsequently affect chromatin structure, compaction or transcription of specific genes and as a result may increase cellular survival. This would suggest that reduction of H1 levels might overcome the effect of SET depletion on survival. To test whether the enhanced survival in SET-depleted cells is indeed related to its H1 eviction activity, we depleted H1 in the presence of absence of SET. A combination of three different siRNAs was used to target all six canonical histone H1 variants [15] and H1 knock down was confirmed by western blot (Fig. 5E). Histone H1 depletion alone does not affect the cellular survival in response to UV irradiation, but reduces the effect of SET KD (Fig. 5F & supplemental fig. 4A). Also, knock down of H1 almost completely overcomes the increased survival to oxidative damage in SET-depleted cells (Supplemental fig. 4B). Together this suggests that the increased DNA damage survival observed in SET-depleted cells is mainly caused by enhanced levels of chromatin bound H1, due to a loss of the histone H1 chromatin eviction function of SET.

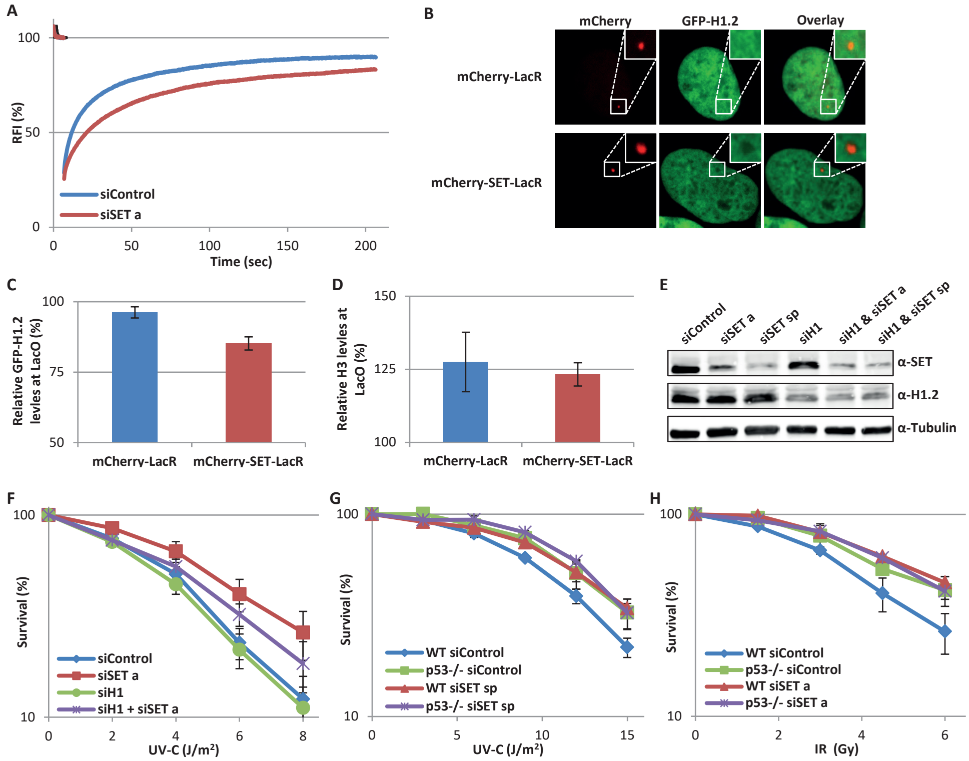

Figure 5: Higher DNA damage resistance in SET-depleted cells is rescued by histone H1 down regulation.

(A) FRAP analysis of stable GFP-H1.2 expressing cells transfected with the indicated siRNAs. A small strip is bleached spanning the nucleus and fluorescent recovery was measured over time. The fluorescent intensity is normalized to the levels before bleaching. N=3 experiments (≥8 cells/experiment), error bars represent SEM. (B) Representative immunofluorescence images of GFP-H1.2 expressing U2OS LacO cells transfected with either mCherry-LacR (top panel) or mCherry-SET-LacR (lower panel) vectors. (C) Quantification of the GFP-H1.2 levels at the LacO, normalized to the average GFP-H1.2 signal in the nucleus. N=10 individual experiments (25 cells/experiment). Error bars represent SEM. (D) Quantification of histone H3 levels at the LacO in cells transfected with the indicated LacR vectors. Average of 3 individual experiments (25 cells/experiment). Error bars represent SEM. (E) Representative immunoblot from WCE from U2OS cells showing the efficiency of the siRNAs targeting SET and histone H1. Tubulin is used as a loading control. (F) Colony survival of U2OS cells transfected with siControl, siSET a and siH1 and treated with UV-C. The relative colony survival, normalized to 0 J/m^2, is plotted against the UV-C dose. Average ±SEM of 5 independent experiments. (G-H) Colony survival of Hct116 WT and p53-/- cells transfected with siControl or siSET treated with UV (G) or IR (H) The relative colony survival, normalized to the untreated condition, is plotted against the dose. N=2, error bars represent SEM.

SET is not the only protein involved in regulating H1 binding to the chromatin. CHD8, a member of the chromodomain helicase DNA-binding (CHD) family, was shown to recruit histone H1 to p53 regulated promoters in response to DNA damage. Enhanced H1 binding at these promoters hampered gene expression and thereby inhibited apoptosis [14]. Together with our data, showing that SET-depleted cells display enhanced levels of chromatin bound H1 (Fig. 5A-C) and reduced apoptosis in response to DNA damage (Fig. 1G), this led to the hypothesis that SET might be involved in regulation of the p53-response after different types of DNA damage. Indeed, clonogenic survival experiments show that knock out of p53 resulted in a similar resistance to DNA damage as SET depletion (Fig. 5G-H). Importantly, knock down of SET had no effect on the cell survival in p53 KO cells, indicating that SET and p53 function in the same pathway. Together these data are in line with a model in which the reduced levels of apoptosis in response to DNA damage observed in SET-depleted cells (Fig. 1G) is likely the result of an inhibition of the p53 pathway, due to reduced H1 unloading from the chromatin.

DISCUSSION

To further study the role of histone H1 and H1-interacting proteins in the DDR, we performed an interaction screen for GFP-tagged H1.2 using mass spectrometry and identified the proto-oncogenic protein SET as an H1 interactor. With cell imaging assays we showed that SET affects the chromatin deposition of H1 in living cells, in line with previously proposed H1-chaperoning functions of SET [16, 24]. In addition, SET is implicated in several other cellular processes, independent of its H1-chaperoning function. SET also functions as a PP2A inhibitor [17], implicated in chromatin remodeling during transcription [22, 23] and inhibits CBP/p300-mediated acetylation [20, 21]. Interestingly, depletion of SET resulted in enhanced cellular resistance to many types of structurally diverse DNA lesions (Fig.3 & Supplemental fig. 2), which are targeted by different repair pathways. Previously it was found that SET functions in the response to DSBs by recruiting KAP1 and HP1 to lesions, thereby shifting the balance between HR and NHEJ [28]. However, we found that KAP1-depleted cells did not cause enhanced resistance to DNA damage (Fig. 3A-B), suggesting that SET-dependent damage resistance is independent of KAP1 and likely caused by another function of SET. No effect of SET depletion was found on repair efficiency of either UV-induced lesions (Fig. 2) or DSBs [28], suggesting that SET is not a general suppressor of DNA repair. Together these data suggest that SET functions in a response more common between all types of DNA damages, like DNA damage signaling or chromatin remodeling.

Despite the observation that DNA damage signaling by phosphorylation of H2AX is affected by SET (Fig. 4C) [28], yH2AX appeared not to be involved in the DNA damage resistance of SET-depleted cells (Fig. 4E-G). Instead we found that chromatin-bound histone H1 levels are important for the increased survival (Fig. 5F & Supplemental fig. 4). We showed that, in vivo, SET assists the removal of H1 from chromatin (Fig. 5A-C) and depletion of SET leads to an excess of chromatin bound H1. Importantly, the effect of SET on DNA damage resistance can be reversed by depleting H1, corroborating the hypothesis that removal of histone H1 from the chromatin by its chaperone function is needed for efficient induction of cell death in response to DNA damage.

Previously it was found that enhanced histone H1 promoter binding can negatively regulate the activation of p53-regulated genes [14]. Activation of the p53-pathway is a common response to DNA damage [42] and therefore we investigated if SET was involved in this response. Indeed we found that SET and p53 act in the same pathway (Fig. 5G-H), suggesting a stimulatory role for SET in p53-mediated apoptosis. Therefore it is tempting to speculate that SET depletion leads to enhanced H1 binding to p53-regulated promoter thereby repressing the DNA damage-induced activation of pro-apoptotic genes and preventing cell death in response to DNA damage. Chromodomain helicase DNA-binding enzyme CHD8 is implicated in controlling H1 occupancy at p53-regulated promoters and depletion of CHD8 leads to increased apoptosis after UV irradiation and etoposide treatment [14]. Since CHD8 and SET have opposing effects on both cellular survival after DNA damage and on H1 chromatin occupancy, a delicate balance between CHD8 and SET activity might define the expression levels of p53-regulated genes and therefore apoptosis. Disturbance of this balance may lead to an altered apoptotic response and cause genomic instability, as suggested by the notion that both SET, as a fusion gene with CAN resulting from chromosomal translocations [43], and altered CHD8 expression [44] are implicated in oncogenic transformation.

It is currently not known if SET distinctively removes H1 from specific genomic locations or affects constant turnover of histone H1 proteins chromatin-wide. Our FRAP studies show a substantial immobilization of H1 upon SET depletion (Fig. 5A), which is unlikely to be solely caused by binding to p53-target promoters. It is thus likely that also expression of other genes is altered, which may contribute to the affected DDR upon SET depletion. Future studies should determine if SET indeed alters the expression of p53-regulated pro-apoptotic genes. In contrast to our data, it was shown that SET can also interfere with apoptosis by inhibiting p53 acetylation [45, 46]. Therefore, SET seems to have both an inhibitory and activating function in p53-mediated apoptosis. Moreover, the inhibitory effect of SET on PP2A activity, which is an important phosphatase implicated in DDR, may further confound the dissection of the molecular mechanism of SET in the DDR.

It is intriguing to note that SET sensitizes cells to DNA damage, as thus far most proteins found to be involved in the DDR, like DNA repair and damage signaling proteins, protect cells against genomic insults. Possibly this is a mechanism to prevent the formation of mutations, in which SET actively stimulates cell death in cells that cannot reliably repair all DNA lesions, similarly to the established pro-apoptotic role of p53 in the DDR [42]. In summary, we identified a new role for histone H1 and its chaperone SET in the DDR, in which unloading of H1 from chromatin is necessary for efficient induction of apoptosis in response to DNA damage.

METHODS

Cell lines and cell culture

U2OS, HeLa, Hct116 and XP4PA cells were cultured in DMEM/F10 medium (Lonza) supplemented with 10% fetal calf serum (FCS) and 1% penicillin-streptomycin (PS, P0781 Sigma). C5RO cells were cultured in F10 supplemented with 15% FCS and 1% PS. Mouse embryonic stem cells (mES) were cultured in DMEM/BRL-conditioned medium containing 10%FCS, 1%PS, 1% non-essential amino acids (Lonza), 0.2% β-mercaptoehtanol (Invitrogen) and 1000 U/ml leukemia inhibitory factor on gelatin (0.1%) pre-coated dishes. For stable isotope labeling by amino acids in cell culture (SILAC) experiments, cells were cultured for at least 10 cell doublings in lysine and arginine deficient DMEM (Thermo Scientific) with 10% dialyzed FCS (Invitrogen), 1% PS, 1% non-essential amino acids and 1% ultraglutamine (200 mM Lonza), supplemented with either light [^{12}C6]lysine (73 μg/mL, Sigma) and [^{12}C6, ^{14}N4]arginine (42 μg/mL, Sigma) or similar concentrations of heavy [^{13}C6]lysine and [^{13}C6, ^{15}N4]arginine (Cambridge Isotope Laboratories). All cells were cultured at 37°C and 5% CO_2 in a humidified incubator. For UV treatments, cells were washed with phosphate-buffered saline (PBS) and irradiated with using a 254 nm Philips TUV UV-C lamp. Transfections with RNAi were performed with RNAiMax (Invitrogen) according to the manufacturer's protocol 3 days before treatments; siControl: UGGUUUACAUGUCGACUAA; siSETa: UCUCCAAAGAAUUUCAUCUGAAU; siSETsp: smart pool Dharmacon (L-019586-00-0005); siH1: CCUUUAAACUCAACAAGAA, CCUUCAAACUCAACAAGAA, CAGUGAAACCCAAAGCAAA [15]; siXPC: CUGGAGUUUGAGACAUAUC; siXPA: CUGAUGAUAAACACAAGCUUA; siH2AX a: GUCUCCCAGAAGACAGUGA; siH2AX b: CAACAAGAAGACGCGAAUC; siKAP1: GCAUGAACCCCUUGUGCUG. Transfections with mCherry-LacR, mCherry-SET-LacR and GFP-H2AX vectors (2 μg) are performed with Fugene (Promega) according to manufacturer's protocol 16 h before fixation, unless stated otherwise. For these experiments a U2OS (2-6-3) cell line containing a chromosomal array of 256 lac operator repeats and a CFP reporter gene harboring 24 repeats of the MS2 bacteriophage RNA hairpins was used. The mCherry-SET-LacR vector was made by ligating a PCR product containing the SET cDNA into the mCherry-LacR construct digested with AscI. GFP-H1.2 construct was made by cloning a PCR product from a H1.2-Flag (kind gift from Kyosuke Nagata) in a pENTR4-eGFP-C1 vector, followed by an LR clonase reaction to a pLenti-CMV vector [47]. Stably expressing GFP-H1.2 cell lines were made by lentiviral transduction. Medium containing lentivirus was harvested 2 days after transient transfection of HEK293 cells with pLenti-CMV-GFP-H1.2, pMDLg/pRRE, pRSV-REV and pMD2.G constructs. Control (scrambled) and SET shRNA oligos, used in mES cells, had a forward MluI site overhang and a reverse ClaI site overhang. In addition, an NdeI site was inserted after the terminating signal of 5 "T" nucleotides to allow oligo insertion verification. Single stranded oligonucleotides were purchased (IDT) and hybridized to make double stranded oligos using standard hybridization procedures. Hybridized oligonucleotides were inserted into pLVTHM vector between MluI and ClaI sites. Lentiviral particles were prepared by transfecting pLVTHM-shSET, LV-VSVG and CMV-dr8.9-dvpr packaging plasmids into HEK 293T cells using Lipofectamine2000 (Invitrogen). Low passage R1 ESCs were infected with low titer of lentiviral particles to prevent multiple integrations. Several GFP positive colonies were picked, clonally expanded and checked for highest knockdown efficiency.

Identification of GFP-H1.2 interactors with MS

GFP-H1.2 containing protein complexes were enriched from nuclear extracts of SILAC labelled HeLa cells stably expressing GFP-H1.2 by immunopurification with GFP-trap beads (Chromotek) as described previously [48]. In short, GFP-H1.2 expressing or WT SILAC labeled HeLa cells from six 15 cm dishes were harvested by scraping in PBS. Nuclei were isolated by resuspending cells in 2x pellet volume Hepes buffer (10 mM Hepes pH 7.6, 1.5 mM $MgCl_2$, 10 mM KCl, 0.5 mM DTT and protease inhibitor cocktail (Roche)), douncing the cells using pestle A of a Dounce homogenizer and centrifugation for 10 min at 3000 rpm. Nuclei were lysed in Hepes buffer B (20 mM Hepes pH 7.6, 1.5 mM $MgCl_2$, 150 mM NaCl, 25% Glycerol, 0.5 mM DTT and protease inhibitor cocktail (Roche)) using pestle B from the dounce homogenizer. Chromatin was fragmented by MNase (25U, Sigma) digestion for 1h at 4°C. Lysates were cleared by centrifugation (15 min at 13.000 rpm) and incubated with GFP-trap beads (Chromotek) for 4h at 4°C. Beads were washed four times in Hepes buffer B and mixed together. Proteins were eluted with Laemmli sample buffer and loaded onto a 4-15% gradient SDS-PAGE gel (Biorad). After running, the gel was fixed and stained with Roti-blue (Carl Roth GmbH) according to manufacturer's protocol. Gel lanes were cut into 2-mm slices using an automatic gel slicer and subjected to in-gel reduction with dithiothreitol, alkylation with iodoacetamide and digestion with trypsin (Promega, sequencing grade) [49]. Nanoflow LC-MS/MS was performed on a quadrupole Orbitrap (Q-Exactive, Thermo Fisher Scientific) mass spectrometer equipped with an EASY-nLC 1000 (Thermo Fisher Scientific). Peptide samples were loaded onto ReproSil C18 reversed phase column (20 cm x 75 μm) and eluted with a linear gradient (70 min) from 5 to 80% acetonitrile containing 0.1% formic acid at a constant flow rate of 300 nl/min. Fragmentation of the peptides was performed in a data-dependent acquisition (DDA) mode. MS1 spectra were collected at a resolution of 70,000, with an automated gain control (AGC) target of 1^{E6} and a max injection time of 50 ms. The 10 most intense ions were selected for MS/MS. Precursors were filtered according to charge state (2-7z), and monoisotopic peak assignment. Previously interrogated precursors were dynamically excluded for 30 s. Peptide precursors were isolated with a quadrupole mass filter set to a width of 2.0 Th. MS experiments were performed in duplo with label swap to easily exclude contaminants and reduce false positive hits. Raw MS data was analyzed using MaxQuant software (version 1.3.0.5) [50, 51] with false protein discovery rate set at 1% and minimum peptide length of 7. MS/MS spectra were searched against the human Uniprot fasta database (version 2013) using Andromeda search engine [51]. Contaminants and reverse hits were removed.

Clonogenic survival assays

Cells were seeded in 6-well plates a day before treatment (U2OS and mES 400 cells/well, Hct116 250 cells/well). Cells were treated with a single doses of UV-C or IR, continuous exposure to $KBrO_3$ (Sigma) or H_2O_2 (Sigma) or treated for 1 hour with Mytomycin C (Kyowa) or 24 h with Hydroxyurea (Sigma) or Illudin S at the indicated concentrations. Each experiment was performed in triplicate. After 6-8 days the colonies were fixed and stained with 50% methanol, 43% H_2O, 7% acetic acid and 0.1% Brilliant blue R (Sigma). Number of colonies was counted using a GelCountTM (Oxford Optronix, version 1.1.2.0). The survival was plotted as the relative amount of colonies after treatment compared to the non-treated samples.

FRAP

GFP-H1.2 expressing HeLa cells were seeded on coverslips and kept at 37°C and 5% CO_2. A Leica sp5 confocal laser scanning microscope with a 63x oil immersion objective. Leica LAS AF software was used for image acquisition. Imaging was performed at 1400 Hz with a line averaging of 2 and a 12x zoom. For FRAP analysis a strip of 32 pixels high, spanning the entire width of the cell nucleus was bleached using a 488 nm laser with high laser power (1 frame, 100%). Recovery of the fluorescent signal was measured every 0,2 seconds for 200 seconds. Fluorescent intensity was normalized to pre-bleach values.

Immunofluorescence

Cells were grown on glass 24 mm coverslips. Cells were fixed in 2% paraformaldehyde in PBS containing 0.1% Triton X-100 and washed 2 times for 10 min in PBS with 0.1% Triton X-100 and one time in PBS with 0.15% Glycine and 0.5% BSA. For 6-4PP and histone H3 staining, cells were incubated for 5 min in freshly made 0.07 M NaOH. Cells were incubated for 1-2 h with the indicated primary antibodies in PBS with 0.15% Glycine and 0.5% BSA and subsequently washed 5 times with PBS with 0.1% Triton. After washing, the cells were incubated for 1-2 h with secondary antibodies in PBS with 0.15% Glycine and 0.5% BSA and DAPI (0.1 ug/ml) or Sytox green (0.5 μM, Life technologies). Cells were washed 5 times with PBS containing 0.1% Triton X-100 and mounted using Aqua Poly/Mount (Polysciences). For cytochrome C release assays, cells were grown in glass bottom 96 well plates (Greiner). 32 h before fixation cells were UV-irradiated and the caspase inhibitor (Q-VD-OPH, 20 μM, MP Biomedicals) was added. Above described staining procedure was used and after secondary antibody staining cells were washed in PBS with Triton X-100, fixed with 2% paraformaldehyde and stored in PBS. Antibodies used: mouse-anti-6-4PP (1:1000, Cosmo), goat-anti-H3 (1:250, Santacruz), mouse-anti-Cytochrome C (1:100, BD Biosciences) and mouse-anti-phospho-H2AX (Ser139) (1:1000, Millipore). Images were acquired using a Leica sp5 confocal scanning microscope (Cytochrome C) with a 20X HCX PL APO CS 0.7 NA objective or a Zeis LSM700 confocal microscope equipped with a 40X oil Plan-apochromat 1.4 NA objective. Images were analyzed using ImageJ software [52].

Westernblotting

Whole cell extracts were made by scraping cells in Laemmli buffer and boiling for 3 min. Lysates were separated on SDS-PAGE gels and transferred to PVDF membranes (0.45 μm, Millipore). Blots were blocked with 5% milk (Sigma) in PBS-Tween (PBS with 0.05% Tween) and incubated 1 h or o/n with primary antibodies. Blot were washed 5 times for 5 min with PBS-Tween and incubated with secondary fluorescent antibodies (Sigma) for 1 h, followed by another 5 washes in PBS-Tween. Antibodies are visualized using an Odyssey CLX Infrared Imaging System (LI-COR Biosciences). Primary antibodies used: mouse-anti-phospho-H2AX (Ser139) (1:1000, Millipore), mouse-anti-Tubulin (1:5000, Sigma), rabbit-anti-SET (1:1000, Abcam), rabbit-anti-XPA (1:250, Santacruz), mouse-anti-KAP1 (1:1000, Abnova), rabbit-anti-H1.2 (1:1000, Abcam)

Unscheduled DNA synthesis (UDS)

C5RO cells were seeded on 24 mm coverslips and cultured under low serum (1%) to accumulate cells in G0-phase cells. Cells were irradiated with 16 J/m^2 and incubated for 3 h in medium containing EdU (5 µM, Invitrogen) and 5-fluorodeoxyuridine (1 µM, Sigma), followed by a 15 min chase of medium containing thymidine. Cells were fixed in 3.6% formaldehyde and permeabilized for 20 min in 0.5% Triton X-100 in PBS. Click-it reaction was performed according to manufacturer's protocol (Invitrogen) and slides were mounted using DAPI vectashield (Vector Laboratories). Images were obtained with a Zeis LSM700 equipped with a 40x 1.3 NA oil immersion Plan apochromat objective.

Recovery of RNA synthesis (RRS)

Cells were cultured on coverslips and irradiated with 6 J/m^2 UV-C or mock treated. Cells were incubated for 2 h in medium containing EU (20 µM, Base Click) at different time points after UV treatment. Cells were fixed in 3.6% formaldehyde and permeabilized in 0.5% Triton X-100 in PBS for 20 min. Click-it reaction is performed according to manufacturer's protocol (Invitrogen) and slides are mounted using DAPI vectashield (Vector Laboratories). Images were obtained with a Zeis LSM700 equipped with a 40x 1.3 NA oil immersion Plan apochromat objective and quantified using ImageJ software [52].

Cell cycle analysis

Cells were labelled with 5 µM BrdU (B5002, Sigma-Aldrich) for 15 minutes at 37°C to identify S-phase cells. Subsequently, cells were harvested and fixed in 70% ethanol overnight at 4°C. Fixed cells were washed with ice-cold PBS and re-suspended in pepsin solution (5 mg pepsin in 10 ml 0.1N HCl) and incubated 20 minutes at RT. After pepsin-treatment blocking solution (PBS + 0.5% Tween-20 + 0.1% BSA) was added and cells were washed. Next, cell were re-suspended in 2N HCl for 12 minutes at 37°C. To neutralize, borate buffer (100 mM, pH8.5) was added and the cells were pelleted. Mouse-anti-BrdU-FITC antibody (1:50, BD Pharming, 556028 Clone 3D4) was added and the cells were incubated for 2 h on ice in the dark. Stained cells were washed in blocking solution and re-suspended in 500 µl PBS supplemented with 12.5 µl RNase A and 1 µl PI (1mg/ml, P3566, Invitrogen). Cell cycle was analysed the next day using BD LSRFortessa (BD Biosciences). Flow Cytometry data was analysed using FlowJo vX.0.7 (Tree Star Inc.).

ACKNOWLEDGMENTS

We thank Kyosuke Nagata for sharing the H1.2-Flag construct. We thank the Erasmus MC optical imaging center (OIC) with help with confocal imaging and image analysis. This work was supported by the Dutch Organization for Scientific Research (NWO) TOP Grants of Earth and Life Sciences and ZonMW (854.11.002 and 912.12.132), European Research Council Advanced Grant (340988-ERC-ID) and Dutch Organization for Scientific Research Earth and Life Sciences VIDI grant (846.13.004).

SUPPLEMENTAL INFORMATION

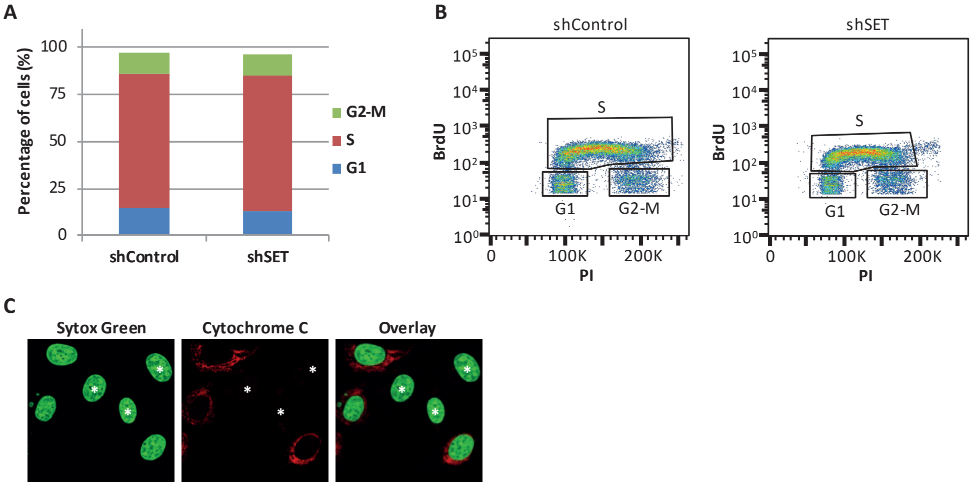

Supplemental figure 1: Depletion of SET leads to enhanced cellular survival after UV irradiation.

(A) Representative plot of BrdU (5 μM) and PI (2 μg/ml) labeled U2OS cells analyzed using FACS. Boxes indicate the G1, S and G2/M populations. (B) Plot of BrdU (5 μM) and PI (2 μg/ml) labeled mES cells analyzed using FACS. Boxes indicate the G1, S and G2/M populations. (C) Representative immunofluorescence images of cells treated with UV (6 J/m^2) and the caspase inhibitor Q-VD-OPH (20 μM). Asterisks (*) indicate apoptotic cells characterized by cytochrome C release.

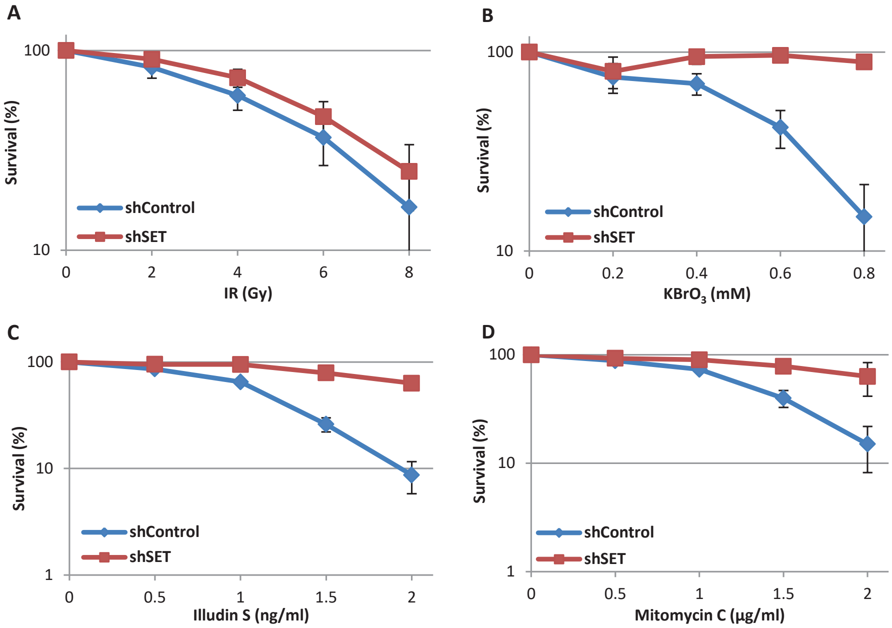

Supplemental figure 2: SET depletion leads to increased resistance to DNA damage. Clonogenic survival assays with mES cell expressing shControl or shSET treated with IR (A) potassium bromate (B), illudin S (C) or mitomycin C (D). The relative colony survival, normalized to untreated conditions, is plotted against the dose. Average ±SEM of at least 2 individual experiments.

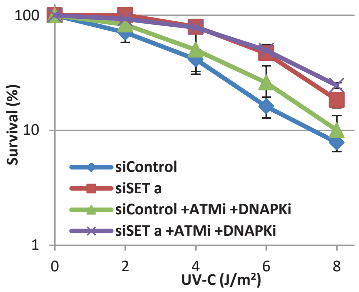

Supplemental figure 3: Altered DNA damage signaling is not the cause of the enhanced survival in SET-depleted cells.
Colony UV-survival experiments of cells treated with ATM and DNA-PK inhibitor. The number of colonies at 0 J/m^2 is normalized to 100%. Average ±SEM of 2 independent experiments.

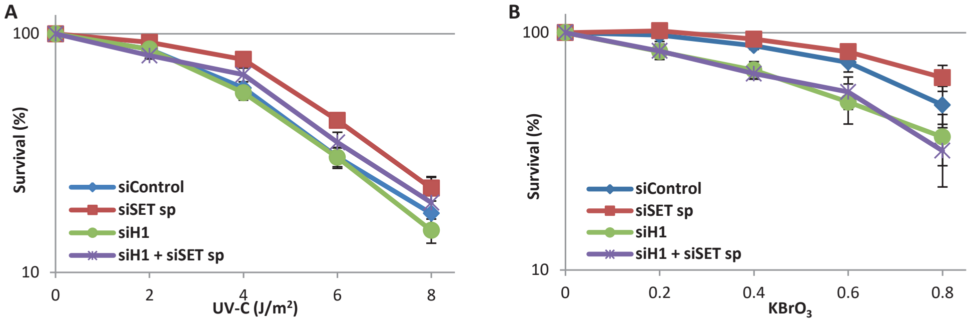

Supplemental figure 4: Higher DNA damage resistance in SET-depleted cells is impeded by histone H1 down regulation.
Colony UV-survivals of U2OS cells transfected with siControl, siH1 and siSET sp treated with UV (N=5) (A), or potassium bromate (N=4) (B). Relative colony number, normalized to untreated conditions, is plotted against dose and error bars represent SEM.

Supplemental table 1: GFP-H1.2 interaction assay.
This table list 48 GFP-H1.2 interacting proteins identified by MS.
Protein names: Name of protein
Gene names: Name of gene
GFP-H1.2/GFP Fw.: Normalized heavy(UV)/Light(Mock) SILAC ratio from experiment 1
GFP-H1.2/GFP Rev.: Normalized light(UV)/Heavy(Mock) SILAC ratio from experiment 2
# of ident. pept. fw.: Number of peptides identified for this protein in exp 1
# of ident. pept. rev.: Number of peptides identified for this protein in exp 2

Protein names	Gene names	GFP-H1.2/ GFP Fw.	GFP-H1.2/ GFP Rev.	# of ident. pept. fw.	# of ident. pept. rev.
Histone H2B type 1-O;Histone H2B type 1-B;Histone H2B type 2-E	HIST1H2BO	10.66	13.17	22	20
Activated RNA polymerase II transcriptional coactivator p15	SUB1	6.40	4.46	4	3
Histone H1.2;Histone H1.3	HIST1H1C	5.41	12.80	27	27
Polymerase delta-interacting protein 2	POLDIP2	4.36	0.23	1	1
Barrier-to-autointegration factor	BANF1	4.02	5.46	8	7
Bromodomain-containing protein 3	BRD3	3.80	1.56	3	9
Histone H3.3;Histone H3.3C;Histone H3	H3F3A	3.75	4.64	12	15
Histone H3.2;Histone H3.1t	HIST2H3A	3.70	12.51	14	15
Coiled-coil domain-containing protein 86	CCDC86	3.60	5.85	15	14
Inhibitor of growth protein 4	ING4	3.53	3.54	3	3
Poly [ADP-ribose] polymerase 1	PARP1	3.30	8.08	59	65
High mobility group protein HMG-I/HMG-Y	HMGA1	3.30	10.52	3	2
Histone H2A.Z;Histone H2A.V;Histone H2A	H2AFZ	3.28	17.17	7	6
Histone H4	HIST1H4A	3.28	9.97	20	22
Histone H3.1	HIST1H3A	3.20	3.39	14	15
Histone H1.5	HIST1H1B	3.20	9.28	22	19
Non-histone chromosomal protein HMG-14	HMGN1	3.17	NaN	1	1
Fc receptor-like protein 3	FCRL3	3.14	30.35	1	1
Histone H2A.x	H2AFX	3.12	3.55	8	5
Core histone macro-H2A.1;Histone H2A	H2AFY	3.11	9.62	19	20
Thymocyte nuclear protein 1	THYN1	3.11	3.24	7	5
Exportin-2	CSE1L	3.08	2.14	2	23
Histone H1.4	HIST1H1E	3.06	18.11	27	24
Zinc finger protein 644	ZNF644	3.06	2.42	3	5

Protein names	**Gene names**	**GFP-H1.2/ GFP Fw.**	**GFP-H1.2/ GFP Rev.**	**# of ident. pept. fw.**	**# of ident. pept. rev.**
Chromatin accessibility complex protein 1	CHRAC1	3.05	6.83	2	2
Ceramide glucosyltransferase	UGCG	3.03	NaN	1	0
	NUMA1	3.03	3.31	101	122
UPF0688 protein C1orf174	C1orf174	2.96	21.60	2	2
TATA-box-binding protein	TBP	2.95	2.75	2	2
Chromodomain Y-like protein 2	CDYL2	2.93	4.98	7	7
GTP-binding nuclear protein Ran	RAN	2.93	8.48	12	12
Methyl-CpG-binding protein 2	MECP2	2.93	2.42	4	3
Polyhomeotic-like protein 2	PHC2	2.88	3.58	2	4
Protein MB21D1	MB21D1	2.85	4.08	18	10
Zinc finger protein 280C	ZNF280C	2.82	NaN	5	3
X-ray repair cross-complementing protein 5	XRCC5	2.82	5.16	34	37
Chromobox protein homolog 5	CBX5	2.80	5.50	9	9
WD repeat-containing protein 5	WDR5	2.79	2.30	8	11
PC4 and SFRS1-interacting protein	PSIP1	2.79	8.06	17	19
X-ray repair cross-complementing protein 6	XRCC6	2.78	5.43	35	41
Zinc finger protein 444	ZNF444	2.77	NaN	1	1
Histone H1.0	H1F0	2.75	9.72	7	8
Protein SSX1;Protein SSX8	SSX1	2.75	0.63	2	3
Cytoskeleton-associated protein 2	CKAP2	2.74	NaN	10	5
High mobility group nucleosome-binding domain-containing protein 5	HMGN5	2.73	11.11	10	10
Histone H1x	H1FX	2.71	7.72	6	7
N-alpha-acetyltransferase 40	NAA40	2.71	6.52	5	8
Protein SET	SET	2.70	5.51	6	7

REFERENCES

1. Jackson, S.P. and J. Bartek, The DNA-damage response in human biology and disease. Nature, 2009. 461(7267): p. 1071-8.
2. Hoeijmakers, J.H., DNA damage, aging, and cancer. N Engl J Med, 2009. 361(15): p. 1475-85.
3. Riley, T., et al., Transcriptional control of human p53-regulated genes. Nat Rev Mol Cell Biol, 2008. 9(5): p. 402-12.
4. Soria, G., S.E. Polo, and G. Almouzni, Prime, repair, restore: the active role of chromatin in the DNA damage response. Molecular Cell, 2012. 46(6): p. 722-34.
5. Smerdon, M.J., DNA repair and the role of chromatin structure. Curr Opin Cell Biol, 1991. 3(3): p. 422-8.
6. Mandemaker, I.K., W. Vermeulen, and J.A. Marteijn, Gearing up chromatin: A role for chromatin remodeling during the transcriptional restart upon DNA damage. Nucleus, 2014. 5(3): p. 203-210.
7. Lans, H., J.A. Marteijn, and W. Vermeulen, ATP-dependent chromatin remodeling in the DNA-damage response. Epigenetics & Chromatin, 2012. 5.
8. Escargueil, A.E., et al., What histone code for DNA repair? Mutat Res, 2008. 658(3): p. 259-70.
9. Dinant, C., et al., Enhanced chromatin dynamics by FACT promotes transcriptional restart after UV-induced DNA damage. Mol Cell, 2013. 51(4): p. 469-79.
10. Yuan, J., R. Adamski, and J. Chen, Focus on histone variant H2AX: to be or not to be. FEBS Lett, 2010. 584(17): p. 3717-24.
11. Park, J.H., et al., Mammalian SWI/SNF complexes facilitate DNA double-strand break repair by promoting gamma-H2AX induction. EMBO J, 2006. 25(17): p. 3986-97.
12. Adam, S., S.E. Polo, and G. Almouzni, Transcription Recovery after DNA Damage Requires Chromatin Priming by the H3.3 Histone Chaperone HIRA. Cell, 2013. 155(1): p. 94-106.
13. Murga, M., et al., Global chromatin compaction limits the strength of the DNA damage response. J Cell Biol, 2007. 178(7): p. 1101-8.
14. Nishiyama, M., et al., CHD8 suppresses p53-mediated apoptosis through histone H1 recruitment during early embryogenesis. Nat Cell Biol, 2009. 11(2): p. 172-82.
15. Thorslund, T., et al., Histone H1 couples initiation and amplification of ubiquitin signalling after DNA damage. Nature, 2015. 527(7578): p. 389-93.
16. Kato, K., M. Okuwaki, and K. Nagata, Role of Template Activating Factor-I as a chaperone in linker histone dynamics. J Cell Sci, 2011. 124(Pt 19): p. 3254-65.
17. Li, M., H. Guo, and Z. Damuni, Purification and characterization of two potent heat-stable protein inhibitors of protein phosphatase 2A from bovine kidney. Biochemistry, 1995. 34(6): p. 1988-96.
18. Christensen, D.J., et al., SET oncoprotein overexpression in B-cell chronic lymphocytic leukemia and non-Hodgkin lymphoma: a predictor of aggressive disease and a new treatment target. Blood, 2011. 118(15): p. 4150-8.
19. Hung, M.H. and K.F. Chen, Reprogramming the oncogenic response: SET protein as a potential therapeutic target in cancer. Expert Opin Ther Targets, 2017. 21(7): p. 685-694.
20. Loven, M.A., et al., A novel estrogen receptor alpha-associated protein, template-activating factor ibeta, inhibits acetylation and transactivation. Mol Endocrinol, 2003. 17(1): p. 67-78.
21. Seo, S.B., et al., Regulation of histone

acetylation and transcription by inhat, a human cellular complex containing the set oncoprotein. Cell, 2001. 104(1): p. 119-130.

22. Gamble, M.J., et al., The histone chaperone taf-i/set/inhat is required for transcription in vitro of chromatin templates. mol Cell Biol, 2005. 25(2): p. 797-807.
23. Okuwaki, M. and K. Nagata, Template activating factor-i remodels the chromatin structure and stimulates transcription from the chromatin template. J Biol Chem, 1998. 273(51): p. 34511-34518.
24. Zhang, Q., et al., Eviction of linker histone H1 by NAP-family histone chaperones enhances activated transcription. Epigenetics Chromatin, 2015. 8: p. 30.
25. Dunkern, T.R., G. Fritz, and B. Kaina, Ultraviolet light-induced DNA damage triggers apoptosis in nucleotide excision repair-deficient cells via Bcl-2 decline and caspase-3/-8 activation. Oncogene, 2001. 20(42): p. 6062-6038.
26. Limsirichaikul, S., et al., A rapid non-radioactive technique for measurement of repair synthesis in primary human fibroblasts by incorporation of ethynyl deoxyuridine (EdU). Nucleic Acids Res, 2009. 37(4): p. e31.
27. Nakazawa, Y., et al., A semi-automated non-radioactive system for measuring recovery of RNA synthesis and unscheduled DNA synthesis using ethynyluracil derivatives. DNA Repair (Amst), 2010. 9(5): p. 506-16.
28. Kalousi, A., et al., The nuclear oncogene SET controls DNA repair by KAP1 and HP1 retention to chromatin. Cell Rep, 2015. 11(1): p. 149-63.
29. Hanasoge, S. and M. Ljungman, H2AX phosphorylation after UV irradiation is triggered by DNA repair intermediates and is mediated by the ATR kinase. Carcinogenesis, 2007. 28(11): p. 2298-304.
30. Rogakou, E.P., et al., DNA double-stranded breaks induce histone H2AX phosphorylation on serine 139. J Biol Chem, 1998. 273(10): p. 5858-68.
31. Ward, I.M. and J. Chen, Histone H2AX is phosphorylated in an ATR-dependent manner in response to replicational stress. J Biol Chem, 2001. 276(51): p. 17759-62.
32. Mogi, S. and D.H. Oh, gamma-H2AX formation in response to interstrand crosslinks requires XPF in human cells. DNA Repair (Amst), 2006. 5(6): p. 731-40.
33. Zhang, Y., et al., Oxidative stress-induced DNA damage of mouse zygotes triggers G2/M checkpoint and phosphorylates Cdc25 and Cdc2. Cell stress Chaperones, 2016. 21(4): p. 687-96.
34. Marteijn, J.A., et al., Nucleotide excision repair-induced H2A ubiquitination is dependent on MDC1 and RNF8 and reveals a universal DNA damage response. J Cell Biol, 2009. 186(6): p. 835-47.
35. Beuzer, P., J.P. Quivy, and G. Almouzni, Establishment of a replication fork barrier following induction of DNA binding in mammalian cells. Cell Cycle, 2014. 13(10): p. 1607-16.
36. Guleria, A. and S. Chandna, ATM kinase: Much more than a DNA damage responsive protein. DNA Repair (Amst), 2016. 39: p. 1-20.
37. Sirbu, B.M. and D. Cortez, DNA damage response: three levels of DNA repair regulation. Cold Spring Harb Perspect Biol, 2013. 5(8): p. a012724.
38. Block, W.D., et al., Selective inhibition of the DNA-dependent protein kinase (DNA-PK) by the radiosensitizing agent caffeine. Nucleic Acids Res, 2004. 32(6): p. 1967-1972.
39. Sarkaria, J.N., et al., Inhibition of ATM and ATR kinase activities by the radiosensitizing agent, caffeine. Cancer Res, 1999. 59(1): p. 1375-82.

40. Rommelaere, J. and M. Errera, The Effect of Caffeine on the Survival of U.V.-irradiated Diploid and Tetraploid Chinese-hamster Cells. Int J Radiat Biol, 1972. 22(3): p. 285-291.
41. Polo, S.E. and G. Almouzni, Chromatin dynamics after DNA damage: The legacy of the access-repair-restore model. DNA Repair (Amst), 2015. 36: p. 114-21.
42. Lieberman, H.B., et al., p53 and RAD9, the DNA Damage Response, and Regulation of Transcription Networks. Radiat Res., 2017. 187(4): p. 424-432.
43. von Lindern, M., et al., Characterization of the translocation breakpoint sequences of two DEK-CAN fusion genes present in t(6;9) acute myeloid leukemia and a SET-CAN fusion gene found in a case of acute undifferentiated leukemia. Genes Chromosomes Cancer, 1992. 5(3): p. 227-34.
44. Damaschke, N.A., et al., Frequent disruption of chromodomain helicase DNA-binding protein 8 (CHD8) and functionally associated chromatin regulators in prostate cancer. Neoplasia, 2014. 16(12): p. 1018-27.
45. Wang, D., et al., Acetylation-regulated interaction between p53 and SET reveals a widespread regulatory mode. Nature, 2016. 538(7623): p. 118-122.
46. Kim, J.Y., et al., Inhibition of p53 acetylation by INHAT subunit SET/TAF-Ibeta represses p53 activity. Nucleic Acids Res, 2012. 40(1): p. 75-87.
47. Campeau, E., et al., A versatile viral system for expression and depletion of proteins in mammalian cells. PLoS One, 2009. 4(8): p. e6529.
48. Aydin, O.Z., et al., Human ISWI complexes are targeted by SMARCA5 ATPase and SLIDE domains to help resolve lesion-stalled transcription. Nucleic Acids Res, 2014. 42(13): p. 8473-85.
49. Schwertman, P., et al., An immunoaffinity purification method for the proteomic analysis of ubiquitinated protein complexes. Anal Biochem, 2013. 440(2): p. 227-36.
50. Cox, J., et al., A practical guide to the MaxQuant computational platform for SILAC-based quantitative proteomics. Nat Protoc, 2009. 4(5): p. 698-705.
51. Cox, J., et al., Andromeda: a peptide search engine integrated into the MaxQuant environment. J Proteome Res, 2011. 10(4): p. 1794-805.
52. Schindelin, J., et al., Fiji: an open-source platform for biological-image analysis. Nat Methods, 2012. 9(7): p. 676-82.

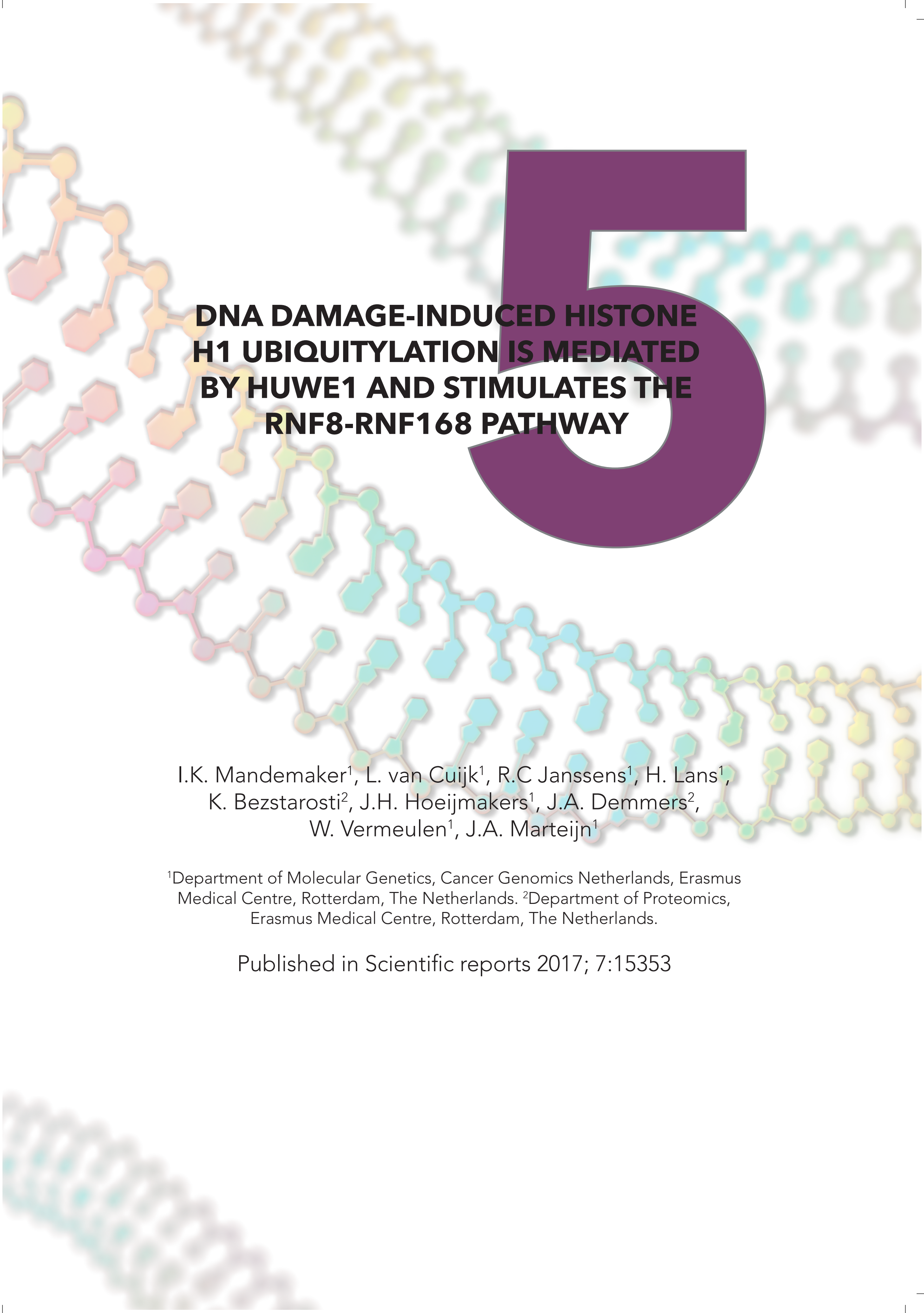

5

DNA DAMAGE-INDUCED HISTONE H1 UBIQUITYLATION IS MEDIATED BY HUWE1 AND STIMULATES THE RNF8-RNF168 PATHWAY

I.K. Mandemaker[1], L. van Cuijk[1], R.C Janssens[1], H. Lans[1],
K. Bezstarosti[2], J.H. Hoeijmakers[1], J.A. Demmers[2],
W. Vermeulen[1], J.A. Marteijn[1]

[1]Department of Molecular Genetics, Cancer Genomics Netherlands, Erasmus Medical Centre, Rotterdam, The Netherlands. [2]Department of Proteomics, Erasmus Medical Centre, Rotterdam, The Netherlands.

Published in Scientific reports 2017; 7:15353

ABSTRACT

The DNA damage response (DDR), comprising distinct repair and signalling pathways, safeguards genomic integrity. Protein ubiquitylation is an important regulatory mechanism of the DDR. To study its role in the UV-induced DDR, we characterized changes in protein ubiquitylation following DNA damage using quantitative di-Gly proteomics. Interestingly, we identified multiple sites of histone H1 that are ubiquitylated upon UV-damage. We show that UV-dependent histone H1 ubiquitylation at multiple lysines is mediated by the E3-ligase HUWE1. Recently, it was shown that poly-ubiquitylated histone H1 is an important signalling intermediate in the double strand break response. This poly-ubiquitylation is dependent on RNF8 and Ubc13 which extend pre-existing ubiquitin modifications to K63-linked chains. Here we demonstrate that HUWE1-depleted cells showed reduced recruitment of RNF168 and 53BP1 to sites of DNA damage, two factors downstream of RNF8-mediated histone H1 poly-ubiquitylation, while recruitment of MDC1, which act upstream of histone H1 ubiquitylation, was not affected. Our data show that histone H1 is a prominent target for ubiquitylation after UV-induced DNA damage. Our data are in line with a model in which HUWE1 primes histone H1 with ubiquitin to allow ubiquitin chain elongation by RNF8, thereby stimulating the RNF8-RNF168-mediated DDR.

INTRODUCTION

DNA integrity is constantly threatened by endogenous and exogenous DNA damaging agents. DNA damage interferes with transcription and replication, causing mutations, chromosomal aberrations and cell death, which may eventually induce malignant transformation and aging [1]. To counteract these deleterious effects cells have evolved an intricate network called the DNA damage response (DDR). This consists of signalling pathways that regulate cell cycle checkpoints and apoptosis, and a set of highly specialized DNA repair mechanisms each capable of repairing a specific subset of DNA lesions. UV-induced helix distorting lesions are typically repaired by nucleotide excision repair (NER) [2]. Helix distorting lesions located at any position in the genome are recognized by the global genome repair (GG-NER) proteins XPC and the UV-DDB complex. DNA lesions in the transcribed strand of active genes that cause stalling of RNA polymerase II initiate transcription-coupled repair (TC-NER). After damage recognition the DNA helix surrounding the lesion is unwound by TFIIH, which together with XPA verifies the lesion [3-6]. Next, RPA stabilizes the repair complex and positions the endonucleases XPG and ERCC1/XPF to excise the damaged DNA [7]. Before the single stranded DNA gap is filled by DNA synthesis by PCNA and the DNA polymerases δ, ε or κ [8] it activates ATR signalling, which subsequently results in phosphorylation of histone H2AX on serine 139 (γH2AX) [9-11]. Phosphorylation of H2AX is a major DDR signalling event initiating the recruitment of many DDR-factors to activate cell cycle checkpoints and stimulate repair. This is induced by many types of genomic insults, such as DNA double strand breaks (DSBs) and stretches of ssDNA following replication fork stalling or NER-mediated excision [12, 13]. MDC1 is directly recruited to γH2AX and functions as a scaffold protein crucial for the recruitment of many downstream DDR factors, such as RNF8, 53BP1 and BRCA1 [10, 14, 15].

The UV-induced DDR (UV-DDR) likely controls the successive reaction steps of NER and signalling pathways and regulates proper functioning of the involved proteins. A growing number of different post translational modifications (PTMs) have been reported in response to UV exposure, including phosphorylation [16], ubiquitylation [17, 18], SUMOylation [19-21] and PARylation [22, 23], likely to allow swift and reversible regulation of the UV-DDR. For example, the UV-damage-specific CRL4DDB2 E3-ligase complex, containing DDB1, DDB2, Cul4 and RBX1, ubiquitylates the GG-NER damage recognition factors DDB2 and XPC [24]. However, not only NER factors are regulated by ubiquitylation, also histones H2A [25, 26], H3 and H4 [27] are ubiquitylated in response to UV, events dependent on the CRL4DDB2 complex and other NER factors. This ubiquitylation of histones results in destabilization of nucleosomes thereby stimulating NER [26]. In addition, histone H2A is ubiquitylated in the RNF8-mediated DDR signalling pathway leading to the recruitment of downstream factors, such as 53BP1 and BRCA1 [10]. In contrast, UV damage-induced stalling of RNA polymerase 2 triggers Ubp8 and Ubp10-dependent deubiquitylation of histone H2B, which is suggested to stimulate repair of lesions in actively transcribed genes [28].

To identify UV-induced changes in protein ubiquitylation in an unbiased manner, we performed an enrichment procedure for ubiquitylated peptides [29] in combination with quantitative proteomics. Tryptic digestion of ubiquitylated proteins results in specific peptides containing a Lys-ε-Gly-Gly (di-Gly) remnant, i.e. the two C-terminal ubiquitin glycine residues covalently attached to the ε-amino group of ubiquitin modified lysines. Ubiquitylated peptides can be enriched by immunopurification using antibodies that specifically recognize this di-Gly remnant, which will increase the identification efficiency of ubiquitylation sites on proteins by MS [29-31]. Using this approach we identified histone H1 as one of the most UV-induced ubiquitylated proteins, with multiple UV-induced ubiquitylation sites. A significant part of these histone H1 ubiquitylation events is mediated by the E3 ligase HUWE1. Recently, also Ubc13 and RNF8 have been shown to ubiquitylate histone H1 at DSBs leading to the recruitment of RNF168 and 53BP1 [32]. RNF8 generates K63 linked poly-ubiquitin chains on H1, most likely on pre-existing ubiquitylation sites [32]. Based on this, we propose a model in which HUWE1 primes histone H1 by ubiquitylation to provide substrates on which RNF8 can generate poly-ubiquitin chains. In line with this model, depletion of HUWE1 results in a reduced damage signalling, as shown by the decreased recruitment of RNF168 and 53BP1 to sites of DNA-damage, while MDC1 and RNF8 remained unaffected, indicating that HUWE1 affects the RNF8-RNF168 pathway downstream of RNF8.

RESULTS

Histone H1 is a major target of UV-induced ubiquitylation

To identify differentially ubiquitylated proteins in response to UV-induced DNA damage we isolated di-Gly modified peptides from mock treated, light (K0R0) labelled U2OS cells and from UV-irradiated (16 J/m^2), heavy (K6R10) labelled U2OS cells using an anti-Lys-ε-Gly-Gly antibody (Supplemental Fig. S1a). Di-Gly enriched peptide mixtures were analysed by LC-MS/MS. Immunoprecipitation with the di-Gly antibody enriched the amount of identified ubiquitylated peptides to 35% of the total amount of identified peptides (Supplemental table S1).

Three independent replicate experiments were performed and peptides were identified and quantified using MaxQuant software [33]. Within these experiments 5467 specific ubiquitylation sites in 3393 proteins were quantified. In total 250 di-Gly-modified peptides showed an increased abundance (UV/mock Log$_2$ SILAC ratio >0.75) in response to UV and 179 di-Gly peptides were found less (UV/mock Log$_2$ SILAC ratio <-0.75) after UV (Supplemental Fig. S1b-c and supplemental table S1). We identified several peptides from proteins that were previously described to be ubiquitylated in response to DNA damage, including XPC [19, 24], DDB2 [34], and FANCD2 [35] (Supplemental Fig. S1c), providing the proof of principle of this approach. While analysis of di-Gly modified peptides cannot reveal whether a protein is modified with a mono-ubiquitin or with a linkage-specific ubiquitin chain, the relative abundance of site-specific di-Gly modified ubiquitin peptides, which are indicative for the types of ubiquitin chains formed, can be quantified. In line with previously reported data [36, 37], we observed a 1.5 fold UV-induced increase in di-Gly modified ubiquitin peptides at lysine 6 (K6), while the abundance of all other di-Gly modified ubiquitin peptides remained largely unaffected (Supplemental Fig. S1d). This suggests that the overall amount of endogenous K6-linked ubiquitin chains is increased after UV-induced DNA damage, indicative for a role of this atypical ubiquitin chain [38] in the UV-DDR. Altogether these data show the validity of our approach to isolate, identify and quantify UV-induced ubiquitylated peptides.

To determine which biological pathways are regulated by ubiquitin in response to UV-irradiation, proteins containing UV-induced ubiquitylation sites were subjected to gene ontology (GO) enrichment analysis. As expected, the functional protein network with the GO-term ‘cellular response to DNA damage stimulus’ was enriched, as represented by several DNA repair proteins. In addition the GO-term ‘chromosome organization’ was enriched (Supplemental Fig. S1e). Interestingly, this biological pathway is mainly represented by several variants of the linker histone H1. Histone H1 functions in chromatin compaction by binding to the nucleosome near the DNA entry and exit point [39]. Multiple histone H1 variants are among the proteins that were identified with the highest fold increase in ubiquitylation in response to UV (Figure 1a). As the globular domain of histone H1 is highly conserved, it is difficult to distinguish for each identified peptide from which H1 variant it originates. However, we do find variant-specific peptides that are more ubiquitylated upon UV-damage for histone H1.0, H1.1, H1.2 and H1.4, indicating that UV-induced ubiquitylation is probably occurring on most histone H1 variants (Figure 1b). Histone H1 peptides not modified by ubiquitin do not change in response to UV (UV/mock $\log_2$ SILAC ratio between 0.75 and -0.75) (Supplemental table S1), indicating that the increase in di-Gly modified histone H1 peptides is caused by increased ubiquitylation, rather than increased histone H1 expression levels. In contrast to histone H1, the SILAC ratios of identified ubiquitylated peptides derived from core histones were barely changed after UV-damage (Figure 1b). However, we do find a loss of H4K60Ub and several histone H2B sites to have reduced ubiquitylation levels after UV irradiation, in line with the described H2B deubiquitylation after RNA polymerase 2 stalling in yeast [28] (Figure 1b). Of note, previous described damage-induced core histone ubiquitylation sites [25-27, 40, 41] were not identified. This might be caused by the very short peptides resulting from tryptic digestion of the lysine and arginine rich histones, which cannot be identified by MS. Interestingly, while thus far most DDR-associated ubiquitylation events on core histones are site-specific, e.g. H2A ubiquitylation on K13/15 [41] and K119 [26], we identified multiple ubiquitylation sites within histone H1, of which almost all are highly UV-responsive, suggesting that histone H1 ubiquitylation is less site-specific (Figure 1b-c). our data show that histone H1 is one of the major targets for ubiquitylation after UV-damage and is the most ubiquitin regulated histone protein.

To validate the UV-induced histone H1 ubiquitylation, as detected by quantitative MS, FLAG-tagged histone H1.2 (FLAG-H1.2) and 6xHis-tagged ubiquitin (His-Ub) were transiently expressed in U2OS cells. Transfected cells were mock treated or UV-irradiated (20 J/m^2) and lysed at the indicated time points (Figure 1d) in a denaturing buffer to disrupt protein-protein interactions and inactivate the 26S proteasome and deubiquitylating enzymes. His-tagged ubiquitylated proteins were isolated and equal pulldown efficiency was confirmed by western blot (Figure 1d, lower panel). Next, the ubiquitylation status of histone H1.2 following UV damage was addressed using anti-FLAG staining. Interestingly, three FLAG-H1.2 bands, differing approximately 8 kDa from each other in size, were identified in the non-irradiated sample (Figure 1d, upper right panel). As they specifically co-purify with His-tagged ubiquitin, these larger bands most likely represent histone H1 species a

Protein name	SILAC ratio UV/mock
XPC	5.83
ZNF280C	3.16
MIPEP	2.70
CETN1/CETN2	2.40
Histone H1.1	**2.16**
FAM111A	2.12
GKAP1	2.06
RPS10	2.05
TRAF2	1.97
RPA3	1.93
Histone H1.4/ H1.3	**1.93**
HLA-A	1.92

c

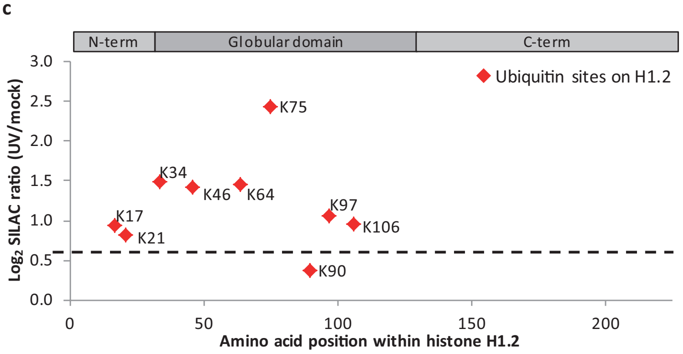

b

Histone	Lysine	Log_2 SILAC ratio (UV/mock)
H1.0	59	0.71
	82	2.02
H1.1	120	1.17
	129	1.11
H1.2	17	0.92
	21	0.80
H1.4	17	1.33
	21	1.24
H1.2-3-4	34	1.47
	46	1.40
H1.1-2-3-4	64	1.43
	75	2.42
H1.1-2-3-4-5	90	0.36
	97	1.05
	106	0.95

Histone	Lysine	Log_2 SILAC ratio (UV/mock)
H2A	96	-0.07
H2AX	120	-0.10
	128	0.25
H2AZ	116	-0.62
	121	-0.02
	122	-0.02
	126	-0.03
H2B	6	-0.19
	12	-0.83
	47	-0.36
	58	0.46
	109	-0.24
	117	-0.75
	121	-0.66
H3.1-2 /H3.3	19	-0.18/-0.18
	24	0.08/0.08
	28	-0.32/-0.23
	37	-0.71/-0.39
	38	-0.66/-0.30
	57	0.27/0.27
	80	-0.10/-0.10
	123	-0.73/-0.73
H4	32	0.09
	60	-1.15
	78	0.43
	80	0.27
	92	0.11

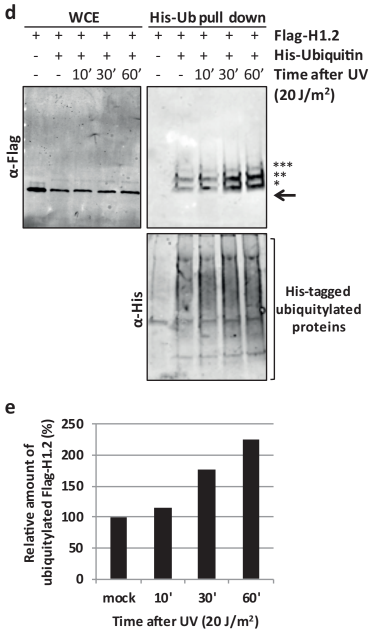
d
WCE
His-Ub pull down
+ + + + + + + + + +
Flag-H1.2
- + + + + - + + + +
His-Ubiquitin
- - 10' 30' 60' - - 10' 30' 60'
Time after UV (20 J/m²)
α-Flag
***
**
*
α-His
His-tagged ubiquitylated proteins
e
250
200
150
100
50
0
Relative amount of ubiquitylated Flag-H1.2 (%)
mock
10'
30'
60'
Time after UV (20 J/m²)

Figure 1: Histone H1 is ubiquitylated in response to UV.
(a) List of the most UV-responsive proteins identified in the di-Gly IPs combined with mass spectrometry in U2OS cells. UV/Mock SILAC ratio is depicted, as determined by Maxquant analysis based on all peptides derived from di-Gly immunopurifications from 3 independent experiments. (b) List of all quantified ubiquitylation sites on histones. Log_2 UV/Mock SILAC ratios as quantified by Maxquant analysis from 3 independent experiments are depicted. More abundant (Log_2>0.75) ubiquitylation sites following UV exposure are shown in red and less abundant (Log_2<-0.75) ubiquitylation sites in blue. When di-Gly modified peptides could not be assigned to specific histone variants due to sequence similarities, all possible variants to which these peptides could be addressed are listed. (c) Graphical representation of the log_2 UV/mock SILAC ratios for the quantified histone H1.2 ubiquitylation sites plotted against

the respective lysine positions within histone H1.2. Quantification by Maxquant analysis from 3 independent experiments. Histone H1 domains are plotted above. Almost all identified ubiquitylation sites are more ubiquitylated in response UV and located within the globular domain of Histone H1.2. (d) U2OS cells transfected with His-Ubiquitin and FLAG-H1.2 were UV-C irradiated at the indicted times before cell lysis. Isolated His-tagged ubiquitylated proteins were analysed by immunoblotting using anti-His and anti-FLAG antibodies as indicated. WCE: whole cell lysate. The arrow (->) indicates the unmodified form of FLAG-H1.2. The asterisks (*) indicate ubiquitin-modified forms of FLAG-H1.2 and the amount of asterisks indicates the expected number of conjugated ubiquitin molecules based on the shift in mass of histone H1. Cropped westernblots are shown, full blots can be found in supplemental information. (e) Quantification of ubiquitylated FLAG-H1.2 signals on western blot after His-Ubiquitin enrichment. Data was normalized to the mock treated signal.

modified with 1, 2 or 3 ubiquitin entities. Since multiple histone H1 ubiquitylation sites were identified by MS (Figure 1b-c), these different ubiquitylated forms might correspond to histone H1 modified with mono-ubiquitin on 1-3 different lysine residues, although H1 poly-ubiquitylation of relative short ubiquitin chains cannot be excluded. The amount of FLAG-H1.2 co-purifying with His-Ub is increased 30 min and 1h after UV irradiation (Figure 1d-e), confirming that histone H1 ubiquitylation is indeed increased in response to UV-irradiation.

The UV-induced histone H1 ubiquitylation is dependent on the E3-ligase HUWE1

Several UV-induced histone modifications are activated by ssDNA gaps mediated by the NER dependent excision of DNA damage, including H2A ubiquitylation [2, 10, 40] and H2AX phosphorylation [9]. To test whether the UV-induced H1 ubiquitylation also depends on NER, we performed di-Gly proteomics experiments and compared XPA-deficient cells (XP-A), in which excision of DNA damage is absent, to XP-A cells rescued by stable GFP-XPA expression [42]. Quantitative mass spectrometry showed that UV-induced H1 ubiquitylation is similar in XPA-deficient and proficient cells, indicating that the H1 ubiquitylation is NER-independent. Some lysines are even slightly more ubiquitylated in XPA deficient cells (Figure 2a & supplemental table S2).

Recently, it was shown that H1 ubiquitylation following double strand break induction was dependent on the E3 ligase RNF8 [32]. Also after UV-induced DNA damage RNF8 is activated [10], however this activation is dependent on NER. This makes RNF8 a less likely candidate to be responsible for our observed H1 ubiquitylation. Another E3-ligase, previously shown to be able to ubiquitylate histone H1 in vitro, is HUWE1 (HECT, UBA, and WWE domain containing protein 1) [43]. In vivo, HUWE1 was found to be involved in the ubiquitylation of histone H2AX in both unperturbed conditions and upon replication stress [44, 45]. In addition, HUWE1 regulates the DDR by targeting different proteins involved in cell cycle checkpoint control, homologous recombination and base excision repair, such as Cdc6 [46], BRCA1 [47], TopBP1 [48] and POLB [49]. To investigate whether HUWE1 is responsible for the UV-induced ubiquitylation of histone H1 we tested the ubiquitylation status of FLAG-H1.2 in cells expressing a doxycycline inducible shRNA targeting HUWE1 [50] (Figure 2d). Interestingly, HUWE1 knockdown resulted in an almost complete absence of the

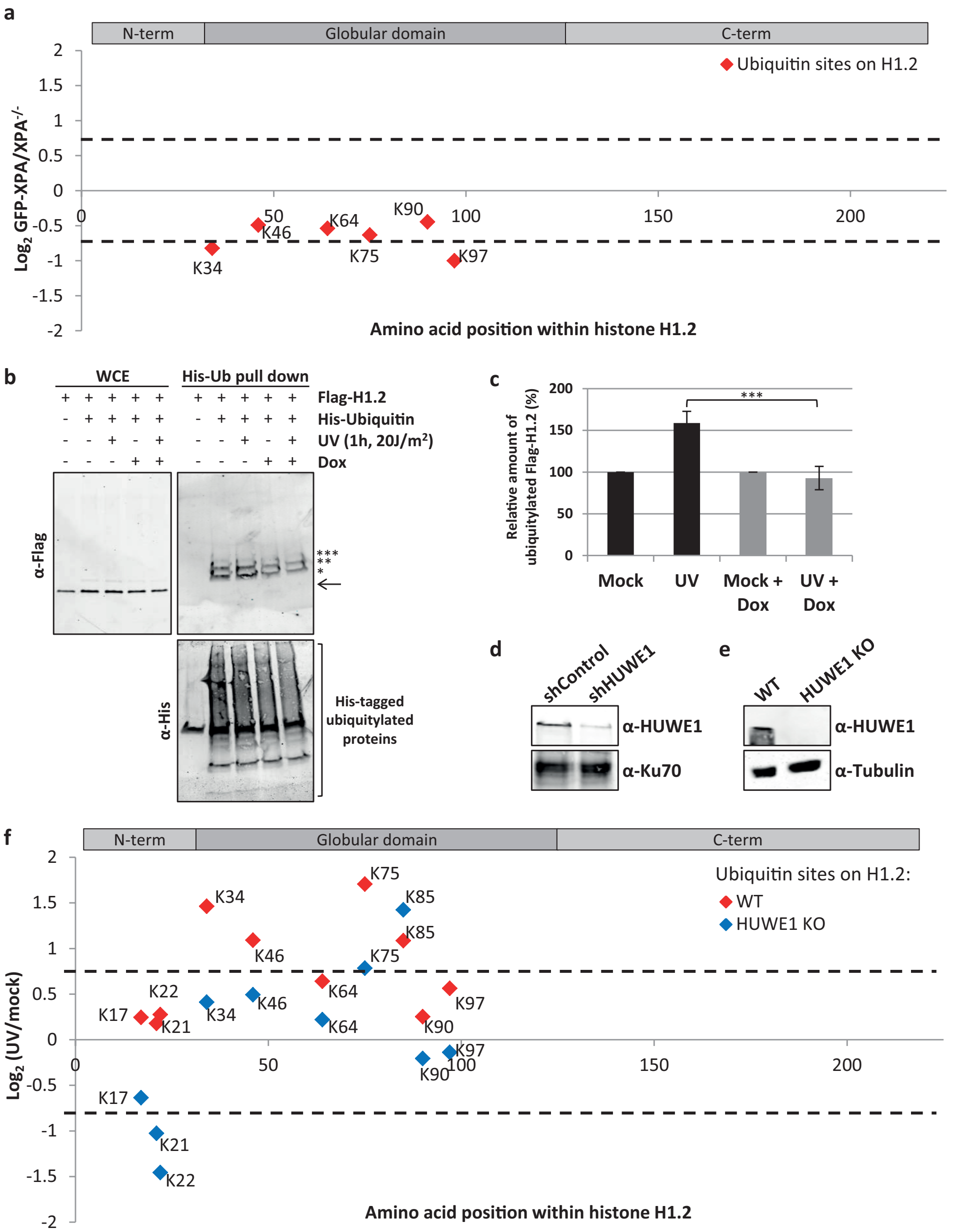

Figure 2: The UV-dependent histone H1 ubiquitylation is dependent on the E3-ligase HUWE1.
(a) Graphical representation of log2 GFP-XPA/XPA-/- SILAC ratio of quantified ubiquitylation sites plotted against the respective lysine positions within histone H1.2. Histone H1 domains are plotted above. Quantification by Maxquant analysis from 1 experiment. (b) U2OS cells were transfected with His-Ub and FLAG-H1.2 were UV-C irradiated (20 J/m^2). To induce expression of the shRNA targeting HUWE1, cells were cultured with doxycycline (1 µg/ml) for 3 days prior to lysis. His-tagged ubiquitylated proteins were isolated 1 hour after UV

exposure and analysed by immunoblotting using anti-His and anti-FLAG antibodies. The arrow (->) indicates the unmodified form of FLAG-H1.2. The asterisks (*) indicate modified forms of FLAG H1.2 and the number of asterisks indicate the expected number of conjugated ubiquitin molecules. Cropped westernblots are shown, full blots can be found in supplemental information. (c) Quantification of ubiquitylated FLAG-H1.2 signals on western blot after His-Ubiquitin enrichment. Data was normalized to the mock treated signals. The average intensity of 8 independent experiments is plotted and error bars represent standard error of the mean. A two-tailed t-test was used (P=0.00498) (d) Western blot showing the knock down efficiency of the shRNA targeting HUWE1. The shHUWE1 is expressed by culturing cells in doxycycline (1 µg/ml) for 3 days. A sample from cells expressing a non-targeting shRNA is taken along as a control. Ku70 staining is used as a loading control. (e) Western blot made from whole cell lysates from WT and HUWE1 KO HeLa cells. Blot was stained with antibodies against HUWE1 and Tubulin. Cropped westernblots are shown, full blots can be found in supplemental information. (f) Graphical representation of $\log_2$ UV/mock SILAC ratio of quantified ubiquitylation sites within histone H1.2 in WT (red) or HUWE1 KO (blue) cells. Quantification by Maxquant analysis from 2 independent experiments. Histone H1 domains are plotted above.

UV-induced Flag-H1.2 ubiquitylation (Figure 2b-c). To exclude doxycycline-induced effects on H1 ubiquitylation we performed a similar experiment using shControl and shHUWE1 cells, both treated with doxycycline (Supplemental Fig S2). Also in this experiment the UV-induced H1 ubiquitylation is absent following HUWE1 depletion. Furthermore, the observed UV-independent decrease of H1 ubiquitylation, suggests a possible role for HUWE1 in the constitutive H1 ubiquitylation as well. To further confirm the HUWE1-dependency on ubiquitylation of endogenous H1 species we used quantitative di-Gly proteomics. UV/mock SILAC ratios of the vast majority of ubiquitylated histone H1 peptides were strongly reduced in HUWE1 KO cells as compared to WT HeLa cells (Figure 2e-f). Of all identified UV-induced ubiquitylation sites, only lysine 85 was not influenced by HUWE1 knock out (KO) (Figure 2f & supplemental table S3), suggesting that probably an additional E3 ligase is involved in H1 ubiquitylation. However, HUWE1 KO severely reduced the levels of histone H1 ubiquitylation on 9 different lysines, indicating that the ubiquitylation levels of histone H1 after UV damage is mainly regulated by HUWE1.

HUWE1 dependent histone H1 ubiquitylation stimulates the RNF8-RNF168 signaling cascade

Although histone H1 was thus far not found to be implicated in the UV-DDR, it was recently described to be modified with K63-linked poly-ubiquitin chains following DSB induction [32]. The E3-ligase RNF8 is recruited to DSBs in a MDC1 and yH2AX-dependent fashion where it, together with the E2-conjugating enzyme UBC13, poly-ubiquitylates histone H1 [32]. The resulting K63-linked poly-ubiquitylated H1 is subsequently bound by the ubiquitin binding domain (UDM1) of the E3-ligase RNF168 which in turn ubiquitylates H2A at lysines K13/K15, stimulating recruitment of downstream factors, such as 53BP1 [32, 41, 51]. Interestingly, using quantitative di-Gly proteomics, it was previously shown that UBC13 depletion barely affects the ubiquitin entities directly coupled to lysines of target proteins [32]. Based on this finding it was hypothesized that UBC13 together with RNF8 mainly conjugates

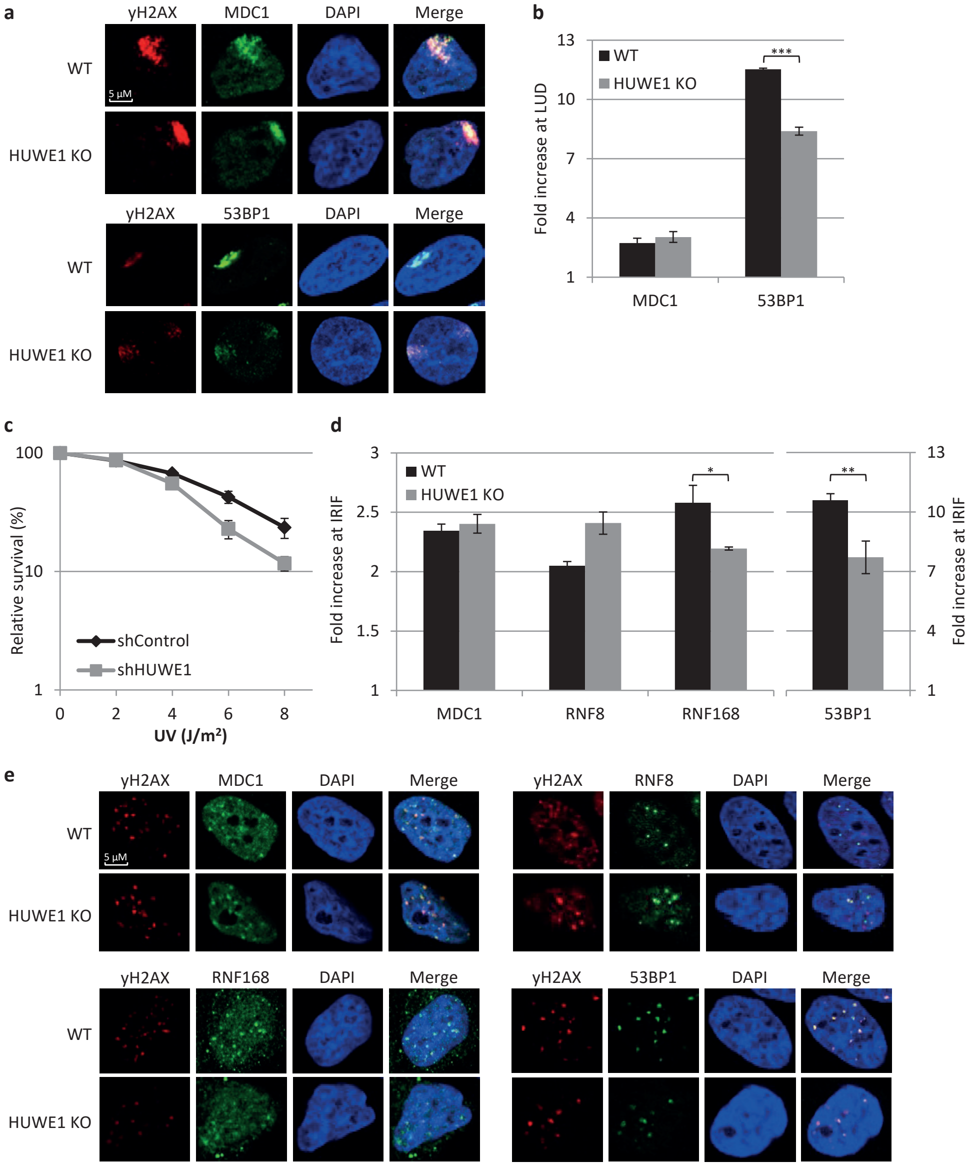

Figure 3: HUWE1 mediated histone H1 ubiquitylation stimulates 53BP1 accumulation to sites of DNA damage.

(a) Representative images of immunofluorescence experiments to study colocalisation of MDC1 (upper panel) or 53BP1 (lower panel) with yH2AX in WT or HUWE1 KO cells. yH2AX is used as damage marker. Local UV damage was induced (60 J/m^2) through a 5 μM micropore filter. Cells were incubated with EdU (20 μM) and fixed 2h after irradiation. (b) Quantification of fold increase of MDC1 and 53BP1 at sites of local UV damage (LUD) in non-S-phase cells. Sites of DNA damage are defined by yH2AX signal. The fold increase is calculated as the ratio of the fluorescent intensity at site of damage over the fluorescent intensity in the rest of the nucleus. Average of 3 independent experiments, with at least 25 cells analysed per experiment, is plotted. Error bars represent SEM. P-value(0.0001) was calculated using a two-tailed t-test. (c) Clonogenic UV-survival experiments in U2OS cells expressing either shControl or shHUWE1. The percentage of surviving colonies is plotted against the UV-C dose. The number of colonies counted at 0 J/m^2 is set as 100% survival. Data represents the average of three independent experiments all done in triplicate and error bars represent standard error of the mean. (d) Quantification of fold increase of MDC1, RNF8, RNF168 and 53BP1 at sites of ionizing radiation-induced foci (IRIF). Double strand breaks are induced by 1 Gy of ionizing radiation and cells were fixed 30 min after damage induction. Sites of DNA damage are defined by yH2AX signal. The fold increase is calculated as the ratio of the fluorescent intensity at sites of damage over the fluorescent intensity in the rest of the nucleus. Average of 3 independent experiments, with at least 75 cells analysed, is plotted. Error bars represent SEM. A two-tailed t-test was used to determine significance of the difference (P= 0.058 (*) and P= 0.018(**)). (e) Representative images of immunofluorescence experiments to study colocalisation of MDC1, RNF8, RNF168 and 53BP1 with yH2AX 30 min after 1Gy in WT or HUWE1 KO cells.

K63-linked ubiquitin chains on pre-existing histone H1 ubiquitin entities. As our ubiquitylation assay suggests that in response to UV damage, HUWE1 mainly stimulates histone H1 modification with either mono-ubiquitin or short poly-ubiquitin chains (Figure 2b), it is possible that HUWE1 provides the initial ubiquitin modification. These ubiquitylated or ‘primed’ histone H1 molecules would then form a substrate for the subsequent poly-ubiquitylation by RNF8 resulting in the accumulation of downstream factors like 53BP1.

Since RNF8-mediated signalling, including H2A ubiquitylation and 53BP1 recruitment, was observed in the UV-DDR [10], it is not unlikely that histone H1 is also K63-linked ubiquitylated by RNF8 after UV damage and that HUWE1 might be involved in priming H1, thereby stimulating this pathway. In line with this hypothesis, immunofluorescence experiments showed reduced levels of 53BP1 at sites of local UV damage (LUD) in HUWE1 KO cells as compared to control cells, while the amount of MDC1, a factor upstream of H1 ubiquitylation, was not affected at LUD (Figure 3a-b). To focus on NER-induced signalling, we used Edu labelling to identify S-phase cells, which were excluded in the analysis to eliminate replication stress generated 53BP1 accumulation at UV-damaged DNA (Supplemental Fig. S3a). Although the intensity of 53BP1 at damaged sites is clearly reduced in HUWE1 KO cells, it is important to note that the colocalization is not lost. This indicates that the DNA damage signalling is not completely absent, as was observed upon knockdown of RNF8 [10], but rather suggests that the signal amplification is affected. Similar results were found in U2OS cells that express a doxycycline inducible shRNA targeting HUWE1 (Supplemental Fig. S3b-c). RNF8 depletion has previously been reported to result in an increased sensitivity to DNA damaging agents [10, 52-54] and therefore we also tested the UV-sensitivity upon HUWE1 depletion using colony survival assays. Both HUWE1 knockdown by dox inducible shRNA expression (Figure 3c) or transient siRNA transfection (Supplemental Fig. S3d-e), each targeting different sequences to exclude off target effects of the siRNA and shRNA, show a mild sensitivity to UV damage compared to control cells.

The RNF8-RFN168-dependent signalling pathway is best described in response to DSBs. To test whether HUWE1 is also involved in the cellular responses to DSBs, we studied the recruitment of the proteins involved in the RNF8-RNF168 pathway to ionizing radiation-induced foci (IRIF) in the presence or absence of HUWE1. Staining for 53BP1 and RNF168, DDR factors that are recruited to DSBs in a histone H1 K63-linked ubiquitylation dependent manner [32], showed reduced signals at IRIF in HUWE1 KO cells compared to control cells (Figure 3d-e). As expected, factors that are recruited upstream of histone H1 poly-ubiquitylation, like MDC1 and RNF8, did not show this reduced recruitment. In line with the effects of HUWE1 during UV-induced signalling, the relative amount of accumulated 53BP1 and RNF168 at IRIF was decreased. However, the number of IRIF showing colocalisation of 53BP1 and RNF168 with γH2AX did not change. Together our data shows that HUWE1 stimulates histone H1 ubiquitylation and affects the recruitment levels of factors downstream of the RNF8-mediated H1 poly-ubiquitylation in response to both UV and IR-induced DNA damage.

DISCUSSION

Our di-Gly quantitative proteomics approach identified H1 as one of the most prominent ubiquitylated proteins following UV-induced DNA damage. This DNA damage-dependent H1 ubiquitylation was found at multiple lysines on histone H1 (Figure 1b-c). H1 ubiquitylation was confirmed by our His-Ub pull downs (Figure 1d) that identified H1 species modified with 1, 2 and 3 ubiquitin entities. Together, with the fact that HUWE1 depletion resulted in a decrease of the UV-induced H1 ubiquitylation (Figure 2), this might suggest that HUWE1 mono-ubiquitylates histone H1 on 1 to 3 different lysine residues, however we cannot exclude that HUWE1 also generates poly-ubiquitin chains on H1. The slower migrating histone H1 bands that were observed in figure 1d and 2a probably do not represent RNF8-mediated K63 poly-ubiquitylation, as these poly-ubiquitin chains display higher molecular weight bands [32]. Therefore, HUWE1-mediated ubiquitylated forms of histone H1 are probably not directly bound by RNF168, as the UDM1-domain of RNF168 preferentially binds to longer ubiquitin chains [32, 55]. Based on our data we propose a model in which HUWE1 is important for the initial damage-induced ubiquitylation of histone H1. This H1 'priming' by ubiquitylation may provide additional substrates for more efficient K63-linked poly-ubiquitylation by UBC13/RNF8, as these proteins most likely elongate pre-existing ubiquitin entities to a K63-linked ubiquitin chain [32, 56-58]. Since HUWE1 is involved in the UV-induced ubiquitylation of multiple lysines on histone H1, it is also likely that chain-extension by RNF8 is not site-specific and might generate ubiquitin chains on several histone H1 sites.

It is not yet known how the E3 ligase activity of HUWE1 towards histone H1 is regulated. Interestingly, UV-induced H1 ubiquitylation is not dependent on active NER (figure 2a). This is in contrast to the activation of the RNF8-RNF168-mediated signalling following UV-induced DNA damage, which is dependent on the presence ssDNA gaps generated by the excision of damaged DNA by the XPF/ERCC1 and XPG endonucleases [2, 9, 10, 40]. This difference in NER-dependency of the HUWE1 and RNF8-mediated H1 ubiquitylation suggests that HUWE1 is presumably activated by a different mechanism than RNF8. Moreover, as our UV-induced H1 ubiquitylation events detected in our di-Gly proteomics approach are NER-independent, these most likely do not represent H1 ubiquitylation events generated by RNF8. Our data further suggest that HUWE1 is also involved in the constitutive ubiquitylation of H1 (Supplemental Fig. S2). The increased H1 ubiquitylation in response to DNA damage (Figure 2b-f) may be derived by activation of HUWE1, which may also explain the previously noted targeting of other DDR proteins by HUWE1 following DNA damage [46-49]. However, the HUWE1-mediated H1 ubiquitylation following DNA damage might also be explained by enhanced accessibility of the targeted lysines of histone H1 due to chromatin changes after DNA damage induction. Of note, recruitment of factors downstream of RNF8 to sites of DNA damage was still observed in the absence of HUWE1, in contrast to RNF8-depleted cells in which recruitment of these factors is almost completely absent [10, 52-54]. However, the amount of accumulation of downstream factors, such as 53BP1, is significantly reduced (Figure 3b-e). While depletion of HUWE1 severely inhibits the DNA-damage-induced histone H1 ubiquitylation, ubiquitylated histone H1 molecules are not completely lost (Figure 2b). These residual HUWE1-independent H1 ubiquitylation may still be sufficient to serve as a substrate for RNF8 and Ubc13. This indicates that HUWE1 can be considered as an important but non-essential player in the RNF8-RNF168 pathway, in which it stimulates signal amplification. Since HUWE1 targets multiple proteins in the DDR, we cannot rule out that these targets might also contribute to the signal amplification. In summary, our data are in line with a two-step model of histone H1 ubiquitylation in response to DNA damage, in which HUWE1 primes histone H1 to stimulate RNF8-Ubc13-mediated K63-linked ubiquitylation and adds an extra player to the ubiquitin-regulated DNA damage-induced signalling pathway [59, 60] (Figure 4).

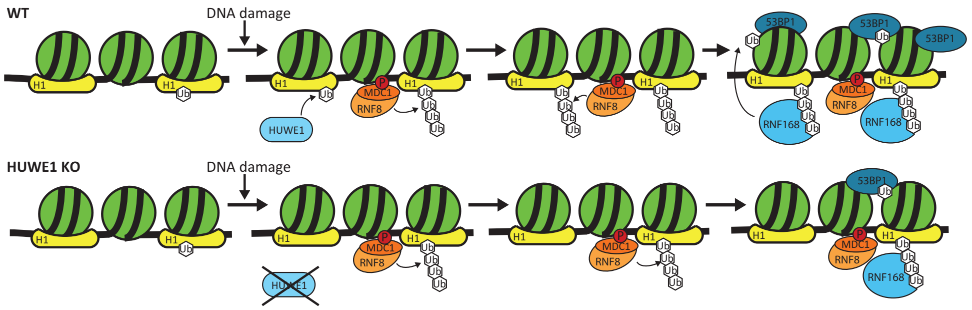

Figure 4: UV-induced H1 ubiquitylation is mediated by HUWE1 and stimulates the RNF8-RNF168 pathway.

Model of HUWE1 functioning in the DNA damage-induced ubiquitin pathway. HUWE1 ubiquitylates histone H1, with a mono-ubiquitin or short poly-ubiquitin chain, in response to DNA damage, thereby providing additional substrates for RNF8-mediated K63-linked poly-ubiquitylation. These K63-chains are recognized and bound by RNF168 which ubiquitylates histone H2A at lysine K13/15, stimulating the recruitment of downstream factors like 53BP1. P=phosphorylation of H2AX, Ub=ubiquitylation.

METHODS

Cell culture

All cells were cultured in DMEM/F10 supplemented with 10% fetal calf serum (FCS) and 1% penicillin-streptomycin (PS, P0781 Sigma) at 37°C and 5% CO$_2$ in a humidified incubator. XP2OS (sv40) cells and the functionally complemented GFP-XPA expressing XP20S cells were described earlier [42]. For SILAC labeling, cells were cultured in DMEM deficient in lysine, arginine and L-glutamine (PAA), supplemented with 10% dialyzed fetal calf serum (Invitrogen), PS and ultra-glutamine (Lonza). Cells were grown in medium containing either 73 μg/ml light [^{12}C6]-lysine and 42 μg/ml [^{12}C6, ^{14}N4]-arginine (Sigma) or similar concentrations of heavy [^{13}C6]-lysine or [^{13}C6, ^{15}N2]-lysine and [^{13}C6, ^{15}N4]-arginine (Cambridge Isotope Laboratories) for at least 10 cell doublings. HUWE1 KO HeLa cells were a kind gift of the Moldovan lab [33] and cultured in 3% oxygen incubators. The U2OS cells expressing shRNA targeting HUWE1 were a kind gift from the lab of Xiaodong Wang and cultured with doxycycline (1 μg/ml) for 3-5 days prior to UV irradiations [34]. SiRNA transfections were performed with RNAiMax (Invitrogen) 3 days prior to UV treatments according to the manufacturer's protocol. The sequences of the used siRNAs were: siControl UGGUUUACAUGUCGACUAA and siHUWE1 GAGUUUGGAGUUUGUGAAGTT [35].

Isolation of ubiquitylated peptides

For di-Gly enrichments either U2OS (Figure 1a-c and supplemental table S1), XP2OS (Figure 2a and supplemental table S2) or HeLa (Figure 2f and supplemental table S3) cells were used. One hour prior to harvesting, SILAC labeled cells were washed with PBS and UV-irradiated (16 J/m^2, 254nm, Philips TUV lamp) or mock treated. Cells were harvested by trypsinization, resuspended in culture medium and cell number was determined using a Z2 coulter particle counter and size analyzer (Beckman coulter). Cells were washed twice with cold phosphate-buffered saline (PBS), and heavy and light labeled cells were mixed in a 1:1 ratio and stored at -80oC until use. Cells were lysed in 7.5 ml denaturing buffer, containing 8 M UREA, 50 mM Tris pH [8.0], 50 mM NaCl, 50 μM MG132 (Biomol), 20 μM PR-619 (LifeSensors) and complete protease inhibitor cocktail (Roche), for 10 min on ice. Following lysis, samples were sonicated 3x for 30 sec with a Soniprep 150 (MSE) and centrifuged at 2500 g at 4°C for 10 min to remove insoluble material. 15-20 mg of protein, as determined by a bicinchoninic acid (BCA) protein assay (Pierce), was reduced with 5 mM dithiothreitol (DTT) and alkylated with 5.5 mM chloroacetamide. Cell lysates were diluted to 4 M urea with 50 mM Tris pH [8.0] and digested with endoproteinase Lys-C (10 μg/mg protein, Wako Chemicals) for 1 hour at RT. Samples were further diluted to 1.6 M urea and incubated overnight at 30°C with proteomics grade trypsin (Roche) at an enzyme to substrate ratio of 1:100. Protease digestion was stopped by addition of trifluoracetic acid (TFA) to a final concentration of 1%. Peptides were purified with 500 mg tC18 SEP-PAK SPE cartridges (Waters) and eluted with 40% acetonitrile (ACN) containing 0.1% TFA. Subsequently, peptides were lyophilized for 48 hours (Scanvac CoolSafe 110-4, Scala Scientific). Lyophilized peptides were dissolved in 1.4 ml of IAP buffer (PTMscan, cell signaling) and incubated with anti-K-ε-GG antibody beads (PTMscan, cell signaling) for 2 hours at 4°C on a rotating unit. Beads were washed three times in IAP buffer followed by two washes in H$_2$O and immunoprecipitated peptides were eluted using 0.1% of trifluoracetic acid (TFA) in H_2O. Eluted peptides were purified using C18 stagetips (ziptipsC18).

Mass spectrometry

Samples were analyzed with a Orbitrap Lumos Tribid mass spectrometer (Thermo Fisher Scientific) or a quadrupole Orbitrap (Q-Exactive, Thermo Fisher Scientific) according to protocols below.

Mass spectra were acquired on an Orbitrap Lumos Tribid mass spectrometer (Thermo Fisher Scientific) coupled to an EASY-nLC 1200 system (Thermo Fisher Scientific). Peptides were separated on an in-house packed 75 μm inner diameter column containing 50 cm CSH130 resin (3.5 μm, 130 Å, Waters) with a gradient of 2–20% (ACN, 0.1% FA) over 150 min at 300 nL/min. The column was kept at 50 °C in an NanoLC oven - MPI design (MS Wil GmbH). For all experiments, the instrument was operated in the data-dependent acquisition (DDA) mode. MS1 spectra were collected at a resolution of 120,000, with an automated gain control (AGC) target of 2E5 and a max injection time of 50 ms. The most intense ions were selected for MS/MS, top speed method 3 seconds cycle time. Precursors were filtered according to charge state (2-7z), and monoisotopic peak assignment. Previously interrogated precursors were dynamically excluded for 70 s. Peptide precursors were isolated with a quadrupole mass filter set to a width of 0.7 Th.

Peptide samples were analyzed on a quadrupole Orbitrap (Q-Exactive, Thermo Fisher Scientific) mass spectrometer equipped with an EASY-nLC 1000 (Thermo Fisher Scientific). Peptide samples were loaded onto ReproSil C18 reversed phase column (20 cm x 75 μm) and eluted with a linear gradient (3 h) from 5 to 80% acetonitrile containing 0.1% formic acid at a constant flow rate of 300 nl/min. Fragmentation of the peptides was performed in a data-dependent acquisition (DDA) mode. MS1 spectra were collected at a resolution of 70,000, with an automated gain control (AGC) target of 1E6 and a max injection time of 50 ms. The 10 most intense ions were selected for MS/MS. Precursors were filtered according to charge state (2-7z), and monoisotopic peak assignment. Previously interrogated precursors were dynamically excluded for 30 s. Peptide precursors were isolated with a quadrupole mass filter set to a width of 2.0 Th.

Data analysis

Raw data files were analyzed using MaxQuant software (version 1.5.1.0) [36]. MS/MS spectra were searched against the human International protein Index (IPI) database (version 3.68), using Andromeda search engine [37]. Spectra were searched with a mass tolerance of 6 ppm. The specificity was set to trypsin, and a maximum of 4 missed cleavages was allowed. Cysteine carbamidomethylation was set as a fixed modification whereas methionine oxidation, N-terminal protein acetylation and di-glycine-lysine were set as variable modifications in Maxquant analysis. A false discovery rate of 0.05 for peptides and a minimum peptide length of 6 were set. Before data analysis, known contaminants and reverse hits were removed from the modification specific peptide list. Scatter plots of the ubiquitylated peptides were generated using Perseus software (version 1.5.4.1). Ubiquitylation sites that were upregulated in response to UV were subjected to Gene Ontology (GO) enrichment analysis (GO_BP4) using the functional annotation tool of DAVID bioinformatics resources [38]. Enriched terms were sorted by p-value.

Isolation of hexa-His-tagged proteins

U2OS cells (70% confluent, 10cm dish) were transfected with 6xHis-tagged ubiquitin (15 µg) and FLAG-tagged histone H1.2 (5 µg) constructs using X-treme gene HP (Roche), one day before cell lysis according to manufacturer's protocol. One hour before lysis, the cells were treated with 20 J/m^2 UV. Cells were washed in PBS and harvested by scraping in 750 µl denaturing urea buffer (8 M urea, 300 mM NaCl, 50 mM Na_2HPO_4, 0.5% NP-40; pH 8.0) supplemented with 10 µM MG132 (Biomol), 10 mM N-ethylmaleimide (Sigma) and complete protease inhibitor cocktail without EDTA (Roche). Lysates were sonicated 3 times for 10 sec with amplitude 12 and centrifuged at 13,000 g and 4°C for 15 min to remove remaining cell debris. Meanwhile 50 µl of Co^{2+} Sepharose beads slurry was equilibrated 3 times with urea buffer. Cleared lysates were incubated with Co^{2+} Sepharose beads for 2 h at 4°C. Subsequently, beads were washed 4 times with urea buffer for 5 min and centrifuged at 3000 rpm for 1 min. His-tagged proteins were eluted by 20 min incubation with urea buffer containing 500 mM EDTA. Eluents were mixed with Laemmli buffer and separated on a Precast BioRad gel 5-14% and transferred to a PVDF membrane (0.45 µm).

Immunoblotting

Cells were lysed in Leammli buffer, separated on 6% SDS-Page gels and transferred to a PVDF membrane. Membranes were blocked with 5% milk in PBS at RT for 1 h and incubated with primary antibodies for 1-2 h. Primary antibodies used: mouse-anti-6xHis-tag (Qiagen #34660, 1:1000), rabbit-anti-FLAG (Sigma E1804, 1:1000), rabbit-anti-HUWE1 (Bethyl A300-486A-2, 1:1000), rabbit-anti-XPC [39] and goat-anti-Ku70 (Santacruz sc-1487, 1:1000). Alexa Fluor 795 donkey anti-mouse antibodies and Alexa Fluor 680 donkey anti-rabbit (LI-COR Biosciences) were used to visualize the proteins using an infrared imaging system (Odyssey; LI-COR Biosciences).

Immunofluorescence

Cells were grown on coverslips until 70-80% confluency. After PBS washing, local UV damage was inflicted by irradiation through 5 µM micropore filters (Milipore). Directly after UV irradiation cells were incubated with EdU (20 µM) containing medium to visualize cells in S-phase. After 2h the cells were washed in PBS and fixed in 2% paraformaldehyde in PBS containing 0.1% triton-X and permeabilized for 20 min in 0,5% Triton-X in PBS. EdU was visualized with a click-it reaction (Click-it EdU imaging kit, Invitrogen) using a 647 nm fluorescent azide (Biotium) according to manufacturer's protocol. After the EdU labelling procedure, cells were washed in PBS containing 0.5% bovine serum albumin (BSA) and 0.15% glycine and stained with primary antibodies for 2 h at RT. Coverslips were washed three times short and twice for 10 min in 0.1% triton-X in PBS and once in PBS with BSA and glycine and subsequently stained with secondary antibodies labeled with alexa fluorochromes 488 and 555 (Invitrogen) and DAPI (0.1 µg/ml) for 1 h at RT. Coverslips were mounted with Aqua Poly/Mount (Polysciences). In experiments using ionizing radiation, cells were fixed 30 min after 1 Gy in 2% paraformaldehyde in PBS containing 0.1% triton-X and permeabilized in 0,1% Triton-X in PBS. Images were obtained using a LSM700 microscope (Carl Zeiss Microimaging Inc.) equipped with a 63× oil immersion lens

(Plan-apochromat, 1.4 NA) and analyzed using ImageJ software [40]. In short data was analyzed using a macro that first defined the cell nucleus by DAPI signal, then identified damage sites (local UV damage or IR induced foci) by yH2AX signal and finally measured the fluorescent signal of the protein of interest at these sites. EdU positive cells were manually excluded. Antibodies used: mouse-α-yH2AX (1:1000, Millipore 05-636); rabbit-α-53BP1 (1:1000, Santacruz sc-22760); rabbit-α-MDC1 (1:500, Abcam ab11171); rabbit-α-yH2AX (1:1000, Abcam ab11174); mouse-α-RNF8 (1:50, Santacruz sc-271462); mouse-α-RNF168 (1:100, Milipore ABE367).

Clonogenic survival assays

For each condition 500 cells/well were seeded in 6-well plates in triplicate. Cells were irradiated with different doses of UV-C one day after seeding and cultured for five days. The cells were fixed and stained in 50% methanol, 43% water, 7% acetic acid and 0.1% brilliant blue (Sigma). The colonies were counted using GelCountTM (Oxford Optronix, version 1.1.2.0).

Statistics

Each experiment was performed at least three times and mean values and standard error of the means (SEM) are shown. To determine if differences between conditions are significant a two-tailed t-test was used. P-values <0.1 (*), <0.05 (**) and <0.005 (***) were considered as significant different.

ACKNOWLEDGEMENTS

We thank Dr. G.L. Moldovan for providing the HUWE1 KO HeLa cells [33] and Dr. Wang for the inducible shHUWE1 U2OS cell line [34]. We thank the Erasmus MC optical imaging center (OIC) with help with confocal imaging and image analysis. This work was supported by the Dutch Organization for Scientific Research (NWO) TOP Grants of Earth and Life Sciences and ZonMW (912.08.031 and 912.12.132), Dutch Organization for Scientific Research Earth and Life Sciences VIDI grant (846.13.004) and European Research Council Advanced Grant (340988-ERC-ID).

AUTHOR CONTRIBUTIONS

I.K.M. designed and performed the majority of the experiments including diGly proteomics and cell biological experiments, analyzed the data; L.v.C. Initiated the project and designed and performed diGly proteomics experiments. R.C.J. performed cell biological experiments; K.B. and J.A.D. performed and supervised mass spectrometry experiments; H.L. and J.H.H. provided advice; W.V. and J.A.M. designed and supervised the project. I.K.M. and J.A.M. wrote the manuscript. All authors reviewed the manuscript.

SUPPLEMENTAL INFORMATION

Supplemental tables can be found online at**:** https://doi.org/10.1038/s41598-017-15194-y

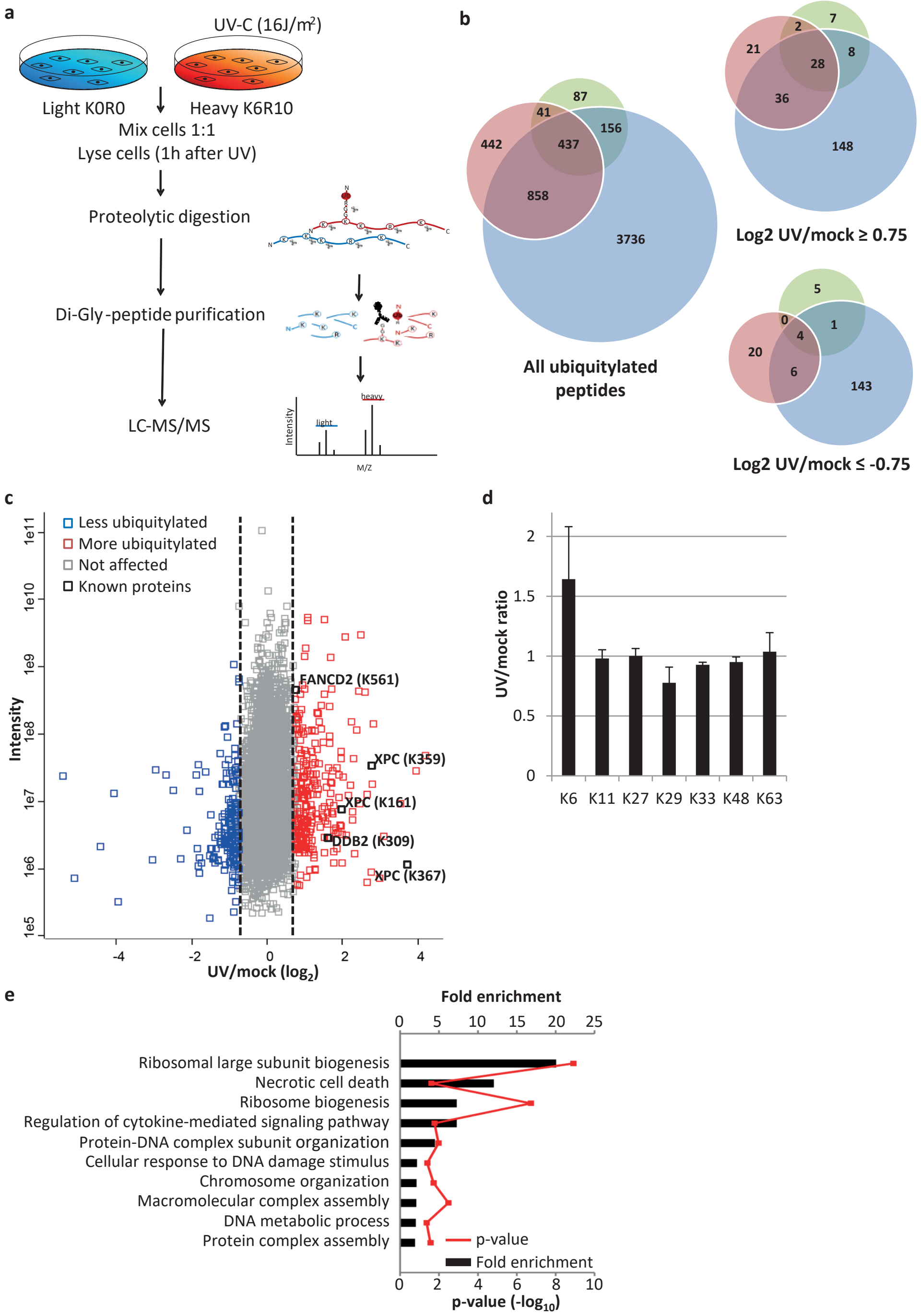

Supplemental figure 1: Isolation of UV-responsive ubiquitylated peptides.
(a) Workflow of SILAC based proteomics approach combined with the isolation of di-Gly peptides to identify UV-responsive ubiquitin sites. Mock treated cells were grown in light (K0R0) medium and UV treated (16J/m^2) cells in heavy (K6R10) medium. One hour after treatments cells were mixed in a 1:1 ratio and lysed in denaturing buffer. Proteins were digested with Lys-C and trypsin after which di-Gly immunopurification was performed. The enriched di-Gly peptides were identified and analysed by LC-MS/MS. (b) Experimental overlap of the identified di-Gly peptides in three biological replicates (experiment #1 red, #2 green and #3 blue). Venn diagrams show the total number of di-Gly peptides identified (left), UV-induced di-Gly sites (top right) and UV-reduced sites (bottom right) quantified in each experiment. (c) Scatter plot with the $\log_2$ SILAC ratio (UV/mock) plotted against the $\log_{10}$ intensity of the identified di-Gly peptides as quantified by Maxquant analysis from 3 independent experiments. Peptides were considered as UV-responsive when its $\log_2$ SILAC ratio was increased or decreased (dotted lines) more than 0.75. Grey: Non-responsive di-Gly peptides; Red: UV-increased ubiquitylated peptides; Blue: UV-reduced ubiquitylated peptides; Black: Increased di-Gly peptides for known UV-dependent ubiquitylated proteins FANCD2, XPC and DDB2. The amino acid position of the modified lysine is shown between brackets. (d) Quantification of the identified di-Gly modified ubiquitin peptides originating from poly-ubiquitin chains, which is a measurement for the abundance of the different ubiquitin chain linkages. Values represent the average of three experiments; error bars indicate SD. (e) Functional annotation of UV-induced ubiquitylation sites ($\log_2$ SILAC ratio >0.75) into biological pathways using DAVID bioinformatics resource. Enriched GO-terms (BP4) (p-value<0.01) are plotted. Bar graph indicates the fold enrichment of biological processes. The fold enrichment defines the ratio between input genes in a pathway over the whole genome in that pathway. The significance (p-value) of the biological pathways was determined by Fisher's exact test and is indicated in red.

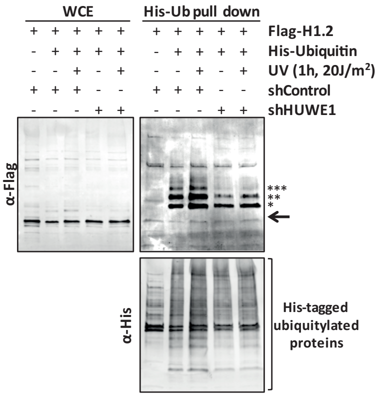
WCE
His-Ub pull down
+ + + + + + + + + + Flag-H1.2
- + + + + - + + + + His-Ubiquitin
- - + - + - - + - + UV (1h, 20J/m²)
+ + + - - + + + - - shControl
- - - + + - - - + + shHUWE1
α-Flag
***
**
*
←
α-His
His-tagged ubiquitylated proteins

Supplemental figure 2: The UV-dependent histone H1 ubiquitylation is dependent on the E3-ligase HUWE1.
U2OS cells, expressing either shControl or shHUWE1, were transfected with His-Ub and FLAG-H1.2 were UV-C irradiated (20 J/m^2). Cells were cultured with doxycycline (1 µg/ml) for 3 days prior to lysis to induce expression of the shRNA. His-tagged ubiquitylated proteins were isolated 1 hour after UV exposure and analysed by immunoblotting using anti-His and anti-FLAG antibodies. The arrow (->) indicates the unmodified form of FLAG-H1.2. The asterisks (*) indicate modified forms of FLAG H1.2 and the number of asterisks indicate the expected number of conjugated ubiquitin molecules based on the shift in mass of histone H1.

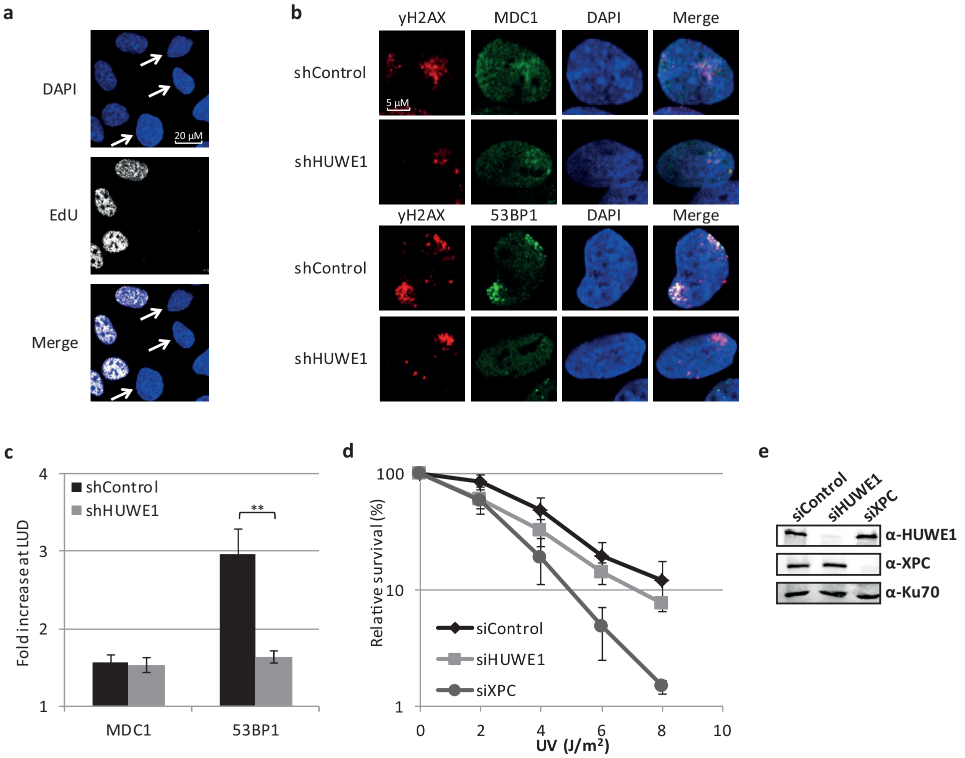

Supplemental figure 3: HUWE1 mediated histone H1 ubiquitylation stimulates 53BP1 accumulation to sites of DNA damage.
(a) Immunofluorescence images showing DAPI and EdU signal in cells treated with EdU (20 µM) for 2 h. Arrows indicate non-S-phase cells. (b) Representative images of immunofluorescence experiments to study colocalisation of MDC1 and 53BP1 with yH2AX in shControl of shHUWE1 expressing cells. Local UV damage was induced (60 J/m^2) through a 5 µM micropore filter. Cells were incubated with EdU (20 µM) and fixed 2h after irradiation.(c) Quantification of fold increase of MDC1 and 53BP1 at sites of local UV damage (LUD). Cells that incorporated high levels of EdU, indicative of S-phase cells, were excluded from analysis. Sites of local UV-induced DNA damage are defined by yH2AX signal. The fold increase is calculated as the ratio of the fluorescent intensity at site of damage over the fluorescent intensity in the rest of the nucleus. Average of 3 independent experiments, in which at least 25 cells were analysed, is plotted. Error bars represent SEM. P-value (0.019) was calculated with a two-tailed t-test. (d) Clonogenic UV-survival experiments in U2OS cells transfected with either siControl, siHUWE1 or siXPC. The percentage of surviving colonies is plotted against the UV-C dose. The number of colonies counted at 0 J/m^2 is set as 100% survival. The data represent the average of three independent experiments, all done in triplicate, and error bars represent standard error of the mean. (e) Western blot showing the knock down efficiency of the siRNAs targeting HUWE1 or XPC. Ku70 is used as a loading control.

REFERENCES

1. Hoeijmakers, J.H., DNA damage, aging, and cancer. N Engl J Med, 2009. 361(15): p. 1475-85.
2. Marteijn, J.A., et al., Understanding nucleotide excision repair and its roles in cancer and ageing. Nat Rev Mol Cell Biol, 2014. 15(7): p. 465-81.
3. Mathieu, N., et al., DNA quality control by a lesion sensor pocket of the xeroderma pigmentosum group D helicase subunit of TFIIH. Curr Biol, 2013. 23(3): p. 204-12.
4. Camenisch, U., et al., Recognition of helical kinks by xeroderma pigmentosum group A protein triggers DNA excision repair. Nat Struct Mol Biol, 2006. 13(3): p. 278-84.
5. Li, C.L., et al., Tripartite DNA Lesion Recognition and Verification by XPC, TFIIH, and XPA in Nucleotide Excision Repair. Mol Cell, 2015. 59(6): p. 1025-34.
6. Sugasawa, K., et al., Two-step recognition of DNA damage for mammalian nucleotide excision repair: Directional binding of the XPC complex and DNA strand scanning. Mol Cell, 2009. 36(4): p. 642-53.
7. de Laat, W.L., et al., DNA-binding polarity of human replication protein A positions nucleases in nucleotide excision repair. Genes Dev, 1998. 12(16): p. 2598-609.
8. Ogi, T., et al., Three DNA polymerases, recruited by different mechanisms, carry out NER repair synthesis in human cells. Mol Cell, 2010. 37(5): p. 714-27.
9. Hanasoge, S. and M. Ljungman, H2AX phosphorylation after UV irradiation is triggered by DNA repair intermediates and is mediated by the ATR kinase. Carcinogenesis, 2007. 28(11): p. 2298-304.
10. Marteijn, J.A., et al., Nucleotide excision repair-induced H2A ubiquitination is dependent on MDC1 and RNF8 and reveals a universal DNA damage response. J Cell Biol, 2009. 186(6): p. 835-47.
11. Marini, F., et al., DNA nucleotide excision repair-dependent signaling to checkpoint activation. Proc Natl Acad Sci U S A, 2006. 103(46): p. 17325-30.
12. Nam, E.A. and D. Cortez, ATR signalling: more than meeting at the fork. Biochem J, 2011. 436(3): p. 527-36.
13. Bartek, J. and J. Lukas, DNA damage checkpoints: from initiation to recovery or adaptation. Curr Opin Cell Biol, 2007. 19(2): p. 238-45.
14. Lukas, J., C. Lukas, and J. Bartek, More than just a focus: The chromatin response to DNA damage and its role in genome integrity maintenance. Nat Cell Biol, 2011. 13(10): p. 1161-9.
15. Zimmermann, M. and T. de Lange, 53BP1: pro choice in DNA repair. Trends Cell Biol, 2014. 24(2): p. 108-17.
16. Bensimon, A., R. Aebersold, and Y. Shiloh, Beyond ATM: the protein kinase landscape of the DNA damage response. FEBS Lett, 2011. 585(11): p. 1625-39.
17. Nouspikel, T., Multiple roles of ubiquitination in the control of nucleotide excision repair. Mech Ageing Dev, 2011. 132(8-9): p. 355-65.
18. van Cuijk, L., W. Vermeulen, and J.A. Marteijn, Ubiquitin at work: The ubiquitous regulation of the damage recognition step of NER. Exp Cell Res, 2014.
19. Poulsen, S.L., et al., RNF111/Arkadia is a SUMO-targeted ubiquitin ligase that facilitates the DNA damage response. J Cell Biol, 2013. 201(6): p. 797-807.
20. Jackson, S.P. and D. Durocher, Regulation of DNA damage responses by ubiquitin and SUMO. Mol Cell, 2013. 49(5): p. 795-807.
21. Bergink, S. and S. Jentsch, Principles of ubiquitin and SUMO modifications in

DNA repair. Nature, 2009. 458(7237): p. 461-7.

22. Sousa, F.G., et al., PARPs and the DNA damage response. Carcinogenesis, 2012. 33(8): p. 1433-40.
23. Pines, A., et al., PARP1 promotes nucleotide excision repair through DDB2 stabilization and recruitment of ALC1. J Cell Biol, 2012. 199(2): p. 235-49.
24. Sugasawa, K., et al., UV-induced ubiquitylation of XPC protein mediated by UV-DDB-ubiquitin ligase complex. Cell, 2005. 121(3): p. 387-400.
25. Kapetanaki, M.G., et al., The DDB1-CUL4ADDB2 ubiquitin ligase is deficient in xeroderma pigmentosum group E and targets histone H2A at UV-damaged DNA sites. Proc Natl Acad Sci U S A, 2006. 103(8): p. 2588-93.
26. Lan, L., et al., Monoubiquitinated histone H2A destabilizes photolesion-containing nucleosomes with concomitant release of UV-damaged DNA-binding protein E3 ligase. J Biol Chem, 2012. 287(15): p. 12036-49.
27. Wang, H., et al., Histone H3 and H4 ubiquitylation by the CUL4-DDB-ROC1 ubiquitin ligase facilitates cellular response to DNA damage. Mol Cell, 2006. 22(3): p. 383-94.
28. Mao, P., et al., UV damage-induced RNA polymerase II stalling stimulates H2B deubiquitylation. Proc Natl Acad Sci U S A, 2014. 111(35): p. 12811-6.
29. Xu, G., J.S. Paige, and S.R. Jaffrey, Global analysis of lysine ubiquitination by ubiquitin remnant immunoaffinity profiling. Nat Biotechnol, 2010. 28(8): p. 868-73.
30. Wagner, S.A., et al., A proteome-wide, quantitative survey of in vivo ubiquitylation sites reveals widespread regulatory roles. Mol Cell Proteomics, 2011. 10(10): p. M111 013284.
31. Kim, W., et al., Systematic and quantitative assessment of the ubiquitin-modified proteome. Mol Cell, 2011. 44(2): p. 325-40.
32. Thorslund, T., et al., Histone H1 couples initiation and amplification of ubiquitin signalling after DNA damage. Nature, 2015. 527(7578): p. 389-93.
33. Cox, J., et al., A practical guide to the MaxQuant computational platform for SILAC-based quantitative proteomics. Nat Protoc, 2009. 4(5): p. 698-705.
34. Matsuda, N., et al., DDB2, the xeroderma pigmentosum group E gene product, is directly ubiquitylated by Cullin 4A-based ubiquitin ligase complex. DNA Repair (Amst), 2005. 4(5): p. 537-45.
35. Garner, E. and A. Smogorzewska, Ubiquitylation and the Fanconi anemia pathway. FEBS Lett, 2011. 585(18): p. 2853-60.
36. Elia, A.E., et al., Quantitative Proteomic Atlas of Ubiquitination and Acetylation in the DNA Damage Response. Mol Cell, 2015. 59(5): p. 867-81.
37. Povlsen, L.K., et al., Systems-wide analysis of ubiquitylation dynamics reveals a key role for PAF15 ubiquitylation in DNA-damage bypass. Nat Cell Biol, 2012. 14(10): p. 1089-98.
38. Kulathu, Y. and D. Komander, Atypical ubiquitylation - the unexplored world of polyubiquitin beyond Lys48 and Lys63 linkages. Nat Rev Mol Cell Biol, 2012. 13(8): p. 508-23.
39. Harshman, S.W., et al., H1 histones: current perspectives and challenges. Nucleic Acids Res, 2013. 41(21): p. 9593-609.
40. Bergink, S., et al., DNA damage triggers nucleotide excision repair-dependent monoubiquitylation of histone H2A. Genes Dev, 2006. 20(10): p. 1343-52.
41. Mattiroli, F., et al., RNF168 ubiquitinates K13-15 on H2A/H2AX to drive DNA damage signaling. Cell, 2012. 150(6): p.

1182-95.
42. Rademakers, S., et al., Xeroderma pigmentosum group A protein loads as a separate factor onto DNA lesions. Mol Biol Cell, 2003. 23(16): p. 2755-67.
43. Liu, Z., R. Oughtred, and S.S. Wing, Characterization of E3Histone, a novel testis ubiquitin protein ligase which ubiquitinates histones. Mol Cell Biol, 2005. 25(7): p. 2819-31.
44. Atsumi, Y., et al., ATM and SIRT6/SNF2H Mediate Transient H2AX Stabilization When DSBs Form by Blocking HUWE1 to Allow Efficient gammaH2AX Foci Formation. Cell Rep, 2015. 13(12): p. 2728-40.
45. Choe, K.N., et al., HUWE1 interacts with PCNA to alleviate replication stress. EMBO Rep, 2016. 17(6): p. 874-86.
46. Hall, J.R., et al., Cdc6 stability is regulated by the Huwe1 ubiquitin ligase after DNA damage. Mol Biol Cell, 2007. 18(9): p. 3340-50.
47. Wang, X., et al., HUWE1 interacts with BRCA1 and promotes its degradation in the ubiquitin-proteasome pathway. Biochem Biophys Res Commun, 2014. 444(4): p. 549-54.
48. Herold, S., et al., Miz1 and HectH9 regulate the stability of the checkpoint protein, TopBP1. EMBO J, 2008. 27(21): p. 2851-61.
49. Parsons, J.L., et al., Ubiquitin ligase ARF-BP1/Mule modulates base excision repair. EMBO J, 2009. 28(20): p. 3207-15.
50. Zhong, Q., et al., Mule/ARF-BP1, a BH3-only E3 ubiquitin ligase, catalyzes the polyubiquitination of Mcl-1 and regulates apoptosis. Cell, 2005. 121(7): p. 1085-95.
51. Bekker-Jensen, S. and N. Mailand, The ubiquitin- and SUMO-dependent signaling response to DNA double-strand breaks. FEBS Lett, 2011. 585(18): p. 2914-9.
52. Mailand, N., et al., RNF8 ubiquitylates histones at DNA double-strand breaks and promotes assembly of repair proteins. Cell, 2007. 131(5): p. 887-900.
53. Kolas, N.K., et al., Orchestration of the DNA-damage response by the RNF8 ubiquitin ligase. Science, 2007. 318(5856): p. 1637-40.
54. Huen, M.S., et al., RNF8 transduces the DNA-damage signal via histone ubiquitylation and checkpoint protein assembly. Cell, 2007. 131(5): p. 901-14.
55. Pinato, S., et al., UMI, a novel RNF168 ubiquitin binding domain involved in the DNA damage signaling pathway. Mol Cell Biol, 2011. 31(1): p. 118-26.
56. Petroski, M.D., et al., Substrate modification with lysine 63-linked ubiquitin chains through the UBC13-UEV1A ubiquitin-conjugating enzyme. J Biol Chem, 2007. 282(41): p. 29936-45.
57. Christensen, D.E., P.S. Brzovic, and R.E. Klevit, E2-BRCA1 RING interactions dictate synthesis of mono- or specific polyubiquitin chain linkages. Nat Struct Mol Biol, 2007. 14(10): p. 941-8.
58. Windheim, M., M. Peggie, and P. Cohen, Two different classes of E2 ubiquitin-conjugating enzymes are required for the mono-ubiquitination of proteins and elongation by polyubiquitin chains with a specific topology. Biochem J, 2008. 409(3): p. 723-9.
59. van Attikum, H. and S.M. Gasser, Crosstalk between histone modifications during the DNA damage response. Trends Cell Biol, 2009. 19(5): p. 207-17.
60. Panier, S. and D. Durocher, Regulatory ubiquitylation in response to DNA double-strand breaks. DNA Repair (Amst), 2009. 8(4): p. 436-43.
61. Cox, J., et al., Andromeda: a peptide search engine integrated into the MaxQuant environment. J Proteome Res, 2011. 10(4): p. 1794-805.
62. Huang da, W., B.T. Sherman, and R.A. Lempicki, Systematic and integrative analysis of large gene lists using DAVID bioinformatics resources. Nat Protoc,

2009. 4(1): p. 44-57.

63. van Cuijk, L., et al., SUMO and ubiquitin-dependent XPC exchange drives nucleotide excision repair. Nat Commun, 2015. 6: p. 7499.
64. Schindelin, J., et al., Fiji: an open-source platform for biological-image analysis. Nat Methods, 2012. 9(7): p. 676-82.

6

DNA DAMAGE-INDUCED REPLICATION STRESS RESULTS IN PA200-PROTEASOME MEDIATED DEGRADATION OF ACETYLATED HISTONES

I.K. Mandemaker[1], I. Kik[1], K. Bezstarosti[2], E. Rijkers[2], H. Lans[1], J.H. Hoeijmakers[1], J.A. Demmers[2], W. Vermeulen[1] and J.A. Marteijn[1]

[1]Department of Molecular Genetics, Cancer Genomics Netherlands, Erasmus University Medical Center, Rotterdam, The Netherlands. [2]Proteomics Centre, Erasmus University Medical Center, Rotterdam, The Netherlands

ABSTRACT

Histone acetylation influences protein interactions and chromatin accessibility and plays an important role in the regulation of transcription, replication and DNA repair. Conversely, DNA damage affects these crucial cellular processes and induces changes in histone acetylation. However, a comprehensive overview of the effects of DNA damage on the histone acetylation landscape is currently lacking. To quantify changes in histone acetylation we developed an unbiased quantitative mass spectrometry analysis on affinity-purified acetylated histone peptides, generated by differential parallel proteolysis. This resulted in the identification of a large number of histone acetylation sites. We observed a remarkable overall reduction of acetylated histone residues in response to DNA damage, indicative of an overall loss of histone acetyl-modifications. This decrease is mainly caused by DNA damage-induced replication stress coupled to specific proteasome-dependent loss of acetylated histones. Strikingly, this degradation of acetylated histones is independent of ubiquitylation but requires the PA200-proteasome activator, a complex that specifically targets acetylated histones for degradation. The uncovered replication stress-induced degradation of acetylated histones may represent an important chromatin-modifying response to cope with replication stress.

INTRODUCTION

DNA transacting processes such as transcription, replication and DNA repair take place in the context of chromatin. Chromatin is a highly organized structure in which DNA is wound around nucleosomes. Nucleosomes consist of an octamer of histone proteins, containing a histone H3-H4 heterotetramer flanked by two histone H2A-H2B heterodimers. The linker histone H1 binds linker DNA entering and exiting nucleosomes, thereby regulating chromatin compaction [1]. Histones are a target for many post-translational modifications (PTMs), like methylation, phosphorylation, ubiquitylation and acetylation, that are predominantly located at histone tails protruding from the nucleosome [2]. Histone PTMs can directly influence the strength of the histone interactions with each other and with the DNA [2]. Furthermore, several PTMs provide a docking site for specific readers, like chromatin remodeling complexes containing bromodomains that have affinity for acetylated histones [3]. Together this interplay of histone PTMs and chromatin remodeling proteins controls the accessibility of the chromatin thereby playing an important role in transcription, replication and DNA repair.

For example, histone PTMs play a crucial role during DNA repair and DNA damage signaling [2, 4, 5]. Histone acetylation was one of the first histone PTMs, shown to be involved in DNA repair. More than 3 decades ago it was found that after UV irradiation histones undergo a wave of rapid hyperacetylation followed by a hypoacetylation phase [6]. UV light causes helix-distorting lesions such as 6-4 photoproducts (6-4PP) and cyclobutane pyrimidine dimers (CPD), which block transcription and interfere with replication. These lesions can be removed by a specific DNA repair mechanism called nucleotide excision repair (NER) [7]. The fact that hyperacetylated nucleosomes both increased chromatin accessibility in vivo and stimulated repair efficiency [8], led to the formulation of the access-repair-restore concept [9]. This model proposed that chromatin is remodeled by ATP-dependent chromatin remodelers, histone chaperones and modifying enzymes to provide access of repair proteins to damaged sites. After repair the chromatin conformation is restored to pre-damage conditions to preserve epigenetic information and inhibit DNA damage signaling [9, 10]. Over the years several histone acetyltransferases (HATs) have been implicated in the response to UV damage [11-14]. For instance, p300 interacts with PCNA and is associated with newly synthesized DNA after UV irradiation [14]. UV-induced H3K9/K14 acetylation by GCN5 increases nucleosome accessibility at the repressed MFA2 locus in yeast [11, 15] through binding of the RSC remodeling complex, which stimulated CPD repair [16]. In human cells, GCN5 is necessary for efficient recruitment of NER factors and repair [17]. In addition to H3 acetylation, also histone H4 is rapidly acetylated after UV by ING2 leading to the recruitment of XPA to the lesion [13]. Notably, besides acetylation also deacetylation plays an important role during the UV-DDR. For instance, histone deacetylase enzymes (HDACs) 1 and 2 are recruited to damaged sites by the DNA damage recognition proteins, DDB1 and DDB2, resulting in H3K56 deacetylation [18].

Although these studies underscore the crucial interplay of histone acetylation and DNA repair, thus far a comprehensive overview of UV-induced histone acetylation and deacetylation events during repair, but also caused by UV-induced replication or transcription blocks is missing. Changes in histone modifications are often studied using modification-specific antibodies [15, 19]. However, these techniques rely on the specificity and availability of antibodies and unknown modification sites can therefore not be identified. Especially the acetylation status of histone H2A and H2B after UV irradiation remains largely unclear. In this study we used a quantitative mass spectrometry approach to identify histone acetylation changes in response to UV irradiation in an unbiased manner. Surprisingly, we found that UV damage induces a histone-wide reduction in acetylation levels. This loss of acetylated histones was not dependent on active transcription or NER. Instead, we show that it is the result of replication stress-induced histone degradation by a specific type of proteasome, containing the PA200 subunit, which recognizes acetylated proteins.

RESULTS

Isolation of acetylated histone peptides

To identify the effects of UV-induced DNA damage on histone acetylation in an unbiased and quantitative manner we used a stable isotope labeling by amino acids in cell culture (SILAC) MS based approach. Cells labelled with light-isotope-containing amino acids (K0R0) were mock treated and cells labelled with heavy-isotope-containing amino acids (K6R10) were UV irradiated (16 J/m^2) 1 hour before harvesting. In order to increase detection and quantification of histone acetylation sites, including less abundant ones, we established an isolation procedure to enrich for acetylated histone peptides. To this end we combined histone acid extraction [20, 21] with recently developed acetyl-lysine immunoprecipitation (Ac-IP) procedures [22, 23] (Figure 1A). Histones were isolated by a two-step histone acid extraction protocol: extracting first linker histone H1 and the high mobility group proteins, followed by isolation of the core histones. Specificity of the histone extraction was confirmed by comparing the pellet fraction containing the precipitated non-acid-soluble proteins with the histone H1 and the core histone fractions using Coomassie staining (Figure 1B). Protein bands of the expected sizes of H1 (21 kDa) and the core histones (10-15 kDa) could be detected in the designated lanes. The presence of histone H1.2 in the histone H1 fraction and histone H2B in the core histone fraction was confirmed by western blot analysis. Furthermore, the induction of yH2AX following UV irradiation [24, 25] indicates that histone PTMs are preserved during the acid extraction procedure (Figure 1C). Prior to digestion the isolated H1 and core histone fractions were pooled. To obtain peptide sizes that are compatible with MS analysis to ensure a high coverage of all histone proteins, we split our sample in fractions, each digested with a different protease; trypsin, pepsin or GluC (Figure 1A). The trypsin fraction was further split in four and digested for different durations. After pooling these differential digested fractions, this approach led to the detection of many different unique and overlapping peptides, covering 74-98% of the core histone sequences and 27-62% of the different histone H1 variants (Figure 1D and Supplemental table 1).

Acetylated peptides were isolated by Ac-IP and measured on LC-MS/MS. While several acetylated histone peptides could already be identified without the specific isolation procedure (Supplemental table 1), the Ac-IP resulted in a 4-fold increase in the number of identified unique acetylated histone peptides. We identified 301 different acetylated histone peptides in total, 75% of which carry more than one acetyl-group (supplemental table 2). Within this set of peptides, 40 unique histone acetylation sites were identified, including many previously described sites, like histone H3 acetylation on lysine 9, 14, 18, 23, 27 and 64 [26, 27]. Interestingly, we found H2B to have most unique acetylation sites (Figure 1E). As expected, acetylated sites of core histones were mainly found in the tails [28] whereas lysine 64 of histone H3 was the only acetylated residue found within the globular domains (Supplemental table 3). In contrast to the core histones, the majority of acetyl modified lysines of the linker histone H1 were located in the globular domain [29].

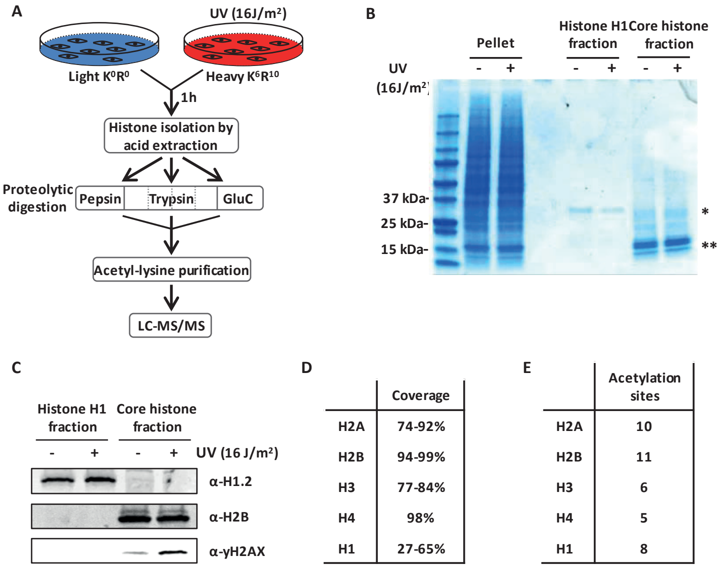
A
UV (16J/m²)
Light K⁰R⁰
Heavy K⁶R¹⁰
1h
Histone isolation by acid extraction
Proteolytic digestion
Pepsin
Trypsin
GluC
Acetyl-lysine purification
LC-MS/MS
B
Pellet
Histone H1 fraction
Core histone fraction
UV (16J/m²)
- +
- +
- +
37 kDa-
25 kDa-
15 kDa-
*
**
C
Histone H1 fraction
Core histone fraction
- + - + UV (16 J/m²)
α-H1.2
α-H2B
α-yH2AX
D
E

	Coverage
H2A	74-92%
H2B	94-99%
H3	77-84%
H4	98%
H1	27-65%

	Acetylation sites
H2A	10
H2B	11
H3	6
H4	5
H1	8

Figure 1: Isolation of acetylated histone peptides.
(A) Schematic overview of the experimental set up to isolate and identify acetylated histone peptides following UV irradiation. SILAC labeled cells are mock or UV (16 J/m^2) treated one hour before harvesting. Heavy and light labelled cells are mixed in a 1:1 ratio followed by acid extraction to isolate histones. Histones are separated in 3 fractions each digested with either pepsin, trypsin or GluC. The limited digestion with trypsin is performed for 2, 10, 30 and 120 min. The different fractions of digested peptides are combined and followed by acetyl-lysine immunopurification. The acetylated-lysine enriched histone peptides are analyzed by LC-MS/MS. (B) Histones were isolated by acid extraction from HeLa cells one hour after UV (16 J/m^2) or mock treatment and were loaded on a 4-15% gradient SDS-PAGE gel and stained with Coomassie Brilliant Blue. The different fractions originate from the same amount of cells and contain the non-acid-soluble proteins (pellet), histone H1 and high mobility group proteins (H1 fraction) or the core histones (core histone fraction). * indicates 21 kDa protein band, most likely representing histone H1. ** indicates several protein bands ranging between 10-15 kDa most likely representing core histones. (C) Western blot of isolated histone fractions from HeLa cells one hour after UV (16 J/m^2) or mock treatment. Western blots were stained with α-histone H1.2 (top panel), α-histone H2B (middle panel) and α-yH2AX (bottom panel). (D) Table listing the coverage of the histone sequences using our peptide digestion procedure by LC-MS/MS analysis. (E) Table listing the number of acetylation sites on core histones identified by MS after acetylated peptide enrichment.

Histone acetylation levels are decreased after UV-irradiation

After validating our approach to efficiently identify histone acetylation sites, we analyzed differences in the extent of histone acetylation one hour after UV-induced DNA damage. To visualize UV-induced changes in the acetylation status, all unique acetyl-modified histone peptides were plotted against their SILAC based UV/mock $\log_2$ ratio (Figure 2A). Surprisingly, the vast majority of the acetylated peptides had a negative normalized SILAC ratio following UV treatment (61% had a UV/mock $\log_2$ ratio < -0.5), indicative of an overall reduction in acetylation level of histones one hour after UV-induced DNA damage (Figure 2B and supplemental table 2). The non-modified histone peptides that, despite the enrichment for acetylated peptides, were present in our sample display UV/mock $\log_2$ SILAC ratios between -0.5 and 0.5, indicating that similar amounts of histone peptides are extracted during the procedure and that the quantity of unmodified histone peptides is not massively changed upon UV irradiation (Figure 2C and supplemental table 2). Together, these data show that overall histone levels in the cell are not significantly changed one hour after UV treatment, suggesting that the UV-induced histone-wide decrease in acetylation levels is rather a consequence of a specific loss of acetylated histones. This loss can be induced either by active deacetylation of histones or by specific degradation of a small subset of acetylated histones. Although most histones display lower acetylation levels after UV, histone H2B and H2A were affected the most (Figure 2B, supplemental figure 1A and supplemental table 2&3). Interestingly, only for histone H2A variant H2AZ sites with increased acetylation after UV irradiation (UV/mock $\log_2$ ratio>0.5) were observed, while its unmodified peptides are not changed (Supplemental table 2&3).

To confirm this histone-wide reduction of acetylation detected by MS, we quantified overall histone acetylation levels on western blot using the α-acetyl-lysine antibody. Western blotting of sonicated whole cell extract (WCE), obtained by lysing HeLa cells directly in Laemmli buffer, showed that the vast majority of the signal from the α-acetyl-lysine antibody is confined in two bands around 10-15 kDa (Figure 2D). This α-acetyl-lysine signal fully overlapped with bands obtained by staining against the different core histones (Supplemental figure 1B) and a similar α-acetyl-lysine signal was obtained from an acid extracted histone fraction (Figure 2D and supplemental figure 1C). This strongly suggests that these low molecular weight acetyl-lysine signals represent acetylated histones and that the majority of lysine modifications with acetyl within the cell take place at the highly expressed and heavily modified core histones. This was further corroborated by the reduction in acetylation signal following incubation with HAT inhibitors and the increase in signal after HDACs were inhibited (Figure 2D). Together this shows that the overall histone acetylation status can be assessed in a quantitative manner by western blot using α-acetyl-lysine staining. In line with our MS results we observed a UV-induced decrease in acetylated histones 1 hour after UV (Figure 2E-F). Interestingly, the histone acetylation levels decreased even further over time. Quantification of the histone acetylation levels normalized to either histone H4 or tubulin showed a 30-50% reduction of acetylated histones 4 hours following UV exposure (Figure 2E-F). Using another acetyl-lysine antibody [22], we confirmed the UV-induced reduction in overall histone acetylation levels by both MS (supplemental table 4) and western blotting experiments (Supplemental figure 1D-E) , excluding the possibility that our results were due to preferred recognition motifs or other biases of the used antibodies.

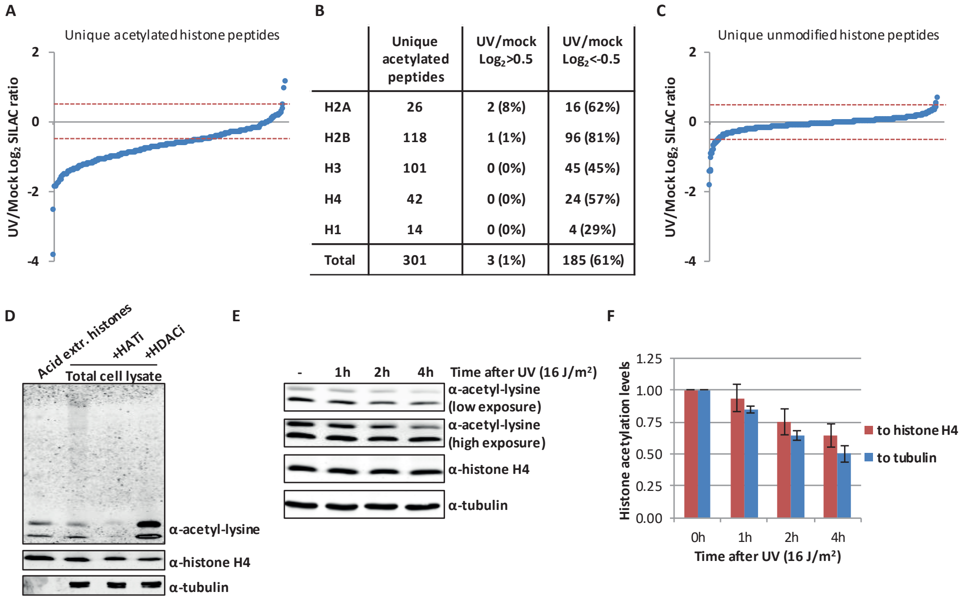

	Unique acetylated peptides	UV/mock $Log_2>0.5$	UV/mock $Log_2<-0.5$
H2A	26	2 (8%)	16 (62%)
H2B	118	1 (1%)	96 (81%)
H3	101	0 (0%)	45 (45%)
H4	42	0 (0%)	24 (57%)
H1	14	0 (0%)	4 (29%)
Total	301	3 (1%)	185 (61%)

Figure 2: UV-induced decrease in acetylated histones.
(A) Identified acetylated histone peptides plotted against their $\log_2$ SILAC ratio (1h after 16 J/m^2 UV/mock), ranked by SILAC ratio. (B) Table listing the number of identified peptides per histone using MS following enrichment of acetylated peptides, and the number of peptides identified that are decreased (UV/mock $\log_2<-0.5$) or increased (UV/mock $\log_2>0.5$) one hour after UV irradiation (16 J/m^2). (C) Identified non-modified histone peptides plotted against their log2 SILAC ratio (1h after 16 J/m^2 UV/mock), ranked by SILAC ratio. (D) Western blot of acid extracted histones and WCE from HeLa cells, treated with HATi (CTK7A, 100 µM and CPTH2, 50 µM) or HDACi (TSA, 1 µM) for 4h or mock treated as indicated. (E) A representative western blot of histone acetylation levels of HeLa cells lysed at indicated time points after UV-irradiation (16 J/m^2). Blots were stained with α-acetyl-lysine (top panels, high and low exposure), α-histone H4 (middle panel) and α-tubulin (bottom panel). (F) Quantification of histone acetylation levels, normalized against either the histone H4 levels (red bars) or tubulin levels (blue bars). Error bars represent SEM. N=5 independent experiments.

Recovery of acetylation levels 16 hours after UV is dependent on NER

To study the temporal behavior of histone acetylation levels after UV irradiation in more detail, western blot experiments were performed with WCE obtained at later time points after UV irradiation. While the acetylation signal was still reduced 8 h after UV, it recovered to levels similar as mock treated cells 16 h after irradiation (Figure 3A (left panel) and B), a time point when most DNA repair is finished [30, 31]. This suggests that repair of UV-induced damage by NER might be necessary for the recovery of histone acetylation levels. Indeed, the recovery of the histone acetylation signal is abolished in cell lines deficient for NER proteins XPC or XPA, indicating that repair of UV-induced DNA damage is crucial for recovery of histone acetylation levels and that the persistent presence of DNA damage prevents this (Figure 3). Interestingly, in NER-deficient cells a similar loss of acetylated histones was observed compared to NER-proficient cells in the first 8 h after UV, showing that the UV-induced decrease in acetylated histones is not dependent on DNA damage recognition or on repair by NER (Figure 3). Together these data suggest that the trigger for the observed decrease in histone acetylation levels and occurs upstream or in parallel of the damage recognition step of NER.

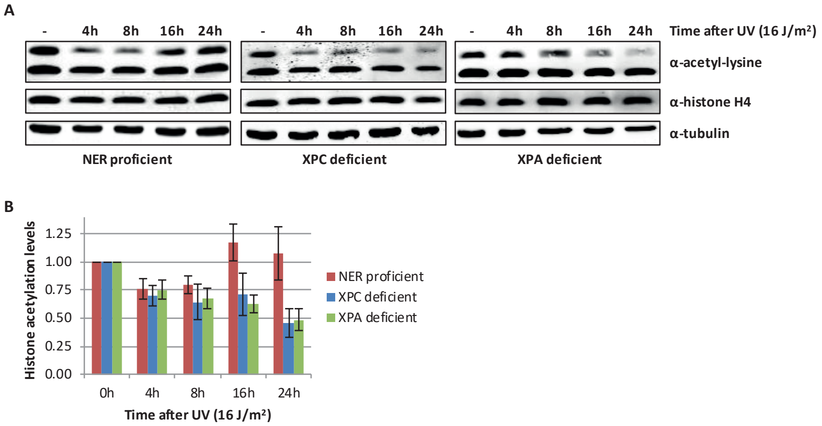

Figure 3: The recovery of histone acetylation levels at later time points after UV is dependent on NER.

(A) Representative western blots of WCE from NER-proficient HeLa cells and NER-deficient XP4PA (XP-C) and XP2OS (XP-A) cells obtained at indicated time points after UV irradiation (16 J/m2) and stained with the indicated antibodies. (B) Quantification of histone acetylation levels of NER-proficient cells (HeLa) and NER-deficient (XP-A and XP-C) patient cells at the indicated time points after UV-irradiation (16 J/m^2). Histone acetylation levels are normalized against histone H4 levels. Average of at least 5 independent experiments and error bars represent SEM.

Transcription does not influence the decrease in acetylated histones after UV-irradiation

Persistent UV-induced DNA lesions severely impede transcription and replication [32, 33]. As active transcription is highly associated with increased levels of histone acetylation [2] we tested whether transcription inhibition affects the acetylation status of histones. Transcription was impeded by THZ1 and flavopiridol, which both inhibit transcription preceding productive elongation, and α-amanitin that blocks elongating RNAPII [34]. In contrast to UV, the histone acetylation levels remain rather stable after transcription inhibition, indicating that transcription inhibition is not the main cause of the UV-induced loss of acetylated histones (Figure 4A-B). However, even though chemical transcription inhibition did not result in a decrease in acetylated histones, we could not exclude that active transcription or lesion stalled RNAPII might initiate this UV-induced process. To test this, cells were pre-treated with the transcription inhibitors THZ1 or flavopiridol to deplete cells of elongating RNAPII before UV irradiation. This, however, did not affect the decrease in histone acetylation levels after UV irradiation (Figure 4C-D), indicating that the UV-induced loss of acetylated histones is a process independent of transcription.

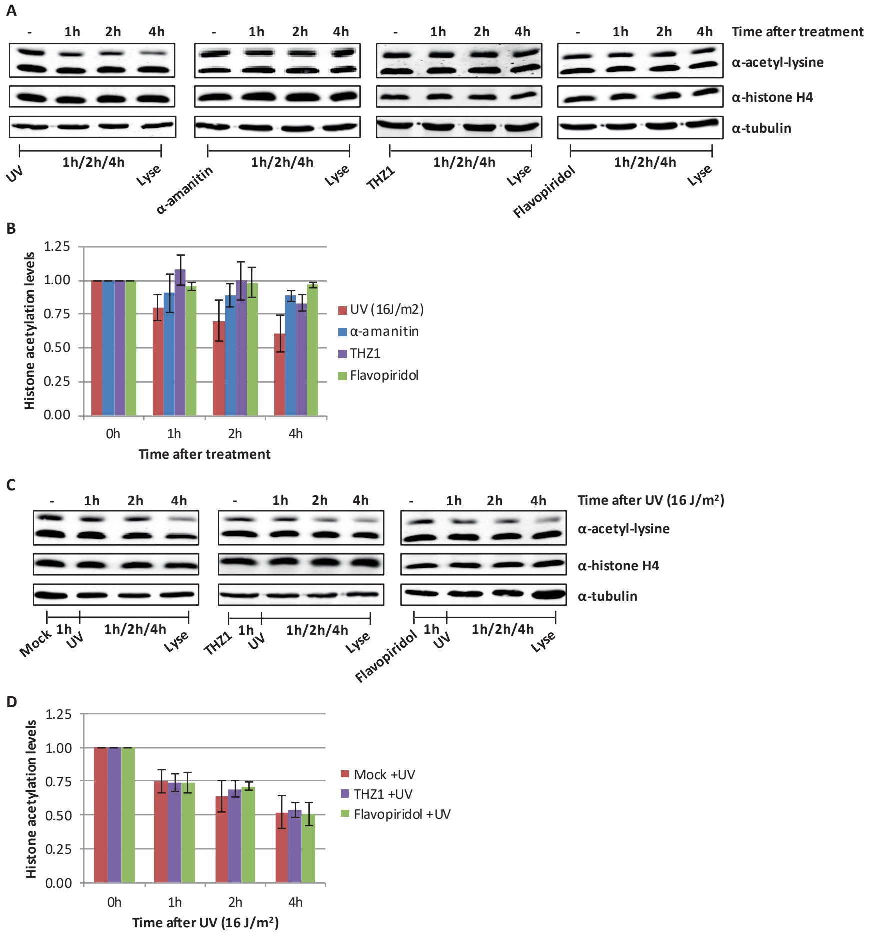

Figure 4: Loss of acetylated histones is independent of transcription inhibition. (A) Representative western blots of histone acetylation levels of HeLa cells lysed at indicated time points after UV irradiation (16 J/m^2, left panel), α-amanitin (second panel, 100 μg/ml), THZ1 (third panel, 1 μM) or flavopiridol (right panel, 1 μM) treatment. Blots were stained with α-acetyl-lysine (top panel), α-histone H4 (middle panel) and α-tubulin (bottom panel). (B) Quantified histone acetylation levels, normalized against histone H4 levels for quantification. Average of at least 3 experiments. Error bars represent SEM. (C) Representative western blots of histone acetylation levels of HeLa cells pre-treated with transcription inhibitors (mock (left), THZ1 (middle, 1 μM) or flavopiridol (right, 1 μM) an hour before UV irradiation and lysed at the indicated time points after UV (16J/m^2). Blots were stained with the indicated antibodies. (D) Quantification of α-acetyl-lysine signal, normalized against histone H4 levels. Average of 5 experiments. Error bars represent SEM.

Decrease in histone acetylation levels is the result of UV-induced replication stress

In addition to transcription inhibition, UV induced DNA lesions also cause replication stress, by slowing down or stalling replication forks, which eventually may result in double strand break induction and mutagenesis. To test whether the loss of acetylated histones is caused by UV-induced replication stress, we induced replication stress in a different manner, by a combination of hydroxyurea (HU) and arabinofuranosyl cytidine (AraC). This way of replication stress induction led to a similar loss of acetylated histones as after UV irradiation (Figure 5A-B). This indicates that replication stress itself can indeed induce a general decrease in histone acetylation levels and suggests that the loss of acetylated histones following DNA damage might be the direct consequence of UV-induced replication stress. To test whether the loss of acetylated histones following UV exposure could be attributed to replication stress, we studied UV-induced effects on histone acetylation in non-replicating cells. To this end, HeLa cells were blocked in S-phase using the Cdc7/CDK9 inhibitor PHA 767491 hydrochloride (Supplemental figure 2A). These cells displayed lower histone acetylation levels under unperturbed conditions (Figure 5C and supplemental figure 2B), which suggests that the high histone acetylation levels in cycling cells are mainly induced by replication related events. However, no additional UV-induced decrease was observed in these cells (Figure 5C-D). Similar results were obtained in contact inhibited non-replicating VH10 cells, which showed less reduction in histone acetylation levels compared to cycling VH10 cells following UV-exposure (Supplemental figure 2C-E). Together these results indicate that the loss of acetylated histones after UV irradiation is mainly the result of replication stress.

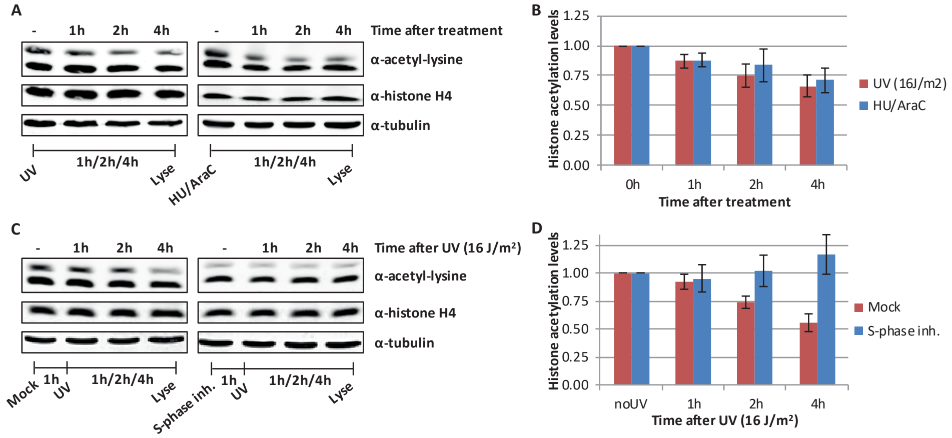

Figure 5: Replication stress induces loss of acetylated histones.
(A) Representative western blots of histone acetylation levels of HeLa cells obtained at the indicated time points after UV irradiation (16 J/m^2) or HU/AraC treatment (100 mM/10 μM). Blots were stained with α-acetyl-lysine (top panel), α-histone H4 (middle panel) and α-tubulin (bottom panel). (B) Quantification of histone acetylation, normalized against histone H4 levels. Average of 5 experiments. Error bars represent SEM. (C) Representative Western blots, stained with the indicated antibodies of HeLa cells pre-treated o/n with an S-phase inhibitor (PHA 767491 hydrochloride, 10 μM) and lysed at indicated time points after UV (16 J/m^2). (D) Quantification of the α-acetyl-lysine signals, normalized against histone H4 levels, average of 5 experiments, error bars represent SEM.

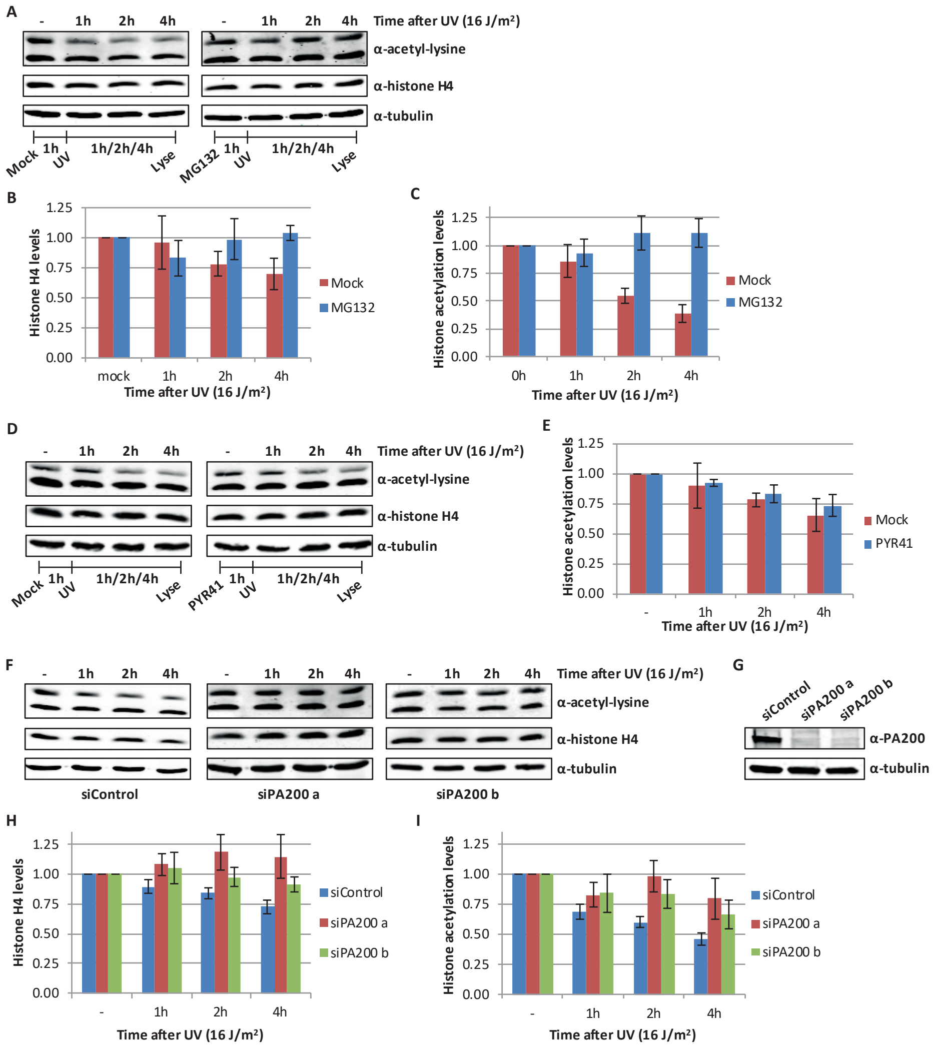

Figure 6: Proteasomal degradation of acetylated histones following replication stress. (A) Western blots of HeLa cells treated with proteasome inhibitor MG132 one hour before UV irradiation and lysed at different time points after UV (16 J/m²). Blots were stained with α-acetyl-lysine (top panel), α-histone H4 (middle panel) and α-tubulin (bottom panel). Quantifications of (B) histone H4 levels and (C) acetylation levels, normalized against tubulin levels. Average of 6 experiments and error bars represent SEM. Representative blots are shown in panel A. (D) Western blots of HeLa cells pre-treated with the E1 enzyme inhibitor PYR-41 (10 μM) one hour before UV irradiation and lysed at different time points after UV (16 J/m²). Blots were stained with the indicated antibodies and representative blots are shown. (E) Quantification of histone acetylation levels, normalized against histone H4 levels, average of 5 experiments. Error bars represent SEM. (F) Representative western blots of siControl or siPA200 (2 independent siRNAs, a and b) transfected cells, lysed at indicated time points after UV-irradiation (16 J/m²). (G) Western blot showing the knock down efficiency of the siRNAs targeting PA200. (H) Quantification of histone H4 and (I) histone acetylation levels, normalized against tubulin and non-treated levels are set as 1. The average of at least 9 independent experiments and SEM is shown.

Acetylated histones are degraded by PA200-proteasome complexes

Besides the reduction in histone acetylation levels, we observed a concomitant decrease in the histone H4 levels after UV irradiation (Figure 6A-B), however to a lesser extent than the loss of acetylated histones (Figure 6C). This suggests that the observed UV-induced decrease in histone acetylation levels could be caused by degradation of a specific subset of acetylated histones. To test this, cells were pre-treated with the proteasome inhibitor MG132 one hour before UV irradiation. Proteasome inhibition completely rescued the UV-induced loss of both acetylated histones and histone H4 (Figure 6A-C). Interestingly, inhibition of the ubiquitin-activating enzyme (E1) using PYR-41, did not rescue the decrease in acetylated histones (Figure 6D-E). This indicates, in contrast to most proteasome dependent protein degradation, that the proteasomal degradation of acetylated histones is independent of protein ubiquitylation. It has been shown that in response to double strand breaks and during spermatogenesis, acetylated histones can be recognized and degraded by a specific proteasome complex independent of protein ubiquitylation [35]. This specific proteasome complex consists of the 20S core complex and the nuclear proteasome activator PA200 [35]. In contrast to the 26S proteasome, in which the 19S regulatory cap recognizes ubiquitylated proteins, the PA200-proteasome complex does not recognize poly-ubiquitin chains but binds to acetylated proteins and targets them for degradation [35]. Therefore, we tested the involvement of PA200 in the UV-induced decrease in histone H4 and histone acetylation levels. siRNA-mediated knockdown of PA200 inhibited the UV-induced proteasomal degradation of acetylated histones (Figure 6F-I). Together these results show that following replication stress, for example induced by UV-induced DNA damage, acetylated histones are degraded by the PA200-20S proteasome complex in an ubiquitin independent manner.

DISCUSSION

To study the effects of UV-induced DNA damage on histone acetylation in an unbiased manner, we established a protocol to efficiently isolate acetyl-modified histone peptides. This stepwise purification approach, consisting of an acid extraction of histones, combined with proteolytic digestion with different proteases in parallel and followed by immuno-purification of acetylated peptides and analysis by mass spectrometry, resulted in the identification of 40 histone acetylation sites originating from over 300 unique peptides. Using this procedure, we uncovered an UV-induced reduction of the vast majority of detected acetylated residues originating from all histones, except for variant H2AZ. Western blot experiments confirmed this UV-induced overall loss of acetylated histones and showed a loss of overall histone acetylation levels up to 40% 4 hours after UV exposure. Thus far most research on histone acetylation was focused on H3 and H4, for example on the role of H4K16Ac in chromatin compaction [36] and H3K9/14Ac in transcription [37] and during the UV-DDR [15-17]. Our data show that acetylation levels of H2A and H2B are more reduced in response to UV than H3 and H4 acetylation levels (Figure 2B, supplemental figure 1A and supplemental table 2&3), suggesting an important role for the regulation of H2A and H2B acetylation levels in the UV-DDR or in the extensive chromatin remodeling processes observed following DNA damage [38, 39]. In contrast to the here described global decrease of histone acetylation, multiple other studies have observed an increase in acetylation in response to UV irradiation [11-13, 15-17, 40]. For example, the UV-induced histone acetylation on H3K9/14 was shown to stimulate efficient NER [17] by opening the chromatin structure as a result of recruitment of the chromatin remodeling complex RSC [16]. This UV-induced acetylation is mediated by histone acetyltransferases GCN5 and p300, which are both found at UV lesions and interact with the UV-DDB complex [11, 12, 15, 17, 41, 42]. We propose that our observed overall loss of histone acetylation is a separate event, that acts independent of the reported histone acetylation events during NER [11-13, 15-17, 40]. First, the large decrease in total histone acetylation levels occurs on all core histones and includes multiple lysines, as shown by our MS experiments, suggesting a chromatin-wide effect in contrast to the reported histone acetylation events that are often lysine specific and are mainly locally observed centered around the DNA lesion [11, 15, 17]. Furthermore, NER-stimulating acetylation was proposed to be facilitated by the recruitment of HATs to the site of DNA damage [14, 17, 41-43], while the here described replication stress-associated loss of acetylated histones is due to proteasomal degradation rather than caused by changes in HATs or HDACs activity. In addition, the degradation of acetylated histones is only observed in cycling cells (Fig. 5C-D), while NER and the previously described histone acetylation events are expected to take place throughout the cell cycle. Finally, we found that the loss of acetylated histones after UV irradiation is not dependent on NER (Figure 3). Our observations suggest that the overall decrease in histone acetylation in response to UV is not directly associated with DNA repair but more a consequence of DNA damage-induced replication stress. In line with this, it was previously observed, using acetyl-histone specific antibodies, that H3K9Ac and H3K56Ac are reduced after hydroxyurea treatment [19]. Of note, unlike the loss of acetylated histones, the recovery of histone acetylation levels after UV-induced replication stress is dependent on NER. Since NER is the only mammalian DNA repair system capable of removing UV-induced lesions [7], its absence will prohibit repair of replication stress inducing UV-lesions. The recovery of histone acetylation levels is likely the result of synthesis of new histones required for the resumption of replication, which are subsequently acetylated, to replace the acetylated histones that were degraded in response to DNA damage. The fact that mainly an overall loss of histone acetylation was observed, despite the existence of two independent and opposing UV-induced histone acetylation influencing events, indicates that in dividing cells the abundant replication stress-induced loss of acetylated histones may shield the detection of more residue-specific and damage-localized acetylation events. To specifically investigate acetylation events that are induced by UV-lesions or active NER, it is thus important to execute experiments in non-replicating cells.

The decrease in histone acetylation levels following replication stress is proteasome dependent and is likely explained by the degradation of a specific subset of histones, i.e. acetylated histones, as the histone acetylation levels are more reduced than the histone levels in response to UV irradiation (Figure 6A-C). Surprisingly, the observed histone degradation is not dependent on ubiquitylation, but instead it depends on the PA200-proteasome that specifically targets acetylated proteins for degradation (Figure 6D-I) [35]. It is not known whether or how PA200 can discriminate between differentially acetylated histones. For example, it is not expected that histones in transcriptionally active regions, which also carry acetylation marks [44], are constantly targeted by the PA200-proteasome. We observed a reduction in almost all acetylated peptides, many of which carried multiple acetyl groups (Supplemental table 2). This might suggest that PA200 may not recognize specific histone marks, but rather targets hyperacetylated histones for degradation. Future studies should uncover if and how PA200 can discriminate between different subsets of acetylated histones, or that for example the activity of the PA200 complex itself is regulated to control histone degradation following replication stress. It is also not clear yet whether incorporated histones can be degraded by the PA200 proteasome or whether histones need to be evicted from chromatin prior to degradation.

An important question that remains to be answered is why histones are degraded in response to replication stress. In response to DNA damage, chromatin is remodeled to a more accessible conformation to enable efficient repair and this might be facilitated by the degradation of histones. In line with this, histone degradation in response to zeocin treatment was recently observed in yeast. This degradation was shown to lead to enhanced chromatin dynamics and recombination rates [45]. This implies that degradation of histones could indeed be necessary to efficiently overcome stalled replication forks. In accordance with this hypothesis, PA200 was found to localize to chromatin in response to DNA damage [46], which suggests that it might locally degrade nucleosomal histones. However, it is unknown whether histones are hyper acetylated near stalled replication forks. Interestingly, in yeast all core histones, except H2AZ, are degraded in response to DNA damage [45]. The only two sites that in our study were identified to be more acetylated in response to UV irradiation are both located on this histone variant (Supplemental table 3), which was previously described to be important for UV survival and CPD repair in yeast [16]. This might imply that also in human cells H2AZ might not be degraded in response to replication stress. However, the function of this UV-induced H2AZ acetylation [16] and why the PA200-proteasome would not recognize this specific histone variant remains unclear.

Another function of replication stress-induced histone degradation might be to prevent an excess of non-incorporated histones. A surplus of histones is expected to be harmful to cells as these proteins may non-specifically bind DNA and RNA and sequester the pool of histone modifying enzymes and chaperones, thereby triggering chromosomal aggregation and transcription block resulting in genome instability [47]. Therefore, in response to replication stress, the production of histones is quickly stopped by inhibiting transcription and degradation of histone mRNA [48, 49] and free histones are sequestered by chaperones [50, 51]. The here described degradation of histones in response to replication stress may represent an additional layer of regulation to control histone levels. Histone degradation to prevent an excess of histones has been previously described in yeast after overexpression of histones, although this process was dependent on Rad53 and ubiquitylation [52]. We observed a strong reduction in histone acetylation levels in non-cycling cells compared to cycling cells (Supplemental figure 2B), which suggests that the histone acetylation signal in cycling cells mainly originates from replication-induced acetylation events. In line with this, it has previously been shown that newly synthesized histone H3/

H4 dimers are acetylated to stimulate incorporation into chromatin [53-55]. During replication the levels of soluble histones are increased. After stalling of replication, histones will no longer be incorporated into the chromatin. These relatively accessible histones may be a specific target for PA200-mediated degradation. Future research is needed to uncover which subset of histones is exactly degraded upon replication stress.

In summary, our data indicates that in response to replication stress acetylated histones are specifically degraded by the PA200-proteasome in an ubiquitin independent manner. This degradation most likely represents an important chromatin-modifying mechanism for cells to cope with stalled replication forks.

MATERIALS AND METHODS

Cell culture and treatments

HeLa and VH10, SV40 or hTert immortalized, cells were cultured in DMEM/F10 (Lonza) supplemented with 10% fetal calf serum (FCS) and 1% penicillin-streptomycin (PS, P0781 Sigma) at 37°C in a humidified incubator containing 5% CO_2. For stable isotope labeling by amino acids in cell culture (SILAC), HeLa cells were cultured for at least 10 cell doublings in lysine, arginine and L-glutamine (PAA) deficient DMEM with 10% dialyzed FCS (Invitrogen), 1% PS and 1% ultraglutamine (200mM Lonza), supplemented with either 73 μg/mL light [^{12}C6]lysine and 42 μg/mL light $^{[12}$C6, ^{14}N4] arginine (Sigma) or similar concentrations of heavy [^{13}C6]lysine and heavy [^{13}C6, ^{15}N4] arginine (Cambridge Isotope Laboratories). For UV treatments cells were washed with phosphate-buffered saline (PBS) and irradiated with 16 J/m^2 (254nm, Philips TUV lamp). To induce replication stress a combination of hydroxyurea (100 mM) and AraC (10μM) was used. Transcription was inhibited using; α-amanitin (0.1mg/ml), THZ1 (1 μM) and flavopiridol (1 μM). To inhibit cell cycle PHA 767491 hydrochloride (10 μM) was added o/n to the culture medium.

Histone isolation and protein digestion

Cells were washed twice with cold PBS, scraped and mixed in a 1:1 ratio based on cell pellet size (UV:mock). The cell pellet was resuspended in 1 volume 5% perchloric acid. After incubating for 10 min, the solution was centrifuged for 10 min at 13,000 rpm. The supernatant containing histone H1 was collected and the procedure was repeated twice. The pellet was then resuspended in 2 volumes 0.4N hydrochloric acid (HCl) and incubated for 15 min before spinning down (10 min 13.000 rpm). This procedure was repeated twice and all supernatants containing the core histones were collected. The histone containing supernatants were precipitated by the addition of trichloric acid to 25% and incubated on ice for 30 min and centrifuged for 20 min at 13,000 rpm. Pellets were washed in acetone with 0.006%HCl and subsequently in acetone and finally the histone pellets were dissolved in 50 mM ammonium bicarbonate. Digestions were performed with proteomics-grade trypsin (Roche, 1:100, 30°C, 2/10/30/120 min) (50% of sample), GluC (100x, o/n, room temperature (RT)) (25% of sample) or on an immobilized pepsin (Pierce) column (in 0.5% trifluoracetic acid (TFA)) (25% of sample). Tryptic and GluC digestion was stopped by acidification to 0.5% TFA. The digested peptides were mixed and subsequently purified using 200 mg tC18 SEP-PAK SPE cartridges (Waters) and eluted with 40% acetonitrile (ACN) containing 0.1% TFA. The peptides were then lyophilized for 48 h (Scanvac CoolSafe 110-4, Scala Scientific).

Ac-K peptide enrichment

Lyophilized peptides were dissolved in 1.4 mL of IAP buffer (PTMscan, cell signaling) and incubated with anti-Ac-K antibody beads (PTMscan, cell signaling) for 2 h at 4°C on a rotating unit. Beads were washed three times in IAP buffer followed by two washes in H_2O and subsequently the peptides were eluted using 0.1% of TFA in H_2O. The enrichments with the anti-Ac-K antibody from Immunechem were performed as described previously [22]. In short, peptides were dissolved in 1.4 ml IP buffer (50 mM MOPS pH7.2, 10 mM sodium phosphate, 50 mM NaCl) and incubated o/n with 62,5 µg anti-Ac-K antibody conjugated to 12 µl protein A beads (GE Healthcare). Beads were washed 3 times in IP buffer and two times with water before peptide elution with 0.15% TFA. Eluted peptides were purified with C18 stage tips (Millipore).

Mass spectrometry

Digested histone peptides, not enriched for acetyl-lysines, were analyzed with an Orbitrap Fusion Tribrid mass spectrometer (Thermo Fisher Scientific) or a quadrupole Orbitrap (Q-Exactive, Thermo Fisher Scientific) and samples enriched for acetylated peptides were analyzed with the Orbitrap Fusion Tribrid mass spectrometer according to protocols below.

Mass spectra were acquired on an Orbitrap Fusion Tribrid mass spectrometer (Thermo Fisher Scientific) coupled to an EASY-nLC 1000 system (Thermo Fisher Scientific). Peptide samples were loaded onto a ReproSil C18 reversed phase column (20 cm x 75 µm ID) and eluted with a gradient of 5-80% (acetonitrile containing 0.1% formic acid) over 90 min at 300 nl/min. For all experiments, the instrument was operated in data-dependent acquisition (DDA) mode. MS1 spectra were collected at a resolution of 120,000, with an automated gain control (AGC) target of 2E5 and a max injection time of 50 ms. The most intense ions were selected for MS/MS, top speed method with a 3 second cycle time. Precursors were filtered according to charge state (2-7z), and monoisotopic peak assignment. Previously interrogated precursors were dynamically excluded for 70 s. Peptide precursors were isolated with a quadrupole mass filter set to a width of 0.7 Th.

Peptide samples were analyzed on a quadrupole Orbitrap (Q-Exactive, Thermo Fisher Scientific) mass spectrometer equipped with an EASY-nLC 1000 (Thermo Fisher Scientific). Peptide samples were loaded onto a ReproSil C18 reversed phase column (20 cm x 75 µm ID) and eluted with a gradient of 5-80% (acetonitrile containing 0.1% formic acid) over 70 min at 300 nl/min. Fragmentation of the peptides was performed in DDA mode. MS1 spectra were collected at a resolution of 70,000, with an automated gain control (AGC) target of 1E6 and a max injection time of 50 ms. The 10 most intense ions were selected for MS/MS. Precursors were filtered according to charge state (2-7z) and monoisotopic peak assignment. Previously interrogated precursors were dynamically excluded for 30 sec and peptide precursors were isolated with a quadrupole mass filter set to a width of 2.0 Th.

Peptide identification

Raw data files were analyzed using MaxQuant software (version 1.5.2.8). MS/MS spectra were searched against a histone database, containing all uniprot entries of which the protein name contains the string "histone" and organism "Homo sapiens", using the Andromeda search engine. The protease specificity was set to nonspecific cleavage. Cysteine carbamidomethylation was included as a fixed modification, whereas methionine oxidation, N-terminal protein acetylation and lysine acetylation were set as variable modifications. A false discovery rate of 0.05 for peptides and a minimum peptide length of 7 were set. Before further data analysis, known contaminants and reverse hits were removed from the modification-specific peptides list.

Western blotting

Cell lysates were made in 2x Laemmli buffer. Lysates were boiled and sonicated with a Diagenode Bioruptor (30 sec on; 30 sec off for 10min) to shear the DNA. Lysates were separated on a 6% SDS-PAGE acrylamide gel and transferred to a PVDF membrane (0.45 µm, Merck Millipore ltd). Membranes were blocked with 5% milk in PBS for 1 hour at RT and incubated with primary antibody for 2 hours at RT or overnight at 4°C. Secondary Alexa Fluor 795 donkey anti-mouse antibodies and Alexa Fluor 680 donkey anti-rabbit antibodies (Sigma) were used to visualize the proteins using an infrared imaging system (Odyssey; LI-COR Biosciences). Quantifications of the signals from the blots were performed using the Odyssey software (LI-COR Biosciences). The total intensity from the two acetyl-lysine bands, representing acetylated histones, was normalized against histone H4 or tubulin signals and the mock treated time point was set as 1. Primary antibodies were: rabbit-α-histone H2B (1:1000, Millipore), mouse-α-phospho-H2A.X (SER139) (1:1000, Millipore), rabbit-α-histone H1.2 (1:1000, Abcam), goat-α-histone H2A (1:200, Santacruz), goat-α-histone H2B (1:100, Santacruz), goat-α-histone H3 (1:1000, Santacruz), mouse-α-histone H4 (1:1000, Abcam), rabbit-α-Acetyl-lysine (1:2000, PTMscan), rabbit-α-Acetyl-lysine (1:1000, Immunechem) and mouse-α-tubulin (1:5000, Sigma Aldrich). For western blots the rabbit-α-Acetyl-lysine from PTMscan was used, except when stated otherwise.

EdU incorporation

Cells were incubated with 20 µM 5-ethynyl-2'-dexoyuridine (EdU, Invitrogen) and 1 µM 5-Fluoro-2'-deoxyuridine for 2 hours. Cells were fixed in 3.6% formaldehyde in PBS and permeabilized in 0,5% Triton-X in PBS. EdU was visualized with a click-it reaction using Alexa fluorophore 488 nm according to manufactures protocol (Invitrogen). Images were obtained using a LSM700 microscope (Carl Zeiss Microimaging Inc.) and analyzed using ImageJ software [56].

ACKNOWLEDGEMENTS

This work is dedicated to the memory of Iris Kik. This work was supported by the Dutch Organization for Scientific Research (NWO) TOP Grants of Earth and Life Sciences and ZonMW (854.11.002 and 912.12.132), European Research Council

Advanced Grant (340988-ERC-ID) and Dutch Organization for Scientific Research Earth and Life Sciences VIDI grant (846.13.004).

AUTHOR CONTRIBUTIONS

I.M. initiated the project and designed and performed the majority of the experiments including proteomics and cell biological experiments and analysed the data; I.K. performed cell biological experiments; E.R. analysed mass spectrometry data. K.B. and J.D. performed and supervised mass spectrometry experiments; H.L. and J.H. provided advice; W.V. and J.M. designed and supervised the project. I.M. and J.M. wrote the manuscript. All authors reviewed the manuscript.

SUPPLEMENTAL INFORMATION

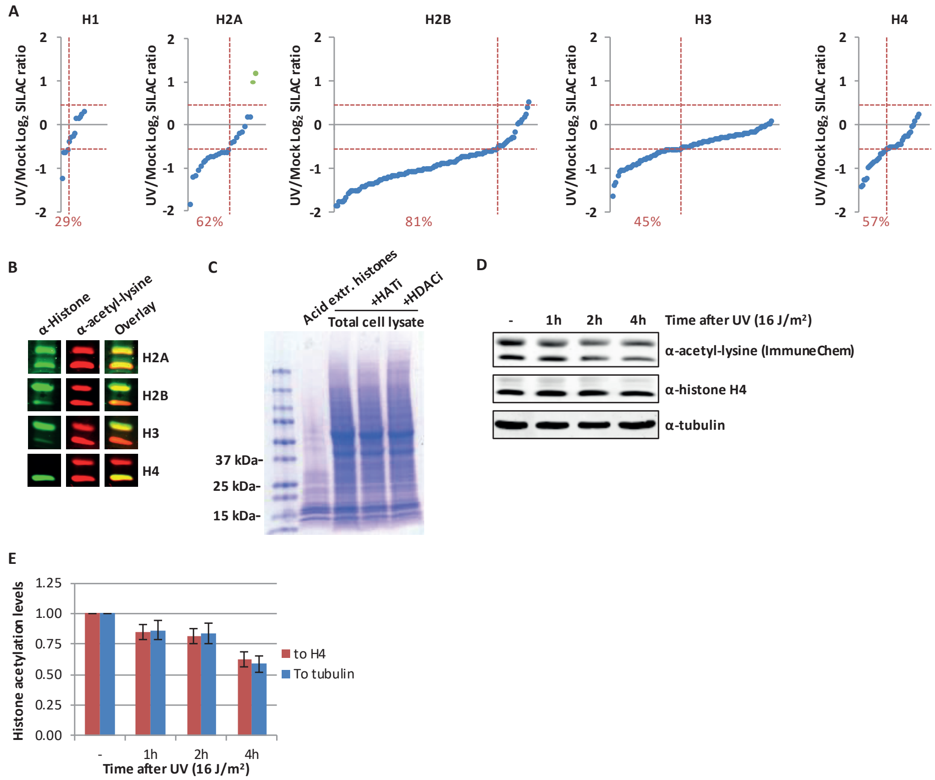

Supplemental figure 1: UV-induced decrease in acetylated histones.

(A) Identified acetylated peptides per histone plotted against their $\log_2$ SILAC ratio (1h after 16 J/m^2 UV/mock), ranked by SILAC ratio. Green dots represent the identified peptides from histone variant H2AZ. The percentage of peptides with a SILAC ratio < -0.5 are indicated in red. (B) Western blots of WCE from HeLa cells stained with α-histone H2A, α-histone H2B, α-histone H3 α-histone H4 (depicted in green) and α-acetyl-lysine (depicted in red) indicating that the strong acetyl-lysine signal of the low molecular weight bands originates from acetylated core histones. (C) Coomassie staining of extracted histones and WCE from the same number of HeLa cells, treated with HATi (CTK7A, 100 μM and CPTH2, 50 μM) or HDACi (TSA, 1 μM) or mock treated. (D) Western blots of HeLa cells lysed at different time points after irradiation with UV (16J/m^2). Blots were stained with α-acetyl-lysine (Immunechem, top panel), α-histone H4 (middle panel) and α-tubulin (bottom panel). (E) Quantification of the α-acetyl-lysine signal normalized against either the histone H4 levels (red bars) or tubulin levels (blue bars). Error bars represent SEM. Quantification is average of 7 experiments and SEM is shown.

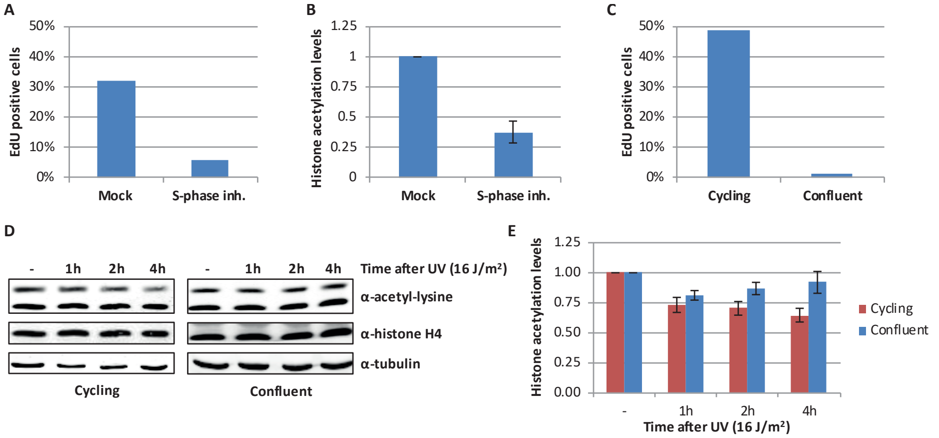

Supplemental figure 2: Loss of acetylated histones is caused by replication stress. (A) Relative amount of HeLa cells positively stained for EdU incorporation (2h, 20 µM), quantified from immunofluorescence images (>120 cells analyzed). (B) Quantification of histone acetylation levels, normalized against histone H4 levels of HeLa cells that are cultured with S-phase inhibitor (10 µM, o/n) or mock treated. (C) Relative amount of EdU positive, cycling or contact inhibited (confluent) VH10 cells, quantified from immunofluorescence images (>100 cells analyzed). (D) Western blots of WCE from confluent (right panel) or cycling (left panel) VH10 cells lysed at different time points after UV (16 J/m^2). Blots were stained with α-acetyl-lysine (top panel), α-histone H4 (middle panel) and α-tubulin (bottom panel). (E) Quantification of histone acetylation levels in confluent or cycling VH10 cells at different time points in which the histone acetylation levels are normalized against histone H4 levels after UV (16 J/m^2). Average of at least 3 experiments. Error bars represent SEM.

Full supplemental tables are available upon request.
The identified acetylated histone peptides from the acetyl-lysine IP experiments using the antibody from PTMscan listed in Supplemental table 2 are shown in the following table.

Histone H1
Histone H2A
Histone H2B
Histone H3
Histone H4

Sequence: Amino acid sequence of the identified peptide
Modifications: List of modifications identified within the peptide.
Gene Names: Name of the gene that peptide is associated with
UV/Mock pooled: Log 2 of the average normalized heavy(UV)/Light(Mock) SILAC ratio from 3 independent experiments analyzed together
UV/mock exp1: Log 2 of the normalized heavy(UV)/Light(Mock) SILAC ratio from experiment 1
UV/mock exp2: Log 2 of the normalized heavy(UV)/Light(Mock) SILAC ratio from experiment 2

Sequence	Modifications	Gene	UV/Mock pooled	UV/mock Exp 1	UV/mock Exp 2
ASGSFKLNKKAASGE	Acetyl (K)	HIST1H1E	0.15	0.20	0.10
IKLGLKSLVSK	Acetyl (K)	HIST1H1E	0.20	NaN	0.20
KASGPPVSELITKAVAASKER	Acetyl (K)	HIST1H1E	-1.22	NaN	-1.22
KNNSRIKLGLKS	Acetyl (K)	HIST1H1E	-0.37	-0.37	NaN
LITKAVAASKE	Acetyl (K)	HIST1H1E	0.26	0.26	-0.11
LKSLVSKGTLVQTKGTG	Acetyl (K)	HIST1H1E	0.33	0.45	-0.16
SETAPAAPAAAPPAEKAPVK	Acetyl (K);Acetyl (Protein N-term)	HIST1H1C	-0.25	-0.25	NaN
SETAPAAPAAPAPAEKTPVK	Acetyl (K);Acetyl (Protein N-term)	HIST1H1E	-0.19	-0.03	-0.55
SGVSLAALKK	Acetyl (K)	HIST1H1E	0.16	NaN	0.16
TAPAAPAAAPPAEKAPVKK	Acetyl (K)	HIST1H1C	-0.54	NaN	-0.54
TAPAAPAAPAPAEKTPVKK	Acetyl (K)	HIST1H1E	-0.26	NaN	-0.26
TAPAAPAAPAPAEKTPVKKK	Acetyl (K)	HIST1H1E	-0.62	NaN	-0.62
TAPAAPAAPAPAEKTPVKKKAR	Acetyl (K)	HIST1H1E	-0.60	NaN	-0.60
VKTPQPKKAAKSPAKA	3 Acetyl (K)	HIST1H1D	NaN	NaN	NaN
AGGKAGKDSGKAK	3 Acetyl (K)	H2AFZ	-0.71	-0.76	-0.62
AGGKAGKDSGKAKAK	4 Acetyl (K)	H2AFV	-0.81	NaN	-0.81
AGGKAGKDSGKAKAK	3 Acetyl (K)	H2AFV	-0.76	-0.78	-0.72
AGGKAGKDSGKAKAKAVSR	4 Acetyl (K)	H2AFV	-0.87	-0.92	-0.83
AGGKAGKDSGKAKAKAVSR	3 Acetyl (K)	H2AFV	-0.42	-0.42	NaN
AGGKAGKDSGKAKAKAVSRSQR	3 Acetyl (K)	H2AFV	-1.83	-1.83	NaN
AGGKAGKDSGKAKTK	4 Acetyl (K)	H2AFZ	-0.72	-1.06	-0.71
AGGKAGKDSGKAKTK	3 Acetyl (K)	H2AFZ	-0.63	-0.45	-0.67
AGGKAGKDSGKAKTKA	4 Acetyl (K)	H2AFZ	-0.64	-0.64	NaN
AGGKAGKDSGKAKTKAVS	3 Acetyl (K)	H2AFZ	-0.57	NaN	-0.57
AGGKAGKDSGKAKTKAVSR	4 Acetyl (K)	H2AFZ	-0.72	-0.67	-0.74
AGGKAGKDSGKAKTKAVSR	3 Acetyl (K)	H2AFZ	-0.27	-0.52	-0.11
AGGKAGKDSGKAKTKAVSR	2 Acetyl (K)	H2AFZ	1.19	1.07	1.32
AGGKAGKDSGKAKTKAVSRSQR	4 Acetyl (K)	H2AFZ	-0.96	-0.97	-0.95
AGGKAGKDSGKAKTKAVSRSQR	3 Acetyl (K)	H2AFZ	-0.67	-0.53	-1.03
AVLLPKKTE	Acetyl (K)	HIST1H2AK	-0.19	-0.13	-0.19
LDSLIKATIAGGGVIPHIHKS	Acetyl (K)	H2AFZ	0.99	NaN	0.99
LPKKTESHKPG	2 Acetyl (K)	HIST2H2AB	-1.17	-1.36	-0.99
NKLLGKVTIAQGGVL	Acetyl (K)	HIST1H2AK	0.19	0.19	NaN
QGGVLPNIQAVLLPKKTE	Acetyl (K)	HIST1H2AK	0.21	NaN	0.21
SGRGKQGGKAR	2 Acetyl (K);Acetyl (Protein N-term)	HIST1H2AK	-1.20	-1.20	NaN
SGRGKQGGKARAK	2 Acetyl (K);Acetyl (Protein N-term)	HIST1H2AK	-1.03	-1.03	NaN
SGRGKQGGKVR	2 Acetyl (K);Acetyl (Protein N-term)	H2AFJ	-0.64	-0.64	NaN
VLLPKKTE	Acetyl (K)	HIST1H2AK	-0.01	-0.02	-0.01
VLLPKKTESHHKAKGK	Acetyl (K)	HIST1H2AK	-0.15	-0.15	NaN
VLLPKKTESHKAKSK	Acetyl (K)	HIST2H2AC	-0.36	-0.36	NaN
AKHAVSEGTKAVTKYTSSK	Acetyl (K)	HIST1H2BI	-0.14	-0.14	NaN
APAPKKGSKKAVTKAQKKD	3 Acetyl (K)	HIST1H2BI	-1.03	NaN	-1.03
APAPKKGSKKAVTKAQKKD	4 Acetyl (K)	HIST1H2BI	-0.63	NaN	-0.63

Sequence	**Modifications**	**Gene**	**UV/Mock pooled**	**UV/mock Exp 1**	**UV/mock Exp 2**
AVTKAQKK	2 Acetyl (K)	HIST1H2BI	0.06	0.06	0.05
GTKAVTKYTSAK	Acetyl (K)	HIST1H2BK	0.26	0.28	0.26
GTKAVTKYTSSK	Acetyl (K)	HIST1H2BI	0.12	0.22	0.08
HAVSEGTKAVTKYTSSK	Acetyl (K)	HIST1H2BI	0.53	0.53	NaN
IQTAVRLLLPGELAKHAVSE	Acetyl (K)	HIST1H2BI	0.06	0.07	0.06
KAVTKAQK	2 Acetyl (K)	HIST1H2BI	-0.62	-0.62	NaN
KAVTKAQKK	3 Acetyl (K)	HIST1H2BI	-0.32	-0.80	0.15
KGSKKAVTK	3 Acetyl (K)	HIST1H2BI	-1.17	-1.45	-0.90
KGSKKAVTKAQK	4 Acetyl (K)	HIST1H2BI	-0.76	-0.85	-0.60
KGSKKAVTKAQK	3 Acetyl (K)	HIST1H2BI	-0.71	-1.18	-0.66
KGSKKAVTKAQKK	3 Acetyl (K)	HIST1H2BI	-1.02	-1.02	-0.70
KGSKKAVTKAQKK	4 Acetyl (K)	HIST1H2BI	-0.72	-0.72	-0.51
KGSKKAVTKAQKK	5 Acetyl (K)	HIST1H2BI	-0.37	-0.88	0.01
KGSKKAVTKAQKKD	3 Acetyl (K)	HIST1H2BI	-1.15	NaN	-1.15
KGSKKAVTKAQKKD	4 Acetyl (K)	HIST1H2BI	-0.48	-1.27	-0.46
KGSKKAVTKAQKKDGK	4 Acetyl (K)	HIST1H2BI	-0.68	-0.88	-0.48
KGSKKAVTKAQKKDGK	3 Acetyl (K)	HIST1H2BI	-0.52	NaN	-0.52
KGSKKAVTKAQKKDGK	5 Acetyl (K)	HIST1H2BI	0.03	-0.77	0.05
KGSKKAVTKAQKKDGKK	4 Acetyl (K)	HIST1H2BI	-0.87	NaN	-0.87
KGSKKAVTKAQKKDGKKR	3 Acetyl (K)	HIST1H2BI	-1.23	-1.23	NaN
KGSKKAVTKAQKKDGKKR	4 Acetyl (K)	HIST1H2BI	-0.84	-1.40	-0.73
KGSKKAVTKAQKKDGKKR	5 Acetyl (K)	HIST1H2BI	-0.29	-1.06	-0.17
KGSKKAVTKVQK	4 Acetyl (K)	HIST2H2BF	-0.55	NaN	-0.55
KGSKKAVTKVQKK	4 Acetyl (K)	HIST2H2BF	-0.60	-1.20	-0.43
KGSKKAVTKVQKK	3 Acetyl (K)	HIST2H2BF	-0.41	NaN	-0.41
KGSKKAVTKVQKKD	4 Acetyl (K)	HIST2H2BF	-0.56	NaN	-0.56
KGSKKAVTKVQKKDGK	5 Acetyl (K)	HIST2H2BF	-1.49	NaN	-1.49
KGSKKAVTKVQKKDGK	4 Acetyl (K)	HIST2H2BF	-0.58	NaN	-0.58
KGSKKAVTKVQKKDGKKR	4 Acetyl (K)	HIST2H2BF	-0.66	NaN	-0.66
LAKSAPAPKKG	Acetyl (K)	HIST1H2BL	-1.30	-1.30	NaN
LLLPGELAKHAVSEGTK	Acetyl (K)	HIST1H2BI	0.19	NaN	0.19
PDPAKSAPAPKKG	2 Acetyl (K)	HIST1H2BH	-1.11	NaN	-1.11
PDPAKSAPAPKKGSK	3 Acetyl (K)	HIST1H2BH	-1.35	NaN	-1.35
PDPAKSAPAPKKGSK	2 Acetyl (K)	HIST1H2BH	NaN	NaN	NaN
PDPAKSAPAPKKGSKK	2 Acetyl (K)	HIST1H2BH	-1.36	-1.36	NaN
PDPAKSAPAPKKGSKKAVT	4 Acetyl (K)	HIST1H2BH	-1.11	-1.11	NaN
PDPAKSAPAPKKGSKKAVT	3 Acetyl (K)	HIST1H2BH	-0.99	-1.13	-0.84
PDPAKSAPAPKKGSKKAVT	2 Acetyl (K)	HIST1H2BH	-0.98	-0.98	NaN
PDPAKSAPAPKKGSKKAVTK	3 Acetyl (K)	HIST1H2BH	-1.75	-1.75	NaN
PDPAKSAPAPKKGSKKAVTKAQK	4 Acetyl (K)	HIST1H2BH	-1.65	NaN	-1.65
PDPAKSAPAPKKGSKKAVTKAQK	5 Acetyl (K)	HIST1H2BH	-1.06	NaN	-1.06
PDPAKSAPAPKKGSKKAVTKAQKK	5 Acetyl (K)	HIST1H2BH	-0.87	NaN	-0.87
PDPAKSAPAPKKGSKKAVTKAQKKD	4 Acetyl (K)	HIST1H2BH	-0.88	NaN	-0.88

Sequence	**Modifications**	**Gene**	**UV/Mock pooled**	**UV/mock Exp 1**	**UV/mock Exp 2**
PDPAKSAPAPKKGSKKAVTKAQKKD	5 Acetyl (K)	HIST1H2BH	-0.71	NaN	-0.71
PDPAKSAPAPKKGSKKAVTKVQK	4 Acetyl (K)	HIST2H2BF	-1.02	-1.27	-0.77
PDPAKSAPAPKKGSKKAVTKVQKKD	5 Acetyl (K)	HIST2H2BF	-1.48	NaN	-1.48
PDPAKSAPAPKKGSKKAVTKVQKKD	4 Acetyl (K)	HIST2H2BF	-0.94	-1.75	-0.92
PELAKSAPAPKKGSK	2 Acetyl (K)	HIST1H2BL	-1.39	NaN	-1.39
PELAKSAPAPKKGSKK	2 Acetyl (K)	HIST1H2BL	-1.82	-1.82	NaN
PELAKSAPAPKKGSKKAVT	3 Acetyl (K)	HIST1H2BL	-1.14	-1.14	NaN
PEPAKSAPAPKKG	2 Acetyl (K)	HIST1H2BI	-1.05	-1.76	-1.05
PEPAKSAPAPKKGS	2 Acetyl (K)	HIST1H2BI	-1.00	NaN	-1.00
PEPAKSAPAPKKGSK	2 Acetyl (K)	HIST1H2BI	-1.50	-1.83	-1.42
PEPAKSAPAPKKGSK	3 Acetyl (K)	HIST1H2BI	-1.23	NaN	-1.23
PEPAKSAPAPKKGSKK	2 Acetyl (K)	HIST1H2BI	-1.53	-1.74	-1.47
PEPAKSAPAPKKGSKK	4 Acetyl (K)	HIST1H2BI	-1.51	NaN	-1.51
PEPAKSAPAPKKGSKK	3 Acetyl (K)	HIST1H2BI	-0.95	-1.46	-0.62
PEPAKSAPAPKKGSKKA	3 Acetyl (K)	HIST1H2BI	-0.84	NaN	-0.84
PEPAKSAPAPKKGSKKAVT	5 Acetyl (K)	HIST1H2BI	-1.40	-1.40	NaN
PEPAKSAPAPKKGSKKAVT	2 Acetyl (K)	HIST1H2BI	-1.33	-1.33	NaN
PEPAKSAPAPKKGSKKAVT	4 Acetyl (K)	HIST1H2BI	-1.18	-1.33	-0.98
PEPAKSAPAPKKGSKKAVT	3 Acetyl (K)	HIST1H2BI	-1.08	-1.16	-0.71
PEPAKSAPAPKKGSKKAVTK	5 Acetyl (K)	HIST1H2BI	-1.84	NaN	-1.84
PEPAKSAPAPKKGSKKAVTK	2 Acetyl (K)	HIST1H2BI	-1.73	-1.85	-1.40
PEPAKSAPAPKKGSKKAVTK	4 Acetyl (K)	HIST1H2BI	-1.50	-1.46	-1.53
PEPAKSAPAPKKGSKKAVTK	3 Acetyl (K)	HIST1H2BI	-1.32	-1.65	-1.13
PEPAKSAPAPKKGSKKAVTKAQK	3 Acetyl (K)	HIST1H2BI	-1.15	-1.15	NaN
PEPAKSAPAPKKGSKKAVTKAQK	4 Acetyl (K)	HIST1H2BI	-0.99	-1.08	-0.93
PEPAKSAPAPKKGSKKAVTKAQK	5 Acetyl (K)	HIST1H2BI	-0.87	-1.21	-0.86
PEPAKSAPAPKKGSKKAVTKAQK	2 Acetyl (K)	HIST1H2BI	NaN	NaN	NaN
PEPAKSAPAPKKGSKKAVTKAQKK	6 Acetyl (K)	HIST1H2BI	-0.93	-1.46	-0.78
PEPAKSAPAPKKGSKKAVTKAQKK	5 Acetyl (K)	HIST1H2BI	-0.46	NaN	-0.46
PEPAKSAPAPKKGSKKAVTKAQKKD	6 Acetyl (K)	HIST1H2BI	-1.20	NaN	-1.20
PEPAKSAPAPKKGSKKAVTKAQKKD	3 Acetyl (K)	HIST1H2BI	-1.16	-1.39	-1.16
PEPAKSAPAPKKGSKKAVTKAQKKD	4 Acetyl (K)	HIST1H2BI	-0.90	-1.04	-0.89
PEPAKSAPAPKKGSKKAVTKAQKKD	5 Acetyl (K)	HIST1H2BI	-0.84	-1.37	-0.83
PEPSKSAPAPKKG	2 Acetyl (K)	HIST1H2BN	-1.03	NaN	-1.03
PEPSKSAPAPKKGSKKAVT	3 Acetyl (K)	HIST1H2BN	-1.05	-1.05	NaN
PEPSKSAPAPKKGSKKAVT	4 Acetyl (K)	HIST1H2BN	-1.05	-1.05	NaN
PEPSKSAPAPKKGSKKAVTKAQKKD	4 Acetyl (K)	HIST1H2BN	-0.85	NaN	-0.85
PEPTKSAPAPKKG	2 Acetyl (K)	HIST1H2BD	-1.40	NaN	-1.40
PEPTKSAPAPKKGSKK	3 Acetyl (K)	HIST1H2BD	-1.54	-1.54	NaN
PEPTKSAPAPKKGSKKAVT	4 Acetyl (K)	HIST1H2BD	-1.32	-1.32	NaN
PEPTKSAPAPKKGSKKAVT	3 Acetyl (K)	HIST1H2BD	-0.89	NaN	-0.89
PEPTKSAPAPKKGSKKAVTK	4 Acetyl (K)	HIST1H2BD	-1.74	NaN	-1.74
PEPTKSAPAPKKGSKKAVTK	3 Acetyl (K)	HIST1H2BD	-1.48	NaN	-1.48

Sequence	**Modifications**	**Gene**	**UV/Mock pooled**	**UV/mock Exp 1**	**UV/mock Exp 2**
PEPTKSAPAPKKGSKKAVTKAQK	4 Acetyl (K)	HIST1H2BD	-1.12	-1.12	NaN
PEPTKSAPAPKKGSKKAVTKAQK	5 Acetyl (K)	HIST1H2BD	-0.99	NaN	-0.99
PEPVKSAPVPKKGSKKAIN	3 Acetyl (K)	HIST1H2BM	-1.28	-1.28	NaN
SAPAPKKGSKK	3 Acetyl (K)	HIST1H2BI	-1.10	NaN	-1.10
SAPAPKKGSKKAVT	3 Acetyl (K)	HIST1H2BI	-0.63	-0.73	-0.58
SAPAPKKGSKKAVTK	4 Acetyl (K)	HIST1H2BI	-1.24	NaN	-1.24
SAPAPKKGSKKAVTK	3 Acetyl (K)	HIST1H2BI	-1.22	NaN	-1.22
SAPAPKKGSKKAVTKAQK	2 Acetyl (K)	HIST1H2BI	-1.71	NaN	-1.71
SAPAPKKGSKKAVTKAQK	4 Acetyl (K)	HIST1H2BI	-0.75	NaN	-0.75
SAPAPKKGSKKAVTKAQK	3 Acetyl (K)	HIST1H2BI	-0.69	NaN	-0.69
SAPAPKKGSKKAVTKAQK	5 Acetyl (K)	HIST1H2BI	-0.66	NaN	-0.66
SAPAPKKGSKKAVTKAQKK	3 Acetyl (K)	HIST1H2BI	-1.12	NaN	-1.12
SAPAPKKGSKKAVTKAQKK	4 Acetyl (K)	HIST1H2BI	-0.80	NaN	-0.80
SAPAPKKGSKKAVTKAQKK	5 Acetyl (K)	HIST1H2BI	-0.70	-1.60	-0.62
SAPAPKKGSKKAVTKAQKKD	2 Acetyl (K)	HIST1H2BI	-1.04	NaN	-1.04
SAPAPKKGSKKAVTKAQKKD	4 Acetyl (K)	HIST1H2BI	-0.65	NaN	-0.65
SAPAPKKGSKKAVTKAQKKD	5 Acetyl (K)	HIST1H2BI	-0.47	NaN	-0.47
SAPAPKKGSKKAVTKAQKKDGK	4 Acetyl (K)	HIST1H2BI	-1.34	-2.15	-0.54
SAPAPKKGSKKAVTKAQKKDGK	3 Acetyl (K)	HIST1H2BI	-0.83	NaN	-0.83
SAPAPKKGSKKAVTKAQKKDGK	5 Acetyl (K)	HIST1H2BI	-0.60	NaN	-0.60
SAPAPKKGSKKAVTKAQKKDGK	6 Acetyl (K)	HIST1H2BI	-0.27	NaN	-0.27
SAPAPKKGSKKAVTKVQKK	4 Acetyl (K)	HIST2H2BF	-0.70	NaN	-0.70
SAPAPKKGSKKAVTKVQKK	5 Acetyl (K)	HIST2H2BF	-0.69	NaN	-0.69
SAPAPKKGSKKAVTKVQKKD	3 Acetyl (K)	HIST2H2BF	NaN	NaN	NaN
SKKAVTKAQKK	3 Acetyl (K)	HIST1H2BI	-0.45	NaN	-0.45
SKKAVTKAQKKD	3 Acetyl (K)	HIST1H2BI	-0.58	NaN	-0.58
SKKAVTKAQKKD	4 Acetyl (K)	HIST1H2BI	-0.27	NaN	-0.27
SKKAVTKAQKKDGK	3 Acetyl (K)	HIST1H2BI	-0.72	NaN	-0.72
VRLLLPGELAKHAVSE	Acetyl (K)	HIST1H2BI	0.41	0.41	NaN
AARKSAPATGGVKKPHRYRPGTVA	Acetyl (K)	HIST2H3A	-0.96	-0.96	NaN
AARKSAPATGGVKKPHRYRPGTVAL	Acetyl (K)	HIST2H3A	-1.01	-1.01	NaN
AARKSAPSTGGVKKPHRYRPGTVAL	Acetyl (K)	H3F3A	-1.62	-1.62	NaN
ARTKQTARKSTGGKAPR	2 Acetyl (K)	HIST2H3A	-0.90	-0.80	-1.40
ARTKQTARKSTGGKAPRKQ	2 Acetyl (K)	HIST2H3A	-0.70	-0.56	-0.84
ARTKQTARKSTGGKAPRKQL	2 Acetyl (K)	HIST2H3A	NaN	NaN	NaN
ARTKQTARKSTGGKAPRKQLA	2 Acetyl (K)	HIST2H3A	-0.67	-0.67	NaN
ARTKQTARKSTGGKAPRKQLAT	2 Acetyl (K)	HIST2H3A	-0.62	-0.62	NaN
ARTKQTARKSTGGKAPRKQLATK	3 Acetyl (K)	HIST2H3A	-1.38	NaN	-1.38
GKAPRKQL	2 Acetyl (K)	HIST2H3A	-0.38	NaN	-0.38
GKAPRKQLA	2 Acetyl (K)	HIST2H3A	-0.17	-0.10	-0.23
GKAPRKQLA	Acetyl (K)	HIST2H3A	-0.16	-0.20	-0.05
GKAPRKQLAT	2 Acetyl (K)	HIST2H3A	-0.07	NaN	-0.07
GKAPRKQLATK	2 Acetyl (K)	HIST2H3A	-0.57	-0.17	-0.64

Sequence	**Modifications**	**Gene**	**UV/Mock pooled**	**UV/mock Exp 1**	**UV/mock Exp 2**
GKAPRKQLATK	Acetyl (K)	HIST2H3A	-0.27	-0.27	NaN
GKAPRKQLATKA	2 Acetyl (K)	HIST2H3A	-0.35	-0.23	-0.35
GKAPRKQLATKA	3 Acetyl (K)	HIST2H3A	-0.11	-0.11	NaN
GKAPRKQLATKA	Acetyl (K)	HIST2H3A	0.02	NaN	0.02
GKAPRKQLATKAA	Acetyl (K)	HIST2H3A	-0.57	-0.42	-0.72
GKAPRKQLATKAA	2 Acetyl (K)	HIST2H3A	-0.28	0.12	-0.33
GKAPRKQLATKAA	3 Acetyl (K)	HIST2H3A	0.11	0.11	NaN
GKAPRKQLATKAAR	3 Acetyl (K)	HIST2H3A	-0.40	-0.39	-0.43
GKAPRKQLATKAAR	Acetyl (K)	HIST2H3A	-0.22	-0.22	NaN
GKAPRKQLATKAAR	2 Acetyl (K)	HIST2H3A	0.03	-0.60	-0.32
GKAPRKQLATKAARKS	4 Acetyl (K)	HIST2H3A	-0.99	-0.99	NaN
GKAPRKQLATKVA	Acetyl (K)	HIST3H3	-0.41	-0.63	-0.19
GKAPRKQLATKVA	2 Acetyl (K)	HIST3H3	-0.21	NaN	-0.21
IRKLPFQRL	Acetyl (K)	HIST2H3A	-0.16	-0.17	0.27
KQLATKAAR	2 Acetyl (K)	HIST2H3A	-0.22	-0.03	-0.22
KQLATKAAR	Acetyl (K)	HIST2H3A	-0.02	-0.01	-0.02
KQLATKAARK	2 Acetyl (K)	HIST2H3A	-1.06	-1.31	-0.80
KQLATKAARKSAPATGGVKKPHR	2 Acetyl (K)	HIST2H3A	-0.86	NaN	-0.86
KSTGGKAPR	2 Acetyl (K)	HIST2H3A	-0.47	-0.18	-0.76
KSTGGKAPRKQ	3 Acetyl (K)	HIST2H3A	-0.56	-0.39	-0.73
KSTGGKAPRKQ	2 Acetyl (K)	HIST2H3A	-0.37	-0.26	-0.37
KSTGGKAPRKQL	3 Acetyl (K)	HIST2H3A	-0.59	-0.42	-0.73
KSTGGKAPRKQL	2 Acetyl (K)	HIST2H3A	-0.57	-0.42	-0.65
KSTGGKAPRKQLA	3 Acetyl (K)	HIST2H3A	-0.89	NaN	-0.89
KSTGGKAPRKQLA	2 Acetyl (K)	HIST2H3A	-0.43	-0.43	NaN
KSTGGKAPRKQLAT	3 Acetyl (K)	HIST2H3A	-1.03	-0.81	-1.25
KSTGGKAPRKQLAT	2 Acetyl (K)	HIST2H3A	-0.35	-0.29	-0.56
KSTGGKAPRKQLATK	3 Acetyl (K)	HIST2H3A	-0.94	-0.38	-0.96
KSTGGKAPRKQLATK	2 Acetyl (K)	HIST2H3A	-0.55	-0.43	-0.55
KSTGGKAPRKQLATK	Acetyl (K)	HIST2H3A	-0.49	-0.48	-0.92
KSTGGKAPRKQLATKA	3 Acetyl (K)	HIST2H3A	-0.76	-0.31	-0.84
KSTGGKAPRKQLATKA	2 Acetyl (K)	HIST2H3A	-0.30	-0.25	-0.63
KSTGGKAPRKQLATKA	Acetyl (K)	HIST2H3A	-0.28	-0.21	-0.35
KSTGGKAPRKQLATKAAR	2 Acetyl (K)	HIST2H3A	-0.61	-0.57	-0.68
KSTGGKAPRKQLATKAAR	4 Acetyl (K)	HIST2H3A	-0.60	-0.60	NaN
KSTGGKAPRKQLATKAAR	Acetyl (K)	HIST2H3A	-0.26	-0.26	NaN
KSTGGKAPRKQLATKAAR	3 Acetyl (K)	HIST2H3A	-0.19	-0.43	-0.97
KSTGGKAPRKQLATKAARK	2 Acetyl (K)	HIST2H3A	-0.96	-0.70	-0.92
KSTGGKAPRKQLATKAARK	3 Acetyl (K)	HIST2H3A	-0.87	-0.51	-0.97
KSTGGKAPRKQLATKAARK	4 Acetyl (K)	HIST2H3A	-0.69	-0.53	-0.88
KSTGGKAPRKQLATKVAR	3 Acetyl (K)	HIST3H3	-0.48	NaN	-0.48
LATKAARKSAPATG	2 Acetyl (K)	HIST2H3A	-0.22	NaN	-0.22
LIRKLPFQRL	Acetyl (K)	HIST2H3A	-0.16	-0.16	NaN

Sequence	Modifications	Gene	UV/Mock pooled	UV/mock Exp 1	UV/mock Exp 2
LLVRKLPFQR	Acetyl (K)	N/A	-0.20	-0.13	-0.24
LLVRKLPFQRL	Acetyl (K)	N/A	0.02	0.02	NaN
LLVRKLPFQRLVRE	Acetyl (K)	N/A	-0.32	-0.15	-0.48
LVRKLPFQRL	Acetyl (K)	N/A	-0.18	-0.18	NaN
QLATKAAR	Acetyl (K)	HIST2H3A	-0.04	0.13	-0.11
QTARKSTGGKAPR	2 Acetyl (K)	HIST2H3A	-1.15	NaN	-1.15
QTARKSTGGKAPRKQ	2 Acetyl (K)	HIST2H3A	-0.53	-0.53	NaN
QTARKSTGGKAPRKQLA	2 Acetyl (K)	HIST2H3A	-1.03	-1.03	NaN
QTARKSTGGKAPRKQLAT	2 Acetyl (K)	HIST2H3A	-0.41	-0.41	NaN
QTARKSTGGKAPRKQLATK	Acetyl (K)	HIST2H3A	-0.81	-0.81	NaN
QTARKSTGGKAPRKQLATK	3 Acetyl (K)	HIST2H3A	-0.75	-0.75	NaN
QTARKSTGGKAPRKQLATK	2 Acetyl (K)	HIST2H3A	-0.74	-0.49	-0.75
QTARKSTGGKAPRKQLATKA	2 Acetyl (K)	HIST2H3A	-0.74	NaN	-0.74
QTARKSTGGKAPRKQLATKA	Acetyl (K)	HIST2H3A	-0.33	-0.33	NaN
QTARKSTGGKAPRKQLATKAAR	4 Acetyl (K)	HIST2H3A	-1.32	NaN	-1.32
QTARKSTGGKAPRKQLATKAAR	2 Acetyl (K)	HIST2H3A	-0.82	-0.62	-0.82
QTARKSTGGKAPRKQLATKAAR	Acetyl (K)	HIST2H3A	-0.49	-0.48	-0.49
QTARKSTGGKAPRKQLATKAAR	3 Acetyl (K)	HIST2H3A	-0.29	-0.70	-0.97
RKSTGGKAPRKQLATK	2 Acetyl (K)	HIST2H3A	-0.96	NaN	-0.96
STGGKAPRKQ	2 Acetyl (K)	HIST2H3A	-0.77	-0.77	-0.66
STGGKAPRKQLA	2 Acetyl (K)	HIST2H3A	-0.33	-0.20	-0.42
STGGKAPRKQLAT	2 Acetyl (K)	HIST2H3A	-0.25	-0.25	NaN
STGGKAPRKQLATK	2 Acetyl (K)	HIST2H3A	-0.50	-0.50	NaN
STGGKAPRKQLATK	Acetyl (K)	HIST2H3A	-0.47	-0.32	-0.63
STGGKAPRKQLATKA	3 Acetyl (K)	HIST2H3A	-0.50	0.00	-0.61
STGGKAPRKQLATKA	Acetyl (K)	HIST2H3A	-0.38	-0.25	-0.50
STGGKAPRKQLATKA	2 Acetyl (K)	HIST2H3A	-0.25	-0.23	-0.58
STGGKAPRKQLATKAAR	3 Acetyl (K)	HIST2H3A	-0.55	-0.40	-0.70
STGGKAPRKQLATKAAR	2 Acetyl (K)	HIST2H3A	-0.55	-0.36	-0.60
STGGKAPRKQLATKAAR	Acetyl (K)	HIST2H3A	-0.32	-0.22	-0.41
STGGKAPRKQLATKVA	2 Acetyl (K)	HIST3H3	-3.78	-3.78	NaN
TARKSTGGKAPRKQLA	2 Acetyl (K)	HIST2H3A	-0.42	NaN	-0.42
TARKSTGGKAPRKQLATK	2 Acetyl (K)	HIST2H3A	-0.64	-0.64	-0.73
TARKSTGGKAPRKQLATK	3 Acetyl (K)	HIST2H3A	-0.55	-0.55	NaN
TGGKAPRKQ	2 Acetyl (K)	HIST2H3A	-0.25	-0.09	-0.41
TGGKAPRKQLA	2 Acetyl (K)	HIST2H3A	-0.24	-0.11	-0.33
TGGKAPRKQLA	Acetyl (K)	HIST2H3A	-0.14	-0.02	-0.25
TGGKAPRKQLATK	2 Acetyl (K)	HIST2H3A	-0.57	-0.19	-0.85
TGGKAPRKQLATK	Acetyl (K)	HIST2H3A	-0.45	-0.45	-0.45
TGGKAPRKQLATKA	2 Acetyl (K)	HIST2H3A	-0.28	-0.06	-0.47
TGGKAPRKQLATKAA	3 Acetyl (K)	HIST2H3A	-0.59	NaN	-0.59
TGGKAPRKQLATKAA	2 Acetyl (K)	HIST2H3A	-0.17	0.05	-0.28
TGGKAPRKQLATKAAR	2 Acetyl (K)	HIST2H3A	-0.08	-0.08	NaN

Sequence	**Modifications**	**Gene**	**UV/Mock pooled**	**UV/mock Exp 1**	**UV/mock Exp 2**
TKAARKSAPATG	2 Acetyl (K)	HIST2H3A	-0.02	NaN	-0.02
GGKGLGKGGAKR	3 Acetyl (K)	HIST1H4A	-0.77	NaN	-0.77
GGKGLGKGGAKR	2 Acetyl (K)	HIST1H4A	-0.28	-0.28	NaN
GGKGLGKGGAKR	Acetyl (K)	HIST1H4A	0.00	0.12	-0.04
GGKGLGKGGAKRHR	3 Acetyl (K)	HIST1H4A	-0.24	-0.33	-0.87
GKGGKGLG	2 Acetyl (K)	HIST1H4A	-0.48	-0.45	-0.50
GKGGKGLGKGGAK	3 Acetyl (K)	HIST1H4A	-0.51	-0.63	-0.51
GKGGKGLGKGGAK	2 Acetyl (K)	HIST1H4A	-0.45	-0.44	-0.66
GKGGKGLGKGGAKR	3 Acetyl (K)	HIST1H4A	-0.92	-0.60	-0.95
GKGGKGLGKGGAKR	4 Acetyl (K)	HIST1H4A	-0.51	-0.80	-0.56
GKGGKGLGKGGAKR	2 Acetyl (K)	HIST1H4A	-0.50	-0.42	-0.84
GKGGKGLGKGGAKR	Acetyl (K)	HIST1H4A	-0.24	-0.21	-0.29
GKGGKGLGKGGAKRHR	3 Acetyl (K)	HIST1H4A	-0.91	-0.71	-0.95
GKGGKGLGKGGAKRHR	4 Acetyl (K)	HIST1H4A	-0.88	-0.88	NaN
GLGKGGAKR	2 Acetyl (K)	HIST1H4A	-0.23	-0.22	-0.56
GLGKGGAKRHR	2 Acetyl (K)	HIST1H4A	-0.49	-0.49	-0.71
HRKVLRDNIQGITKPAIR	Acetyl (K)	HIST1H4A	-0.64	NaN	-0.64
LGKGGAKR	2 Acetyl (K)	HIST1H4A	-0.18	-0.18	NaN
RGKGGKGLG	2 Acetyl (K)	HIST1H4A	-0.51	-0.51	-0.91
RKVLRDNIQGITKPAIR	Acetyl (K)	HIST1H4A	-0.50	NaN	-0.50
SGRGKGGKGLG	2 Acetyl (K);Acetyl (Protein N-term)	HIST1H4A	-0.55	-0.50	-0.61
SGRGKGGKGLG	2 Acetyl (K)	HIST1H4A	-0.03	-0.24	0.19
SGRGKGGKGLGK	2 Acetyl (K)	HIST1H4A	-1.25	-1.25	NaN
SGRGKGGKGLGK	2 Acetyl (K);Acetyl (Protein N-term)	HIST1H4A	-0.59	-0.59	NaN
SGRGKGGKGLGKG	3 Acetyl (K)	HIST1H4A	-0.80	NaN	-0.80
SGRGKGGKGLGKG	3 Acetyl (K);Acetyl (Protein N-term)	HIST1H4A	-0.73	-0.67	-0.78
SGRGKGGKGLGKG	2 Acetyl (K)	HIST1H4A	-0.44	-0.44	NaN
SGRGKGGKGLGKGG	3 Acetyl (K);Acetyl (Protein N-term)	HIST1H4A	-2.48	-2.60	-2.41
SGRGKGGKGLGKGGA	3 Acetyl (K);Acetyl (Protein N-term)	HIST1H4A	0.19	0.19	NaN
SGRGKGGKGLGKGGAK	3 Acetyl (K)	HIST1H4A	-0.82	-0.88	-0.81
SGRGKGGKGLGKGGAK	3 Acetyl (K);Acetyl (Protein N-term)	HIST1H4A	-0.62	-0.68	-0.62
SGRGKGGKGLGKGGAKR	4 Acetyl (K);Acetyl (Protein N-term)	HIST1H4A	-0.98	-0.98	NaN
SGRGKGGKGLGKGGAKR	4 Acetyl (K)	HIST1H4A	-0.50	-0.69	-0.95
SGRGKGGKGLGKGGAKR	3 Acetyl (K)	HIST1H4A	-0.34	-0.35	-0.84
SGRGKGGKGLGKGGAKR	2 Acetyl (K)	HIST1H4A	-0.16	-0.16	NaN
SGRGKGGKGLGKGGAKRH	3 Acetyl (K)	HIST1H4A	-1.35	-1.35	NaN
SGRGKGGKGLGKGGAKRH	4 Acetyl (K);Acetyl (Protein N-term)	HIST1H4A	-1.20	-1.16	-1.33
SGRGKGGKGLGKGGAKRHR	4 Acetyl (K);Acetyl (Protein N-term)	HIST1H4A	-1.24	NaN	-1.24
SGRGKGGKGLGKGGAKRHR	4 Acetyl (K)	HIST1H4A	-0.65	-0.64	-1.40
SGRGKGGKGLGKGGAKRHR	2 Acetyl (K)	HIST1H4A	-0.44	-0.27	-0.61
SGRGKGGKGLGKGGAKRHRK	4 Acetyl (K);Acetyl (Protein N-term)	HIST1H4A	-1.39	-1.39	-1.35
TRGVLKVFLE	Acetyl (K)	HIST1H4A	0.10	NaN	0.10
TVTAMDVVYALKR	Acetyl (K)	HIST1H4A	0.27	NaN	0.27

REFERENCES

1. Zhu, P. and G. Li, Structural insights of nucleosome and the 30-nm chromatin fiber. Curr Opin Struct Biol, 2016. 36: p. 106-15.
2. Kouzarides, T., Chromatin modifications and their function. Cell, 2007. 128(4): p. 693-705.
3. Langst, G. and L. Manelyte, Chromatin Remodelers: From Function to Dysfunction. Genes (Basel), 2015. 6(2): p. 299-324.
4. Escargueil, A.E., et al., What histone code for DNA repair? Mutat Res, 2008. 658(3): p. 259-70.
5. van Attikum, H. and S.M. Gasser, Crosstalk between histone modifications during the DNA damage response. Trends Cell Biol, 2009. 19(5): p. 207-17.
6. Ramanathan, B. and M.J. Smerdon, Changes in nuclear protein acetylation in u.v.-damaged human cells. Carcinogenesis, 1986. 7(7): p. 1087-94.
7. Marteijn, J.A., et al., Understanding nucleotide excision repair and its roles in cancer and ageing. Nat Rev Mol Cell Biol, 2014. 15(7): p. 465-81.
8. Ramanathan, B. and M.J. Smerdon, Enhanced DNA repair synthesis in hyperacetylated nucleosomes. J Biol Chem, 1989. 264(19): p. 11026-34.
9. Smerdon, M.J., DNA repair and the role of chromatin structure. Curr Opin Cell Biol, 1991. 3(3): p. 422-8.
10. Green, C.M. and G. Almouzni, When repair meets chromatin. First in series on chromatin dynamics. EMBO Rep, 2002. 3(1): p. 28-33.
11. Teng, Y., Y. Yu, and R. Waters, The Saccharomyces cerevisiae histone acetyltransferase Gcn5 has a role in the photoreactivation and nucleotide excision repair of UV-induced cyclobutane pyrimidine dimers in the MFA2 gene. J Mol Biol, 2002. 316(3): p. 489-99.
12. Kim, M.K., et al., The role of p300 histone acetyltransferase in UV-induced histone modifications and MMP-1 gene transcription. PLoS One, 2009. 4(3): p. e4864.
13. Wang, J., M.Y. Chin, and G. Li, The novel tumor suppressor p33ING2 enhances nucleotide excision repair via inducement of histone H4 acetylation and chromatin relaxation. Cancer Res, 2006. 66(4): p. 1906-11.
14. Hasan, S., et al., Transcription coactivator p300 binds PCNA and may have a role in DNA repair synthesis. Nature, 2001. 410(6826): p. 387-91.
15. Yu, Y., et al., UV irradiation stimulates histone acetylation and chromatin remodeling at a repressed yeast locus. Proc Natl Acad Sci U S A, 2005. 102(24): p. 8650-5.
16. Duan, M.R. and M.J. Smerdon, Histone H3 lysine 14 (H3K14) acetylation facilitates DNA repair in a positioned nucleosome by stabilizing the binding of the chromatin Remodeler RSC (Remodels Structure of Chromatin). J Biol Chem, 2014. 289(12): p. 8353-63.
17. Guo, R., et al., GCN5 and E2F1 stimulate nucleotide excision repair by promoting H3K9 acetylation at sites of damage. Nucleic Acids Res, 2011. 39(4): p. 1390-7.
18. Zhu, Q., et al., Damaged DNA-binding protein down-regulates epigenetic mark H3K56Ac through histone deacetylase 1 and 2. Mutat Res, 2015. 776: p. 16-23.
19. Tjeertes, J.V., K.M. Miller, and S.P. Jackson, Screen for DNA-damage-responsive histone modifications identifies H3K9Ac and H3K56Ac in human cells. EMBO J, 2009. 28(13): p. 1878-89.
20. Bergink, S., et al., DNA damage triggers nucleotide excision repair-dependent monoubiquitylation of histone H2A. Genes Dev, 2006. 20(10): p. 1343-52.

21. Citterio, E., et al., ATP-dependent chromatin remodeling by the Cockayne syndrome B DNA repair-transcription-coupling factor. Molecular and Cellular Biology, 2000. 20(20): p. 7643-7653.
22. Elia, A.E., et al., Quantitative Proteomic Atlas of Ubiquitination and Acetylation in the DNA Damage Response. Mol Cell, 2015. 59(5): p. 867-81.
23. Svinkina, T., et al., Deep, Quantitative Coverage of the Lysine Acetylome Using Novel Anti-acetyl-lysine Antibodies and an Optimized Proteomic Workflow. Mol Cell Proteomics, 2015. 14(9): p. 2429-40.
24. Marteijn, J.A., et al., Nucleotide excision repair-induced H2A ubiquitination is dependent on MDC1 and RNF8 and reveals a universal DNA damage response. J Cell Biol, 2009. 186(6): p. 835-47.
25. Hanasoge, S. and M. Ljungman, H2AX phosphorylation after UV irradiation is triggered by DNA repair intermediates and is mediated by the ATR kinase. Carcinogenesis, 2007. 28(11): p. 2298-304.
26. Turner, B.M., Cellular memory and the histone code. Cell, 2002. 111(3): p. 285-91.
27. Kallin E, Z.Y., Chromatin remodeling, in Encyclopedia of biological chemistry., L.M. Lennarz WJ, Editor. 2004, Academic Press: London. p. 456-462.
28. Sadakierska-Chudy, A. and M. Filip, A comprehensive view of the epigenetic landscape. Part II: Histone post-translational modification, nucleosome level, and chromatin regulation by ncRNAs. Neurotox Res, 2015. 27(2): p. 172-97.
29. Wisniewski, J.R., et al., Mass spectrometric mapping of linker histone H1 variants reveals multiple acetylations, methylations, and phosphorylation as well as differences between cell culture and tissue. Mol Cell Proteomics, 2007. 6(1): p. 72-87.
30. van Cuijk, L., et al., SUMO and ubiquitin-dependent XPC exchange drives nucleotide excision repair. Nat Commun, 2015. 6: p. 7499.
31. Choi, J.H., et al., Highly specific and sensitive method for measuring nucleotide excision repair kinetics of ultraviolet photoproducts in human cells. Nucleic Acids Res, 2014. 42(4): p. e29.
32. Orren, D.K., L.N. Petersen, and V.A. Bohr, Persistent DNA damage inhibits S-phase and G2 progression, and results in apoptosis. Mol Biol Cell, 1997. 8(6): p. 1129-42.
33. Steurer, B. and J.A. Marteijn, Traveling Rocky Roads: The Consequences of Transcription-Blocking DNA Lesions on RNA Polymerase II. J Mol Biol, 2016.
34. Bensaude, O., Inhibiting eukaryotic transcription: Which compound to choose? How to evaluate its activity? Transcription, 2011. 2(3): p. 103-108.
35. Qian, M.X., et al., Acetylation-mediated proteasomal degradation of core histones during DNA repair and spermatogenesis. Cell, 2013. 153(5): p. 1012-24.
36. Shogren-Knaak, M.I., H.; Sun, J.M.; Pazin, M.J.; Davie, J.R.; Peterson, C.L., Histone H4-K16 acetylation controls chromatin structure and protein interactions. Science, 2006. 311: p. 844-847.
37. Agalioti, T.C., G.; Thanos, D., Deciphering the transcriptional histone acetylation code for a human gene. Cell, 2002. 111(3): p. 381-92.
38. Lans, H., J.A. Marteijn, and W. Vermeulen, ATP-dependent chromatin remodeling in the DNA-damage response. Epigenetics & Chromatin, 2012. 5.
39. Soria, G., S.E. Polo, and G. Almouzni,

Prime, repair, restore: the active role of chromatin in the DNA damage response. Molecular Cell, 2012. 46(6): p. 722-34.
40. Brand, M., et al., UV-damaged DNA-binding protein in the TFTC complex links DNA damage recognition to nucleosome acetylation. EMBO J, 2001. 20(12): p. 3187-96.
41. Rapic-Otrin, V., et al., Sequential binding of UV DNA damage binding factor and degradation of the p48 subunit as early events after UV irradiation. Nucleic Acids Res, 2002. 30(11): p. 2588-98.
42. Datta, A., et al., The p48 subunit of the damaged-DNA binding protein DDB associates with the CBP/p300 family of histone acetyltransferase. Mutat Res, 2001. 486(2): p. 89-97.
43. Yang, X., et al., Histone acetyltransferase 1 promotes homologous recombination in DNA repair by facilitating histone turnover. Journal of Biological Chemistry, 2013. 288(25): p. 18271-82.
44. Kurdistani, S.K., S. Tavazoie, and M. Grunstein, Mapping global histone acetylation patterns to gene expression. Cell, 2004. 117(6): p. 721-33.
45. Hauer, M.H., et al., Histone degradation in response to DNA damage enhances chromatin dynamics and recombination rates. Nat Struct Mol Biol, 2017. 24(2): p. 99-107.
46. Blickwedehl, J., et al., Role for proteasome activator PA200 and postglutamyl proteasome activity in genomic stability. Proc Natl Acad Sci U S A, 2008. 105(42): p. 16165-70.
47. Singh, R.K., et al., Excess histone levels mediate cytotoxicity via multiple mechanisms. Cell Cycle, 2010. 9(20): p. 4236-44.
48. Dominski, Z., et al., A 3' exonuclease that specifically interacts with the 3' end of histone mRNA. Mol Cell, 2003. 12(2): p. 295-305.
49. Kaygun, H. and W.F. Marzluff, Translation termination is involved in histone mRNA degradation when DNA replication is inhibited. Mol Cell Biol, 2005. 25(16): p. 6879-88.
50. Cook, A.J., et al., A specific function for the histone chaperone NASP to fine-tune a reservoir of soluble H3-H4 in the histone supply chain. Mol Cell, 2011. 44(6): p. 918-27.
51. Groth, A., et al., Human Asf1 regulates the flow of S phase histones during replicational stress. Mol Cell, 2005. 17(2): p. 301-11.
52. Gunjan, A. and A. Verreault, A Rad53 kinase-dependent surveillance mechanism that regulates histone protein levels in S. cerevisiae. Cell, 2003. 115(5): p. 537-49.
53. Sobel, R.E., et al., Conservation of deposition-related acetylation sites in newly synthesized histones H3 and H4. Proc Natl Acad Sci U S A, 1995. 92(4): p. 1237-41.
54. Li, Q., et al., Acetylation of histone H3 lysine 56 regulates replication-coupled nucleosome assembly. Cell, 2008. 134(2): p. 244-55.
55. Verreault, A., De novo nucleosome assembly: new pieces in an old puzzle. Genes Dev, 2000. 14(12): p. 1430-8.
56. Schindelin, J., et al., Fiji: an open-source platform for biological-image analysis. Nat Methods, 2012. 9(7): p. 676-82.

7

DISCUSSION

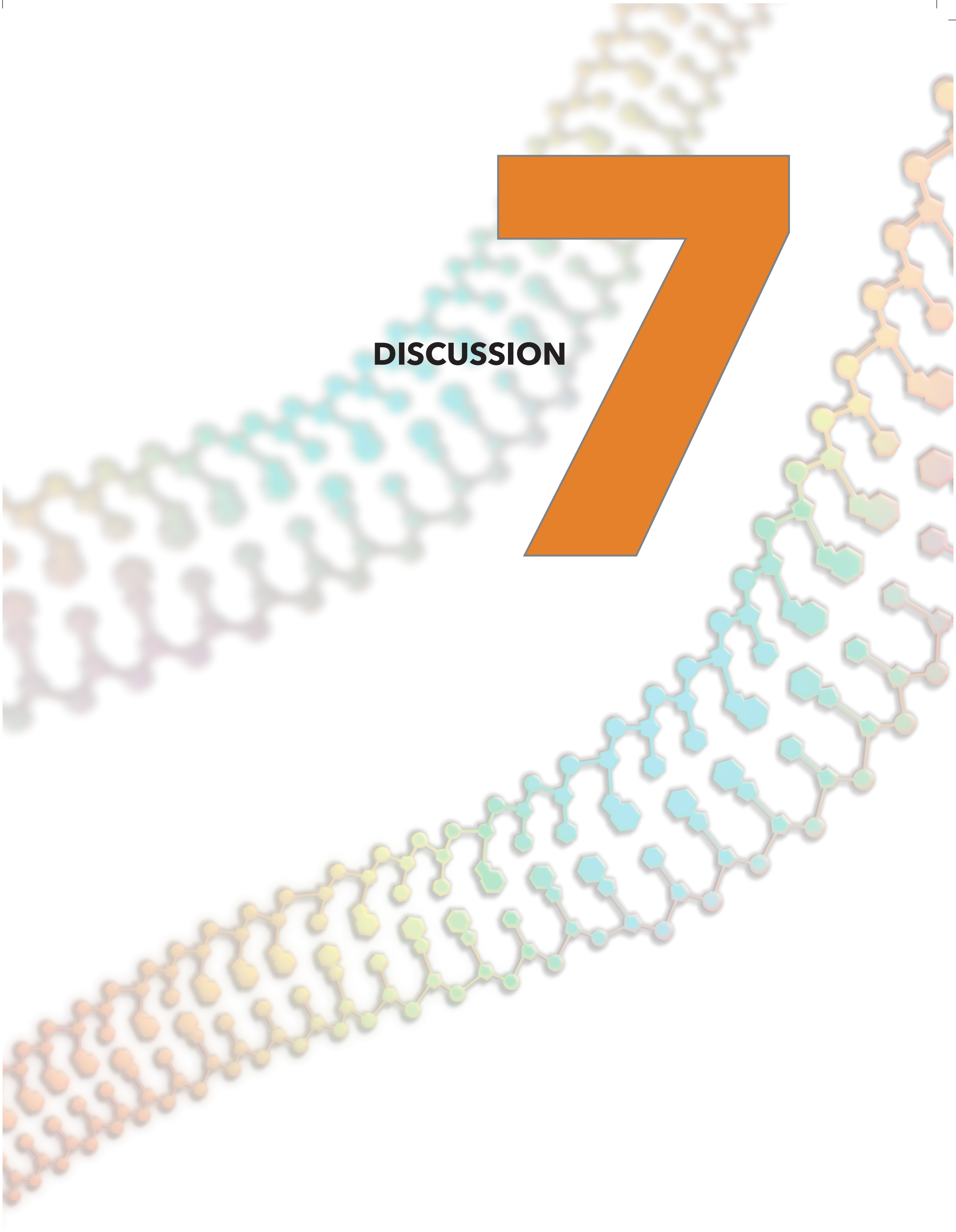

Chromatin is a well-known regulator of all DNA-associated processes, including DNA repair. Thus far most research on the interplay between chromatin and the DNA damage response (DDR) has focused on the core histones and how they are affected by ATP-dependent chromatin remodelers, histone chaperones and post-translational modifications (PTMs). For example, it was shown that different ATP-dependent chromatin remodeling complexes are important for the efficient initiation of NER in response to UV-induced DNA damage [1]. The most well-known example of a DNA damage-induced PTM is the phosphorylation of the histone H2A variant H2AX at serine 139 [2, 3]. Phosphorylation of H2AX plays an important role in the maintenance of genome stability by initiating the activation of cell cycle checkpoints and stimulating the recruitment of repair factors. Core histones are very immobile, as they are stably incorporated in nucleosomes. Consequently, epigenetic changes on these histones by PTMs can be considered as rather stable [4]. This makes core histones useful targets for DNA damage signaling events as modified histones are not easily translocated away from damaged sites. However, enhanced histone exchange by histone chaperones, or replacement of core histones by specific histone variants may occur in response to DNA damage, which may add more plasticity to the rigid chromatin fiber and eventually stimulate repair efficiency [5]. The linker histone H1 is a more dynamic element of chromatin than core histones and binds on the surface of the nucleosome to the DNA exit and entry points. Initially it was thought that H1 had merely a structural role in chromatin compaction thereby acting as transcription repressor. However, over the years it became clear that H1 can be modified and bound by other proteins and is actively involved in transcription regulation, heterochromatin formation and the DDR [6-9].

HISTONE H1 IS AN IMPORTANT PLAYER IN THE DNA DAMAGE RESPONSE

One of the first indications that histone H1 is involved in the DDR came from experiments using mouse embryonic stem cells, in which three of the six canonical H1 variants were knocked out (TKO H1 mES cells) [7, 10]. These cells are hyper resistant to ionizing radiation (IR), hydroxyurea and methyl methanesulfonate and displayed increased checkpoint signaling [7]. In contrast, later it was shown that these cells were more sensitive to doxorubicin and etoposide treatment [8]. This contradictory findings may be the result of different functions of histone H1, as loss of H1 reduces chromatin compaction [10] but also decreases suppression of p53-mediated gene expression [8]. Reduced chromatin compaction enables easier access of repair factors to DNA lesions, which can lead to enhanced resistance. However when p53-regulated apoptosis is not suppressed properly, there will be more cell death in response to DNA damage, resulting in enhanced sensitivity. Future studies are necessary to uncover the exact underlying mechanism of this striking difference in survival rate.

In chapter 6 we showed that acetylated histones are degraded upon UV-induced replication stress by PA200-containing proteasome complexes. In this chapter we mainly focused on the acetylation levels of core histones as the antibodies against acetylated-lysine did not show a clear band around the expected size of H1 on western blot, which indicates that the endogenous levels of acetylated H1 proteins is probably relatively low. However, our proteomics data show that, like for core histones, acetylated peptides derived from the N-terminus of histone H1 are less abundant in response to UV irradiation. This suggests that also acetylated H1 entities may be degraded in response to UV-induced replication stress, possibly to reduce chromatin compaction or stimulate p53-mediated apoptosis.

In addition, DNA damage-induced ubiquitylation of H1 has recently been shown to be an important step in the RNF8-RNF168-mediated ubiquitin signaling pathway [9]. Our data presented in Chapter 5 are in line with a two-step model of histone H1 ubiquitylation in response to DNA damage in which HUWE1 primes H1 with mono-ubiquitin entities, thereby stimulating RNF8/Ubc13-mediated K63-linked poly-ubiquitylation and recruitment of downstream DDR factors, such as 53BP1. It is not clear yet how the activity of HUWE1 is regulated and if it, like RNF8, requires phosphorylation of H2AX and MDC1 recruitment to damage sites. However, as we observed that HUWE1-mediated H1 ubiquitylation in response to UV irradiation is independent of XPA, it is likely not dependent on ATR and yH2AX. Previously, it was observed that reduced H1 levels lead to enhanced H2AX phosphorylation, the initial step of the RNF8-RNF168-mediated DDR pathway, in response to DNA damage [7, 9]. It is conceivable that proper recruitment of downstream factors, like 53BP1 and BRCA1, initiate a negative feedback loop that reduces yH2AX signaling to prevent hyper-activation of the DDR. However, when recruitment of 53BP1 or BRCA1 is impaired, for example due to lower H1 levels, H2AX may be persistently phosphorylated. This signaling pathway needs to be tightly regulated, not only to achieve a swift and efficient induction following DNA damage, but also to switch off this signaling pathway when repair has taken place or to prevent over-activation and propagation of the signaling. The RNF8-RNF168 pathway is likely controlled by different processes, as the deubiquitylating enzymes USP3 and USP16 counteract the RNF8-RNF168-mediated ubiquitylation [11, 12] and TRIP12 and UBR5 are involved in regulating RNF168 levels [13]. Moreover, the RNF168 paralog RNF169 binds ubiquitylated chromatin thereby competing with 53BP1 and BRCA1 recruitment to damage sites [14, 15]. Initiation of DDR through H1 may represent another safeguard to avoid excessive signaling, since due to its relative high turnover compared to core histones, PTMs are only transiently present around DNA lesions. In addition, ubiquitylation decreases the binding strength between histone H1 and chromatin [9], which might further enable histone chaperones to remove H1 from damaged sites, thereby restricting downstream signaling events.

Histone H1 levels affect the RNF8-RNF168-mediated ubiquitin signaling pathway, as depletion of H1 leads to reduced recruitment of downstream factors [9]. In line with this, local reduction of H1 levels by SET overexpression (Chapter 5), decreases the levels of BRCA1 colocalization with DSB [16]. In contrast, similar amounts of 53BP1 recruitment to IR-induced foci were observed in TKO H1 mES cells compared to WT cells [7]. These cells have a 50% reduction of total histone H1 levels, however the amount of chromatin bound H1 might still be sufficient for efficient RNF8-RNF168-mediated signaling. Interestingly, as shown by experiments overexpressing HMGN1 which competes with H1 for chromatin binding, not the absolute H1 levels, but rather the amount of H1 molecules incorporated in the chromatin determines the efficiency of this signaling pathway [9].

Specific enzymes are involved in the loading and releasing of H1 from the chromatin. For example, SET was identified as a histone H1 chaperone, involved in the removal of H1 from chromatin [17, 18]. Our data presented in Chapter 4 show that depletion of SET leads to enhanced levels of chromatin bound H1 and a striking enhanced resistance to a wide variety of structurally unrelated DNA lesions. This increased resistance to genotoxic agents does not seem to be derived from enhanced repair capacity as SET depletion does not change NER efficiency (chapter 4). These observation suggest that SET is most likely involved in a more general cell survival mechanism, such as the p53-mediated apoptotic pathway. In line with this we suggest that induction of p53-controlled genes is in part regulated by SET (Chapter 4), as we observed that SET and p53 act in the same pathway. Based on these data we propose a model in which enhanced binding of H1 on p53-regulated promoters inhibits the induction of pro-apoptotic genes, resulting in higher resistance to DNA damage. Therefore, loss of SET will have consequences, as by avoiding the apoptotic emergency response the risk of propagation of cells with DNA damage-induced mutations will increase. Histone H1 can repress gene expression by enhancing chromatin compaction and by recruiting transcriptional repressors to promoters [6], which makes it an ideal candidate for the regulation of stress-induced genes. Interestingly, it was found that the chromatin remodeler CHD8 recruits H1 to p53-regulated promoters in response to DNA damage. As SET and CHD8 have antagonistic functions [8], the balance in activity of these chaperones in response to DNA damage may determine the amount of chromatin-bound histone H1 and, as a result, influence expression of p53-regulated genes and cellular survival. This indicates that not only the amount of chromatin-bound histone H1 is important, but also the genomic location where H1 is incorporated is of significance in the DDR.

We describe a stimulatory role for SET in apoptosis which might indicate that SET is a tumor suppressor gene, but surprisingly SET is found to be overexpressed in many types of cancer [19-23]. CHD8 levels are, in contrast, found decreased in prostate cancer [24]. Possibly not the absolute levels of SET are important in tumorigenesis, but the balance between CHD8 and SET and as a result the levels and localization of H1. Also SET overexpression could be a compensatory mechanism in cells that carry other mutations that inhibit DNA damage signaling. The obtained results described in this thesis provide additional evidence that histone H1 is an important player in the DDR, by both functioning in DNA damage signaling and transcriptional regulation. The output of H1 itself is likely regulated at different levels, through post translation modifications, differential mobility, localization and protein levels. Therefore, it would be interesting to further study these properties in tumors and investigate the potential of histone H1 as a target for cancer treatments.

CHROMATIN REMODELING DURING THE DDR; MORE THAN OPEN-REPAIR-RESTORE

The access-repair-restore model has provided a convenient framework for hypothesis-driven research on the interplay between chromatin and DNA damage. However, the naïve view that chromatin is solely an obstacle for repair has been changed over the past years, as many studies have showed that chromatin is an active player in the DDR [1, 3, 5, 25, 26]. More recent, an updated version of this model has been proposed. In this prime-repair-restore paradigm [27] the different steps are not considered as sequential and unidirectional but also include overlapping stages that may occur simultaneously. The priming step prepares chromatin for repair and damage signaling by its decondensation, incorporation of specific histone variants and the addition of histone modifications. The restore step does no longer only contain restoration to pre-damaged conditions to maintain epigenetic information, but is extended with incorporation of specific histone variants and modifications that may locally alter functional properties of chromatin [27]. For instance, both the transcription inhibition following DNA damage and its subsequent recovery following DNA repair may require changes in chromatin conformation, histone modifications or incorporation of specific histone variants [25, 28]. In our review (Chapter 3) we summarize and discuss the current literature on how chromatin is prepared for transcription restart after repair of UV-induced transcription inhibition. Cells that have repaired the UV-induced lesions need to restore transcription to pre-damage states. As DNA-damage induced transcription block can take up to several hours, there is probably a high demand for the formation of new transcripts compared to cells under unperturbed conditions. Histone chaperones HIRA [29] and FACT [30] are shown to be necessary for efficient transcription recovery in response to UV irradiation. The exchange of histones by these factors may provide sufficient chromatin plasticity to allow efficient transcription re-initiation. The exchanged histones might also carry specific modifications thereby changing the epigenetic state of the chromatin and stimulating transcription. The methyltransferase DOT1L can further stimulate the assembly of transcription machineries by providing an more accessible chromatin structure [31].

The experiments described in this thesis provide additional evidence that the function of chromatin remodeling and histone modifications in response to DNA damage indeed extends beyond the classical access-repair-restore model. For example, besides damage-induced transcriptional repression, a specific set of stress-response genes are induced in response to UV-irradiation [32-34]. These genes are implicated in e.g. general stress response, DNA repair or apoptosis [33] and many are tightly regulated in a p53-dependent manner. Our data suggest that SET and H1 chromatin binding are both implicated in p53-regulated gene expression. It is however also likely that other transcription factors, ATP-dependent chromatin remodelers, histone chaperones and PTMs are involved in the precise regulation of these genes.

DNA damage by definition occurs in the context of chromatin, which makes it a convenient platform for damage signaling and allows efficient spreading of the signal along the chromatin fiber. Over the years, many histone modifications were found to be regulated in response to DNA damage [35-37]. However, since both chromatin and DNA damage affect DNA transacting processes, like transcription, replication and repair, it remains difficult to distinguish if chromatin changes are required to regulate the DDR or are indirectly caused by DNA damage-induced transcription or replication block. To differentiate whether changes in histone PTMs can be linked to DNA repair or to transcription or replication stress, systematic comparative experiments should be performed by e.g. comparing cycling versus non-cycling cells, cells treated with transcription inhibitors or in repair-deficient versus repair-

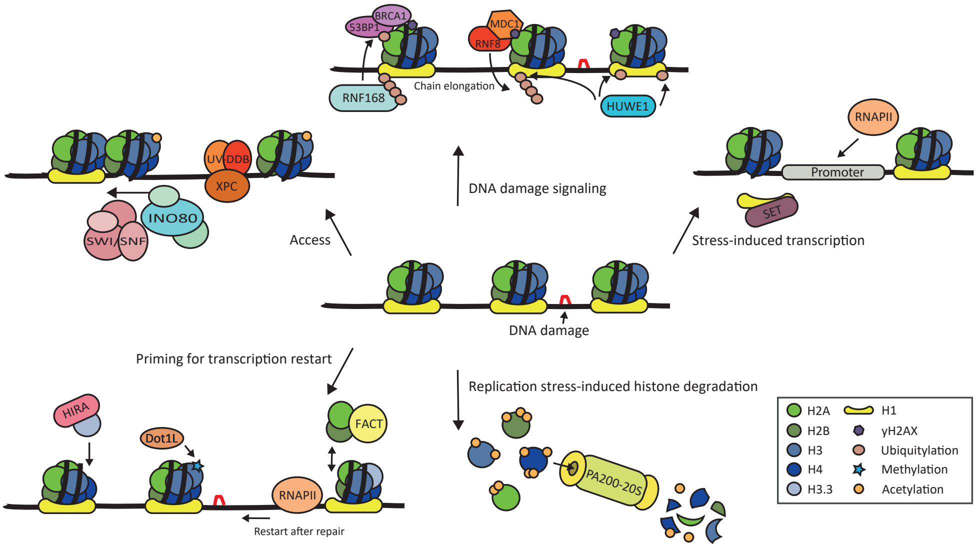
BRCA1
53BP1
MDC1
RNF8
RNF168
Chain elongation
HUWE1
UV-DDB
XPC
INO80
SWI/SNF
Access
DNA damage signaling
RNAPII
Promoter
SET
Stress-induced transcription
DNA damage
Priming for transcription restart
HIRA
Dot1L
FACT
RNAPII
Restart after repair
Replication stress-induced histone degradation
PA200-20S
H2A
H1
H2B
γH2AX
H3
Ubiquitylation
H4
Methylation
H3.3
Acetylation

Figure 1: Graphical representation of the different functions of chromatin changes in response to UV-induced DNA damage.

By definition, DNA lesions are always located within chromatin (center). To allow repair proteins to access DNA lesions, chromatin is remodeled to a more open structure by the concerted action of ATP-dependent chromatin remodelers, histone chaperones and post translational modifications (top left). The stable nature of core histones makes chromatin a perfect platform for DNA damage signaling events. In response to DNA damage, H2AX is phosphorylated, leading to the recruitment of MDC1 and RNF8. The E3 ligase HUWE1 most likely primes histone H1 with mono-ubiquitin entities that are subsequently elongated to K63-linked poly-ubiquitin chains by RNF8. These K63-chains are recognized and bound by RNF168 that, in turn, ubiquitylates H2A, and as a result downstream factors, like 53BP1 and BRCA1, are recruited to damage sites (top middle). In response to DNA damage, also transcription of specific stress-responsive genes is induced. These include, for example, p53-controlled genes. Histone H1 binding to p53-regulated promoters inhibits the expression of these genes. SET facilitates the removal of H1 from the chromatin thereby allowing the induction of apoptosis, which might be mediated via p53-dependent gene transcription (top right). The histone chaperones HIRA and FACT and the methyltransferase Dot1L are thought to prime the chromatin to stimulate transcription recovery after UV-lesions are removed by the specific transcription-coupled NER process (bottom left). UV-damage can also lead to replication stress, after which acetylated histones are specifically degraded by the PA200-proteasome. This might be necessary to open up the chromatin structure, prevent an excess of histones or to regulate replication. It is currently not known whether chromatin-bound or free histones are degraded (bottom right). After repair is finished, DNA damage signaling and stress induced transcription need to be stopped and chromatin needs to be restored to pre-damage conditions to preserve epigenetic information. It is perhaps even more enigmatic how this latter chromatin mark erasing process is achieved.

proficient cells. While different histone PTMs that are affected by DNA damage have been studied using PTM-specific histone antibodies, their identification depends on the availability, quality and specificity of these antibodies. The unbiased quantitative mass spectrometry approach described in chapter 6, in which different proteases are used in parallel to achieve a high coverage of histone proteins followed by an enrichment for acetylated peptides, resulted in the identification of many new UV-damage induced histone acetylation events. To further uncover DNA-damage induced chromatin changes and to functionally link these to the DDR, this approach can be extended to study other histone PTMs, using other enrichment procedures for modified peptides.

Our approach uncovered that replication stress induces an overall loss of acetylated histones due to degradation by the non-canonical PA200-containing proteasome complex (chapter 6). What the exact function of this process is during the UV-DDR remains unknown. However, as we additionally found that non-cycling cells have lower histone acetylation levels than cycling cells, we propose that high levels of acetylated histones might be necessary for replication. Previously it was shown that replication forks slowdown in the absence of sufficient histone levels [38]. Therefore it is tempting to speculate that degradation of acetylated histones may be an additional regulatory mechanism to slowdown replication fork progression in response to DNA damage, thereby giving the cell more time to repair DNA damage and avoiding additional encounters of replication forks with DNA lesions. However future studies are necessary to reveal the specific cellular function of histone degradation in response to UV-induced replication stress.

To summarize, the findings presented in this thesis have identified and partly disclosed additional control mechanisms to be added to growing number of chromatin-mediated DDR processes, including a role for chromatin in the regulation of transcription following DNA damage (Chapters 3 & 4) and DNA damage signaling (Chapter 5) (Figure 1). In addition to histones incorporated in the chromatin, also total histone levels are regulated following DNA damage and may play a role in the regulation of replication and the cell cycle (Chapter 6). Thus far many chromatin regulating proteins were found to stimulate repair and cellular survival in response to DNA damage. Interestingly however, in this thesis we showed that also specific chromatin modifying factors exist that negatively affect survival. This indicates that chromatin remodeling in response to DNA damage is a tightly regulated and intricate process, involving many different proteins that regulate the delicate balance between repair and transcription, replication and apoptosis, thereby preserving genome integrity and preventing tumorigenesis.

REFERENCES

1. Lans, H., J.A. Marteijn, and W. Vermeulen, ATP-dependent chromatin remodeling in the DNA-damage response. Epigenetics & Chromatin, 2012. 5.
2. Rogakou, E.P., et al., DNA double-stranded breaks induce histone H2AX phosphorylation on serine 139. J Biol Chem, 1998. 273(10): p. 5858-68.
3. Lukas, J., C. Lukas, and J. Bartek, More than just a focus: The chromatin response to DNA damage and its role in genome integrity maintenance. Nat Cell Biol, 2011. 13(10): p. 1161-9.
4. Kimura, H. and P.R. Cook, Kinetics of core histones in living human cells: little exchange of H3 and H4 and some rapid exchange of H2B. J Cell Biol, 2001. 153(7): p. 1341-53.
5. Mandemaker, I.K., W. Vermeulen, and J.A. Marteijn, Gearing up chromatin: A role for chromatin remodeling during the transcriptional restart upon DNA damage. Nucleus, 2014. 5(3): p. 203-210.
6. Hergeth, S.P. and R. Schneider, The H1 linker histones: multifunctional proteins beyond the nucleosomal core particle. EMBO Rep, 2015. 16(11): p. 1439-53.
7. Murga, M., et al., Global chromatin compaction limits the strength of the DNA damage response. J Cell Biol, 2007. 178(7): p. 1101-8.
8. Nishiyama, M., et al., CHD8 suppresses p53-mediated apoptosis through histone H1 recruitment during early embryogenesis. Nat Cell Biol, 2009. 11(2): p. 172-82.
9. Thorslund, T., et al., Histone H1 couples initiation and amplification of ubiquitin signalling after DNA damage. Nature, 2015. 527(7578): p. 389-93.
10. Fan, Y., et al., H1 linker histones are essential for mouse development and affect nucleosome spacing in vivo. Mol Cell Biol, 2003. 23(13): p. 4559-72.
11. Nicassio, F., et al., Human USP3 is a chromatin modifier required for S phase progression and genome stability. Curr Biol, 2007. 17(22): p. 1972-7.
12. Shanbhag, N.M., et al., ATM-dependent chromatin changes silence transcription in cis to DNA double-strand breaks. Cell, 2010. 141(6): p. 970-81.
13. Gudjonsson, T., et al., TRIP12 and UBR5 suppress spreading of chromatin ubiquitylation at damaged chromosomes. Cell, 2012. 150(4): p. 697-709.
14. Chen, J., et al., Ring finger protein RNF169 antagonizes the ubiquitin-dependent signaling cascade at sites of DNA damage. J Biol Chem, 2012. 287(33): p. 27715-22.
15. Povlsen, L.K., et al., Systems-wide analysis of ubiquitylation dynamics reveals a key role for PAF15 ubiquitylation in DNA-damage bypass. Nat Cell Biol, 2012. 14(10): p. 1089-98.
16. Kalousi, A., et al., The nuclear oncogene SET controls DNA repair by KAP1 and HP1 retention to chromatin. Cell Rep, 2015. 11(1): p. 149-63.
17. Kato, K., M. Okuwaki, and K. Nagata, Role of Template Activating Factor-I as a chaperone in linker histone dynamics. J Cell Sci, 2011. 124(Pt 19): p. 3254-65.
18. Zhang, Q., et al., Eviction of linker histone H1 by NAP-family histone chaperones enhances activated transcription. Epigenetics Chromatin, 2015. 8: p. 30.
19. Christensen, D.J., et al., SET oncoprotein overexpression in B-cell chronic lymphocytic leukemia and non-Hodgkin lymphoma: a predictor of aggressive disease and a new treatment target. Blood, 2011. 118(15): p. 4150-8.
20. Jiang, Q., et al., The set gene is a potential oncogene in human colorectal adenocarcinoma and oral squamous cell carcinoma. Mol Med Rep, 2011. 4(5): p.

993-9.

21. Leopoldino, A.M., et al., SET protein accumulates in HNSCC and contributes to cell survival: antioxidant defense, Akt phosphorylation and AVOs acidification. Oral Oncol, 2012. 48(11): p. 1106-13.
22. Li, C., et al., Quantitative proteomics reveal up-regulated protein expression of the SET complex associated with hepatocellular carcinoma. J Proteome Res, 2012. 11(2): p. 871-85.
23. Ouellet, V., et al., SET complex in serous epithelial ovarian cancer. Int J Cancer, 2006. 119(9): p. 2119-26.
24. Damaschke, N.A., et al., Frequent disruption of chromodomain helicase DNA-binding protein 8 (CHD8) and functionally associated chromatin regulators in prostate cancer. Neoplasia, 2014. 16(12): p. 1018-27.
25. Polo, S.E. and G. Almouzni, Chromatin dynamics after DNA damage: The legacy of the access-repair-restore model. DNA Repair (Amst), 2015. 36: p. 114-21.
26. Zhang, L., et al., The chromatin remodeling factor BRG1 stimulates nucleotide excision repair by facilitating recruitment of XPC to sites of DNA damage. Cell Cycle, 2009. 8(23): p. 3953-3959.
27. Soria, G., S.E. Polo, and G. Almouzni, Prime, repair, restore: the active role of chromatin in the DNA damage response. Molecular Cell, 2012. 46(6): p. 722-34.
28. Steurer, B. and J.A. Marteijn, Traveling Rocky Roads: The Consequences of Transcription-Blocking DNA Lesions on RNA Polymerase II. J Mol Biol, 2016.
29. Adam, S., S.E. Polo, and G. Almouzni, Transcription Recovery after DNA Damage Requires Chromatin Priming by the H3.3 Histone Chaperone HIRA. Cell, 2013. 155(1): p. 94-106.
30. Dinant, C., et al., Enhanced chromatin dynamics by FACT promotes transcriptional restart after UV-induced DNA damage. Mol Cell, 2013. 51(4): p. 469-79.
31. Oksenych, V., et al., Histone Methyltransferase DOT1L Drives Recovery of Gene Expression after a Genotoxic Attack. Plos Genetics, 2013. 9(7).
32. Derheimer, F.A., et al., RPA and ATR link transcriptional stress to p53. Proc Natl Acad Sci U S A, 2007. 104(31): p. 12778-83.
33. Riley, T., et al., Transcriptional control of human p53-regulated genes. Nat Rev Mol Cell Biol, 2008. 9(5): p. 402-12.
34. Garinis, G.A., et al., Persistent transcription-blocking DNA lesions trigger somatic growth attenuation associated with longevity. Nat Cell Biol, 2009. 11(5): p. 604-15.
35. Elia, A.E., et al., Quantitative Proteomic Atlas of Ubiquitination and Acetylation in the DNA Damage Response. Mol Cell, 2015. 59(5): p. 867-81.
36. Dabin, J., A. Fortuny, and S.E. Polo, Epigenome Maintenance in Response to DNA Damage. Mol Cell, 2016. 62(5): p. 712-27.
37. van Attikum, H. and S.M. Gasser, Crosstalk between histone modifications during the DNA damage response. Trends Cell Biol, 2009. 19(5): p. 207-17.
38. Mejlvang, J., et al., New histone supply regulates replication fork speed and PCNA unloading. J Cell Biol, 2014. 204(1): p. 29-43

APPENDIX &

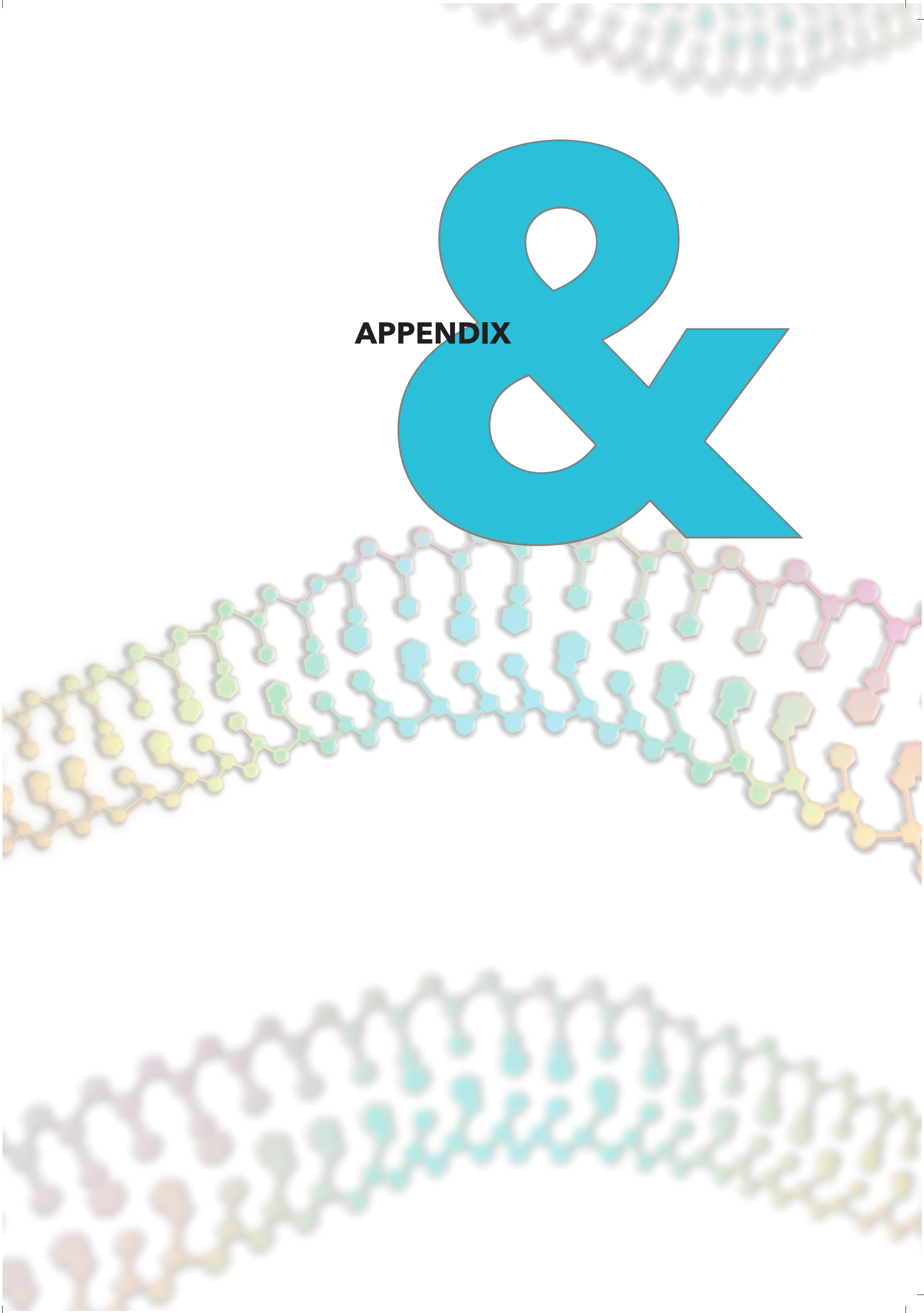

SUMMARY

The blueprint of our cells, the DNA, is constantly threatened by damaging agents of both exogenous and endogenous sources. To preserve DNA functionality and sequence a complex network of biological reactions, called the DNA damage response (DDR), has evolved. The DDR consist of many pathways that are involved in recognition, signaling and repair of DNA damage and that control replication, transcription and cell death. Different damaging agents can generate structurally very diverse DNA lesions that are repaired by different DNA repair pathways. For instance, ionizing radiation (IR) induces double strand DNA breaks which, dependent on the cell cycle phase, are repaired by homologous recombination or non-homologous end-joining. Nucleotide excision repair (NER) is involved in the repair lesions induced by UV irradiation, which mainly consist of 6-4 photoproducts and cyclobutane pyrimidine dimers. An overview of the different DNA repair mechanisms can be found in **Chapter 1**.

The importance of efficient DNA repair is highlighted by several rare recessive disorders, caused by mutations in DNA repair genes. One of these syndroms is trichothiodystrophy (TTD), which is characterized by brittle hair and nails, ichthyosis, impaired intelligence and anemia. About 50% of the patients are also sensitive to UV light, which is due to a mutation in the transcription and repair factor TFIIH. To dissect the pathophysiological contributions of unrepaired DNA lesions and impaired transcription, we studied the consequences of a non-photosensitive TTD-causing mutation in the general transcription factor IIE, subunit 2 (TFIIEβ) in **Chapter 2**. We showed that this mutation leads to a reduction in the protein levels of the TFIIE complex and a striking temperature-sensitive transcription defect. Also we found a late-stage hematopoietic differentiation defect by differentiating induced pluripotent stem cells (iPS), derived from patient fibroblasts, to erythroid cells. Our data confirm that TTD-specific features are mainly derived from subtle transcription defects, which are mostly evident in differentiated cells.

By definition, DNA transacting processes, like transcription and repair, take place in the context of chromatin. The main building blocks of chromatin are nucleosomes, consisting of DNA wrapped around histones, which small positively charged proteins. There are different chromatin structures, like heterochromatin, inaccessible dense chromatin, and euchromatin that has a more open conformation. The accessibility of chromatin is constantly altered by the concerted action of ATP-dependent chromatin remodelers, histone chaperones and post translational modifications (PTMs). The access-repair-restore model describes the importance of chromatin remodeling during the DDR, for example, to activate DNA damage signaling and to allow DNA repair proteins to access and repair lesions. In **Chapter 3** we provide an overview of chromatin remodeling during the UV-DDR and give a specific example showing three factors, HIRA, FACT and Dot1L, that stimulate the last step of transcription-coupled NER, the transcription restart.

As most chromatin-related DNA damage research has thus far focused on the core histones, not much is known about the function of histone H1 in the DDR. Therefore we studied H1 and its histone chaperone SET in **Chapter 4**. We found that cells depleted of SET are resistant to many different DNA damaging agents. However, this damage resistance was not caused by affecting DNA repair, but rather a result of reduced apoptosis upon DNA damage. We found that SET is involved in the removal of H1 from chromatin and that the increased DNA damage resistance in SET down regulated cells can be counteracted by co-depleting H1. Also we show that SET and p53 are epistatic in the induction of apoptosis in response to DNA damage. Together with recent data showing that DNA damage-induced H1 binding at promoters suppresses the expression of p53-responsive genes, this suggests a novel role for SET, in which its H1 chaperoning function is necessary for induction of apoptosis in response to DNA damage.

Modification by ubiquitin is a post translational modification important in the DDR. For example, several NER factors are modified with ubiquitin. In **Chapter 5** we found that also histone H1 is a major target of ubiquitylation in response to UV-damage and that ubiquitin E3-ligase HUWE1 is responsible for this. Previously it was found that RNF8 poly-ubiquitylates histone H1 in response to IR leading to recruitment of downstream factors. However, in contrast to HUWE1, RNF8 is not involved in the ligation of primary ubiquitin entities on H1 but most likely extends pre-existing ubiquitin modifications. We found that HUWE1 stimulates the RNF8 pathway, both after IR and UV irradiation. Our data are in line with the model that HUWE1 ubiquitylates histone H1 in response to DNA damage followed by K63-linked chain elongation by RNF8.

Histone acetylation, which neutralizes positively charged lysines and as a result untightens the interaction between histone and DNA, is another PTM previously shown to stimulate NER. However, thus far a complete overview of histone acetylation events in response to UV irradiation was missing. In **Chapter 6** we used a combination of different techniques to isolate acetylated histone peptides and quantitative mass spectrometry and found that there is an overall reduction in acetylated histones in response to UV irradiation. We found that this was the result of replication stress-induced degradation of acetylated histones. In contrast to general proteasomal degradation that is ubiquitin-driven, this degradation is mediated by a specific proteasome complex containing the PA200 subunit, which targets acetylated proteins. This degradation of acetylated histones is most likely a mechanism for cells to cope with replication stress.

In **Chapter 7**, we further discuss the emerging role of histone H1 in the DDR. Also we argue that chromatin remodeling during the DDR goes beyond the access-repair-restore model. Chromatin remodeling in response to DNA damage involves many different processes and regulates the fine balance between repair, replication, transcription and apoptosis. The findings presented in this thesis have identified novel processes that can be added to this growing list of chromatin-mediated DDR mechanisms.

Samenvatting

De blauwdruk van onze cellen, het DNA, wordt continu bedreigd door schadelijke stoffen, die ontstaan als bijproducten van processen in ons eigen lichaam of afkomstig zijn van bronnen van buitenaf. Om desondanks toch de functionaliteit en de sequentie van het DNA te kunnen behouden, is er tijdens evolutie een complex netwerk van biologische reacties, de DNA-schade respons (DDR) genaamd, ontstaan. De DDR bestaat uit vele processen die betrokken zijn bij herkenning, signalering en reparatie van DNA-schade en celdeling, transcriptie en celdood regelen. Diverse schadelijke stoffen veroorzaken structureel zeer uiteenlopende DNA-laesies, die elk gerepareerd kunnen worden door specifieke DNA-herstelprocessen. Bijvoorbeeld, ioniserende straling (IR) induceert dubbelstrengs DNA-breuken die, afhankelijk van de fase van de cel cyclus, worden gerepareerd door homologe recombinatie of “non-homologous end joining". Nucleotide excisie reparatie (NER) is betrokken bij het herstellen van DNA laesies geïnduceerd door UV straling, welke voornamelijk bestaan uit 6-4 fotoproducten en pyrimidine dimeren. Een overzicht van de verschillende DNA-reparatiemechanismen kan gevonden worden in **Hoofdstuk 1**.

Het belang van efficiënte DNA-reparatie wordt benadrukt door verscheidende zeldzame recessieve ziektes die worden veroorzaakt door mutaties in DNA-reparatiegenen. Een van deze syndromen is trichothiodystrofie (TTD), wat wordt gekarakteriseerd door zeer broze nagels en haren, ichtyosis, verstandelijke beperking en anemie. Ongeveer de helft van de patiënten zijn daarnaast ook gevoelig voor UV licht, wat in de meeste gevallen uitgelegd kan worden door een mutatie in de transcriptie- en reparatiefactor TFIIH. Om te ontleden wat niet-gerepareerde DNA-laesies en problemen met genexpressie bijdragen aan de symptomen van TTD, hebben wij de gevolgen van een niet-fotogevoelige TTD-veroorzakende mutatie in de algemene transcriptiefactor IIE, subunit 2 (TFIIEβ), onderzocht in **Hoofdstuk 2**. We laten zien dat deze mutatie leidt tot een afname in de expressie van de algemene transcriptiefactor TFIIE en tot een temperatuurgevoelig defect in transcriptie. Pluripotente stamcellen, geïnduceerd vanuit patiëntfibroblasten, tonen, wanneer ze gedifferentieerd worden tot erytrocyten, een laat-stadium hematopoïetisch differentiatiedefect. Deze data bevestigen dat de TTD-specifieke symptomen vooral veroorzaakt worden door subtiele genexpressiemankementen, welke het sterkst tot uiting komen in gedifferentieerde cellen.

DNA-gerelateerde processen, zoals transcriptie en DNA-reparatie, vinden per definitie plaats in de context van chromatine. De voornaamste bouwstenen van chromatine zijn nucleosomen, die bestaan uit histonen omwikkeld door DNA. Er zijn verschillende chromatinestructuren, zoals ontoegankelijk, compact heterochromatine en euchromatine, wat een lossere conformatie heeft. De toegankelijkheid van het chromatine wordt constant veranderd door de gezamenlijke actie van ATP-afhankelijke chromatine remodelers, histon chaperonnes en histon post-translationele modificaties (PTMs). Het herstructureren van chromatine speelt een belangrijke rol tijdens de DDR, bijvoorbeeld om het gemakkelijker te maken voor reparatie-eiwitten om DNA-laesies te binden en repareren of door het activeren van DNA-schade signalering. In **Hoofdstuk 3** geven we een overzicht van chromatine reorganisatie tijdens de UV-DDR. We geven hierbij een specifiek voorbeeld van drie factoren, HIRA, FACT en Dot1L, die de laatste stap van transcriptie-gekoppeld NER, de transcriptie herstart, stimuleren.

Omdat tot op heden chromatine-gerelateerd DNA-schade onderzoek zich vooral heeft gefocust op de histonen die de kern van het nucleosoom vormen, is er weinig bekend over de functie van histon H1, die aan de buitenkant van het nucleosoom bindt, in de DDR. Daarom hebben wij in **Hoofdstuk 4** H1 en de histon chaperonne SET bestudeerd. We hebben ontdekt dat cellen met verlaagde SET expressie resistent zijn tegen veel verschillende DNA-beschadigende stoffen. Echter deze resistentie tegen DNA-schade werd niet veroorzaakt doordat DNA-reparatie verbeterd was, maar bleek het resultaat te zijn van een verminderde DNA-schade-geïnduceerde celdood (apoptose). Onze data laten zien dat SET betrokken is bij het verwijderen van H1 van het chromatine. In lijn met deze vinding, hebben wij ook gevonden dat de verhoogde resistentie, veroorzaakt door verlaging van SET expressie, tegengegaan kan worden door ook expressie van histon H1 te verminderen. Daarnaast tonen wij aan dat SET en p53 beide belangrijk zijn voor de stimulatie van apoptose na DNA-schade. Samen met recente data die laat zien dat DNA-schade-geïnduceerde H1 binding de expressie van p53-gereguleerde genen onderdrukt, laten wij een potentiele nieuwe rol voor SET zien, waarin de H1 chaperonnefunctie van SET belangrijk is voor de inductie van apoptose na DNA-schade.

Modificatie met ubiquitine is een PTM die een belangrijke rol speelt in de DDR. In **Hoofdstuk 5** hebben wij gevonden dat histon H1 een belangrijk doelwit is van ubiquitinering in reactie op UV-schade en dat de ubiquitine E3-ligase HUWE1 hier verantwoordelijk voor is. Het is eerder aangetoond dat RNF8 histon H1 poly-ubiquitineerd in reactie op IR wat leidt tot de rekrutering van factoren die later in het proces betrokken zijn. RNF8 lijkt echter, in tegenstelling tot HUWE1, niet betrokken bij de hechting van de eerste ubiquitine op H1, maar verlengt waarschijnlijk reeds bestaande ubiquitine modificaties verder tot ketens. Wij hebben gevonden dat HUWE1 het RNF8-pathway stimuleert na zowel IR als UV-straling. Onze data zijn in overeenkomst met het model dat HUWE1 histon H1 ubiquitineert in reactie op DNA-schade, wat gevolgd wordt door een K63-gekoppelde verlenging van de ubiquitineketen door RNF8.

Histonacetylatie, een andere PTM betrokken bij de DDR, neutraliseert positief geladen lysines met als resultaat een minder sterke binding tussen histon en DNA. Tot op heden is er echter geen compleet overzicht gemaakt van histonacetylatiereacties als gevolg van UV-straling. In **Hoofdstuk 6** hebben we een combinatie van verschillende technieken gebruikt om geacetyleerde histonpeptiden te isoleren en kwantificeren. Hierbij hebben we een algeheel verlies van geacetyleerde histonen na UV-bestraling geobserveerd. Dit verlies was het gevolg van replicatiestress-geïnduceerde afbraak van geacetyleerde histonen. Echter, in contrast met basale proteasomale afbraak, wat gedreven wordt door ubiquitinatie, is deze afbraak gereguleerd door een speciaal proteasomaal complex. Dit complex bevat een PA200-eiwit en herkent specifiek geacetyleerde eiwitten en breekt deze af. Deze degradatie van geacetyleerde histonen na UV-straling is waarschijnlijk een mechanisme waardoor cellen beter om kunnen gaan met replicatiestress.

In **Hoofdstuk 7** gaan we dieper in op de steeds duidelijker wordende rol van histon H1 in de DDR. We beargumenteren ook dat de herstructurering van het chromatine tijdens de DDR verder gaat dan het bestaande "access-repair-restore" model. Dit model beschrijft hoe chromatine is gereorganiseerd na DNA-schade, door eerst het beschadigde chromatine toegankelijk te maken om DNA-reparatie mogelijk te maken. Als dit is voltooid, wordt het chromatine weer hersteld naar condities vergelijkbaar met onbeschadigd DNA om zo epigenetische informatie te bewaren. Veel verschillende processen zijn betrokken bij de veranderingen aan het chromatine na DNA-schade en samen reguleren deze de delicate balans tussen reparatie, celdeling, transcriptie en apoptose. De in deze thesis gepresenteerde bevindingen tonen nieuwe processen die toegevoegd kunnen worden aan de groeiende lijst van door chromatine-gereguleerde DDR-mechanismen.

CURRICULUM VITAE

Name:	Imke Karlijn Mandemaker
Date of birth:	14 October 1989
Place of birth:	Schijndel, The Netherlands
Email:	imke.mandemaker@gmail.com

Education

2010-2012	Master Molecular Life Sciences, Radboud University, Nijmegen, The Netherlands (cum laude)
2007-2010	Bachelor Molecular Life Sciences, Radboud University, Nijmegen, The Netherlands
2001-2007	Gymnasium Bernrode, Heeswijk, The Netherlands

Work experience

2017-present	Postdoc, Department of Physiological Chemistry, Ludwig-Maximilians-Universität München, Germany
2012-2017	PhD student, Department of Molecular Genetics, Erasmus MC, Rotterdam, The Netherlands
2012	Research internship, Institute for Cell and Molecular Biosciences, University of Newcastle, Newcastle upon Tyne, United Kingdom
2010-2011	Research internship, Department of Molecular Biology, Radboud University, Nijmegen, The Netherlands
2010	Research internship, Department of Biomolecular Chemistry, Radboud University, Nijmegen, The Netherlands

PUBLICATIONS

Mandemaker IK, van Cuijk L, Janssens RC, Lans H, Bezstarosti K, Hoeijmakers JH, Demmers JA, Vermeulen W, Marteijn JA. *DNA damage-induced histone H1 ubiquitylation is mediated by HUWE1 and stimulates the RNF8-RNF168 pathway.* Scientific reports 2017, 7:15353

Theil AF, Mandemaker IK, van den Akker E, Swagemakers SMA, Raams A, Wüst T, Marteijn JA, Giltay JC, Colombijn RM, Moog U, Kotzaeridou U, Ghazvini M, von Lindern M, Hoeijmakers JHJ, Jaspers NGJ, van der Spek PJ, Vermeulen W. *Trichothiodystrophy causative TFIIEβ mutation affects transcription in highly differentiated tissue.* Hum Mol Genet. 2017, doi: 10.1093/hmg/ddx351

Mandemaker IK, Vermeulen W, Marteijn JA. *Gearing up chromatin: A role for chromatin remodeling during the transcriptional restart upon DNA damage*. Nucleus 2014, 5(3):203-10

Ederveen TH, Mandemaker IK, Logie C. *The human histone H3 complement anno 2011.* Biochim Biophys Acta. 2011, 1809(10):577-86

PHD PORTFOLIO

Courses

Biomedical English writing and communication	2015
Biostatistical Methods I: Basic Principles	2015
Epigenetic regulation in health and disease	2014
Genome maintenance and stability	2014
Technology facilities: Proteomics	2014
The microscopic image analysis: from theory to practice	2014
Literature discussion	2014
Genetics	2013
Cell and developmental biology	2013
Safely working in the Laboratory	2012
Biochemistry and biophysics	2012
In vivo imaging from molecule to organism	2012

Teaching

I. Kik, BSc Biologie en Medisch laboratorium onderzoek	2015-2016
T. Goncalves Vaz, BSc Biomedical Sciences	2014-2015
Q. Hartman, BSc Forensic Laboratory Research	2013-2014
Werkcollege Genetics course, bachelor Nanobiology	2013-2015

Conferences and meetings

Molecular Genetic workdiscussion, oral presentations	2012-2017
NER-Vermeulen group discussions, oral presentations	2012-2017
Literature discussions	2012-2017
MGC DNA repair meeting, Rotterdam/Leiden, The Netherlands, oral presentations	2012-2017
Cancer Genomics meeting, oral presentation	2017
14th Dutch Chromatin meeting, Leiden, The Netherlands, poster presentation	2016
CGC meeting; Genomic instability in Cancer, Amsterdam, The Netherlands	2016
Responses to DNA damage: from molecule to disease, Egmond aan zee, The Netherlands	2016
IMB conference: DNA repair and genome stability in a chromatin environment, Mainz, Germany, poster presentation	2015
13th Dutch Chromatin meeting, Nijmegen, The Netherlands, poster presentation	2015
25th MGC symposium, Leiden, The Netherlands	2015
MGC PhD workshop, Maastricht, The Netherlands, oral presentation	2015
12th Dutch Chromatin meeting, Utrecht, The Netherlands, poster presentation	2014
24th MGC symposium, Rotterdam, The Netherlands	2014
EMBO Histone variants meeting, Strasbourg, France, oral presentation	2014
MGC PhD workshop, Munster, Germany, poster presentation	2014
11th Dutch Chromatin meeting, Rotterdam, The Netherlands, poster presentation	2013
2nd Chromatin symposium, Egmond aan zee, The Netherlands	2013
MGC PhD workshop, Luxembourg, Luxembourg	2013
10th Dutch Chromatin meeting, Amsterdam, The Netherlands	2012
22nd MGC symposium, Leiden, The Netherlands	2012

ACKNOWLEDGEMENTS/DANKWOORD

My thesis is done! I have been working hard to get to this point and couldn't have done it without the great support from so many people.

First I would like to thank all my colleagues in the NER group (Bert Jaap, jij hoort hier natuurlijk ook bij!). This thesis wouldn't have been there without the help from all of you. I cannot recall how many times I asked every one of you to watch my gels, fix my samples, take out my blots, split my cells or stain my survivals. However, I do know this happened often, very often and I am very grateful for your help. In addition, everyone was always willing to discuss experiments, protocols and data. But what I appreciated most over the past years was the atmosphere in the lab. I really had a great time and enjoyed coming to work. Over the years, many of you stopped being just my colleagues, but became my friends. Thank you for all the fun we had during all the lunches, coffee breaks, lab days and all other activities we organized.

In addition I also want to specifically thank some people.

Jurgen, ik heb met veel plezier met je samen gewerkt tijdens mijn promotie. Je had altijd tijd voor vragen en ik heb enorm veel van je geleerd de afgelopen jaren (ik neem nu eindelijk controles mee in mijn proeven!). Bedankt dat je me hebt gestimuleerd om zelf met ideeën voor proeven en projecten te komen en dat ik vervolgens ook de vrijheid heb gekregen om deze uit te voeren. Ook buiten de wetenschappelijke discussies om stond je deur altijd open voor een praatje. Bedankt voor de support, maar zeker ook voor de gezelligheid.

Wim, ook bij jou stond de deur altijd open voor vragen en ik heb daar naar het einde van mijn promotie toe ook steeds meer gebruik van gemaakt. Verder kwam je altijd met nuttige input tijdens de werkbesprekingen en ik heb hier veel van geleerd. Ook bedankt voor de de leuke lab stap dagen.

En dan mijn paranimfen; Mariangela, jij bent een van de liefste en zorgzaamste mensen die ik ken. Ik heb enorm veel lol met je gehad zowel binnen en buiten het lab. Hopelijk werken we over een aantal jaren weer beide in Nederland! Marjolein, wat begrijpen wij elkaar toch goed. We delen vaak dezelfde mening, en gelukkig ook dezelfde humor, wat tot vele leuke momenten heeft geleid. Karen en Serena, ook al had ik officieel maar 2 paranimfen, voor mij vallen jullie ook onder deze noemer. Vanaf het eerste moment konden we goed met elkaar opschieten en we hebben uren gekletst in het kantoor, in het lab of in de trein. Dames, bedankt voor alles waar jullie me bij hebben geholpen, maar vooral voor alle gezelligheid en steun tijdens mijn PhD.

My students, Quirine, Tiago and Iris, thank you for all the hard work and enthusiasm. Iris, ik ben trots dat jij als coauteur op een van mijn papers staat. Helaas heb jij dit zelf niet meer mee mogen maken.

Also thanks to all coateurs on my papers, for the experiments, discussions and all the input.

Alle leden van de promotiecommissie; Bedankt voor het lezen van dit proefschrift, jullie tijd en de nuttige tips.

Many thanks also go to all my other colleagues at the department of Molecular Genetics, the theme and other collaborating groups and supporting staff. Everybody was always willing to share knowledge and equipment and to help with different techniques and analyzing methods, which stimulated my research tremendously. I also realy enjoyed the chats that I had with many of you in the hallway, cell culture, on PhD retreats and during the activities outside the lab.

Ook wil ik graag mijn vrienden bedanken. Doordat velen van jullie zelf ook promoveren, begrijpen jullie precies wat een PhD doen inhoudt. De struggles, de hoogtepunten, de momenten van stress of frustratie, maar ook die van blijdschap. Ik heb de afgelopen jaren alles met jullie kunnen delen en bespreken. Ook bedankt voor alle ontspannen momenten; de etentjes, het (beach)volleyballen, de terrasjes, het squashen, de weekendjes weg en alle gekke activiteiten die we gedaan hebben.

Aruna, als ik “aiuto” roep, dan zijn jullie er altijd voor me, of het nu is om met me te proosten of om me te redden!

Esther, jij hebt een zesde zintuig ontwikkeld waardoor je altijd precies wist wanneer je me moest appen of een kaartje (of reisgids van München) moest sturen. Je hebt zo ontzettend met me meegeleefd de afgelopen jaren. Ik ben ontzettend gelukkig om jou als vriendin te hebben.

Enorm veel steun heb ik ook gevoeld vanuit mijn familie; Mama, papa, Jorik, Jouke en Maud bedankt voor alles. Mam en pap, jullie zijn er altijd als ik jullie nodig heb en dat betekent heel veel voor me. Gelukkig heb ik de afgelopen tijd geleerd om wat vaker naar jullie wijze adviezen te luisteren. Ook de betrokkenheid en interesse vanuit mijn schoonfamilie heb ik enorm gewaardeerd.

Sander, er zijn geen woorden voor hoeveel ik jou wil bedanken. Je hebt altijd aan mijn zijde gestaan, wat er ook gebeurde. Samen kunnen we niet alleen elk avontuur aan, maar het ook nog eens leuker maken dan ik ooit had kunnen dromen. Ik kan niet wachten op ons volgende avontuur!